

INFORMATION TO USERS

This material was produced from a microfilm copy of the original document. While the most advanced technological means to photograph and reproduce this document have been used, the quality is heavily dependent upon the quality of the original submitted.

The following explanation of techniques is provided to help you understand markings or patterns which may appear on this reproduction.

1. The sign or "target" for pages apparently lacking from the document photographed is "Missing Page(s)". If it was possible to obtain the missing page(s) or section, they are spliced into the film along with adjacent pages. This may have necessitated cutting thru an image and duplicating adjacent pages to insure you complete continuity.
2. When an image on the film is obliterated with a large round black mark, it is an indication that the photographer suspected that the copy may have moved during exposure and thus cause a blurred image. You will find a good image of the page in the adjacent frame.
3. When a map, drawing or chart, etc., was part of the material being photographed the photographer followed a definite method in "sectioning" the material. It is customary to begin photoing at the upper left hand corner of a large sheet and to continue photoing from left to right in equal sections with a small overlap. If necessary, sectioning is continued again – beginning below the first row and continuing on until complete.
4. The majority of users indicate that the textual content is of greatest value, however, a somewhat higher quality reproduction could be made from "photographs" if essential to the understanding of the dissertation. Silver prints of "photographs" may be ordered at additional charge by writing the Order Department, giving the catalog number, title, author and specific pages you wish reproduced.
5. PLEASE NOTE: Some pages may have indistinct print. Filmed as received.

Xerox University Microfilms

300 North Zeeb Road
Ann Arbor, Michigan 48106

76-24,653

MILLER, Thomas William, 1946-
THE TRANSIENT RESPONSE OF ADAPTIVE
ARRAYS IN TDMA SYSTEMS.

The Ohio State University, Ph.D.,
1976
Engineering, electronics and
electrical

Xerox University Microfilms, Ann Arbor, Michigan 48106

© 1976

THOMAS WILLIAM MILLER

ALL RIGHTS RESERVED

THE TRANSIENT RESPONSE OF ADAPTIVE ARRAYS IN TDMA SYSTEMS

DISSERTATION

Presented in Partial Fulfillment of the Requirements for
the Degree Doctor of Philosophy in the Graduate
School of The Ohio State University

By

Thomas William Miller, B.S., M.S.

* * * * *

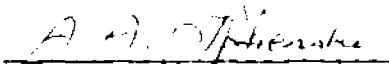
The Ohio State University

1976

Reading Committee:

Dr. A. A. Ksienski
Dr. R. J. Huff
Dr. R. T. Compton

Approved By



Adviser
Department of Electrical
Engineering

ACKNOWLEDGMENTS

This report, OSURF Number 4116-1 was prepared by the Electro-Science Laboratory, Department of Electrical Engineering, The Ohio State University Research Foundation, Columbus, Ohio. Research was conducted under Contract F30602-75-C-0061, Task No. 6523. Mr. Stuart Talbot was the Rome Air Development Center Program Monitor for this research.

The author wishes to express his sincere appreciation to his graduate adviser, Professor A. A. Ksienski, for his guidance and suggestions during the course of this work. A debt of gratitude is also owed to Professors R. J. Huff and R. T. Compton for their guidance and critical review of the text. Special thanks are also due to Messrs. R. Caldecott, C. H. Boehnker, R. C. Taylor, and S. Monett for their contributions to the instrumentation phase of the work.

The material contained in this report is also used as a dissertation submitted to the Department of Electrical Engineering, The Ohio State University as partial fulfillment for the degree Doctor of Philosophy.

VITA

September 10, 1946... Born - Cleveland, Ohio

1968..... B.S.E.E., Carnegie-Mellon University,
Pittsburgh, Pennsylvania

1968-1971..... Graduate Research Assistant,
ElectroScience Laboratory, The Ohio
State University, Columbus, Ohio

1971..... M.Sc., The Ohio State University,
Columbus, Ohio

1971-1976..... Graduate Research Associate,
ElectroScience Laboratory, The Ohio
State University, Columbus, Ohio

PUBLICATIONS

- "Imperfect Differential Detection of a Biphase Modulated Signal -- An Experimental and Analytical Study," Report 2738-5, 23 August 1971, The Ohio State University ElectroScience Laboratory, Department of Electrical Engineering; prepared under Contract F30602-69-C-0112 for Rome Air Development Center, Griffiss Air Force Base, Ohio.
- "Additional Experimental Results Relevant to TDMA-System Synchronization," (co-authors, R.J. Huff, D.C. Upp, J.D. Clover), Report 2738-8, March 1972, The Ohio State University ElectroScience Laboratory, Department of Electrical Engineering; prepared under Contract F30602-69-C-0112 for Rome Air Development Center, Griffiss Air Force Base, Ohio.
- "A Satellite Simulation with a TDMA-System Compatible Adaptive Array," (co-authors, R. Caldecott, R.J. Huff), Report 3364-4, January 1976, The Ohio State University ElectroScience Laboratory, Department of Electrical Engineering, prepared under Contract F30602-72-C-0162 for Rome Air Development Center, Griffiss Air Force Base, Ohio.

FIELDS OF STUDY

Major Field: Electrical Engineering

Studies in Digital Systems. Professors R.B. Lackey and
K.J. Breeding

Studies in Communications. Professor C.E. Warren

Studies in Applied Mathematics. Professor H.D. Colson

Studies in Probability and Statistics. Professor R.C. Srivastava

TABLE OF CONTENTS

	Page
ACKNOWLEDGMENTS	ii
VITA	iii
LIST OF TABLES	vii
LIST OF FIGURES	viii
 Chapter	
I INTRODUCTION	1
II TDMA - ADAPTIVE ARRAY DESIGN OBJECTIVES	4
A. Introduction	4
B. The TDMA Signaling Concept	4
C. Abbreviated Description of the Prototype TDMA Modems	5
D. Basic Considerations Relevant to the Utilization of ANSAs in TDMA Systems	8
III MATHEMATICAL MODEL	19
A. Introduction	19
B. Signal Structure and Array Geometry	19
C. Optimum Spatial Filtering in a Narrowband Environment	27
D. The Reference Signal	32
IV TRANSIENT RESPONSE OF THE LMS ALGORITHM	36
A. Introduction	36
B. Description of the LMS Algorithm	36
C. Ideal LMS Algorithm	41
D. Effects of Control Loop Noise	60
1. Introduction	60
2. Digital LMS Algorithm	60
E. The Effects of Weight Jitter on Desired Signal Coherence	91
1. Introduction	91

TABLE OF CONTENTS (continued)

Chapter		Page
	2. Desired Signal Amplitude and Phase Jitter	92
	3. Effects of Weight Jitter on Coherent Detection	99
V	TRANSIENT RESPONSE AND SIGNAL ESTIMATION	113
	A. Introduction	113
	B. Estimating the Desired Signal Direction of Arrival Vector	114
	C. Estimating the Input Signal Covariance Matrix	137
	D. Comparison with LMS Algorithm Transient Response	155
VI	AN EXPERIMENTAL TDMA - ADAPTIVE ARRAY SYSTEM	170
	A. Introduction	170
	B. Description of the Experimental System	171
	1. Description of Bench-Test Configuration and General Operating Principles	171
	2. Input Signal Synthesis	173
	3. Adaptive Processor Configuration	175
	4. Reference Signal Processor Description ...	181
	5. Multiplexer and Limiter Subsystem	184
	6. Control Waveform Subsystem	187
	7. The Bit Error Probability Measure	190
	C. Practical Design Considerations Relevant to the Implementation of the Analog LMS Algorithm	192
	1. Introduction	192
	2. Delays in the Feedback Loop	193
	3. Amplitude and Phase Error in the Weight Multipliers	199
	4. Weight Multiplier Feedthru	203
	5. D.C. Offsets and Dynamic Range Considerations	205
	6. The Effects of Higher Order Poles in the Feedback Loop	218
	D. Experimental Performance with a Constant Envelope Signal	224
	1. Introduction	224
	2. Waveform Processing Gain	224

TABLE OF CONTENTS (continued)

Chapter	Page
3. Performance with Small Loop Gain	227
4. Steady-State Performance With Weight Jitter	239
E. Experimental Performance Under Pulsed Desired Signal Conditions	266
VII SUMMARY AND CONCLUSIONS	286
APPENDIX I	291
APPENDIX II	295
APPENDIX III	296
REFERENCES	301

LIST OF TABLES

Table		Page
I	The eigenvalues, eigenvectors, and optimum signal-to-noise ratio for several values of the angular separation parameter ψ	50
II	An upper bound on the variance of the desired signal phase at the array output for $R_{\Delta} = 0$ and $R_{\Delta} \neq 0$ for several values of the angular separation parameter ψ	98
III	Conditions under which simulation results in Figures 18-20 were obtained	133
IV	Conditions under which simulation results in Figures 30-34 were obtained. Average values of the normalized output signal-to-noise ratio are also given	162
V	Experimental performance of the range tracking loop for several values of P_i/P_s under c.w. and wideband (563 KHz bandwidth) interference conditions	262

LIST OF FIGURES

Figure		Page
1	The TDMA modem signaling formats	6
2	Functional diagram of the previous ASP	12
3	Block diagram of the reference waveform generator	13
4	Functional diagram of the present ASP	15
5	Array geometry and signal environment	20
6	Analog adaptive processor model	39
7	Digital adaptive processor model	40
8	The output signal-to-noise ratio versus β for several values of the normalized adaption time	51
9	The output signal-to-noise ratio versus β for several values of the normalized adaption time	52
10	The output signal-to-noise ratio versus β for several values of the normalized adaption time	55
11	The output signal-to-noise ratio versus β for several values of the normalized adaption time	56
12	Upper and lower bounds on the (normalized) ratio of the excess noise power to the noise power without jitter	90
13	The minimum output signal-to-noise ratio required to obtain the performance level g	111
14	The minimum output signal-to-noise ratio required to obtain the performance level g	112
15	The probability that the average output signal-to-noise ratio, normalized to T_0 , is less than -3 dB versus T_0 and the number of samples (k) for several different array sizes	129
16	The average normalized output signal-to-noise ratio versus $T_0 k$ for several different array sizes	131
17	The standard deviation of $\hat{\rho}$ normalized to $\bar{\rho}$	132

LIST OF FIGURES (continued)

Figure		Page
18	The average normalized output signal-to-noise ratio versus T_0k for a four-element array	134
19	The average normalized output signal-to-noise ratio versus T_0k for a four-element array	135
20	The average normalized output signal-to-noise ratio versus T_0k for a four-element array	136
21	The average normalized output signal-to-noise ratio versus the optimum output signal-to-noise ratio for several different sample sizes (k)	144
22	The average normalized output signal-to-noise ratio versus the optimum output signal-to-noise ratio for several different sample sizes (k)	145
23	The average normalized output signal-to-noise ratio versus the optimum output signal-to-noise ratio for several different sample sizes (k)	146
24	The average normalized output signal-to-noise ratio versus the number of samples for a four-element array	148
25	The average normalized output signal-to-noise ratio versus the number of samples for a four-element array	149
26	The average normalized output signal-to-noise ratio versus the number of samples for a four-element array	150
27	The average normalized output signal-to-noise ratio versus the number of samples for a four-element array	151
28	The average normalized output signal-to-noise ratio versus the number of samples for a four-element array	152
29	The average normalized output signal-to-noise ratio versus the number of samples for a four-element array	153

LIST OF FIGURES (continued)

Figure		Page
30	The average normalized output signal-to-noise ratio versus the number of samples for six different algorithms	160
31	The average normalized output signal-to-noise ratio versus the number of samples for six different algorithms	165
32	The average normalized output signal-to-noise ratio versus the number of samples for six different algorithms	166
33	The average normalized output signal-to-noise ratio versus the number of samples for six different algorithms	167
34	The average normalized output signal-to-noise ratio versus the number of samples for six different algorithms	168
35	A functional block diagram of the satellite simulator/adaptive spatial processor bench-test	172
36	Input signal synthesis	174
37	Normalized broadside pattern of a four-element 1.5 λ -spaced linear array	176
38	Functional diagram of the present LMS algorithm implementation showing greater detail	177
39	Relative phase and amplitude characteristics of the 70 MHz i.f. bandpass amplifier	178
40	D.C. voltage measured at the baseband amplifier output versus the array input signal frequency	180
41	Functional diagram of the waveform processor	183
42	(a) Error monitor output signal (LRF) initial conditions set	185
	(b) Weight #2 control voltage, continuous adaption ...	185
43	Functional diagram of the multiplexer and limiter subsystem	186

LIST OF FIGURES (continued)

Figure		Page
44	The suppression characteristic of the bandpass limiter versus the input signal-to-noise ratio	188
45	Relationships of the control waveforms to the TDMA format	189
46	Performance of the differential detector/bit timing synchronization subsystem versus the input bit energy to noise density ratio (LRF)	191
47	A functional representation of the waveform processing used in the sampled-data delay-locked loops	192
48	Adaptive processor model with feedback delays	194
49	A closed loop representation of the LMS algorithm when $\tau_{ij} = 0$, $\tau_{2j} = 0$, and $\tau_{3i} = \tau_3$ for $i, j=1, 2, \dots, m$	200
50	The response of $y_n(t)$ versus adaption time (normalized to the n^{th} time constant) for several different initial weights	201
51	Weight control model with signal feedthru	204
52	Adaptive processor model with control-loop d.c. offsets	207
53	Signal spectra within the LMS control loop	216
54	Adaptive processor model with a low-pass filter in the feedback loop	220
55	The effect of the low-pass filter cutoff frequency on the poles of the feedback loop	223
56	Measurements showing the interference protection afforded by waveform processing at the differential detector for a bandspreading ratio of 16:1	225
57	The bit error probability versus the interference-to-desired signal ratio at the input to the bandpass limiter with wideband interference	228

LIST OF FIGURES (continued)

Figure		Page
58	Performance of the experimental system versus the bit energy-to-noise density ratio at the detector input using quadrature and biphase modulation	229
59	Performance of the experimental system versus the bit energy-to-noise density ratio using the range tracking loop to synchronize the transmit time base ..	230
60	Performance of the experimental system versus the bit energy-to-noise density ratio in the HRF	231
61	Performance of the experimental system versus the input interference-to-signal ratio for two values of the separation parameter ψ	233
62	Performance of the experimental system versus the input interference-to-signal ratio for several values of the separation parameter ψ	234
63	Performance of the experimental system versus the input interference-to-signal ratio for $\psi = 60^\circ$	236
64	Performance of the experimental system versus the input interference-to-signal ratio for $\psi = 30^\circ$	237
65	The array output signal-to-noise ratio versus the input interference-to-signal ratio	238
66	Performance of the experimental system versus the input interference-to-signal ratio for $\psi = 30^\circ$ with and without down-link noise added	242
67	Performance of the experimental system for $P'_S/\sigma^2 = 4$ dB	242
68	Performance of the experimental system for $\psi = 60^\circ$, and $P'_S/\sigma^2 = 0$ dB	244
69	Performance of the experimental system versus the input interference-to-signal ratio for $\psi = 30^\circ$	250
70	Performance of the experimental system for $P'_S/\sigma^2 = -4$ dB	251
71	Performance of the experimental system versus the input interference-to-signal ratio for $\psi = 60^\circ$	255

LIST OF FIGURES (continued)

Figure		Page
72	Performance of the experimental system for $\psi = 30^\circ$...	256
73	Performance of the experimental system versus the input interference-to-signal ratio for $\psi = 30^\circ$	258
74	Performance of the experimental system versus the input interference-to-signal ratio for $\psi = 60^\circ$	259
75	Performance of the experimental system versus the input interference-to-signal ratio for $\psi = 60^\circ$	268
76	Performance of the experimental system with $E_b/N_0 \approx 11.9$ dB and a reference signal level of 68.5 mv rms	269
77	The output signal-to-noise ratio versus adaption time (normalized to the preamble interval) for several values of P_J/P_S under the same conditions as in Figure 75	272
78	The output signal-to-noise ratio versus the normalized adaption time for several values of P_J/P_S under the same conditions as in Figure 76	273
79	The output signal-to-interference ratio versus the normalized adaption time for several values of P_J/P_S under the same conditions as in Figure 75	275
80	The output signal-to-interference ratio versus the normalized adaption time for several values of P_J/P_S under the same conditions as in Figure 76	276
81	Performance of the experimental system versus the input interference-to-signal ratio with and without the range tracking loop enabled	277
82	The output signal-to-noise ratio versus the normalized adaption time for $w(t_0) = [0]$ and $w(t_0) = (3.4 + j 3.4)[1, 1, 1, 1] = \beta R_{Xd}$	280
83	The output signal-to-interference ratio versus the normalized adaption time for $w(t_0) = [0]$ and $w(t_0) = (3.4 - j 3.4)[1, 1, 1, 1] = \beta R_{Xd}$	281
84	The output signal-to-noise ratio versus the normalized adaption time for $\psi = 30^\circ$. See text for parameter values	283

LIST OF FIGURES (continued)

Figure		Page
85	The output signal-to-noise ratio versus the normalized adaption time for $\psi = 30^\circ$. See text for parameter values	284
86	LMS loop showing points referenced in the specifications	300

CHAPTER I

INTRODUCTION

Adaptive antenna arrays are currently the subject of extensive investigation for radar and communications systems applications. The interest in this area stems from the fact that an adaptive array automatically establishes pattern nulls in directions from which undesired signals are received and provides gain to the desired signal. An adaptive array therefore offers the capability of improving system performance by enhancing the ability to acquire and track desired signals, even when the undesired signal sources have much higher levels relative to the desired signal. This latter capability is one of the fundamental advantages of adaptive arrays compared to conventional waveform processing techniques which generally require a large spectrum spreading factor to obtain comparable levels of undesired signal suppression.

An adaptive array is an array of antenna elements followed by an adaptive processor. An adaptive processor functions to combine the element outputs to optimize the output signal according to an appropriate performance criterion. Early work in the area of adaptive arrays considered adaptive processing as an optimal control problem. Widrow, et al. [1], presented the basic feedback algorithms which seek to minimize the mean square error between the array output signal and the desired signal. Applebaum [2] developed the control law theory of side-lobe cancellers using maximization of the output signal-to-noise ratio as a performance criterion. The theory of adaptive arrays has since been developed to satisfy the requirements of radar and communications system applications. In radar applications, the desired signal direction of arrival is generally presumed known a priori. This a priori knowledge is utilized to steer the main beam on the desired signal while rejecting all other signals. Griffiths [3] presented a modification to Widrow's least mean square (LMS) algorithm which can be applied to the known direction of arrival case. Brennan, et al. [4], along with Widrow [5] developed first order approximations to the effects of noise in the control loops assuming the presence of the desired signal does not contribute significantly to the weight solutions. This assumption was also employed by Reed, et al. [6], in an analysis which showed that an adaptive processor which is calculated directly from a sample covariance matrix of the input signals converges rapidly to an optimum processor in an arbitrary signal environment. Other results related to the radar applications can be found in [7,8,9]. In communications systems, the application addressed herein, an adaptive

array must generally be implemented without a a priori knowledge of the desired signal direction of arrival since sources of desired signal are located at unknown positions. An overview of various techniques which can be used to distinguish between desired and undesired signal sources in the unknown direction of arrival case was presented by Baird, et al. [10]. The choice of a technique tends to be dictated by the specific communications application. The power inversion techniques [e.g., 11], which rely on very rapid nulling of high-level interfering signals characteristic to the feedback algorithms, have shown promise where little or no a priori information regarding the desired signal waveform is available, e.g., during a prelockup phase before code timing has been established in a coded communications channel. One problem with this approach is that the adaptive processor gradually forms a null on the desired signal. Nulling of the desired signal was prevented in Widrow's algorithm by subtracting the desired signal, which was assumed known, from the array output and then using the result as the error signal in the feedback loop. Using Widrow's basic algorithm, Riegler and Compton [12] showed that nulling of the desired signal can also be prevented if a reference signal which adequately resembles the desired signal is subtracted from the array output to form the error feedback signal. Huff [13] and Reinhard [14,15] extended this idea to a coded communications application. The basic feasibility of using a delay-lock loop to establish initial code timing under high-level interfering signal conditions has also been demonstrated [16]. Koleszar [17] developed techniques for determining the statistics and spectral characteristics of the adaptive array weights when the desired signal is corrupted by additive random noise.

The purpose of this research was to generalize previous work to coded communication system applications where the desired signals received at the array are pulsed. A time division multiple access (TDMA) communications system is an example of one such application. The effectiveness of utilizing an adaptive array to improve the signal-to-noise ratio in such a system is highly dependent upon the ability to rapidly form a beam on the pulsed desired signal. Since interfering signals could be pulsed, the pattern nulls should also be formed as rapidly as possible in order to minimize loss of data. Consequently, a major portion of this study was devoted to investigating, both analytically and experimentally, the transient response characteristics of adaptive arrays.

A brief description of the TDMA system concept, followed by an overview of factors to be considered in selecting a specific approach to implementing a TDMA/adaptive array system, are presented in Chapter II. In Chapter III, the complex envelope representation of the input signals and appropriate performance measures are formulated. Optimal solutions for the adaptive processor are then presented. In Chapter IV, the ideal transient and steady-state performance of digital and analog models of the LMS algorithm and the modified

(Griffith's) LMS algorithm are reviewed. The relationship between initial weights and loop convergence is also discussed. Then, the effects of control loop noise on the array output signal and on coherent detection of that signal are examined in detail. The analysis represents an extension of the work by Brennan, et al. [4], to the coded communications application in which the presence of the desired signal cannot be neglected and the desired signal direction of arrival may or may not be assumed known a priori. Second order effects of control loop noise are also taken into account. The analysis differs from the research conducted by Koleszar [17] in that the effects of loop noise on the array output signal are determined under high-level input interfering signal conditions. The results of this analysis will serve as a basis for determining an upper limit on the rate of convergence of the LMS algorithm. The transient response of the LMS algorithm is compared with the response of the direct matrix inversion technique in Chapter V. An analysis of a technique for estimating the desired signal direction of arrival vector assuming an ideal reference signal is then presented. One purpose of this analysis was to determine the length of averaging time required to obtain an adequate estimate of the direction of arrival vector for use in initializing or modifying the LMS algorithm, thereby improving adaptive array performance. The experimental performance of a TDMA/adaptive processor system, implemented using the LMS algorithm, is described in Chapter VI. The adaptive processor employs waveform processing to generate the reference signal. Experimental measurements of data bit errors which occurred upon detecting a bandpass limited adaptive array output signal plus additive noise in a differential (DPSK) detector are presented. These data were obtained under steady-state, transient, and high control loop noise conditions with c.w., moderate bandwidth, and wide bandwidth interfering signals successively applied to the adaptive array inputs. The experimental results are compared, where appropriate, with the analytical results derived in Chapter IV. A summary and conclusions are given in Chapter VII.

CHAPTER II

TDMA - ADAPTIVE ARRAY DESIGN OBJECTIVES

A. Introduction

Abbreviated descriptions of the TDMA signaling concept [18,19] and the prototype TDMA modems used in performing the experiments described in Chapter VI are presented in the following two subsections. These descriptions are followed by an overview of the factors considered in selecting a specific approach to implementing a jointly operational TDMA/adaptive array satellite communications system. The reports cited contain detailed descriptions of the TDMA and adaptive array investigations completed previously. Most of the discussions presented in this chapter were documented previously in [20].

B. The TDMA Signaling Concept

In TDMA satellite communication systems, the time continuum is divided into non-overlapping intervals or slots, each of which is (normally) allocated for the relaying of signal from no more than one terminal at a time. The slots are normally defined with respect to the time base of a signal present on the satellite down-link designated as the network clock signal (NCS). At each user terminal, the time base of a locally-generated signal (clock) is aligned with the time base of the received NCS to establish a local receive clock. In turn, a transmit clock is timed so that pulses transmitted by the terminal during intervals identified from the transmit clock occupy assigned time slots on arriving at the satellite. Normally, the information needed to maintain proper transmitter time is obtained by estimating the error in arrival time of pulses transmitted by the terminal as they are received on the down-link relative to the local receive clock.

The TDMA techniques developed at The Ohio State University rely on the use of two coupled sampled-data delay-lock loops at each user terminal to maintain the desired timing relationships between the transmit and receive clock signals and the NCS. Baseband waveforms having appropriate correlation properties, e.g., pseudo-noise (PN) codes, are impressed as digital phase

modulation on each pulse processed by the loops. Properly designed, the synchronizing loops will maintain the transmit and receive timing errors at values which are small relative to the duration of the symbols which comprise the modulation waveforms. Consequently, a single local receive clock can be used at a terminal to time the demodulation of all data carrying pulses present on the down-link to that terminal. Moreover, a single clock signal can be employed within the satellite to generate signals which are synchronized with respect to the received signals. This latter clock signal can be generated autonomously within the satellite if the NCS is generated in synchronism with it by a satellite-borne subsystem. As should become evident subsequently, a satellite-borne adaptive array which sequentially forms main beams in directions from which desired, pulsed-envelope signals are received and nulls in directions from which undesired signals are received can be implemented with relative ease if the system design is based on the autonomous generation of a single clock signal within the satellite.

C. Abbreviated Description of the Prototype TDMA Modems

The four prototype TDMA modems which were implemented to demonstrate the practical feasibility of the TDMA technique developed previously can be configured to establish either a lower-rate format (LRF) or a higher-rate format (HRF) as shown in Figure 1. To utilize the LRF, the received signal power to single-sided noise density ratio (P_r/N_0) associated with the smallest terminal in the network must equal or exceed 51 dB, and the satellite channel must have a bandwidth of approximately 500 KHz. The respective values for the HRF are 60 dB and 4 MHz. Each prototype modem can simultaneously accommodate an I/O device which operates asynchronously at an average data rate of 75 bps, e.g., a teleprinter, and a device which operates synchronously at a 2400 bps average data rate, e.g., a vocoder. When the modems are configured to establish the HRF, data are transmitted at an instantaneous rate of 87.6 Kbps. Pseudo-noise (PN) codes are employed to spread the signal spectrum by a factor of sixteen to provide a moderate amount of protection against multipath and interference. In the LRF mode, the data are conveyed at an instantaneous rate of either 10.95 Kbps or 87.6 Kbps; the corresponding spectrum spreading factors are sixteen and two, respectively. The modems can be configured in either a two-phase mode wherein each signal pulse is bi-phase modulated by a PN code to effect spectrum spreading or a four-phase mode wherein a pair of PN codes is employed to quadrature phase modulate each signal pulse. Data are always conveyed via antipodal, differential phase shift keying, and each modem is equipped with a single differential

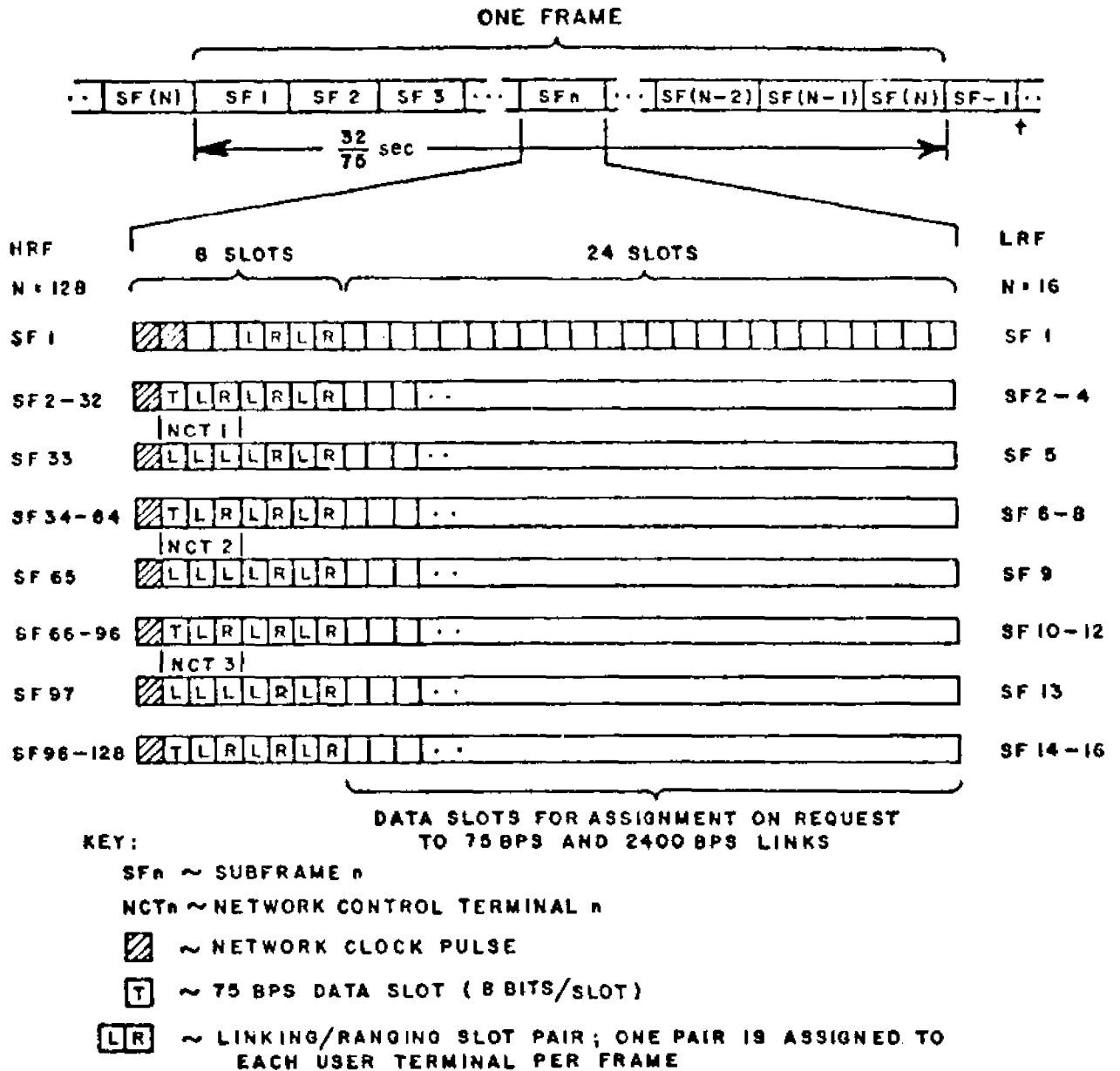


Figure 1. The TDMA modem signaling formats.

detector which is utilized to detect multiple signals in time sequence. Eight data symbols are transmitted in each time slot utilized to convey data except when operation in the LRF is enabled and data are being conveyed at an 87.6 Kbps rate. When the exception applies, sixty-four data bits are transmitted in each data slot. The first signaling interval within each slot which conveys data is allocated to the transmission of a one-bit "preamble" which is processed intrinsically within the differential detector to establish the reference "vector" needed to detect the first data symbol conveyed in the slot.

Essentially one-fourth of the TDMA signaling format is allocated for use in performing "overhead" functions; the remainder of the format is normally allocated to the user terminals in real time on a priority, demand-assignment basis* and is utilized exclusively to convey data between I/O devices. The overhead signals include one NCS, one control signal per network control terminal, and one link/range (L/R) signal per user terminal (see Figure 1). The modems are implemented so that a NCS is generated at a terminal and transmitted on the up-link in addition to other signals when a transmit clock switch is placed in an on position. However, no requirement exists for generating the NCS within a modem, i.e., the NCS can be generated autonomously within the signal relay, e.g., within the satellite.

Each L/R signal is transmitted during two consecutive pre-assigned slots--a L/R slot pair--once per frame. The L/R signal transmitted by a given terminal is generated in synchronism with a transmit clock and is subsequently received by that terminal on the down-link. On receipt, the L/R pulse is processed to estimate its error in arrival time relative to a locally-generated receive clock. This latter clock is maintained in synchronism with the received NCS. The time base of the transmit clock is corrected as appropriate to maintain the estimated error in arrival time within acceptable bounds. Each L/R signal is also utilized to convey data-slot assignment requests to a network control terminal, to request links with one or more terminals after an assignment has been received, to transmit suitable responses to link requests, to terminate links, and to relinquish data slot assignments after they are no longer needed. These functions are performed, in part, by transmitting one appropriately-coded sixteen-bit control word in each L/R slot pair.

Three or fewer network control terminals (NCTs) assign data slots on a priority, demand-assignment basis in accord with a network control algorithm. Each NCT transmits a twenty-four bit

*A manual-assignment capability is also provided to simplify testing.

network control word in three consecutive overhead slots--LLL slots (see Figure 1)--once per frame (in addition to a L/R signal). Appropriately-coded control words are made available to the TDMA modems by a minicomputer which executes the network control algorithm.* Each network control word destined for a given terminal conveys, in part, the terminal's address, a data slot allocation, and either an authorization to utilize the designated allocation or a request to terminate utilization of that allocation. Detailed descriptions of how the overhead slots are utilized are contained in [19].

D. Basic Considerations Relevant to the Utilization of ATISAs in TDMA Systems

An adaptive array is considered to consist of an array of antenna elements, appropriate front-end amplifiers and down-converters, and an adaptive spatial processor (ASP). Unlike in a conventional array, the signals received by the array elements in an adaptive array are not combined in a fixed manner to generate an array output signal. Rather, the array output signal--normally an IF signal--is generated by processing the received signals within the ASP in accord with an adaptive spatial processing algorithm. Generally, the array output signal is formed by (effectively) multiplying each received signal by a complex weighting coefficient which can vary with time and summing the weighted signals. For a given set of weighting coefficients, an equivalent conventional array having the same structure as the adaptive array could be implemented. Thus, at any given instant, an adaptive array (of the type being discussed) can be characterized by an effective pattern which is dependent, in part, on the number of elements in the array, the element characteristics, and the manner in which the elements are spatially distributed. If the weighting coefficients are properly calculated (generated), the effective pattern would exhibit preferred characteristics, and will be modified automatically to maintain those characteristics should the temporal and/or spatial characteristics of the composite signal incident on the array change with time. For example, pattern nulls will be established and maintained in directions from which undesired signals are incident on the array if the weighting coefficients are generated in an appropriate manner.

In the TDMA application, the adaptive array would ideally form a main beam in the direction from which any given desired-signal pulse is to be received immediately prior to the receipt of that pulse and in a negligibly-short interval of time, and pattern nulls in direction from which undesired signals are

*Only terminals which are to be configurable as NCTs need be equipped with minicomputers.

incident on the array. Since the undesired signals could also be time-varying, the pattern nulls should also be established in negligibly-short time intervals. Of course, a main beam and a pattern null cannot be formed in the same direction (if the spectral of the desired and undesired signals overlap and the desired and undesired signals are similarly polarized), nor can appropriate changes in the (effective) array pattern be made instantaneously, i.e., the signal transmitted on the down-link will not exhibit a suitably high desired signal-to-noise ratio until after an appropriate pattern is formed. Clearly, each of the many time-orthogonal pulsed (desired) signals could be processed by a single ASP in a manner whereby the weights (spatial filter) associated with each signal would appear to be held between pulses by sampling the weights at the end of each received pulse, storing the sampled weights in an appropriate manner, and initializing the weights at the beginning of each pulse to the appropriate stored values. A suitably-high signal-to-noise ratio may be obtained using this technique provided (1) that the desired signal direction of arrival is approximately constant between pulses, (2) the angular separation between the desired and undesired signal source is sufficiently large, and (3) an appropriate reference signal is available at the array processor for distinguishing desired and undesired signal sources. These requirements must be met regardless of the adaptive algorithm selected for implementing the adaptive array. Condition 1 represents a valid assumption in the present application. Condition 2 can normally be satisfied by selecting an array geometry capable of accommodating the closest angular separation which is expected to be encountered in a particular application. The third condition represents a more demanding requirement since the desired signal is modulated by an unknown data stream and its direction of arrival is initially unknown. Moreover, the desired signal cannot initially be assumed to arrive at the satellite in synchronism with the TDMA format. Since it is desirable to synchronize the desired signal and derive a reference signal as rapidly as possible and to obtain an adequate signal-to-noise ratio in time varying signal environments as well, attention was necessarily focused on providing a capability for forming an appropriate pattern in a short interval of time.

In the TDMA application being considered, undesirable signals should be suppressed within one or two data slots in order to prevent the occurrence of burst errors having lengths greater than the maximum burst length that can be accommodated by a practical error correcting codec. This implies adaptive array response times on the order of several hundred microseconds or less for the HRF mode of operation (about eight times longer in the LRF). As will be shown in Chapter V, this rate of convergence may be achieved in theory for arbitrarily low input desired signal to

undesired signal ratios by directly computing the weights based on a sample covariance matrix of the input signals and on an estimate of the desired signal direction of arrival. Unfortunately, this high rate of convergence cannot be achieved in practice due to limited real-time computer speeds* and non-ideal circuit components used for implementing the weight controls. The direct calculation approach also has the disadvantages that the number of calculations required per unit time is approximately proportional to m^3 and that the number of circuit components is approximately proportional to m^2 , where m is the number of complex weight controls (equal to the number of antenna elements in the present application)--a requirement which could present serious difficulties even for moderate array sizes, e.g., for an array of sixteen elements.

Of the alternative approaches considered for implementing the adaptive array, the LMS algorithm was selected. In addition to satisfying the speed requirements of the TDMA application over a wide range of signal conditions, the LMS algorithm has the advantage that (1) wideband analog circuits can be used to implement the ASP, (2) circuit complexity is proportional to m rather than m^2 or m^3 , (3) the feedback loop tends to compensate for circuit imperfections, and (4) means for obtaining a reference signal and for inserting that information into the feedback loop are readily effected.

The most direct approach to implementing the LMS algorithm with analog circuits is illustrated in Figure 2. In an ASP of the type illustrated, the n^{th} received signal (where $n = 1, 2, \dots, m$) is effectively weighted by the complex coefficient w_n^* by separating the signal into in-phase and quadrature components and multiplying the components by real weights $w_{n1} = \text{Re}\{w_n^*\}$ and $w_{n2} = \text{Im}\{w_n^*\}$, respectively. Each real weight assumes an arbitrary value in a range $[-w_{\text{max}}, w_{\text{max}}]$ where w_{max} is a positive number: the maximum gain of the weighting circuits. The weights are maintained at values which result in the error signal being minimized in an LMS sense by the feedback control loops. Should the error signal be correlated with the signal present at the input to any given weighting circuit, the value of the weight is automatically changed in a manner which results in the amplitude of the error signal being reduced. It has been shown that the desired signal to interference plus thermal noise power ratio associated with the array output signal is maximized on minimizing the error signal in a LMS sense if the reference signal is sufficiently like the

*This limitation is not necessarily based on the time required to invert the covariance matrix. Formidable difficulties are encountered in processing the input signals at the Nyquist rate, and in maintaining the accuracies required for implementing the optimum filter under high-level interference conditions.

desired signal, the desired and interfering signals are sufficiently different, and the time constant associated with the response of the ASP to the highest level signal incident on the array is maintained at a sufficiently large value.

Ideally, reference signal $r(t)$ (see Figure 2) would be an amplitude-scaled version of the desired signal incident on the array since the feedback control circuits would operate to prevent all signals unlike $r(t)$ from existing at the array output. In a communication system application, a suitable reference signal cannot normally be generated within the adaptive array on an autonomous basis since the desired signal is modulated by an unknown data stream. However, it has been shown that the array output signal can be temporally processed to generate an adequate reference signal if a pseudo-noise (PN) coded (spread spectrum) desired signal is to be received provided (1) the spectrum of the data-carrying desired signal is spread by a factor of approximately eight or more, (2) the spectrum spreading code can be generated autonomously within the adaptive array, and (3) proper synchronization between the time bases of the received desired signal and a clock signal generated within the adaptive array can be maintained. A suitable reference waveform generator can be implemented as shown in Figure 3. As is well known, the desired-signal to interfering-signal power ratio associated with the signal present at the output of the bandpass filter in a processor configured as shown in Figure 3 will be larger than the desired-signal to interfering-signal power ratio associated with the signal present at the processor's input (provided the conditions delineated above are satisfied). The factor by which the desired-signal to interfering-signal ratio is increased is normally designated as the (waveform) processing gain and is nominally equal to the rate at which the spectrum spreading code is generated divided by the bandwidth of the bandpass filter. Since any practical filter introduces a non-zero envelope delay, the phase of the reference signal generated will be incorrect following transitions in the desired signal's phase resulting from the impression of data on the coded carrier until the phase transitions have "propagated-through" the filter. The control loops can be prevented from responding improperly during the intervals of time when the phase of the reference signal is incorrect by forcing the error signal to zero or holding the weights constant during an appropriate portion of each signaling (bit) interval. This approach is practical provided the filter parameters are specified so that the phase-transition lag time does not exceed approximately one-third of the data bit duration. A lag time approximately equal to one-fourth of the data bit duration results when a double-tuned circuit having a 3 dB bandwidth approximately equal to three

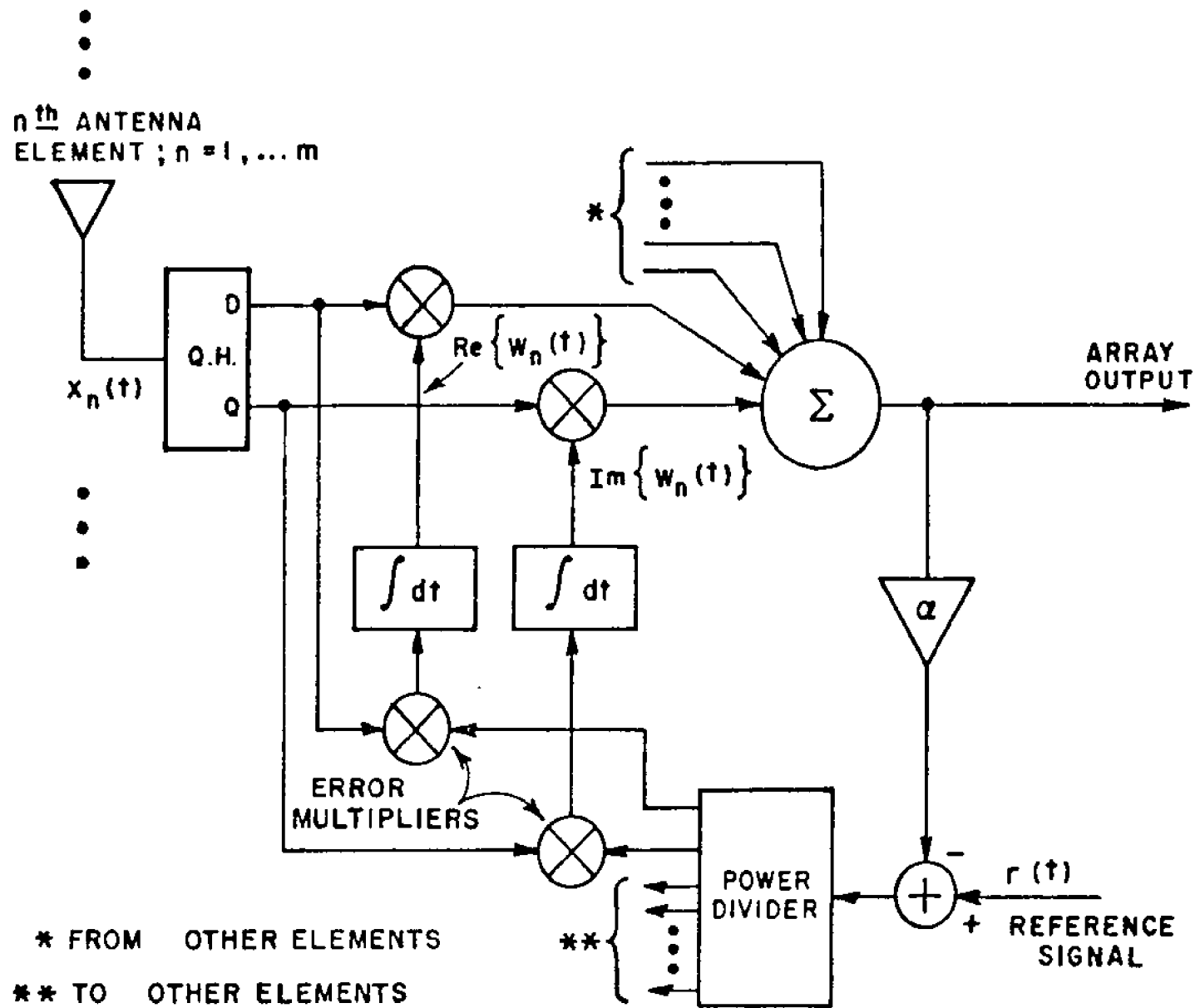


Figure 2. Functional diagram of the previous ASP.

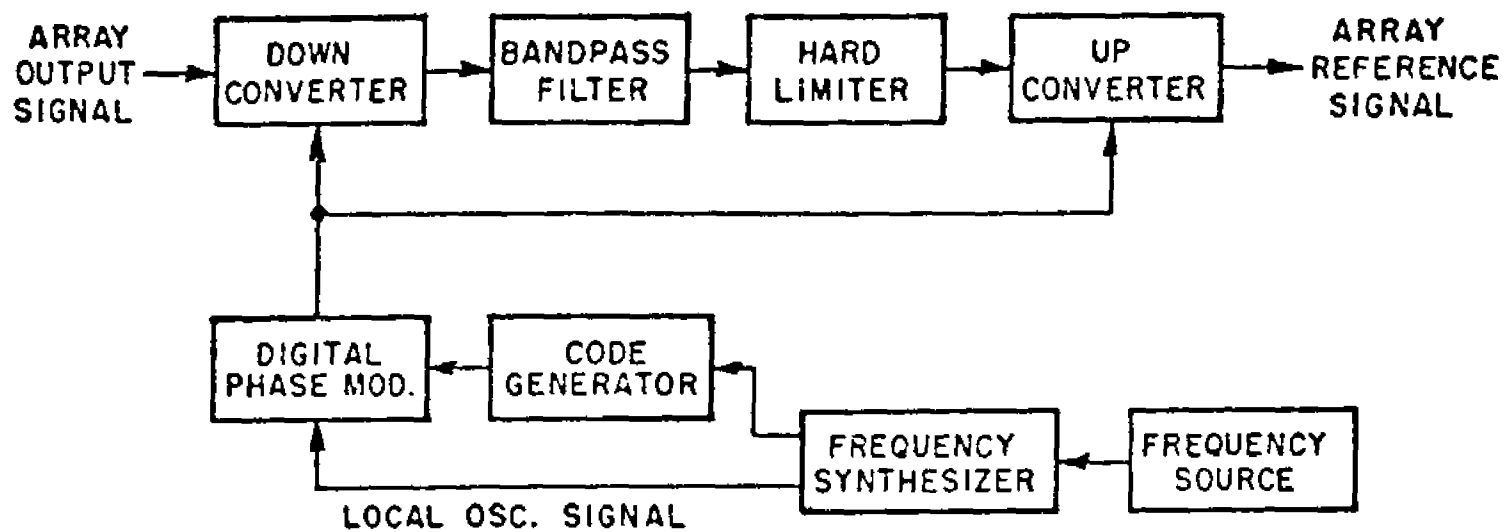


Figure 3. Block diagram of the reference waveform generator.

times the data rate is utilized to implement the filter.* Note that the amplitude of the array reference signal is maintained at a preferred value by a suitable limiter circuit (see Figure 3).

An experimental four-channel 30 MHz IF ASP and a reference waveform generator configured in accord with Figures 2 and 3, respectively, were implemented previously and operated in conjunction with a differential detector [14, 15]. It was shown that a spectrum spreading factor of only ten is adequate to result in interference suppression capabilities which do not differ significantly from the capabilities provided when an ideal reference signal is utilized. Overall, the implementation of practical ASPs which provide very significant interference suppression capabilities was shown to be feasible. A spatial processing gain of 65 dB resulted when each of the four signals applied to the ASP consisted of a desired signal, a thermal noise signal containing approximately the same power as the desired signal, and a c.w. interfering signal having an amplitude 25 dB larger than the desired signal's amplitude. Circuit limitations precluded increasing the interference-to-signal ratio above 25 dB. Intolerable intermodulation resulted when the amplitude of the interfering signal was excessively large. At the other extreme, the amplitude of the desired signal was not reducible below a minimum value due to non-ideal offset voltage characteristics of the circuits utilized to multiply the input signals by the error signal. Four-quadrant transconductance multipliers were employed which were implemented with wideband analog integrated circuits (CA3049s). No alternative approach to implementing four-quadrant multipliers having adequate bandwidths was identified. Since a reasonable attempt was made to optimize the multiplier design, it was concluded that an ASP capable of accommodating an interference-to-signal ratio greater than 25 dB would best be configured so that the utilization of four-quadrant multipliers would not be required.

Although perhaps not obvious, it has been shown that the LMS algorithm is implemented by an ASP configured as shown in Figure 4 if the IF amplifiers following the input signal by (down-converted) error signal multipliers have suitably large bandwidths. Only one wideband quadrature hybrid and m four-quadrant multipliers are required to implement this latter configuration, where m represents the number of signals processed. In contrast, m wideband quadrature hybrids and $2m$ four-quadrant multipliers are required to implement the former configuration. More importantly,

*The utilization of a multiple-pole (sharp cutoff) filter having a bandwidth only moderately larger than the data rate would maximize the processing gain. However, the phase-transition lag time would be unacceptably large if such a filter were to be employed.

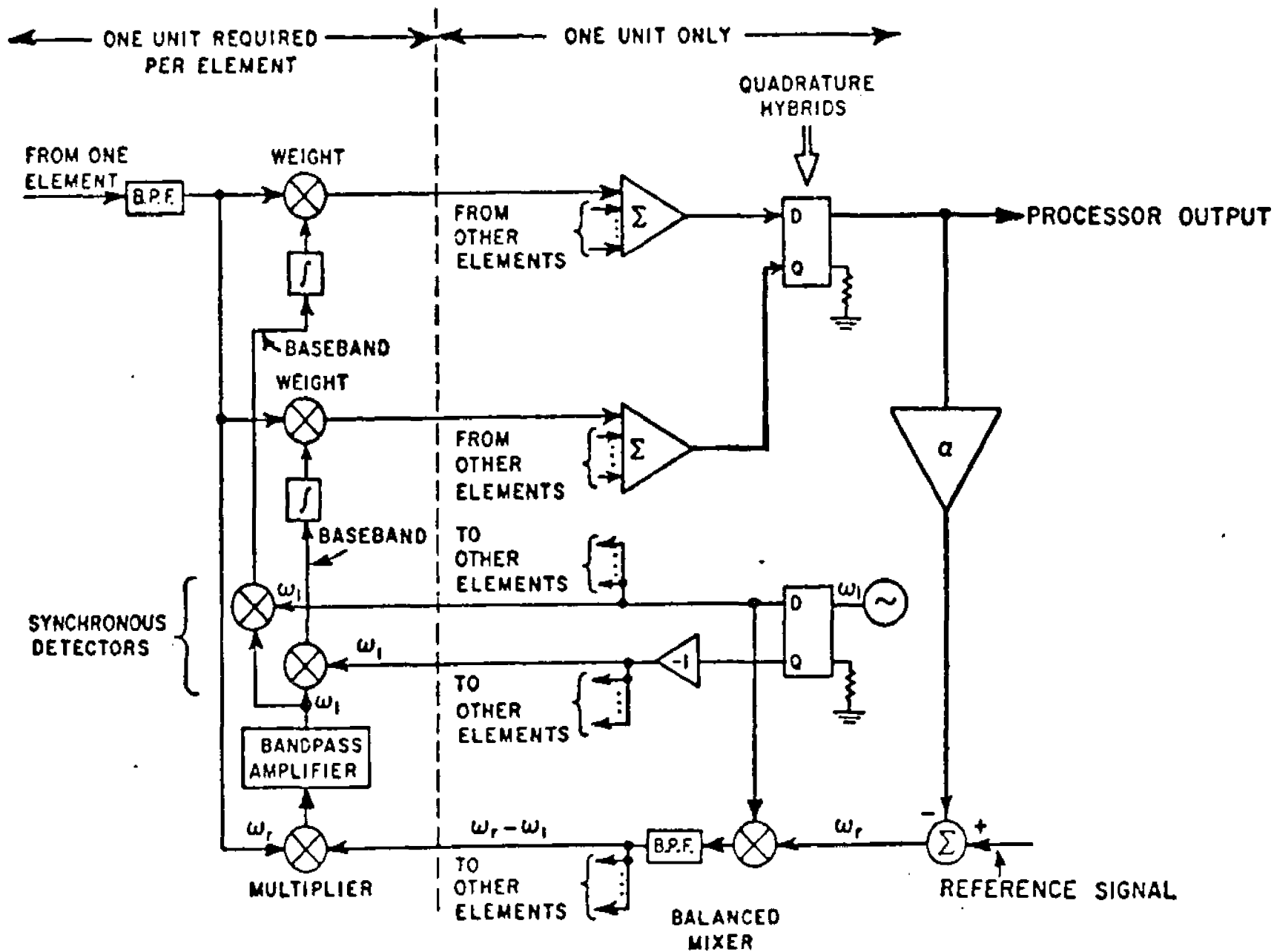


Figure 4. Functional diagram of the present ASP.

offset voltages generated by the m input signal by down-converted error signal multipliers do not affect the dynamic range of the control loops since the product components of interest are IF signals. These IF signals are transformed into in-phase and quadrature weights, respectively. Of course, offset voltages will still exist at the inputs of the integrators. However, the baseband signals can readily be generated by passive mixers which each have a constant envelope, narrowband, high-level signal applied at one input port and, under steady-state conditions, a low-level signal at the other input port. Consequently, the offset voltages at the integrator inputs can be maintained at small values. A high loop gain can readily be achieved without imposing an unreasonable dynamic range requirement on the four-quadrant multipliers by suitably amplifying the IF product signals. These considerations are discussed in greater detail in section VI C.

The ASP in the experimental TDMA/adaptive array system is configured in accord with Figure 4; the reference signal applied to the ASP is generated by a reference waveform generator configured essentially in accord with Figure 3. Four PN codes are generated autonomously within the satellite, i.e., in synchronism with a free-running "clock." These codes are identical in structure to four codes which are generated with each TDMA modem. One pair of codes or one code from that pair is utilized to generate either a quadrature or biphase coded LO signal in the reference waveform generator, depending on the position of a $2\phi/4\phi$ switch. When comparable switches in TDMA modems are appropriately positioned, the coded LO signal and coded carrier signals generated within the TDMA modems are identically modulated. Similarly, a second pair of codes or one code from the pair is employed to generate a network clock signal (NCS) which is identical to the NCS transmitted by a TDMA modem when the modems are not being operated in conjunction with the adaptive array. Generating the NCS and the coded LO signal synchronously within the satellite results in the signals transmitted by the TDMA modems arriving at the satellite in synchronism with the coded LO signal.

As previously noted, the spectra of all overhead signals transmitted by the modems are always spread by a factor of sixteen. The spectra of the data carrying signals are also spread by a factor of sixteen except when the modems are configured to establish the LRF and 64 data symbols are being conveyed in each data slot. The spectra of signals which convey 64 bits in a slot are spread by a factor of two. Since a spectrum spreading factor of two is not adequate to permit a suitable reference signal to be generated, the reference waveform generator has been implemented so that only signals having spectra spread by a factor of sixteen can be accommodated. Thus, when the TDMA modems are being operated in conjunction with the satellite, the data channel assignments utilized must be selected so that eight data bits are transmitted in each data slot.

It is well-known that the transient response of the LMS algorithm is dependent on the signal environment and on the circuit gains used in the feedback loop. In the remainder of this report, techniques for maximizing the convergence rate of the LMS algorithm are evaluated. The scope of the analysis presented in Chapter IV extends beyond the specific implementation discussed in this section so that alternative approaches for structuring the LMS algorithm could be examined. The analytical models presume that an ideal reference signal is available at the adaptive array. As previously discussed, this is a good approximation in the experimental system provided the signals are appropriately synchronized. The ability of the SDDL to acquire and maintain synchronization in a jointly operational TDMA/adaptive array system is evaluated experimentally in Chapter VI. Two methods for inserting desired signal information into the LMS feedback loop are addressed in the analysis. In one method, the ideal reference signal is inserted into the feedback loop as in Figure 4. The second method uses the desired signal direction of arrival to provide desired signal discrimination. The latter method may appear inappropriate insofar as the ASP implementation previously described is concerned, since the desired signal direction of arrival and the reference signal are initially unknown. However, as presently implemented, each pulsed desired signal is preceded by a preamble interval during which only the PN code is transmitted* (i.e., no data are transmitted). Since this code is presumed known at the adaptive array, an ideal reference signal can be generated autonomously within the ASP during the preamble. It is thus possible to estimate the desired signal direction of arrival during this interval, as will be shown. It is also possible to use an ideal reference signal during the preamble when the LMS algorithm is structured as in Figures 2 or 4. Finally, a weight management subsystem wherein the weights are sampled, stored, and "recalled" is no longer necessary to obtain acceptable system performance, since an adequate (array) output signal-to-noise ratio can be obtained prior to data detection by adapting during the preamble interval. For this reason and the fact that a significant reduction in circuit complexity/cost could be obtained, the weight management subsystem was omitted from the experimental TDMA/adaptive array system. The prototype TDMA/adaptive array has been designed so that each preamble transmitted by a TDMA modem need only span one time-slot. The experimental TDMA/adaptive array system is described in greater detail in Chapter VI and in [20].

The analytical results presented in Chapter IV establish a basis for designing an adaptive array which responds rapidly to changing signal environments. It is shown that the rate of response is related to the input signal bandwidth and is limited

*This requires a minor modification in the TDMA modems.

by the level of control loop noise which can be tolerated. The effects of control loop noise on the performance of phase detectors is also investigated. When applicable, these results are compared to the experimental results in Chapter VI. For the purposes of comparison, the transient response of the direct computation methods are examined analytically and numerically in Chapter V. A technique for estimating the desired signal direction of arrival is also presented.

CHAPTER III

MATHEMATICAL MODEL

A. Introduction

This chapter provides the necessary mathematical background and definitions required in subsequent chapters. A description of an assumed antenna array geometry and signal structure is given. A spatial filter which linearly combines the received signal in each antenna element to achieve an optimum signal-to-noise ratio is derived. The performance of this filter is then compared to the performance of filters developed under other performance criteria assuming narrowband signals. The method employed to distinguish the input signal from noise is described in the last section.

B. Signal Structure and Array Geometry

The assumed array geometry is illustrated in Figure 5. It consists of m sensors (or elements) positioned in a three-dimensional coordinate frame which has its origin near the array phase center. The position of the k th antenna element ($k = 1, 2, \dots, m$) with respect to the origin is specified by the vector d_k and is assumed known. The signal environment is assumed to consist of p signals which are assumed to propagate towards the antennas in a non-dispersive homogeneous medium with propagation velocity v . Unless otherwise noted, the angle-of-arrival of the i th signal, which is denoted by the unit vector a_i ($i = 1, 2, \dots, p$) is assumed constant. The signal emitted from the first source ($i=1$) is defined as the desired signal (DS), while the signals from the other $p-1$ sources are defined as interfering signals. To emphasize the relationship between the signal environment and adaptive array performance, the output of each element is modeled as a time delayed version of signals arriving at the origin of coordinates plus internally generated thermal noise. The effects of non-ideal antenna elements will not be addressed; however, these effects can be included in any results presented by an appropriate transformation of the input signal waveforms.

The i^{th} signal at the coordinate origin may be represented, in general, by an amplitude and phase modulated carrier of the form

$$\epsilon_i(t) = \alpha_i(t) \cos(\omega_c t + \phi_i(t) + \theta_i) \quad i = 1, 2, \dots, p \quad (1)$$

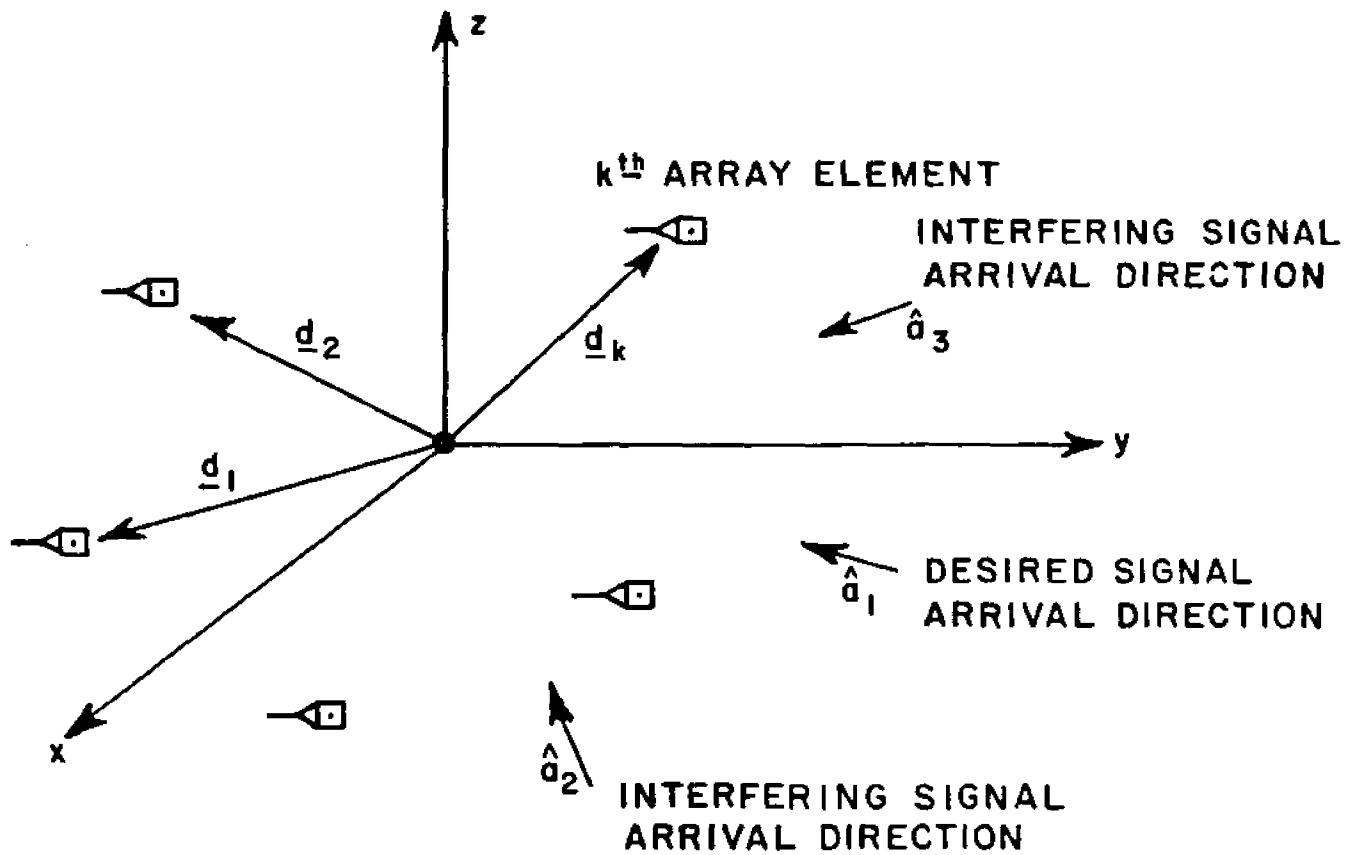


Figure 5--Array geometry and signal environment.

where ω_c represents the carrier frequency in radians, $\phi_i(t)$ and $\alpha_i(t)$ represent the phase and amplitude modulations, and θ_i represents an initial (constant) phase angle. The spectrum of $\xi_i(t)$ is assumed bandlimited to $0 < \omega < 2\omega_c$. Whenever possible, signals will be expressed in their complex envelope representation to simplify the notation. Denoting the complex envelope of $\xi_i(t)$ by $\tilde{\xi}_i(t)$, it follows that

$$\tilde{\xi}_i(t) = \frac{\alpha_i(t)}{\sqrt{2}} \exp [j (\phi_i(t)) + \theta_i] \quad ; \quad i = 1, 2, \dots p. \quad (2)$$

Similarly, thermal noise generated in the k^{th} element can be expressed in the form

$$\delta_k(t) = \beta_k(t) \cos (\omega_c t + \psi_k(t)) \quad . \quad (3)$$

The associated complex envelope representation is

$$\tilde{\delta}_k(t) = \frac{\rho_k(t)}{2} \exp(j \psi_k(t)) \quad ; \quad k = 1, 2, \dots, n \quad (4)$$

where $\beta_k(t)$ and $\psi_k(t)$ represent amplitude and phase, respectively.

For the purposes of analysis in later chapters, interfering signals and element thermal noise will be modeled as sample functions from stationary, zero-mean random processes. Thermal noise will be assumed uncorrelated between elements. Further, these processes are assumed partially characterized by the following ensemble averages:

$$E[\tilde{\xi}_i(t) \tilde{\xi}_j^*(t - \tau)] = \begin{cases} P_i R_i(\tau) & i = j \\ 0 & i \neq j \end{cases} \quad i, j = 2, 3, \dots, p \quad (5)$$

$$E[\tilde{\delta}_k \tilde{\delta}_\ell^*(t - \tau)] = \begin{cases} \sigma^2 R_\sigma(\tau) & k = \ell \\ 0 & k \neq \ell \end{cases} \quad k, \ell = 1, 2, \dots, m \quad (6)$$

where $R_i(0) = 1$
 $R_\sigma(0) = 1$

and P_i and σ^2 represent per-element input powers associated with the i th source and thermal noise, respectively. It can be shown that the corresponding cross-correlation functions of the real input signals (Equations (1) and (3)) are related to Equations (5) and (6) by

$$E[\xi_i(t) \xi_j(t - \tau)] = \text{Re} \left\{ e^{j\omega_c \tau} E[\tilde{\xi}_i(t) \tilde{\xi}_j^*(t - \tau)] \right\} \quad (7)$$

An arbitrary stationary process $\xi_i(t)$ with zero mean can be written in the form [21]

$$\xi_i(t) = a_i(t) \cos \omega_c t + b_i(t) \sin \omega_c t \quad (8)$$

where $a_i(t)$ and $b_i(t)$ are real processes. Since $\xi_i(t)$ is assumed a stationary, zero-mean process, it follows that $a_i(t)$ and $b_i(t)$

are also stationary, zero-mean processes. If the spectral density of $\xi_i(t)$ is an even function about the carrier frequency, then its complex envelope can be shown to have the following properties [21]:

$$\begin{aligned} P_i^* R_i(\tau) &= E[a(t)a(t - \tau)] \\ &= E[b(t)b(t - \tau)] \\ &= R_{aa}(\tau) \end{aligned} \tag{9}$$

and

$$E[\tilde{\xi}_i(t) \tilde{\xi}_i(t - \tau)] = 0 \tag{10}$$

which implies that $R_i(\tau)$ is real and that the in-phase and quadrature components of the signal $\xi_i(t)$ are uncorrelated. In addition, if $\tilde{\xi}_i(t)$ is modeled as a sample function from a zero-mean Gaussian process (and Equations (9) and (10) are satisfied), then a moment theorem for complex Gaussian processes, derived by Reed [22], can be applied. As a consequence of this theorem,

$$\begin{aligned} (a) \quad E[Z_1^* Z_2^* Z_3] &= 0 \\ (b) \quad E[Z_1^* Z_2^* Z_3 Z_4] &= E[Z_1^* Z_3] E[Z_2^* Z_4] + E[Z_2^* Z_3] E[Z_1^* Z_4] \end{aligned} \tag{11}$$

where Z_i ($i = 1, 2, 3, 4$) represents a sample $Z(t_i)$ of the Gaussian, zero-mean process $Z(t)$. The properties of narrowband complex Gaussian processes given in Equations (9)-(11) will be employed in Chapters IV and V.

With the exception of a portion of the analysis presented in Chapter V, the desired signal is assumed to be biphasic (or quadrature) modulated with PN code(s) in order to obtain results applicable to the TDMA signals. When biphasic data are to be conveyed, they are added modulo-two with the PN code(s) prior to modulation. The ratio of the code rate to the data rate, denoted as the spectrum-spreading-ratio, is assumed to have an integer value greater than or equal to one.

The desired signal (DS) is to be distinguished from all other signals present at the array input and thus will be designated by

special notation. The DS, observed from the origin of the coordinate frame in Figure 5, is defined by

$$\tilde{s}(t) = \tilde{\xi}_1(t) \quad . \quad (12)$$

Under the biphase (or quadrature) assumption, the DS has a constant envelope, as opposed to the random envelopes assumed for interference and thermal noise. That is,

$$P'_s \equiv P'_1 = E[\tilde{s}(t) \tilde{s}^*(t)] = \tilde{s}(t) \tilde{s}^*(t) \quad (13)$$

where P'_s represents the per-element input desired signal power. Except in Chapter V, $s(t)$ is assumed to be a deterministic signal.

The arrival of the i^{th} signal at the output of the k^{th} element, $\tilde{\xi}_{ik}(t)$, is delayed τ_{ik} seconds with respect to the coordinate origin, where*

$$\tau_{ik} = \frac{\langle \underline{a}_i, \underline{d}_k \rangle}{v} \quad . \quad (14)$$

Thus,

$$\begin{aligned} \tilde{\xi}_{ik}(t) &= \tilde{\xi}_i(t - \tau_{ik}) \exp[-j\omega_c \tau_{ik}] & i = 1, 2, \dots, p \quad . \\ & & k = 1, 2, \dots, m \quad (15) \end{aligned}$$

All signals present at the array input will be assumed narrowband with respect to the array bandwidth; that is, the maximum differential delay between elements is assumed much smaller than the reciprocal of the array bandwidth. In this case, the effects of envelope delay in Equation (15) can be neglected, permitting the approximation

$$\tilde{\xi}_i(t - \tau_{ik}) = \tilde{\xi}_i(t) \quad . \quad (16)$$

The output $\tilde{x}_k(t)$ of the k^{th} antenna element is composed of the sum of all delayed directional sources plus thermal noise:

* $\langle \underline{x}, \underline{y} \rangle$ denotes the inner product of the m -dimensional vectors \underline{x} and \underline{y} .

$$\tilde{x}_k(t) = \tilde{s}(t) \exp [-j \omega_c \tau_{ik}] \quad (17)$$

$$+ \sum_{i=2}^P \tilde{\xi}_i(t) \exp [-j \omega_c \tau_{ik}] + \tilde{\delta}_k(t) \quad ; k = 1, 2, \dots, m$$

For notational convenience, the outputs of the m antenna elements at time t will be written as the m -dimensional complex-type vector

$$\underline{\tilde{x}}(t) = \begin{bmatrix} \tilde{x}_1(t) \\ \tilde{x}_2(t) \\ \vdots \\ \tilde{x}_m(t) \end{bmatrix} \quad (18)$$

The m -dimensional vector defined by

$$\underline{v}_i = \begin{bmatrix} e^{-j \omega_c \tau_{i1}} \\ e^{-j \omega_c \tau_{i2}} \\ \vdots \\ e^{-j \omega_c \tau_{im}} \end{bmatrix} \quad ; i = 1, 2, \dots, m \quad (19)$$

is a vector directed along the DOA of the i^{th} directional source and will be denoted as the direction-delay vector associated with that signal. The instantaneous input desired signal vector, $\underline{\tilde{s}}(t)$, and the instantaneous input noise vector, $\underline{\tilde{u}}(t)$, are defined in terms of \underline{v}_i as

$$(a) \quad \underline{\tilde{s}}(t) = \tilde{s}(t) \underline{v}_1 \quad (20)$$

$$(b) \quad \underline{\tilde{u}}(t) = \sum_{i=2}^P \tilde{\xi}_i(t) \underline{v}_i + \tilde{\delta}(t)$$

where

$$\underline{\tilde{\delta}}(t) = \begin{bmatrix} \delta_1(t) \\ \delta_2(t) \\ \vdots \\ \delta_m(t) \end{bmatrix}$$

represents the input thermal noise vector. That the input desired signal and noise vectors could be written as in Equation (20) is a consequence of assumptions regarding the antenna elements. For non-isotropic and non-identical array elements, the only modification required in Equation (20) is to multiply the k^{th} component of each vector \underline{v}_i ($i = 1, 2, \dots, p$) by a complex scalar $f_k(\underline{v}_i)$ ($k = 1, 2, \dots, n$) which is functionally dependent upon the arrival direction a_i of the i^{th} signal. Other effects such as mutual coupling and aperture blockage, which alter the relative phases of each $\delta_i(t)\underline{v}_i$ in Equation (20), may also be included in modeling the received signal structure, although the modifications to Equation (20) would generally be more involved.

From Equations (17)-(20), the output of the m antenna elements may be expressed as

$$\underline{\tilde{x}}(t) = \underline{\tilde{s}}(t) + \underline{\tilde{u}}(t) \quad . \quad (21)$$

The covariance matrices associated with each of these three input vectors may be determined as follows:*

$$\begin{aligned} K_x &\equiv E\{ \underline{\tilde{x}}(t) \underline{\tilde{x}}^\dagger(t - \tau) \} \Big|_{\tau=0} & (22) \\ &= E\{ [\underline{\tilde{s}}(t) + \underline{\tilde{u}}(t)] [\underline{\tilde{s}}(t) + \underline{\tilde{u}}(t)]^\dagger \} \\ &= \underline{s} \underline{s}^\dagger + M \end{aligned}$$

where

*The symbol \dagger denotes the complex conjugate transpose of a matrix or vector, and the complex conjugate of a scalar.

$$M \equiv E[\underline{\hat{u}}(t)\underline{\hat{u}}^{\dagger}(t)] = \sum_{i=2}^m P_i \underline{v}_i \underline{v}_i^{\dagger} + \sigma^2 I$$

$$\underline{s} \equiv \sqrt{P_s} \underline{v}_1$$

The $m \times m$ matrices K_X and M , which represent the input covariance and noise covariance matrices, respectively, are positive definite and Hermitian. It, therefore, follows that (1) their inverses exist and (2) each can be transformed by a unitary transformation into a diagonal matrix with real elements. The unitary transformation and diagonal matrix associated with K_X will be denoted by the $m \times m$ matrices P and Λ , respectively. Thus,

$$PK_X P^{-1} = \Lambda \tag{23}$$

where $PP^{-1} = PP^{\dagger} = I$

and

$$\Lambda = \begin{bmatrix} \lambda_1 & 0 & 0 & \cdots & 0 \\ 0 & \lambda_2 & 0 & \cdots & 0 \\ 0 & 0 & \lambda_3 & \cdots & 0 \\ \vdots & & & & \vdots \\ 0 & 0 & 0 & & \lambda_m \end{bmatrix}$$

The elements of Λ are the eigenvalues of K_X . Since K_X is positive definite,

$$\lambda_k > 0 \quad ; \quad k = 1, 2, \dots, m \tag{24}$$

Several additional definitions will be required in later chapters. The total input power, input desired signal power, and input noise power will be denoted by P_I , P_S , and P_N , respectively. They are related to other system parameters as follows:*

* $TR(K_X)$ denotes the trace of the matrix K_X .

$$P_S = E\{\underline{s}^\dagger(t)\underline{\tilde{s}}(t)\} = \underline{s}^\dagger \underline{s} = mP'_S \quad (25)$$

$$P_N = E\{\underline{u}^\dagger(t)\underline{\tilde{u}}(t)\} = \text{TR}(M) = m \sum_{i=2}^P P'_i$$

$$P_I = E\{\underline{x}^\dagger(t)\underline{\tilde{x}}(t)\} = \text{TR}(K_X) = \sum_{k=1}^m \lambda_k = P_S + P_N$$

C. Optimum Spatial Filtering in a Narrowband Environment

The antenna element outputs are correlated since each contains delayed versions of the p received signals (see Equation (17)). It is this property which permits partial cancellation of undesired signals without cancelling a desired signal coming from a different direction, i.e., a spatial processor can be implemented by applying the sensor outputs to an appropriate combining network (spatial filter). The purpose of this section is to derive a spatial filter which processes the sensor outputs to maximize the desired signal and minimize undesired signals at its output. The input signals will be assumed stationary and narrowband with respect to the array bandwidth.

The proposed spatial filter, linearly combines (or weights) the outputs of each element, $\tilde{x}_k(t)$, to generate a scalar output $\tilde{y}(t)$. That is,

$$\tilde{y}(t) = w_1^* \tilde{x}_1(t) + w_2^* \tilde{x}_2(t) + \dots + w_m^* \tilde{x}_m(t) \quad (26)$$

The weights w_k are complex to convey phase as well as amplitude control. When w_k is viewed as the k th component of the m -dimensional weight vector* \underline{w} , Equation (26) becomes

$$\tilde{y}(t) = \underline{w}^\dagger \underline{x}(t) = \underline{w}^\dagger \underline{s}(t) + \underline{w}^\dagger \underline{u}(t) \quad (27)$$

*For notational convenience, the vectors \underline{w} and \underline{R}_{Xd} (defined later) will be written as w and R_{Xd} , respectively. When either of these vectors is written with a subscript, e.g., w_i , it will denote the i th component of that vector.

The spatial filter w which optimizes the output signal-to-noise ratio will first be determined.

The total power at the output of the spatial filter is defined as

$$\begin{aligned} P_T &\equiv E[\tilde{Y}^+(t) \tilde{Y}(t)] \\ &= E \{ [w^\dagger \underline{\tilde{s}}(t) + w^\dagger \underline{\tilde{u}}(t)] [\underline{\tilde{s}}^+(t)w + \underline{\tilde{u}}^+(t)w] \} \end{aligned} \quad (28)$$

If the weight vector is fixed at some arbitrary value, then Equation (28) reduces to

$$P_T = w^\dagger \underline{s} \underline{s}^\dagger w + w^\dagger M w = S_0 + N_0 \quad (29)$$

where

$$S_0 \equiv E[w^\dagger \underline{\tilde{s}}(t) \underline{\tilde{s}}^+(t) w]$$

and

$$N_0 \equiv E[w^\dagger \underline{\tilde{u}}(t) \underline{\tilde{u}}^+(t) w]$$

The parameters S_0 and N_0 defined above represent the output desired signal and output noise powers, respectively. Thus, the output signal-to-noise ratio $[(S/N)_0]$, given w , may be expressed as

$$\left(\frac{S}{N}\right)_0 = \frac{S_0}{N_0} = \frac{w^\dagger \underline{s} \underline{s}^\dagger w}{w^\dagger M w} \quad (30)$$

A least upper bound (LUB) for this ratio will be determined as a function of w assuming a fixed signal environment. The LUB will be denoted as the optimum output signal-to-noise ratio, and the filter w which achieves this optimum will be denoted the optimum weight vector (usually w_{opt}).

The maximum value of Equation (30), for a given signal environment, will be evaluated by following the procedure introduced by Reed, et al. [6]. First, an upper bound on Equation (30) will be derived, then a filter w_{opt} which achieves this bound will be given. Define the operator

$$(X, Y) = X^\dagger M Y$$

where M is the $m \times m$ noise covariance matrix and X and Y are arbitrary m -component complex vectors. Since M is positive definite Hermitian, it is easy to show that the above-defined operator satisfies the axioms of a complex-type scalar product [23]. In terms of this scalar product, Equation (30) becomes

$$\left(\frac{S}{N}\right)_0 = \frac{(w, M^{-1}\underline{s}) (M^{-1}\underline{s}, w)}{(w, w)} \quad (31)$$

By the Schwartz inequality

$$(X, Y)^2 \leq (X, X) (Y, Y) \quad . \quad (32)$$

Thus, Eq. (31) is bounded above by

$$\left(\frac{S}{N}\right)_0 \leq \frac{(w, w) (M^{-1}\underline{s}, M^{-1}\underline{s})}{(w, w)} = (M^{-1}\underline{s}, M^{-1}\underline{s}) = \underline{s}^+ M^{-1} \underline{s} \quad . \quad (33)$$

This upper bound is independent of w and therefore holds for all complex vectors w . If a vector w can be found such that

$$\left(\frac{S}{N}\right)_0 = \underline{s}^+ M^{-1} \underline{s} \equiv T_0 \quad (35)$$

then $\underline{s}^+ M^{-1} \underline{s}$ is the LUB and the vector w is optimum. One such solution for w , is given by

$$w = w_{opt} = \beta_1 M^{-1} \underline{s} \quad (36)$$

where β_1 is an arbitrary (non-zero) complex-type scalar. Substituting Equation (36) into Equation (30), one obtains

$$\begin{aligned}
\left(\frac{S}{N}\right)_0 &= \frac{\underline{w}^\dagger \underline{s} \underline{s}^\dagger \underline{w}}{\underline{w}^\dagger \underline{M} \underline{w}} & (37) \\
&= \frac{|\beta_1|^2 \underline{s}^\dagger \underline{M}^{-1} \underline{s} \underline{s}^\dagger \underline{M}^{-1} \underline{s}}{|\beta_1|^2 \underline{s}^\dagger \underline{M}^{-1} \underline{s}} \\
&= \underline{s}^\dagger \underline{M}^{-1} \underline{s} \equiv T_0
\end{aligned}$$

where T_0 is defined as the optimum output signal-to-noise ratio for a given stationary signal environment; w_{opt} is the filter which achieves this optimum.

The fact that neither the amplitude nor phase of w_{opt} affects $(S/N)_0$ is both obvious and significant, e.g., neither the amplitude nor phase of $\underline{s}(t)$ are required in determining w_{opt} . The advantage of this manifests itself not only in estimating the desired signal DOA, but also in estimating M , as should become apparent in subsequent chapters.

Next, consider a weight vector calculated from the inverse of the input covariance matrix:

$$w_0 = \beta_2 k_x^{-1} \underline{s} \quad (38)$$

where β_2 is an arbitrary (complex) constant. From Equation (22),

$$w_0 = \beta_2 (M + \underline{s} \underline{s}^\dagger)^{-1} \underline{s} .$$

Using a well-known matrix inversion lemma [24], w_0 reduces to

$$\begin{aligned}
w_0 &= \beta_2 [M^{-1} - M^{-1} \underline{s} (1 + \underline{s} M^{-1} \underline{s})^{-1} \underline{s} M^{-1}] \underline{s} & (39) \\
&= \beta_2 M^{-1} \underline{s} \left(1 - \frac{\underline{s}^\dagger M^{-1} \underline{s}}{1 + \underline{s}^\dagger M^{-1} \underline{s}} \right) \\
&= \beta_2 \left(\frac{1}{1 + \underline{s}^\dagger M^{-1} \underline{s}} \right) M^{-1} \underline{s} \\
&= \frac{\beta_2}{1 + T_0} M^{-1} \underline{s} \\
&= \beta_3 M^{-1} \underline{s}
\end{aligned}$$

where $\beta_3 = \frac{\beta_2}{1 + T_0}$.

Since β_3 is a complex constant, filter w_0 (compare Equation (39) with Equation (36)) also maximizes the output signal-to-noise ratio [25].

The filter $\sqrt{P_s'} k_x^{-1} \underline{s}$ is the well-known Weiner filter, which minimizes the mean-squared error (MSE) between the filter output signal and $s(t)$; that is, it minimizes

$$\begin{aligned}
J_{\text{MSE}} &= E \{ \hat{s}(t) - \tilde{y}(t) \}^2 & (40) \\
&= E \{ (\hat{s}(t) - w^\dagger \underline{\tilde{x}}(t)) (\hat{s}^\dagger(t) - \underline{\tilde{x}}^\dagger(t) w) \}
\end{aligned}$$

By Equations (13) and (22), this reduces to

$$J_{\text{MSE}} = P_s' = 2 \operatorname{Re} \{ \sqrt{P_s'} \underline{s}^\dagger w \} + w^\dagger k_x w \quad . \quad (41)$$

Equation (41) has a unique minimum [1], which occurs for

$$w = w_{\text{MMSE}} = \sqrt{P_s'} k_x^{-1} \underline{s} \quad (42)$$

for which the minimum mean-square error becomes

$$\begin{aligned}
 J_{\text{MMSE}} &= P'_S (1 - \underline{s}^+ k_x^{-1} \underline{s}) \\
 &= P'_S \left[1 - \frac{T_o}{1 + T_o} \right] \\
 &= \frac{P'_S}{1 + T_o}
 \end{aligned} \tag{43}$$

The MMSE between the desired signal and the Wiener filter output, normalized to the per-element input desired signal power, is a function of the optimum output signal-to-noise ratio (SNR); as expected, $(J_{\text{MMSE}}) (P'_S)^{-1}$ is smallest when the optimum output SNR is high. The weight vectors w_{opt} and w_{MMSE} maximize $(S/N)_o$ in stationary signal environment consisting of narrowband (with respect to the array bandwidth) uncorrelated signals. Baird and Zahm [1] show this is also true for filters which are based on the maximum likelihood criterion. Since these filters yield the same output SNR, the output SNR will be used to measure performance. This measure will be useful when undesired signals and thermal noise approximate Gaussian processes, since maximizing the SNR also optimizes the probability of detection.

D. The Reference Signal

In the preceding section, it was found that filters which optimize the output SNR are completely determined by the covariance matrix K_x (or M) and by the desired signal DOA vector $\beta \underline{s}$, where β represents an arbitrary complex-type constant. In the application under investigation, highly mobile terminals are to be contained in the TDMA network; thus, it has been presumed that the arrival angles of the desired, time multiplexed signals are not known at the satellite. In order to obtain an estimate of $\beta \underline{s}$, some information must be made available at the array processor to distinguish between desired and undesired signal sources. This information will be assumed to take the form of a locally generated reference signal, $\tilde{r}(t)$, which has the following property:

$$\begin{aligned}
 R_{\text{xd}} &= E [\tilde{\underline{x}}(t) \tilde{r}^+(t)] \\
 &= E \{ [\tilde{\underline{s}}(t) + \tilde{\underline{u}}(t)] \tilde{r}^+(t) \} \\
 &= \tilde{\underline{s}}(t) \tilde{r}^+(t) \\
 &= \beta \underline{s}
 \end{aligned} \tag{44}$$

where R_{xd} is defined as the input cross-correlation vector. Thus, an estimate of β_s is obtained by averaging the input signal vector by reference signal product.

For the purposes of analysis, an ideal reference will be assumed. The ideal assumption is that $\tilde{r}(t)$ is a scaled replica of the desired signal:

$$\tilde{r}(t) = \beta_5 \tilde{s}(t) \quad (45)$$

and $|\tilde{r}|^2 \equiv E[\tilde{r}(t) \tilde{r}^+(t)] = |\beta_5|^2 P'_s$

where $|\tilde{r}|^2$ is a known constant. β_5 is constant for a given desired signal and is a function of the unknown phase and amplitude of $\tilde{s}(t)$. In this case, the cross-correlation vector

$$R_{xd} = \beta_5^* \sqrt{P'_s} \underline{s} = \beta \underline{s} \quad (46)$$

has the magnitude

$$\sqrt{R_{xd}^+ R_{xd}} = |\tilde{r}| \sqrt{P_s} \quad (47)$$

In practice, it is possible to locally generate a (nearly) ideal reference signal if (1) the desired signal contains no data modulation, (2) the time base of the code modulation contained on the desired signal at the array input is aligned with the time base of the processor code to within a few tenths of a code bit (chip) duration, and (3) an accurate estimate of the desired signal carrier frequency is available. These requirements would be satisfied intrinsically by a TDMA system of the type described in Chapter II if (1) the data modulation were to be removed*, (2) a single timing signal were to be employed in the processor to generate both the network clock signal and the processor-generated code, and (3) the offset in frequency between $\tilde{s}(t)$ and $r(t)$ were to be sufficiently small.

*For example, each user could be assigned a preamble interval preceding his data slot during which only the PN code is transmitted.

Of course, it is generally not possible to generate an ideal reference signal when data are to be conveyed. In this case, Reinhard [14] has shown that a reference signal, $r_p(t)$, which satisfies the requirements in Equation (44) can be derived from the array output signal by a processor configured as shown in Figure 3 provided the spectrum-spreading ratio is nominally equal to or greater than eight and the signal-to-noise ratio (of $r_p(t)$) is sufficiently large. The latter requirement is satisfied when the product of the spatial and waveform processing gains exceed the input noise to desired signal power ratio, which is normally the case of interest. When the signal-to-noise ratio of $r_p(t)$ is sufficiently high (approximately 10 dB or higher) and if delays introduced by the waveform processor of Figure 3 are compensated,* then $r_p(t)$ can be approximated by

$$\tilde{r}_p(t) \doteq \beta_6 \frac{w^+ \underline{s}}{\sqrt{w^+ \underline{s} \underline{s}^+ w}} \tilde{s}(t) \quad (48)$$

where

$$\begin{aligned} |\tilde{r}_p|^2 &\equiv E[\tilde{r}(t) \tilde{r}^+(t)] \\ &= |\beta_6|^2 P'_s \end{aligned}$$

Again $|\tilde{r}_p|^2$ is assumed known. If $\beta_5 = \beta_6$, then

$$\tilde{r}_p(t) = \frac{w^+ \underline{s}}{w^+ \underline{s} \underline{s}^+ w} \tilde{r}(t) \quad (49)$$

which shows that $\tilde{r}_p(t)$ approximates $\tilde{r}(t)$ to within a phase factor introduced by the spatial filter w . Near steady-state, this phase factor is essentially constant when the desired signal frequency offset is small [15]. Note that the relative phase angle between the desired signal component of the array output and $r_p(t)$ in Equation (49) is nominally zero, whereas the relative phase can

*The subject of delays introduced by the waveform processor and methods for compensating this delay are addressed in Section VI.B4.

assume an arbitrary value in the range 0° to 360° in the case of an ideal reference signal. For this reason, the transient response of an array processor implemented using a waveform processed reference signal can provide better performance during weight transients compared to case in which a waveform processed reference signal is used (see Section V D).

CHAPTER IV

TRANSIENT RESPONSE OF THE LMS ALGORITHM

A. Introduction

This chapter begins with a brief review of the LMS algorithm weight equation. Two implementations of the weight equation are defined. In the first, weights are updated in a continuous manner according to a differential equation. In the second, weights are updated in discrete steps. Each implementation is then further subdivided by distinguishing between two techniques for inserting a priori desired signal information. Transient and steady-state performance of each of these four cases are analyzed in parts C and D. In part C, a review of the mathematical development pertaining to ideal LMS algorithm response is presented. The ideal assumption is that the weights respond to the average of the instantaneous covariance matrix and/or the average of the instantaneous cross-correlation vector (depending on a priori information assumed). This assumption is shown to be valid when the analog control loop bandwidth is much narrower than the input signal bandwidth, i.e., when the convergence rate is relatively slow. When the loop bandwidth is increased to improve convergence, however, the weights become noisier as they begin to respond to instantaneous signal fluctuations, thus departing from the idealized model. Selection of an optimum loop bandwidth in this case requires a compromise between convergence rate and loop noise. To guide this selection, excess noise at the array output as a function of array parameters is determined for the case of a Gaussian noise environment in part D. In part E, the effects of weight jitter on the output signal phase and on coherent detection are determined when the discrete LMS algorithm is employed.

B. Description of the LMS Algorithm

The analog LMS (ALMS) algorithm is designed to minimize the mean-squared error between the array output and a known reference signal $[r(t)]$ based on a steepest descent minimization procedure. The technique sets the time derivative of the complex weights, $w(t)$, equal to a negative constant times the gradient of the instantaneous mean-square error $[l]$, i.e.,

$$\frac{dw(t)}{dt} = -\beta \nabla_w |\tilde{\epsilon}(t,w)|^2 \quad (50)$$

where

$$\begin{aligned} \tilde{\epsilon}(t,w) &= \hat{r}(t) - \hat{r}(t) \\ &= \hat{r}(t) - w^T(t) \hat{x}(t) \end{aligned} \quad (51)$$

It has been shown elsewhere [1,15] that the vector differential equation for the weights which satisfies Equation (50) is given by

$$\begin{aligned} \frac{dw(t)}{dt} &= 2\beta \tilde{x}(t) \tilde{\epsilon}^*(t) \\ &= \alpha \tilde{x}(t) (\hat{r}^*(t) - \tilde{x}^T(t)w(t)) \\ &= \alpha [\tilde{x}(t)\hat{r}^*(t) - \tilde{x}(t)\tilde{x}^T(t)w(t)] \end{aligned} \quad (52)$$

where the real scalar $\alpha (= 2\beta)$ is defined as the loop gain constant. For an m -element array, this expression represents m coupled differential equations of the form

$$\frac{dw_i(t)}{dt} = \alpha (\tilde{x}_i(t)\hat{r}^*(t) - \tilde{x}_i(t)\tilde{x}_i^T(t)w(t)) ; i = 1, 2, \dots, m \quad (53)$$

Equations (52) and (53) describe the time behavior of the weights for continuous values of t . An algorithm for updating weights in discrete steps can be derived by transforming Equation (52) into the difference equation

$$\frac{w(t_{j+1}) - w(t_j)}{t_{j+1} - t_j} = \alpha (\tilde{x}(t_j)\hat{r}^*(t_j) - \tilde{x}(t_j)\tilde{x}^T(t_j)w(t_j)) ; \quad (54)$$

$$t_j < t_{j+1}$$

where $w(t_{j+1})$ and $w(t_j)$ represent the weights at times t_{j+1} and t_j , respectively, in terms of input data $\hat{r}(t)$ and $\hat{x}(t)$ sampled at time t_j . Equation (54) is referred to as the digital LMS (DLMS) algorithm. As the interval $t_{j+1} - t_j$ approaches zero (for all j), Equations (52) and (54) become identical.

Taking the ensemble average of both sides of Equations (52) and (54) yields

$$\begin{aligned} E \frac{dw(t)}{dt} &= \alpha \{ E[\underline{\tilde{x}}(t)\underline{\tilde{x}}^\dagger(t)] - E[\underline{\tilde{x}}(t)\underline{\tilde{x}}^\dagger(t)w(t)] \} \\ &= \alpha \{ R_{xd} - E[\underline{\tilde{x}}(t)\underline{\tilde{x}}^\dagger(t)w(t)] \} \end{aligned} \quad (55)$$

$$\begin{aligned} E \left[\frac{w(t_{j+1}) - w(t_j)}{t_{j+1} - t_j} \right] &= \alpha \{ E[\underline{\tilde{x}}(t_j)\underline{\tilde{x}}^\dagger(t_j)] - E[\underline{\tilde{x}}(t_j)\underline{\tilde{x}}^\dagger(t_j)w(t_j)] \} \\ &= \alpha \{ R_{xd} - E[\underline{\tilde{x}}(t_j)\underline{\tilde{x}}^\dagger(t_j)w(t_j)] \} \end{aligned} \quad (56)$$

The last step in each of Equations (55) and (56) follows from the assumption that the reference signal is a scaled replica of $\mathfrak{S}(t)$ (see Equation (44)). Equations (55) and (56) motivate the following modifications to Equations (52) and (54):

$$\frac{dw(t)}{dt} = \alpha \{ R_{xd} - \underline{\tilde{x}}(t)\underline{\tilde{x}}^\dagger(t)w(t) \} \quad (57)$$

$$\frac{w(t_{j+1}) - w(t_j)}{t_{j+1} - t_j} = \alpha \{ R_{xd} - \underline{\tilde{x}}(t_j)\underline{\tilde{x}}^\dagger(t_j)w(t_j) \} \quad (58)$$

In Equations (57) and (58), desired signal DOA information is assumed given, whereas in Equations (52) and (54) the reference signal, $r(t)$, is assumed given.

Equations (52), (54), (57), and (58) describe the four basic models of the LMS algorithm considered in this chapter. The analog models, defined by Equations (52) and (57), are illustrated in Fig. 6. To establish a convention for distinguishing between the two analog algorithms, the vector $R_\Delta(t)$ is defined as the difference (at time t) between the (instantaneous) desired signal DOA information inserted into the feedback path and the mean cross-correlation vector. That is (the expression $[0]$ denotes the zero vector),

$$R_\Delta = \underline{\tilde{x}}(t)\underline{\tilde{x}}^\dagger(t) - R_{xd} \quad (59a)$$

or

$$R_\Delta = \hat{R}_{xd} - R_{xd} = [0] \quad (59b)$$

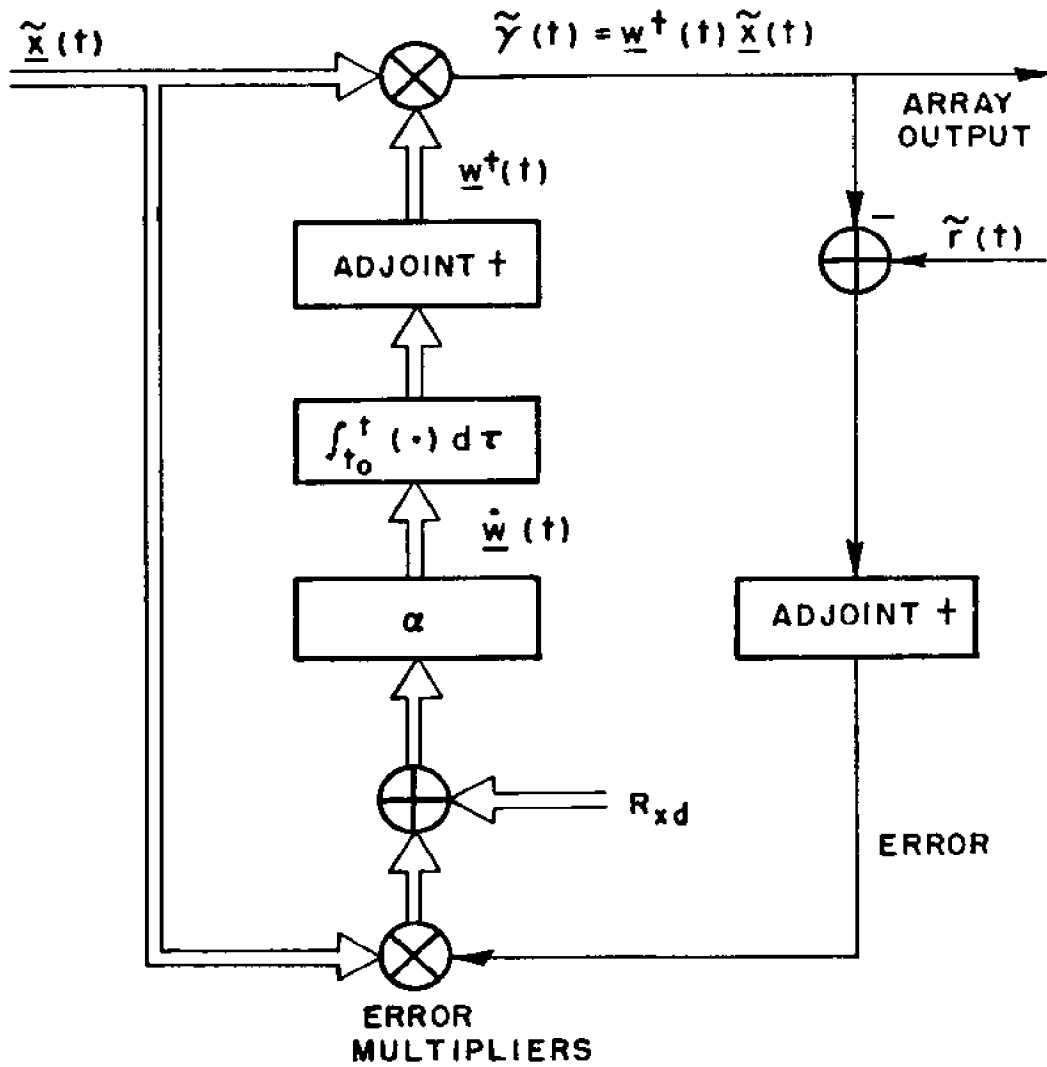


Figure 6--Analog adaptive processor model. In Equation (52), $R_{xd} = [0]$. In Equation (57), $\tilde{\underline{y}}(t) = 0$.

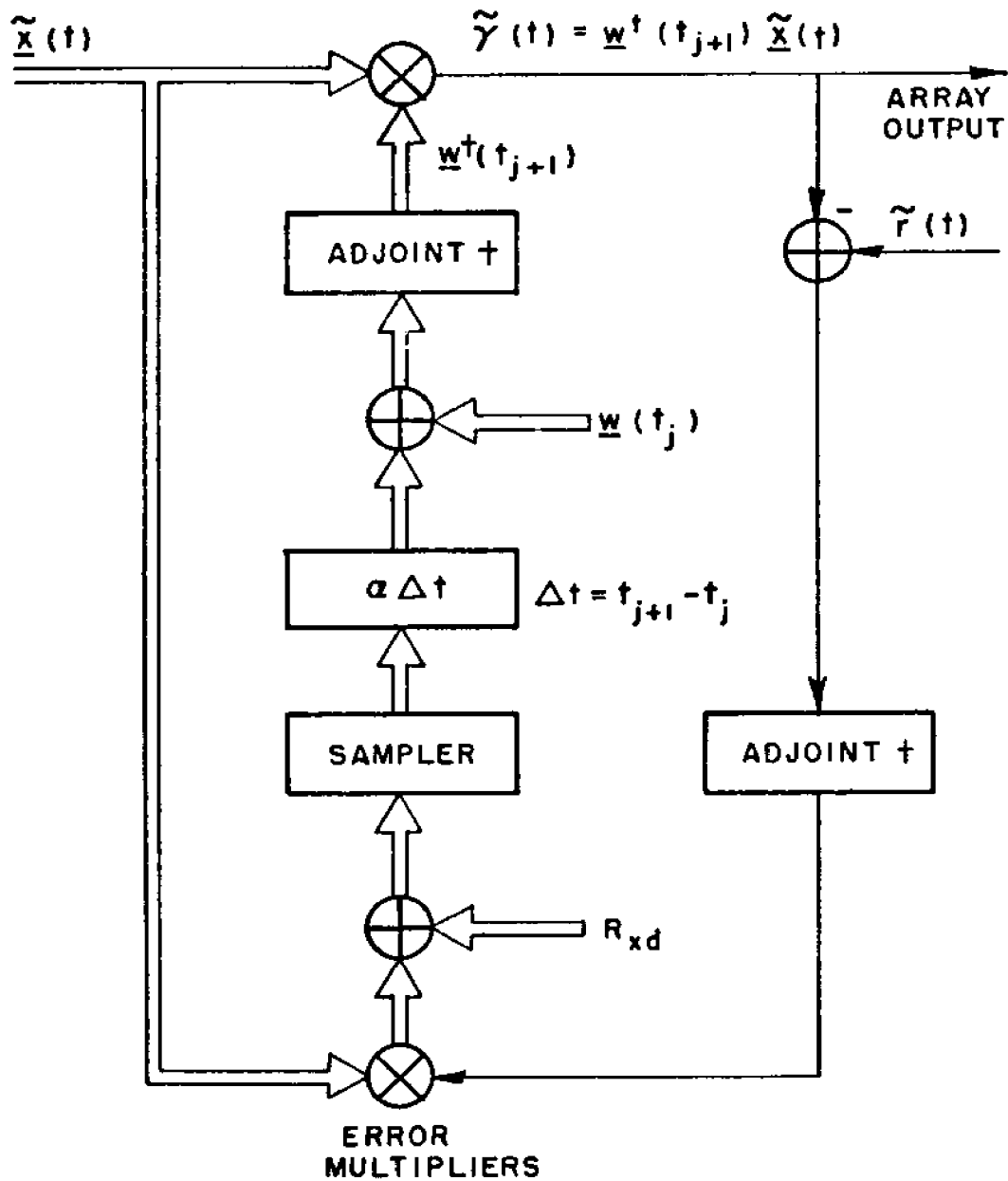


Figure 7--Digital adaptive processor model. In Equation (54), $R_{xd} = [0]$. In Equation (58), $\hat{y}(t) = 0$.

where the explicit time dependence has been suppressed for notational convenience. Equation (59a) applies to an adaptive processing implemented in accord with Equation (52); in later sections, this will be referred to as the $R_{\Delta} \neq [0]$ case. When the processor is implemented in accord with Equation (57), Equation (59b) applies; this will be denoted as the $R_{\Delta} = [0]$ case. Similarly, these definitions and descriptions apply to the digital models defined by Equations (54) and (58) and illustrated in Figure 7.

c. Ideal LMS Algorithm

In this section, the mean transient responses of Equations (52) and (57) will be determined under the assumption that the control loop bandwidth is much narrower than the input signal bandwidth. This result is then compared with the mean response of the DLMS algorithm (Equations (54) and (58)) when $\Delta t \equiv t_{j+1} - t_j$ is assumed equal to the interval between independent samples* of $\underline{\tilde{x}}(t)$.

The mean weight vector, $\bar{w}(t)$, of the ALMS algorithm is obtained by performing an ensemble average of Equation (52) over all signals present. From Equation (55),

$$\begin{aligned} E \frac{dw(t)}{dt} &= \alpha \{ R_{xd} - E[\underline{\tilde{x}}(t)\underline{\tilde{x}}^{\dagger}(t)] \bar{w}(t) \} \\ &\quad - E [\{ \underline{\tilde{x}}(t)\underline{\tilde{x}}^{\dagger}(t) - E[\underline{\tilde{x}}(t)\underline{\tilde{x}}^{\dagger}(t)] \} \{ w(t) - \bar{w}(t) \}] \\ &= \alpha \{ R_{xd} - K_x \bar{w}(t) - E[(\underline{\tilde{x}}(t)\underline{\tilde{x}}^{\dagger}(t) - K_x) (w(t) - \bar{w}(t))] \} \end{aligned} \quad (60)$$

where $\bar{w}(t) \equiv Ew(t)$.

Since $w(t)$ is assumed to vary slowly with respect to $\underline{\tilde{x}}(t)\underline{\tilde{x}}^{\dagger}(t)$, they are negligibly correlated and instantaneous fluctuations of $w(t)$ about its mean are small. This permits the approximation

$$E [(\underline{\tilde{x}}(t)\underline{\tilde{x}}^{\dagger}(t) - K_x) (w(t) - \bar{w}(t))] \approx 0 \quad (61)$$

so that

*Independent samples were assumed in order to simplify the analysis. As should become apparent subsequently, results obtained under this assumption can be used to approximate the mean response for other values of Δt .

$$E \frac{dw(t)}{dt} \triangleq \frac{d\bar{w}(t)}{dt} = \alpha(R_{xd} - K_x \bar{w}(t)) \quad (62)$$

The vector differential equation in (62) defines the ideal ALMS algorithm. To evaluate the characteristics of Equation (62), the eigenvector expansion approach described in Section III B will be adopted. Multiplying both sides of Equation (62) by the $m \times m$ unitary matrix P yields

$$\frac{d}{dt} P\bar{w}(t) = \alpha(P R_{xd} - P K_x P^{-1} P\bar{w}(t)) \quad (63)$$

Defining $\bar{y}_i(t)$ as the projection of $\bar{w}(t)$ onto the i^{th} eigenvector of K_x^* , i.e.,

$$\bar{y}_i(t) = [P\bar{w}(t)]_i \quad (64)$$

results in m decoupled differential equations of the form

$$\frac{d\bar{y}_i(t)}{dt} = \alpha[(P R_{xd})_i - \lambda_i \bar{y}_i(t)] ; i = 1, 2, \dots, m \quad (65)$$

Equation (65) has the solution

$$\bar{y}_i(t) = \left\{ \bar{y}_i(t_0) - \frac{(P R_{xd})_i}{\lambda_i} \right\} e^{-\alpha\lambda_i(t - t_0)} + \frac{(P R_{xd})_i}{\lambda_i} \quad (66)$$

where $\bar{y}_i(t_0)$ denotes the initial value of $\bar{y}_i(t)$. Equation (66) may be written in the vector notation as

$$\bar{y}(t) = e^{-\alpha\Lambda(t - t_0)} [\bar{y}(t_0) - \Lambda^{-1} P R_{xd}] + \Lambda^{-1} P R_{xd} \quad (67)$$

where**

*The notation $[]_i$ represents the i^{th} component of the vector enclosed by the brackets.

**Again, the underbar on the vector $\bar{y}(t)$ is omitted in order to simplify notation.

$$\bar{y}(t) = \begin{bmatrix} \bar{y}_1(t) \\ \bar{y}_2(t) \\ \vdots \\ \bar{y}_m(t) \end{bmatrix}$$

and

$$\exp [-\alpha\Lambda(t - t_0)] \equiv I - \alpha\Lambda(t - t_0) + \frac{1}{2!} [\alpha\Lambda(t - t_0)]^2 - \frac{1}{3!} [\alpha\Lambda(t - t_0)]^3 + \dots$$

$$= \begin{bmatrix} e^{-\alpha\lambda_1(t-t_0)} & 0 & 0 \\ 0 & e^{-\alpha\lambda_2(t-t_0)} & 0 \\ 0 & \dots & \vdots \\ \vdots & \vdots & \vdots \\ 0 & \dots & e^{-\alpha\lambda_n(t-t_0)} \end{bmatrix}$$

Since $\lambda_i > 0$, $\bar{y}_i(t)$ exists for $t > t_0$ and converges to the component of R_{xd} projected onto the i^{th} eigenvector, i.e.,

$$\lim_{t \rightarrow \infty} \bar{y}_i(t) = \frac{(P R_{xd})_i}{\lambda_i} ; i = 1, 2, \dots, m \quad (68)$$

or, in vector form,

$$\lim_{t \rightarrow \infty} \bar{y}(t) = \Lambda^{-1} P R_{xd} \quad (69)$$

The steady-state weight vector is obtained by performing the inverse transformation:

$$\begin{aligned} \lim_{t \rightarrow \infty} \bar{w}(t) &= \lim_{t \rightarrow \infty} P^{-1} \bar{y}(t) = P^{-1} \Lambda^{-1} P R_{xd} \\ &= K_x^{-1} R_{xd} \equiv w_{opt} \end{aligned} \quad (70)$$

This result shows that the weight vector $\bar{w}(t)$, calculated according to the ideal ALMS algorithm (Equation (62)), converges to the optimum weight vector.

The degree to which the solution to Equation (62) approximates the solution to Equation (52) depends on the correlation level between $w(t)$ and $\hat{x}(t)\hat{x}^T(t)$ (or $\hat{x}(t)\hat{r}^T(t)$). This degree of correlation, in turn, depends on the input signal environment as well as the relationship between input signal bandwidth and control loop bandwidth. The impact of these parameters on actual performance will be further evaluated analytically and experimentally in later sections.

Since $\bar{w}(t)$ in Equation (62) is assumed stochastically independent of $x(t)$, the output signal power at time t is given by [see Equation (29)]

$$S_o(t) = \bar{w}^T(t) \underline{s} \underline{s}^T \bar{w}(t) = \bar{y}^T(t) P \underline{s} \underline{s}^T P^{-1} \bar{y}(t) \quad (71)$$

Similarly, the output noise power is given by

$$N_o(t) = \bar{w}^T(t) M \bar{w}(t) = \bar{y}^T(t) \Lambda \bar{y}(t) - S_o(t) \quad (72)$$

Substituting Equation (67) into Equations (71) and (72) yields

$$\begin{aligned} S_o(t) &= \left| \sum_{k=1}^m [(P \underline{s})_k^* \left\{ (P[w(t_0) - \frac{R_{xd}}{\lambda_k}])_k \right. \right. \\ &\quad \left. \left. \cdot e^{-\alpha \lambda_k (t-t_0)} + \frac{(P R_{xd})_k}{\lambda_k} \right\} \right|^2 \\ N_o(t) &= \sum_{k=1}^m \left| \sqrt{\lambda_k} \left\{ (P[w(t_0) - \frac{R_{xd}}{\lambda_k}])_k e^{-\alpha \lambda_k (t-t_0)} \right. \right. \\ &\quad \left. \left. + \frac{(P R_{xd})_k}{\lambda_k} \right\} \right|^2 - S_o(t) \end{aligned} \quad (73)$$

These two expressions indicate the explicit dependence of the ideal ALMS algorithm response time on the eigenvalues of the

covariance matrix, the initial weight vector ($w(t_0)$), and the desired signal DOA (R_{xd}). In general signal environments, all components $\bar{y}_k(t)$ [$k=1,2,\dots,m$] must be near their steady-state value to achieve a nearly optimum output SNR; thus, the adaption time required for convergence is normally proportional to the longest time constant, τ_{max} , where

$$\tau_{max} = (\alpha \lambda_{min})^{-1} \quad (74)$$

The assumption that the control loop bandwidth is much narrower than the input signal bandwidth imposes a lower bound (τ_L) on the shortest time constant. Since the shortest time constant (τ_{min}) is related to τ_{max} by

$$\tau_{min} = \tau_{max} \frac{\lambda_{max}}{\lambda_{min}} \quad (75)$$

one obtains the bound

$$\tau_{max} \geq \frac{\tau_L \lambda_{max}}{\lambda_{min}} \quad (76)$$

Thus, the adaption time required using the ideal ALMS algorithm is, in general, proportional to $\lambda_{max}/\lambda_{min}$.

To relate this result to the signal environment, the eigenvalues must be determined. For narrowband, (temporally) uncorrelated signals, the eigenvalues and eigenvectors of K_x satisfy the eigenvector equation

$$(K_x - \lambda I)e = \sum_{i=1}^p P_i^t \underline{v}_i \underline{v}_i^t + (\sigma^2 - \lambda) I = [0] \quad (77)$$

where $P_s^t = P_1^t$ and e is an eigenvector.

For the case of two directional sources ($p=2$), the eigenvalues and (unnormalized) eigenvectors can be shown [15] to be

(78)

$$\lambda_1 = \sigma^2 + \frac{m}{2} (P_1' + P_2') - \left[\frac{m^2}{4} (P_2' - P_1')^2 + P_1' P_2' |\langle \underline{v}_1, \underline{v}_2 \rangle|^2 \right]^{1/2}$$

$$\lambda_2 = \sigma^2 + \frac{m}{2} (P_1' + P_2') + \left[\frac{m^2}{4} (P_2' - P_1')^2 + P_1' P_2' |\langle \underline{v}_1, \underline{v}_2 \rangle|^2 \right]^{1/2}$$

$$e_1 = - \left\{ \frac{m(P_2' - P_1') + \left[m^2(P_2' - P_1')^2 + 4 P_1' P_2' |\langle \underline{v}_1, \underline{v}_2 \rangle|^2 \right]^{1/2}}{2 P_2' \langle \underline{v}_2, \underline{v}_1 \rangle} \right\} \underline{v}_1 + \underline{v}_2$$

$$e_2 = - \left\{ \frac{m(P_2' - P_1') - \left[m^2(P_2' - P_1')^2 + 4 P_1' P_2' |\langle \underline{v}_1, \underline{v}_2 \rangle|^2 \right]^{1/2}}{2 P_2' \langle \underline{v}_2, \underline{v}_1 \rangle} \right\} \underline{v}_1 + \underline{v}_2$$

$$e_k \quad e_1, e_2 \quad ; \quad k > 2$$

where

$$(P R_{xd})_k = \frac{\langle e_k, R_{xd} \rangle}{(\langle e_k, e_k \rangle)^{1/2}} \quad k = 1, 2, \dots, m$$

Clearly, $\lambda_{\min} = \sigma^2$ when $P < m$. The spread ($\lambda_{\max}/\lambda_{\min}$) in eigenvalues is large when

$$P_i' \gg \sigma^2 \quad i = 1, 2$$

$$\text{or } P_i' \gg P_j' \quad i, j = 1, 2$$

Consequently, from (76), convergence rates can be slow when the input signal power is large in relation to the per-element thermal noise power. Fortunately, the impact of widely spread eigenvalues can be partially alleviated by proper selection of the initial weight vector.

The eigenvectors associated with λ_{\min} (e_3, e_4, \dots, e_m) for the underconstrained array are (spatially) orthogonal to the two directional sources, which implies

$$S_o = \left| \sum_{k=1}^2 (P \underline{s})_k^* \left\{ \left(P[w(t_o) - \frac{R_{xd}}{\lambda_k}] \right)_k e^{-\alpha \lambda_k (t-t_o)} + \frac{(P R_{xd})_k}{\lambda_k} \right\} \right|^2 \quad (79)$$

$$N_o = \sum_{k=1}^2 \left| \sqrt{\lambda_k} \left\{ \left(P[w(t_o) - \frac{R_{xd}}{\lambda_k}] \right)_k e^{-\alpha \lambda_k (t-t_o)} + \frac{(P R_{xd})_k}{\lambda_k} \right\} \right|^2 + \sum_{k=3}^m \left| \sqrt{\lambda_{\min}} (Pw(t_o))_k e^{-\alpha \lambda_{\min} (t-t_o)} \right|^2 \quad (80)$$

Thus, the longest time constant in Equations (79) and (80) may be eliminated if the initial weight vector is chosen orthogonal to the thermal noise eigenvectors (the eigenvectors associated with λ_{\min}).

One such initial weight is the zero vector:

$$w(t_o) = [0] \quad (81)$$

for which

$$S_o = \left| \sum_{k=1}^2 (P \underline{s})_k^* \frac{(P R_{xd})_k}{\lambda_k} \left(1 - e^{-\alpha \lambda_k (t-t_o)} \right) \right|^2 \quad (82)$$

$$N_o = \sum_{k=1}^2 \lambda_k \left| \frac{(P R_{xd})_k}{\lambda_k} \left(1 - e^{-\alpha \lambda_k (t-t_o)} \right) \right|^2 - S_o \quad (83)$$

In this case, the adaption time required for convergence is proportional to either

$$\frac{\lambda_1}{\lambda_2} \quad \text{or} \quad \frac{\lambda_2}{\lambda_1} \quad (84)$$

whichever is largest. In some applications (e.g., when the angular separation between the desired signal and interfering signal is sufficiently large and the per-element thermal noise

power is much smaller than the total input power of each directional source), λ_1 (or λ_2) is considerably larger than λ_{\min} , and thus a significant increase in convergence rate can be achieved by initializing the weights to zero.

A second initial weight which is orthogonal to the thermal noise eigenvectors is given by

$$w(t_0) = b R_{xd} \quad (85)$$

where b is an undetermined constant. In this case, Equation (73) reduces to

$$S_0 = \left| \sum_{k=1}^2 \left[\left(b - \frac{1}{\lambda_k} \right) (P \underline{s})_k^* (P R_{xd})_k e^{-\alpha \lambda_k (t-t_0)} + (P \underline{s})_k^* \frac{(P R_{xd})_k}{\lambda_k} \right] \right|^2 \quad (86)$$

$$N_0 = \sum_{k=1}^2 \left| \sqrt{\lambda_k} \left(b - \frac{1}{\lambda_k} \right) (P R_{xd})_k e^{-\alpha \lambda_k (t-t_0)} + \frac{(P R_{xd})_k}{\sqrt{\lambda_k}} \right|^2 - S_0 \quad (87)$$

Transient response again depends* on λ_1 unless the initial error along e_1 is eliminated by setting

$$b = b_1 \equiv \lambda_1^{-1}$$

Of course, λ_1 is generally unknown. However, the impact of slow response on S_0 and N_0 due to λ_1 (and eigenvalues near λ_1) can at least be reduced by setting b near λ_1^{-1} .

*Assume λ_1 is the smallest eigenvalue larger than λ_{\min} .

To illustrate some concepts discussed above, consider a linear array of four identical antenna elements immersed in an environment containing a directional interfering source 30 dB higher than the desired signal and thermal noise powers. Specifically, let (see Equations (5, 6, and 25))

$$\sigma^2 = 1$$

$$P'_s = P'_i = 1$$

$$I'_2 = 1000$$

The eigenvalues and the optimum (steady-state) output signal-to-noise ratio are given in Table I for several values of relative angular separation (ψ in electrical degrees per element) between interfering and desired signal directions of arrival. For $\psi = 90^\circ$, the interference direction of arrival coincides with the direction of a null in the array pattern when the array is cophased to the desired signal so that $T_0 = mP'_s = P_s$. A closer angular separation causes λ_1 , the eigenvalue associated with desired signal, to decrease, but does not significantly effect λ_{\max} or λ_{\min} . The ratios λ_{\max}/λ_1 and $\lambda_{\max}/\lambda_{\min}$ are very large in all cases.

Employing the ideal LMS algorithm with

$$(\alpha\lambda_{\max})^{-1} = 1 \text{ } \mu\text{sec}$$

results in a maximum time constant of

$$\tau_{\max} = (\alpha\lambda_{\min})^{-1} \approx 4 \text{ msec.}$$

By Equation (82) and (83), the maximum time constant can be reduced by a factor of λ_1/λ_{\min} by setting $w(t_0) = [0]$. For the example in Table I, the degree of improvement is greatest when the array is cophased to desired signal, but decreases rapidly as the angular separation between the interference and desired signal is reduced (i.e., when T_0 is reduced).

When $w(t_0) = \lambda_1^{-1} R_{xd}$, response is very rapid since the maximum time constant in the expressions for S_0 and N_0 equals one microsecond. In order to determine performance for $w(t_0) = \beta\lambda_1^{-1} R_{xd}$, where $\beta \neq 1$, the transient response of the output signal-to-noise ratio (S_0/N_0) was evaluated as a function of β for the $\psi = 60^\circ$ and $\psi = 15^\circ$ cases in Table I. Figures 8 and 9 show S_0/N_0 versus $\beta\lambda$ for several different values of κ , where κ represents the adaption time normalized to the smallest loop time constant, i.e.,

Table I. The Eigenvalues, Eigenvectors, and Optimum Output Signal-to-Noise Ratio for Several Values of the Angular Separation Parameter ψ .

ψ	λ_1	λ_2	λ_k	\hat{e}_1	\hat{e}_2	$\langle \hat{e}_1, v_1 \rangle$	$\langle \hat{e}_2, v_1 \rangle$	T_0
<u>/90°</u>	5	4001	1	0.5 v_1	0.5 v_2	2	0	4
<u>/60°</u>	4.25	4002	1	0.55 v_1 -0.24 v_2	$2.17 \times 10^{-4} v_1$ +0.5 v_2	1.802	0.866	3.244
<u>/45°</u>	3.29	4003	1	0.66 v_1 -0.43 v_2	$3.27 \times 10^{-4} v_1$ +0.5 v_2	1.514	1.306	2.295
<u>/30°</u>	2.2	4004	1	0.91 v_1 -0.76 v_2	$4.2 \times 10^{-4} v_1$ +0.5 v_2	1.09	1.673	1.20
<u>/15°</u>	1.33	4005	1	1.74 v_1 -1.66 v_2	$4.79 \times 10^{-4} v_1$ +0.5 v_2	0.575	1.915	0.331

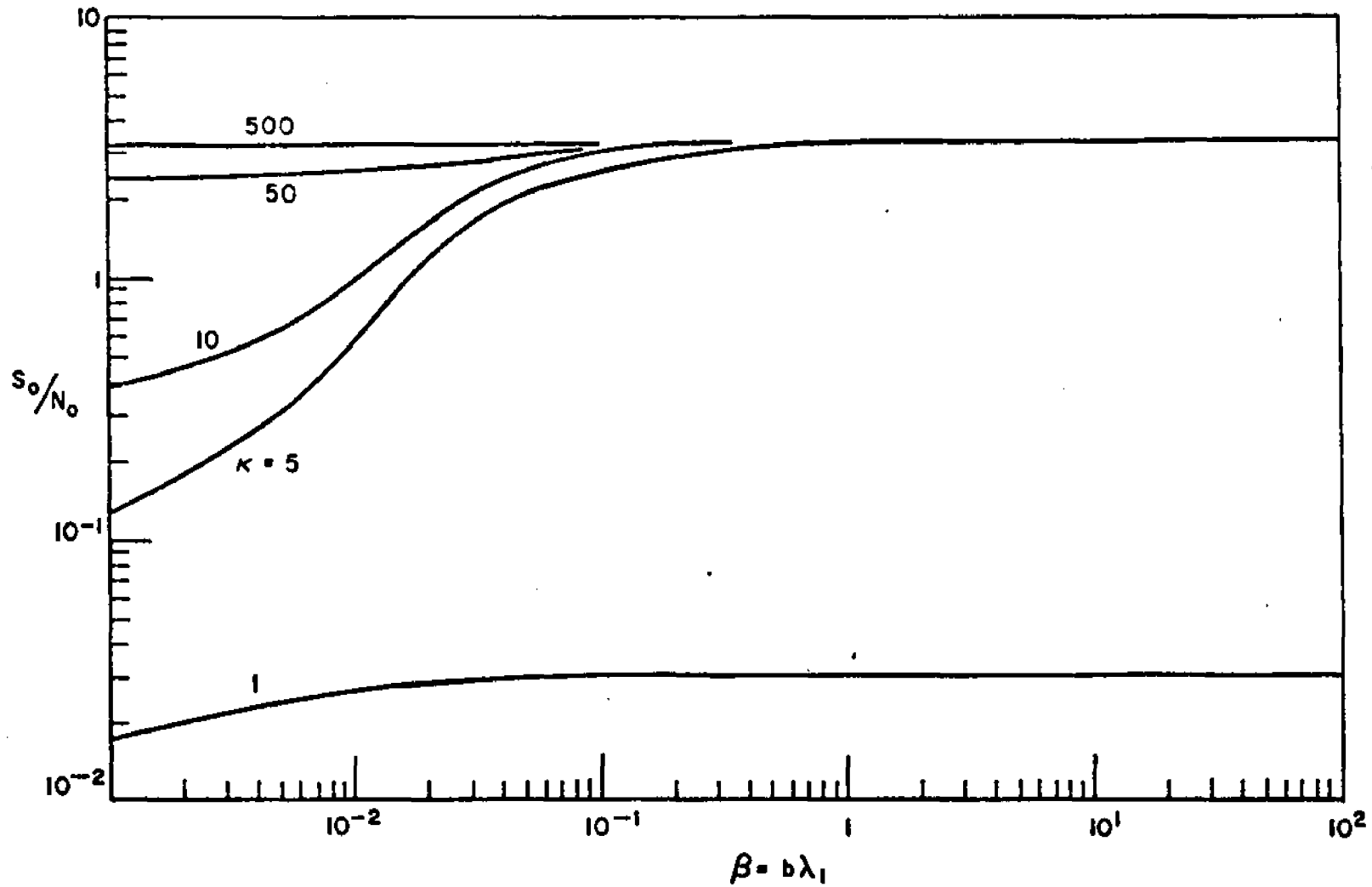


Figure 8--The output signal-to-noise ratio versus β for several values of the normalized adaption time. $\psi = 60^\circ$.

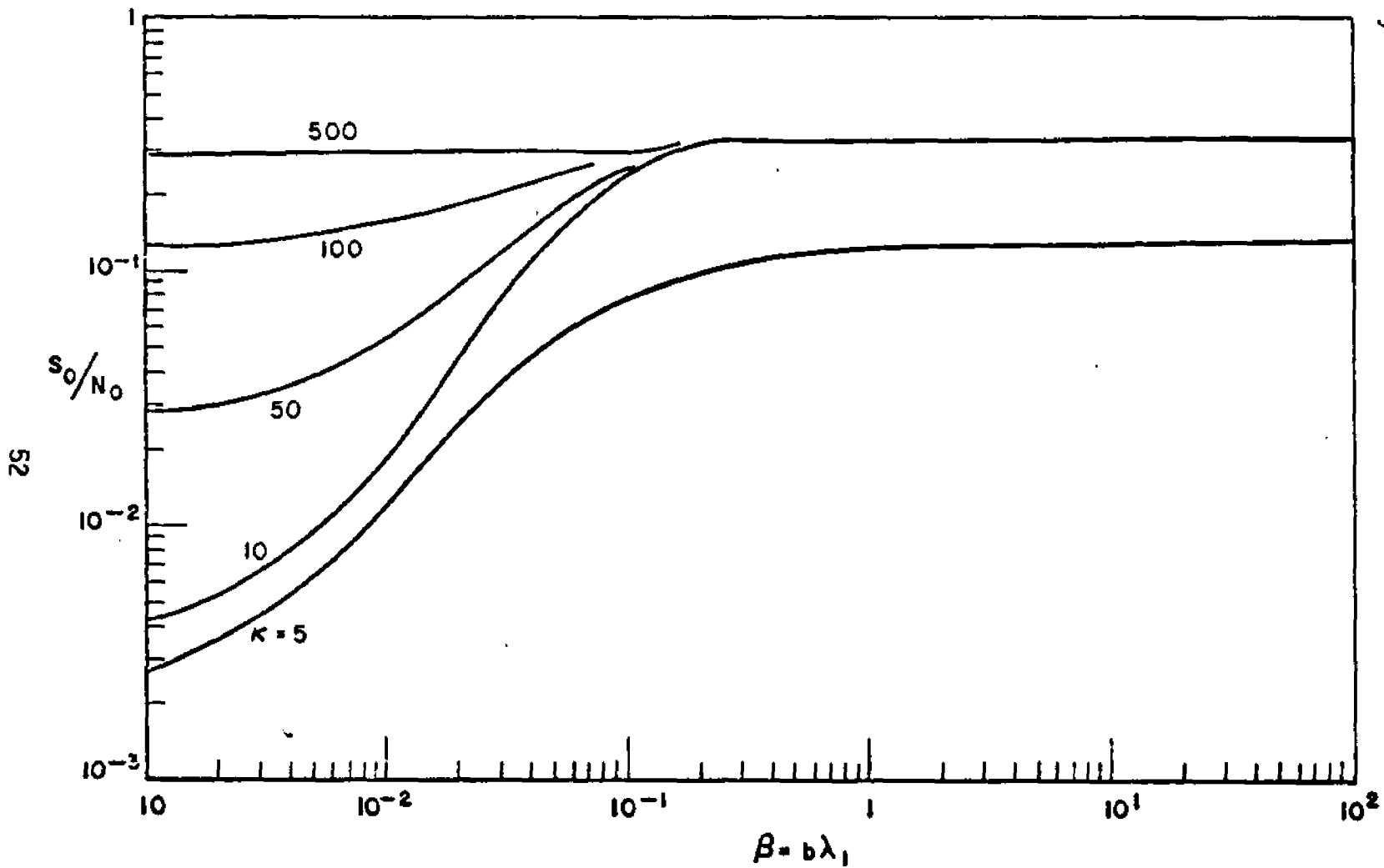


Figure 9--The output signal-to-noise ratio versus β for several values of the normalized adaption time. $\psi = 15^\circ$.

$$\kappa = (t-t_0) (\alpha\lambda_2)^{-1} .$$

The results show that convergence continues to be rapid at both angular separations over a wide range of values for β , which implies that the convergence rate (of S_0/N_0) can be significantly improved by initializing the weight vector to a vector directed along R_{Xd} even though λ_1 is not precisely known. For example, the response obtained in each of the five cases given in Table I for $b = 1$ would be (nearly) the same as the response obtained by setting $b = \lambda_1^{-1}$. Note that the relative responses obtained for the $w(t_0) = [0]$ and $w(t_0) = \lambda_1^{-1} R_{Xd}$ cases can be compared using the results in Figures 8 and 9 since the $w(t_0) = [0]$ case is represented by letting $\beta \rightarrow 0$. In particular, the output signal-to-noise ratio is shown in Figure 9 to converge to within 5 dB of optimum in less than five time constants ($k < 5$) for $\psi = 15^\circ$ and $w(t_0) = \lambda_1^{-1} R_{Xd}$, whereas more than 140 time constants are required to obtain the same performance when $w(t_0) = [0]$.

Although time constants contained in the expression for $\bar{y}_i(t)$ [Equation (66)] are useful in determining the characteristics of the weight response, the "time-constant" associated with convergence of S_0/N_0 (to T_0) may differ significantly from τ_{max} . Again, using the $\psi = 15^\circ$ case as an example, the maximum time constant in the expression* for $y(t)$ is related to the minimum time constant by

$$\tau_{max} = \frac{\alpha\lambda_2}{\alpha\lambda_1} (\alpha\lambda_2)^{-1} = \frac{\alpha\lambda_2}{\alpha\lambda} \tau_{min} \doteq 3011 \tau_{min} \quad (88)$$

Thus, the adaption interval corresponding to τ_{max} is represented by $\kappa = 3011$ in Figure 9. The output signal-to-noise ratio, however, is within 3 dB of optimum for $\kappa \doteq 190$ when $w(t_0) = [0]$. S_0/N_0 converges relatively fast in this case because a deep null is rapidly formed in the direction of the high level interfering signal, which is the only remaining source of initial error. Consequently, S_0/N_0 is large even though S_0 is small relative to its optimum value.

In general signal environments containing more than two directional sources, Equations (86) and (87) become

*The initial weight vector is assumed orthogonal to e_k for $k > 2$.

$$S_o = |\tilde{r}|^2 \left[\sum_{k=1}^p |(P \underline{s})_k|^2 \left\{ \left(b - \frac{1}{\lambda_k} \right) e^{-\alpha \lambda_k (t-t_o)} + \frac{1}{\lambda_k} \right\} \right]^2 \quad (89)$$

$$N_o = |\tilde{r}|^2 \sum_{k=1}^p |P \underline{s}_k|^2 \lambda_k \left\{ \left(b - \frac{1}{\lambda_k} \right) e^{-\alpha \lambda_k (t-t_o)} + \frac{1}{\lambda_k} \right\}^2 - S_o$$

In order to determine a "best" value for b in this case, additional information is required regarding assumed adaption times and signal environment for the particular application. For example, a value for b could be computed such that S_o/N_o versus b is maximized for a given adaption interval $(t-t_o)$ if the signal environment were assumed known. A value for b which provides a "good" response over a wide range of (unknown) signal environments would be more difficult to determine.

Although a detailed study was not conducted, the convergence of S_o/N_o was evaluated for two different values of λ_3 when two high-level interfering signals ($p = 3$) are present; the results are given in Figures 10 and 11. In both cases, the values for $|(P \underline{s})_i|^2/\lambda_i$ ($i = 1, 2, 3$) were selected so that T_o approximated the optimum signal-to-noise ratio of 0.331 obtained for the $\psi = 15^\circ$ case in Table I. Again, the results show that the convergence rate can be significantly improved by setting $w(t_o) = \beta \lambda_1^{-1} R_{Xd}$, and that the convergence rate is relatively insensitive to the value of β .

Some insight regarding the relationship of input signal bandwidth and the ideal ALMS assumption can be obtained by evaluating the mean response of the digital implementation. Successive application of Equation (54) results in an expression for $w(t_n)$ in terms of data collected at times t_1, t_2, \dots, t_{n-1} and the initial weight vector $w(t_1)$. Assuming a constant interval between samples, one obtains

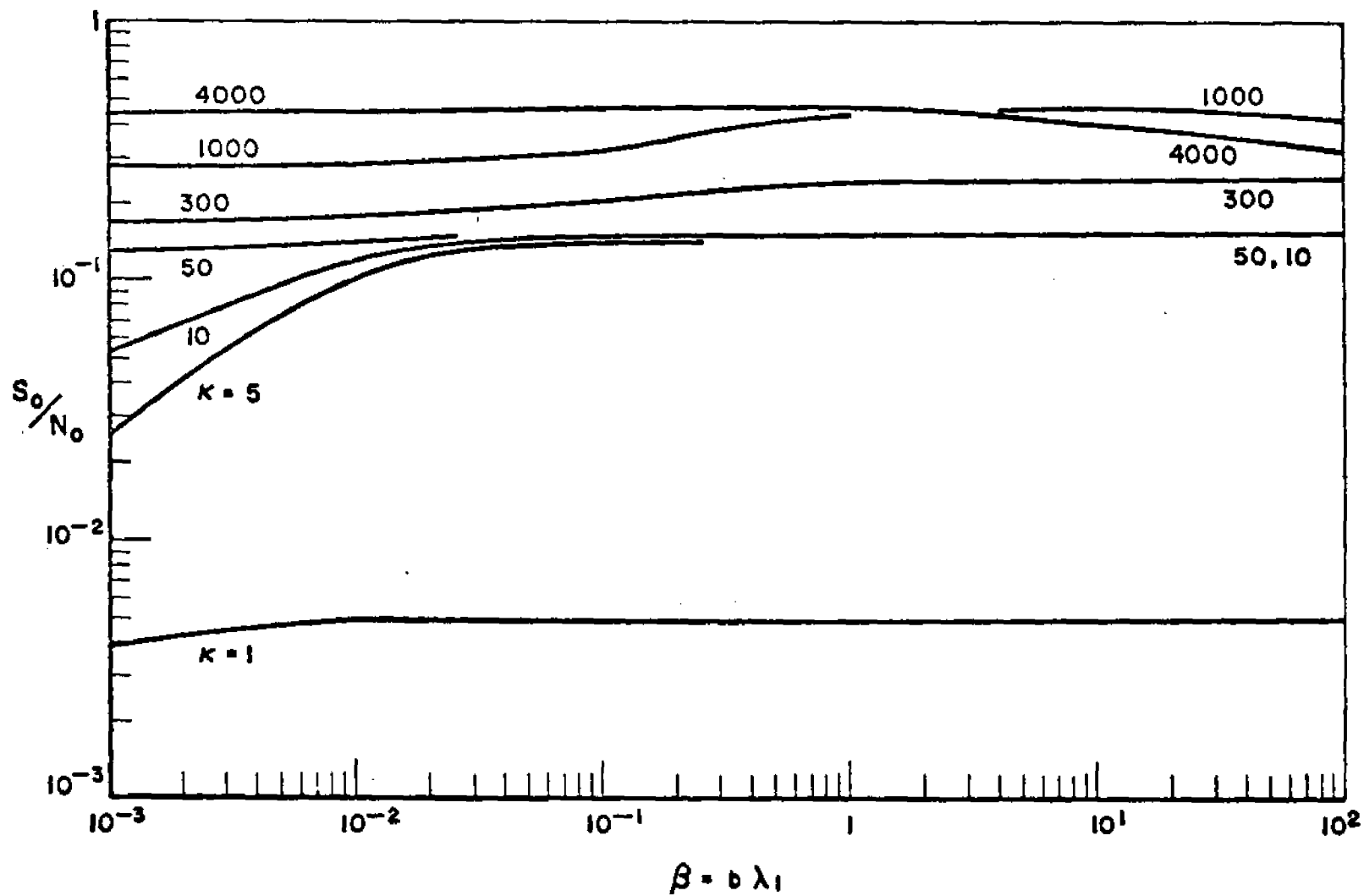


Figure 10--The output signal-to-noise ratio versus β for several values of the normalized adaption time. $\psi = 15^\circ$; $\lambda_3 = 13.3$; $|P_{s1}| = |P_{s2}| = 0.957$.

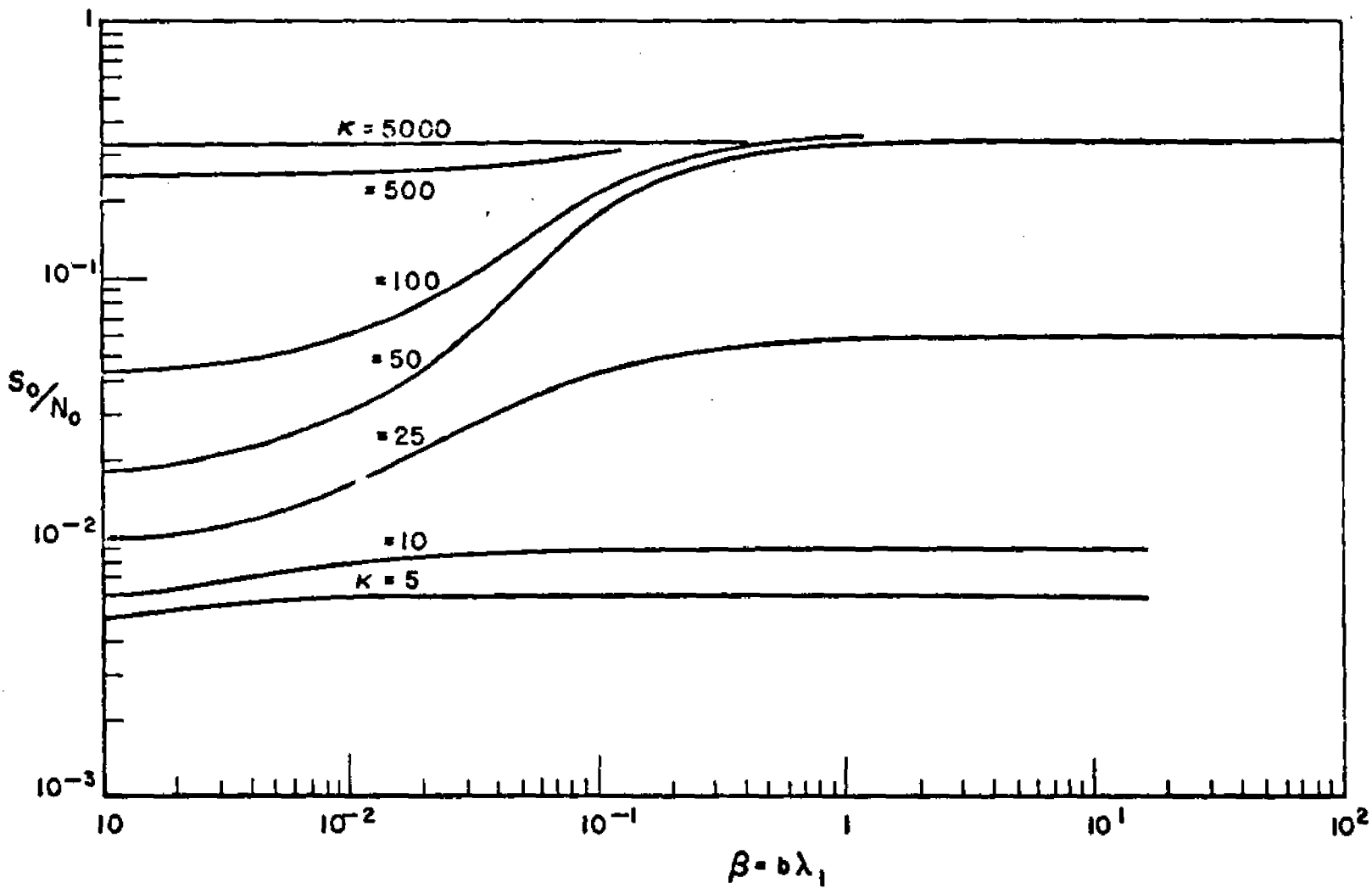


Figure 11--The output signal-to-noise ratio versus β for several values of the normalized adaption time. $\psi = 15^\circ$; $\lambda_3 = 403$; $|P_{s1}| = |P_{s2}| = 0.957$.

$$\begin{aligned}
w(t_n) = & \alpha \Delta t \left\{ \underline{\hat{x}}(t_{n-1}) \hat{r}^\dagger(t_{n-1}) \right. \\
& + \sum_{j=2}^{n-1} \left[\prod_{i=2}^j (I - \alpha \Delta t \underline{\hat{x}}(t_{n-i}) \hat{x}^\dagger(t_{n-i})) \right] \underline{\hat{x}}(t_{n-j}) \hat{r}^\dagger(t_{n-j}) \left. \right\} \\
& + \left\{ \prod_{i=1}^{n-1} [I - \alpha \Delta t \underline{\hat{x}}(t_i) \hat{x}^\dagger(t_i)] \right\} w(t_1)
\end{aligned}$$

where

$$\Delta t \equiv t_k - t_{k-1} \quad ; \quad k = 2, 3, \dots, n \quad .$$

In order to evaluate the ensemble average of Equation (90), it is assumed that Δt equals the interval between independent samples of the input signals contained in $x(t)$. For this choice of Δt , the matrices $\underline{\hat{x}}(t_k) \hat{x}^\dagger(t_k)$ and the vectors $\underline{\hat{x}}(t_i) \hat{r}^\dagger(t_i)$ are also statistically independent for $k \neq i$. Consequently, the ensemble average of the weight vector at time t_n is given by

$$\begin{aligned}
\bar{w}(t_n) \equiv E w(t_n) = & \alpha \Delta t \left\{ E \underline{\hat{x}}(t_{n-1}) \hat{r}^\dagger(t_{n-1}) \right. \\
& + \sum_{j=2}^{n-1} E \left[\prod_{i=2}^j (I - \alpha \Delta t \underline{\hat{x}}(t_{n-i}) \hat{x}^\dagger(t_{n-i})) \right] E \underline{\hat{x}}(t_{n-j}) \hat{r}^\dagger(t_{n-j}) \left. \right\} \\
& + E \left\{ \prod_{i=1}^{n-1} [I - \alpha \Delta t \underline{\hat{x}}(t_i) \hat{x}^\dagger(t_i)] \right\} w(t_1) \\
= & \alpha \Delta t \left\{ R_{xd} + \sum_{j=2}^{n-1} \left[\prod_{i=2}^j (I - \alpha \Delta t K_x) \right] R_{xd} \right\} \\
& + \left\{ \prod_{i=1}^{n-1} [I - \alpha \Delta t k_x] \right\} w(t_1)
\end{aligned}$$

$$= \alpha \Delta t \left\{ \sum_{j=0}^{n-2} (I - \alpha \Delta t K_x)^j \right\} R_{xd} + (I - \alpha \Delta t K_x)^{n-1} w(t_1) .$$

Equation (91) is denoted as the ideal DLMS algorithm.

To evaluate the convergence properties of $\bar{w}(t_n)$ as n grows large, it is again convenient to adopt the eigenvector expansion approach. Multiplying both sides of Equation (91) by the unitary matrix P , yields

$$\begin{aligned} \bar{y}(t_k) \equiv P \bar{w}(t_k) &= \alpha \Delta t \left\{ \sum_{j=0}^{n-2} (I - \alpha \Delta t \Lambda)^j \right\} P R_{xd} \\ &+ (I - \alpha \Delta t \Lambda)^{n-1} \bar{y}(t_1) \end{aligned} \tag{92}$$

which represents m decoupled equations of the form

$$\begin{aligned} \bar{y}_k(t_n) &= \alpha \Delta t \left\{ \sum_{j=0}^{n-2} (1 - \alpha \Delta t \lambda_k)^j \right\} (P R_{xd})_k \\ &+ (1 - \alpha \Delta t \lambda_k)^{n-1} \bar{y}_k(t_1) \\ &= (1 - \alpha \Delta t \lambda_k)^{n-1} \left[\bar{y}_k(t_1) - \frac{(P R_{xd})_k}{\lambda_k} \right] + \frac{(P R_{xd})_k}{\lambda_k} ; \\ &k = 1, 2, \dots, m . \end{aligned} \tag{93}$$

The scalar $\bar{y}_k(t_n)$ converges to $\lambda_k^{-1} (P R_{xd})_k$ provided

$$0 < \alpha \Delta t \lambda_k < 2 . \tag{94}$$

The mean weight vector $\bar{w}(t_n)$ therefore converges to the optimum weight vector $K_x^{-1} R_{xd}$ if the relation in (94) is satisfied for all values of λ_k .

The degree to which the ideal DLMS weights approximate the instantaneous response of Equations (54) and (58) depends on the variance of $w(t_n)$ about $\bar{w}(t_n)$, which, as in the ALMS case, depends on the loop gain constant α and on the signal environment. These effects will also be addressed in the next section.

To show that the ideal ALMS algorithm is a limiting case of the ideal DLMS algorithm, Equation (93) is rewritten as

$$\begin{aligned} \bar{y}_k(t_n) &= (1 - \alpha \Delta t \lambda_k)^{\frac{(n-1)\Delta t}{\Delta t}} \left[\bar{y}_k(t_1) - \frac{(P R_{xd})_k}{\lambda_k} \right] + \frac{(P R_{xd})_k}{\lambda_k} \\ &= (1 - \alpha \Delta t \lambda_k)^{(t_n - t_1)/\Delta t} \left[\bar{y}_k(t_1) - \frac{(P R_{xd})_k}{\lambda_k} \right] + \frac{(P R_{xd})_k}{\lambda_k} \end{aligned} \quad (95)$$

By holding t_k fixed and letting the interval between independent samples approach zero, the expression for $\bar{y}(t_n)$ approaches

$$\lim_{\Delta t \rightarrow 0} \bar{y}_k(t_n) = e^{-\alpha \lambda_k (t_n - t_1)} \left(\bar{y}_k(t_1) - \frac{(P R_{xd})_k}{\lambda_k} \right) + \frac{(P R_{xd})_k}{\lambda_k} \quad (96)$$

which is identical to Equation (66) for $t = t_n$ and $t_1 = t_0$. Even for arbitrary Δt (as long as the samples remain independent), the solution to Equation (66) is approximated by the solution to Equation (95) over a wide range of adaption intervals if

$$\Delta t \ll (\alpha \lambda_k)^{-1} ; \quad k = 1, 2, \dots, m \quad (97)$$

The interval between independent samples can be related to the input signal bandwidth using the sampling theorem. Assuming the input spectra are ideal bandpass with a bandwidth B Hz, then $\Delta t = B^{-1}$. In this case, the limit in Equation (96) is equivalent letting the input signal bandwidth increase without bound, so that the relation given in Equation (97) becomes

$$B \gg \alpha \lambda_k \quad ; \quad k = 1, 2, \dots, m$$

(98)

The above results, together with the fact that the mean of Equation (52) approximates the mean of Equation (57) when the weights are slowly varying with respect to input signal fluctuations, imply that the solution to the ideal ALMS algorithm represents a good approximation to the mean weight response of Equation (52) if the relation in Equation (98) is satisfied, i.e., if the smallest loop time constant is much greater than the inverse of the input signal bandwidth.

D. Effects of Control Loop Noise

1. Introduction

Section C dealt with the transient and steady-state behavior of the mean weight vector $\bar{w}(t)$ (or $\bar{w}(t_n)$). Weights which are controlled according to the DLMS algorithm were shown to converge in the mean provided $\alpha \Delta t \lambda_k < 2$ for all values of λ_k , where λ_k represents the k^{th} eigenvalue of K_x , Δt represents the interval between independent samples of the input signals, and α equals the loop gain constant. It was also shown that the mean weight response of the ALMS algorithms [Equations (52) and (57)] is approximated by the solution to the ideal ALMS algorithm equation when $\alpha \Delta t \lambda_n \ll 1$.

In physical implementations of these algorithms, the weights are controlled by processing random data over a finite time interval. The weights, therefore, tend to respond to instantaneous rather than averaged data, causing them to jitter about their mean values. Weight jitter adds random noise to the array output, thus degrading the output signal-to-noise ratio relative to that predicted by the ideal algorithms. Since the LMS algorithms rely on averaging in the control loop to reduce the impact of instantaneous data fluctuations, the magnitude of excess noise depends on control loop bandwidth relative to input signal bandwidth. In the following two sections, the effects of control loop noise on the output signal-to-noise ratio will be determined when the mean weights are near their steady-state condition. The desired signal will be assumed PM code modulated and the undesired signals will be assumed to approximate sample functions from zero-mean Gaussian processes.

2. Digital LMS Algorithm

The m -dimensional weight vector at time $t = t_k$, in terms of data sampled at time $t = t_{k-1}$, is given by

$$\hat{w}(t_k) = \alpha \Delta t \tilde{x}(t_{k-1}) \tilde{r}^\dagger(t_{k-1}) - \alpha \Delta t \tilde{x}(t_{k-1}) \tilde{x}^\dagger(t_{k-1}) \hat{w}(t_{k-1}) + \hat{w}(t_{k-1})$$

where $\Delta t = t_k - t_{k-1}$ is the interval between independent samples of the input vector $\tilde{x}(t)$. Define the vector $\tilde{z}(t_k)$ as the difference between $\hat{w}(t_k)$ and the optimum weight vector, w_{opt} :

$$\tilde{z}(t_k) = \hat{w}(t_k) - w_{opt} \quad (100)$$

where $w_{opt} = K_X^{-1} R_{xd}$.

Since the mean weights converge to w_{opt} (assuming $\alpha \Delta t \lambda_k < 2$), $\tilde{z}(t_k)$ is a measure of weight jitter when $E \hat{w}(t_k)$ is near steady-state. The magnitude of the additive (or "excess") noise in the array processor's output signal, due to the effects of weight jitter, will be determined by first evaluating the second moment of the process $\tilde{z}(t_k)$. To simplify the analysis, undesired input signals are modeled as sample functions from uncorrelated, zero-mean, Gaussian processes. The desired signal is assumed to be PII code modulated in accord with the TDMA application.

Subtracting w_{opt} from both sides of Equation (99) and rearranging terms yields*

(101)

$$\tilde{z}(t_k) = \alpha \Delta t R_\Delta(t_{k-1}) + [I - \alpha \Delta t K_X] \tilde{z}(t_{k-1}) - \alpha \Delta t \phi(t_{k-1}) \hat{w}(t_{k-1})$$

where

(102)

$$R_\Delta(t_{k-1}) \equiv \tilde{x}(t_{k-1}) \tilde{r}^\dagger(t_{k-1}) - R_{xd}$$

$$\phi(t_{k-1}) \equiv \tilde{x}(t_{k-1}) \tilde{x}^\dagger(t_{k-1}) - K_X$$

*The underbar of the vector $\tilde{z}(t_k)$ has been omitted for notational convenience.

The ensemble average of each element in the random vector R_{Δ} and matrix ϕ is zero:

$$E R_{\Delta}(t_{k-1}) = [0] \quad (103)$$

$$E \phi_{ij}(t_{k-1}) = 0 \quad ; \quad i, j = 1, 2, \dots, m \quad .$$

Since samples of $\hat{x}(t)$ at different sampling instants are independent, it follows that

$$E [R_{\Delta}(t_k) R_{\Delta}^{\dagger}(t_j)] = 0 \quad (104)$$

and

$$E [\phi(t_k) \phi^{\dagger}(t_j)] = 0 \quad ; \quad k \neq j \quad .$$

Employing the eigenvector expansion technique (see Section III), let P be the $m \times m$ unitary matrix which diagonalizes K_x . Further, define the vector $y_{\Delta}(t_k)$ as the transformation of $\hat{z}(t_k)$ into this eigenvector space:

$$y_{\Delta}(t_k) = P \hat{z}(t_k) \quad (105)$$

Multiplying both sides of Equation (101) by P yields the expression

$$\begin{aligned} y_{\Delta}(t_k) &= \alpha \Delta t P R_{\Delta}(t_{k-1}) + [I - \alpha \Delta t \Lambda] y_{\Delta}(t_{k-1}) \\ &\quad - \alpha \Delta t P \phi(t_{k-1}) \hat{w}(t_{k-1}) \\ &= \alpha \Delta t P R_{\Delta}(t_{k-1}) + [I - \alpha \Delta t \Lambda] y_{\Delta}(t_{k-1}) \\ &\quad - \alpha \Delta t P \phi(t_{k-1}) P^{-1} y_{\Delta}(t_{k-1}) - \alpha \Delta t P \phi(t_{k-1}) w_{opt} \quad . \end{aligned} \quad (106)$$

Since $y_{\Delta}(t_k)$ depends only on $y_{\Delta}(t_{k-1})$ and data sampled at $t = t_{k-1}$, its fluctuations are statistically independent of the processes $\phi(t_k)$ and $R_{\Delta}(t_k)$. Utilizing the properties of ϕ and R_{Δ} given in Equations (103) and (104), this implies

$$E y_{\Delta}(t_k) = [I - \alpha\Delta t\Lambda] E y_{\Delta}(t_{k-1}) \quad (107)$$

and

$$\begin{aligned} E y_{\Delta}^{\dagger}(t_k) y_{\Delta}(t_{k-1}) &= \alpha\Delta t E [R_{\Delta}^{\dagger}(t_{k-1}) P^{-1} y_{\Delta}(t_{k-1})] \\ &+ E \left\{ y_{\Delta}^{\dagger}(t_{k-1}) [I - \alpha\Delta t\Lambda] y_{\Delta}(t_{k-1}) \right\} \\ &- \alpha\Delta t E [y_{\Delta}^{\dagger}(t_{k-1}) P\phi^{\dagger}(t_{k-1}) P^{-1} y_{\Delta}(t_{k-1})] \\ &- \alpha\Delta t E [w_{\text{opt}}^{\dagger}\phi^{\dagger}(t_{k-1}) P^{-1} y_{\Delta}(t_{k-1})] \\ &= E \left\{ y_{\Delta}^{\dagger}(t_{k-1}) [I - \alpha\Delta t\Lambda] y_{\Delta}(t_{k-1}) \right\} . \end{aligned} \quad (108)$$

Similarly,

$$\begin{aligned} E [y_{\Delta}^{\dagger}(t_k) y_{\Delta}(t_{k-n})] &= E \left\{ y_{\Delta}^{\dagger}(t_{k-1}) [I - \alpha\Delta t\Lambda]^{n-1} y_{\Delta}(t_{k-n}) \right\} \\ n &= 1, 2, \dots, k-1 . \end{aligned} \quad (109)$$

n iterative applications of Equation (106) generates the vector $y_{\Delta}(t)$ at time $t = t_{k+n}$ in terms of $y_{\Delta}(t_{k-1})$ and data sampled at times $t = t_{k-1}, t_k, t_{k+1}, \dots, t_{k+n-1}$, i.e.,

$$\begin{aligned} y_{\Delta}(t_{k+n}) &= [I - \alpha\Delta t\Lambda]^{n+1} y_{\Delta}(t_{k-1}) \\ &+ \alpha\Delta t \sum_{i=0}^n [I - \alpha\Delta t\Lambda]^i \underline{B}^{k-1+n-i} \end{aligned} \quad (110)$$

where

$$\begin{aligned} \underline{B}^{\ell} &\equiv P R_{\Delta}(t_{\ell}) - p\phi(t_{\ell}) P^{-1} y(t_{\ell}) - p\phi(t_{\ell}) w_{\text{opt}} ; \\ \ell &= k-1, k, \dots, k+n-1 . \end{aligned} \quad (111)$$

The superscript ℓ denotes the value of the vector \underline{B} at time $t = t_{\ell}$. The vector $y_{\Delta}(t_{k+n})$ has the j^{th} component

$$y_{j\Delta}(t_{k+n}) = (1 - \alpha\Delta t\lambda_j)^{n+1} y_{j\Delta}(t_{k-1}) \quad (112)$$

$$+ \alpha\Delta t \sum_{i=0}^n (1 - \alpha\Delta t\lambda_j)^i B_j^{k-1+n-i} \quad ; \quad j = 1, 2, \dots, m$$

where B_j^ℓ denotes the j^{th} component of \underline{B}^ℓ .

The cross-correlation of $y_{j\Delta}$ and $y_{\ell\Delta}$ at $t = t_{k+n}$ is expressed as

$$E\left\{y_{j\Delta}(t_{k+n}) y_{\ell\Delta}^\dagger(t_{k+n})\right\} = \quad (113)$$

$$= (1 - \alpha\Delta t\lambda_j)^{n+1} (1 - \alpha\Delta t\lambda_\ell)^{n+1} E\left\{y_{j\Delta}(t_{k-1}) y_{\ell\Delta}^\dagger(t_{k-1})\right\}$$

$$+ \alpha\Delta t (1 - \alpha\Delta t\lambda_\ell)^{n+1} \sum_{i=0}^n (1 - \alpha\Delta t\lambda_j)^i E\left\{B_j^{k-1+n-i} y_{\ell\Delta}^\dagger(t_{k-1})\right\}$$

$$+ \alpha\Delta t (1 - \alpha\Delta t\lambda_j)^{n+1} \sum_{i=0}^n (1 - \alpha\Delta t\lambda_\ell)^i E\left\{y_{j\Delta}(t_{k-1}) B_\ell^{k-1+n-i}\right\}$$

$$+ (\alpha\Delta t)^2 \sum_{i_1=0}^n \sum_{i_2=0}^n (1 - \alpha\Delta t\lambda_j)^{i_1} (1 - \alpha\Delta t\lambda_\ell)^{i_2}$$

$$\cdot E\left\{B_j^{k-1+n-i_1} B_\ell^{k-1+n-i_2}\right\}.$$

By Equations (103) and (104), and since the process $y_\Delta(t_i)$ is independent of the process $\phi(t_j)$ and $R_\Delta(t_j)$, the ensemble average of the $j\ell^{\text{th}}$ ($j, \ell = 1, 2, \dots, m$) element of the $m \times m$ matrix $E[B^i B^k]$ is zero for $i \neq k$. Similarly, the elements of $E[B^i y_\Delta(t_k)]$ are zero for $i \neq k$. Thus, Equation (113) reduces to

$$E\left\{y_{j\Delta}(t_{k+n}) y_{\ell\Delta}^\dagger(t_{k+n})\right\} \quad (114)$$

$$= (1 - \alpha\Delta t\lambda_j)^{n+1} (1 - \alpha\Delta t\lambda_\ell)^{n+1} E\left\{y_{j\Delta}(t_{k-1}) y_{\ell\Delta}^\dagger(t_{k-1})\right\}$$

$$+ (\alpha\Delta t)^2 \sum_{i=0}^n (1 - \alpha\Delta t\lambda_j)^i (1 - \alpha\Delta t\lambda_\ell)^i$$

$$\cdot E\left\{B_j^{k-1+n-i} B_\ell^{k-1+n-i}\right\}$$

The steady-state condition, where the mean weights are at their steady-state values, is represented in Equation (114) by letting $n \rightarrow \infty$. In this limit, the first term in Equation (114) vanishes. It can also be shown that the term $E B_{j\Delta}^{k-1+n-1} B_{\ell\Delta}^{k-1+n-1}$ becomes independent of n . Thus, under steady-state conditions, the cross-correlation of $y_{j\Delta}(t_{k-n})$ and $y_{\ell\Delta}(t_{k-n})$ may be expressed as

$$E[y_{j\Delta} y_{\ell\Delta}^\dagger] = \lim_{n \rightarrow \infty} (\alpha \Delta t)^2 \sum_{i=0}^n (1 - \alpha \Delta t \lambda_j)^i (1 - \alpha \Delta t \lambda_\ell)^i \cdot E[B_j B_\ell^\dagger] \quad (115)$$

The explicit dependence of $y_{j\Delta}$ and B_j on the variable n has been suppressed in Equation (115) since their values are independent of the number of data samples for n sufficiently large.

The term $E(B_j B_\ell^\dagger)$ in Equation (115) is determined by first evaluating

$$E[C_j C_\ell^\dagger] = E[(R_\Delta - \phi P^{-1} y_\Delta - \phi w_{\text{opt}})_j \cdot (R_\Delta - \phi P^{-1} y_\Delta - \phi w_{\text{opt}})_\ell^*] \quad (116)$$

The ensemble average defined in Equation (116) represents the $i\ell^{\text{th}}$ component of ECC^\dagger , where

$$C^\dagger = [C_1, C_2, \dots, C_m]$$

which is related to EBB^\dagger by

$$E(BB^\dagger) = PE(CC^\dagger)P^{-1} \quad (117)$$

Since ϕ and R_Δ are uncorrelated with y_Δ , all but two of the cross-terms vanish in Equation (116):

$$E(C_j C_\ell^\dagger) = E \left\{ R_{\Delta_j} R_{\Delta_\ell}^\dagger + (\phi P^{-1} y_\Delta)_j (\phi P^{-1} y_\Delta)_\ell^\dagger + (\phi w_{\text{opt}})_j (\phi w_{\text{opt}})_\ell^\dagger - R_{\Delta_j} (\phi w_{\text{opt}})_\ell^\dagger - (\phi w_{\text{opt}})_j R_{\Delta_\ell}^\dagger \right\}. \quad (118)$$

The reference signal is assumed to be a scaled replica of the desired signal waveform; i.e.,

$$\tilde{r}(t) = \frac{|\tilde{x}(t)|}{\sqrt{P_S^\dagger}} \tilde{\xi}_1(t) e^{j\theta} \quad (119)$$

where P_S^\dagger and θ are unknown constants. Separating the input signal into the sum of desired and undesired components

$$\tilde{x}(t) = \tilde{s}(t) + \tilde{u}(t) \quad (120)$$

and using Equations (20, 22, 44, and 102), the following useful properties can be established:

$$|\tilde{r}|^2 \equiv E[\tilde{r}(t) \tilde{r}^\dagger(t)] = \tilde{r}(t) \tilde{r}^\dagger(t) \quad (121)$$

$$R_{\text{xd}} = |\tilde{r}| \sqrt{P_S^\dagger} e^{-j\theta} \underline{v}_1$$

$$\phi(t) = \tilde{u}(t) \tilde{u}^\dagger(t) + \tilde{s}(t) \tilde{u}^\dagger(t) + \tilde{u}(t) \tilde{s}^\dagger(t) - M$$

$$R_\Delta(t) = \tilde{u}(t) \tilde{r}^\dagger(t) .$$

The above relations, together with the properties of complex Gaussian processes [22] outlined in Chapter III C, are used in Appendix I to evaluate Equation (118). The result is shown to be

$$E C_j C_\ell^\dagger = |\tilde{r}|^2 M_{j\ell} - w_{\text{opt}}^\dagger R_{\text{xd}} M_{j\ell} - R_{\text{xd}}^\dagger w_{\text{opt}} M_{j\ell} + E(y_\Delta^\dagger \Lambda y_\Delta) K_{X_{j\ell}} - E(y_\Delta^\dagger P \underline{s} \underline{s}^\dagger P^{-1} y_\Delta) s_j s_\ell^\dagger + w_{\text{opt}}^\dagger K_X w_{\text{opt}} K_{X_{j\ell}} - w_{\text{opt}}^\dagger \underline{s} \underline{s}^\dagger w_{\text{opt}} s_j s_\ell^\dagger . \quad (122)$$

Equation (122) can be further simplified by utilizing the following relations and definitions.

$$w_{\text{opt}} = K_x^{-1} R_{\text{xd}} \quad (123)$$

$$T_o = \underline{s}^\dagger M^{-1} \underline{s}$$

$$R_{\text{xd}}^\dagger K_x^{-1} R_{\text{xd}} = |r|^2 \underline{s}^\dagger K_x^{-1} \underline{s} = |r|^2 \frac{T_o}{1 + T_o} .$$

Thus, Equation (118) becomes

$$\begin{aligned} E C_j C_\ell^\dagger &= |r|^2 \left[\frac{1}{1 + T_o} \right] M_{j\ell} + |\hat{r}|^2 \frac{T_o}{(1 + T_o)^2} s_j s_\ell^\dagger \\ &+ E(y_\Delta^\dagger \Lambda y_\Delta) - E(y_\Delta^\dagger P s s^\dagger P^{-1} y_\Delta) s_j s_\ell^\dagger \end{aligned} \quad (124)$$

which represents the $j\ell^{\text{th}}$ component of the $m \times m$ matrix

$$\begin{aligned} E(CC^\dagger) &= |r|^2 \frac{1}{1 + T_o} M + |\hat{r}|^2 \frac{T_o}{(1 + T_o)^2} \underline{s} \underline{s}^\dagger \\ &+ E(y_\Delta^\dagger \Lambda y_\Delta) K_x - E(y_\Delta^\dagger P \underline{s} \underline{s}^\dagger P^{-1} y_\Delta) \underline{s} \underline{s}^\dagger . \end{aligned} \quad (125)$$

By Equation (117),

$$\begin{aligned} E(\underline{B}\underline{B}^\dagger) &= |r|^2 \frac{1}{1 + T_o} P M P^{-1} + |\hat{r}|^2 \frac{T_o}{(1 + T_o)^2} P \underline{s} \underline{s}^\dagger P^{-1} \\ &+ E(y_\Delta^\dagger \Lambda y_\Delta) \Lambda - E(y_\Delta^\dagger P \underline{s} \underline{s}^\dagger P^{-1} y_\Delta) P \underline{s} \underline{s}^\dagger P^{-1} \\ &= |\hat{r}|^2 \frac{1}{1 + T_o} \Lambda - |r|^2 \frac{1}{(1 + T_o)^2} P \underline{s} \underline{s}^\dagger P^{-1} \\ &+ E(y_\Delta^\dagger \Lambda y_\Delta) \Lambda - E(y_\Delta^\dagger P \underline{s} \underline{s}^\dagger P^{-1} y_\Delta) P \underline{s} \underline{s}^\dagger P^{-1} . \end{aligned} \quad (126)$$

In the high level interference environments of interest, the input desired signal power (P_S) is much smaller than the total input power* (P_I). That is,

$$P_I = \underline{\hat{x}}^\dagger(t) \underline{\hat{x}}(t) = T_R(K_X) = T_R(\Lambda) = \sum_{i=1}^m \lambda_i \gg P_S = \underline{\hat{s}}^\dagger \underline{\hat{s}} \quad (127)$$

Assuming (127) is satisfied*, terms which contain $\underline{s} \underline{s}^\dagger$ in Equation (126) are negligibly small (see Section D of this chapter). Therefore, a good approximation to Equation (126) is given by

$$E(\underline{B}\underline{B}^\dagger) \approx |r|^2 \frac{1}{1+T_0} \Lambda + E y_\Delta^\dagger \Lambda y_\Delta \Lambda \quad (128)$$

The ℓj^{th} component of the matrix in Equation (128) may be expressed as

$$E B_j B_\ell^\dagger = \begin{cases} |r|^2 \frac{1}{1+T_0} \lambda_\ell + E y_\Delta^\dagger \Lambda y_\Delta \lambda_\ell & ; \ell = j \\ 0 & ; \ell \neq j \end{cases} \quad (129)$$

Substituting Equation (129) into Equation (115) yields

$$E y_{j\Delta} y_{\ell\Delta}^\dagger \approx \begin{cases} 0 & ; \ell \neq j \\ \lim_{n \rightarrow \infty} (\alpha \Delta t)^2 \sum_{i=0}^n (1 - \alpha \Delta t \lambda_\ell)^{2i} \cdot \lambda_\ell \left(|r|^2 \frac{1}{1+T_0} + E y_\Delta^\dagger \Lambda y_\Delta \right) & ; \ell = j \end{cases} \quad (130)$$

To obtain a closed form solution to Equation (130), the infinite series and the term $E y^\dagger \Lambda y$ must be evaluated. Assuming $\alpha \Delta t \lambda_\ell < 2$, the infinite series converges to

$$\lim_{n \rightarrow \infty} \sum_{i=0}^n (1 - \alpha \Delta t \lambda_\ell)^{2i} = \frac{1}{\alpha \Delta t \lambda_\ell} \frac{1}{2 - \alpha \Delta t \lambda_\ell} \quad (131)$$

*Although the input desired signal power is assumed much smaller than the total input power, the presence of the desired signal is not neglected.

To find $E y_{\Delta}^{\dagger} \Lambda y_{\Delta}$, $E y_{i_{\Delta}} y_{i_{\Delta}}^{\dagger}$ is multiplied by λ_i and summed from 1 to m;

$$E y_{\Delta}^{\dagger} \Lambda y_{\Delta} = \sum_{i=1}^m y_{i_{\Delta}} y_{i_{\Delta}}^{\dagger} \lambda_i \quad (132)$$

From Equations (130) and (131),

$$E y_{\Delta}^{\dagger} \Lambda y_{\Delta} \approx |r|^2 \frac{1}{1 + T_0} \frac{C}{1 - C} \quad (133)$$

where

$$C \equiv \sum_{i=1}^m \frac{\alpha \Delta t \lambda_i}{2 - \alpha \Delta t \lambda_i} \quad (134)$$

The covariance among components of y_{Δ} is therefore approximated by

$$E(y_{j_{\Delta}} y_{\ell_{\Delta}}^{\dagger}) = \begin{cases} \frac{\alpha \Delta t}{2 - \alpha \Delta t \lambda_{\ell}} |r|^2 \frac{1}{1 + T_0} \frac{1}{1 - C} & ; \ell = j \\ 0 & ; \ell \neq j \end{cases} \quad (135)$$

The variance of the weight vector is therefore given by

$$\begin{aligned} \text{Var}(w) &= \lim_{n \rightarrow \infty} E \left\{ [w(t_n) - \bar{w}(t_n)]^{\dagger} [w(t_n) - \bar{w}(t_n)] \right\} \\ &= \lim_{n \rightarrow \infty} E [\hat{z}^{\dagger}(t_n) \hat{z}(t_n)] \\ &= E y_{\Delta}^{\dagger} y_{\Delta} \\ &= \alpha \Delta t \sum_{i=1}^m \frac{1}{2 - \alpha \Delta t \lambda_i} \frac{|r|^2}{(1 + T_0)(1 - C)} \end{aligned} \quad (136)$$

This result reveals a second condition on the loop gain constant which must be satisfied to insure convergence:

$$C = \sum_{i=1}^m \frac{\alpha \Delta t \lambda_i}{2 - \alpha \Delta t \lambda_i} < 1 \quad (137)$$

Otherwise, the steady-state mean-square error becomes infinite. Relative to Equation (94), inequality (137) represents a smaller upper bound on α . Therefore, Equation (137) establishes a necessary condition on α which must be satisfied to insure that the mean square of the difference between the instantaneous and optimum weight vector is bounded.

The effect of weight jitter on the array output signal will next be determined. The array output power is defined as

$$P_T = E(\hat{w}^\dagger(t_k) \tilde{x}(t) \tilde{x}^\dagger(t) \hat{w}(t_k)) \quad t_k \leq t < t_{k+1} \quad .$$

Assuming $\tilde{x}(t)$ is independent of $\hat{w}(t_k)$ for $t_k < t < t_{k+1}$, the expression for P_T becomes

$$\begin{aligned} P_T &= E[\hat{w}^\dagger(t_k) E(\tilde{x}(t) \tilde{x}^\dagger(t)) \hat{w}(t_k)] & (138) \\ &= E[\hat{w}^\dagger(t_k) K_X \hat{w}(t_k)] \\ &= E\{[\hat{z}(t_k) + w_{opt}]^\dagger K_X [\hat{z}(t_k) + w_{opt}]\} \\ &= E[\hat{z}^\dagger(t_k) K_X \hat{z}(t_k)] + E[\hat{z}^\dagger(t_k) K_X w_{opt}] \\ &\quad + E[w_{opt}^\dagger K_X \hat{z}(t_k)] + w_{opt}^\dagger K_X w_{opt} \quad . \end{aligned}$$

Since $E \hat{z}(t_k) = 0$ when the mean weights are in the steady-state condition, the cross-terms vanish, and Equation (138) reduces to

$$\begin{aligned} P_T &= E \hat{z}^\dagger K_X \hat{z} + w_{opt}^\dagger K_X w_{opt} & (139) \\ &= E y_\Delta^\dagger \Lambda y_\Delta + |\tilde{\gamma}|^2 \frac{T_0}{1 + T_0} \quad . \end{aligned}$$

This expression shows that the total output power consists of a component due to optimum filtering plus an additive component due to weight jitter. The total output noise power, $||_0$, is equal to the total output signal power minus the output desired signal power. That is,

$$\begin{aligned}
N_o &= P_T - w_{opt}^\dagger \underline{s} \underline{s}^\dagger w_{opt} \\
&= E y_\Delta^\dagger \Lambda y_\Delta + N_{o,opt}
\end{aligned}
\tag{140}$$

where

$$N_{o,opt} = w_{opt}^\dagger M w_{opt} = |\tilde{r}|^2 \frac{T_o}{(1 + T_o)^2}
\tag{141}$$

Thus, $E y_\Delta^\dagger \Lambda y_\Delta$ represents excess noise contained in the array output signal due to weight jitter.

Define the performance measure κ as the ratio of excess noise due to jitter normalized to the output noise power without jitter, i.e.,

$$\kappa \equiv \frac{E y_\Delta^\dagger \Lambda y_\Delta}{N_{o,opt}}
\tag{142}$$

From Equations (133) and (141), κ is approximated in high level interfering signal environments by

$$\kappa = \frac{1 + T_o}{T_o} \frac{C}{1 - C}
\tag{143}$$

To maintain an output noise level which is less than 3 dB higher than $N_{o,opt}$ requires that $\kappa < 1$ and

$$C = \sum_{i=1}^m \frac{\alpha \Delta t \lambda_i}{2 - \alpha \Delta t \lambda_i} < \frac{T_o}{1 + 2 T_o}
\tag{144}$$

In theory, it is possible to estimate the eigenvalues of K_x and thus determine C . In practice, however, this generally requires elaborate data processing equipments. Fortunately, it is usually a simple matter to estimate the total input power, which is equal to the sum of the eigenvalues (Equation (127)).

Since all eigenvalues are real and positive,

$$\lambda_i < P_I \quad i = 1, 2, \dots, m$$

which implies

$$C' \equiv \sum_{i=1}^m \frac{\alpha \Delta t \lambda_i}{2 - \alpha \Delta t P_I} = \frac{\alpha \Delta t P_I}{2 - \alpha \Delta t P_I} > C \quad (147)$$

By Equation (147), an upper bound on α which guarantees a total output noise power less than 3 dB above N_{0opt} is obtained by setting

$$C' = T_0 (1 + T_0)^{-1};$$

$$\alpha < \frac{1}{P_I \Delta t} \frac{2 T_0}{1 + 3 T_0} \quad (148)$$

More generally, $\kappa > b$ if

$$\alpha(b) < \frac{1}{P_I \Delta t} \frac{2 b T_0}{1 + 2 b T_0 + T_0} \equiv \alpha_{P_I}(b) \quad (149)$$

where $\alpha_{P_I}(b)$ has been defined as the upper bound on α determined from the total input power.

The value of $\alpha (= \alpha_\lambda(b))$ for which $\kappa = b$ is given more precisely by solving the equation

$$C_\lambda = \sum_{i=1}^m \frac{\alpha_\lambda(b) \Delta t \lambda_i}{2 - \alpha_\lambda(b) \Delta t \lambda_i} = \frac{b T_0}{1 + (b + 1) T_0} \quad (150)$$

Since

$$\alpha_\lambda(b) \Delta t P_I < 2 C_\lambda = \frac{2 b T_0}{1 + (b + 1) T_0}$$

then

$$\alpha_\lambda(b) < \frac{1}{P_I \Delta t} \frac{2 b T_0}{1 + (b + 1) T_0} .$$

The two upper bounds on α such that $\kappa = b$ are thus related by

$$1 < \frac{\alpha_\lambda(b)}{\alpha_{P_I}(b)} < 2 . \quad (151)$$

This result shows that, given $\kappa = b$, the corresponding value for α can be determined to within a factor of two of the exact value if the total input power is known.

If the ratio of excess noise to $N_{o_{opt}}$ is viewed as a function of α , Δt , T_o , and P_I , then it is bounded by

$$\frac{\alpha \Delta t P_I}{2 - \alpha \Delta t P_I} \frac{1 + T_o}{T_o} < \kappa < \frac{\alpha \Delta t P_I}{1 - \alpha \Delta t P_I} \frac{1 + T_o}{T_o} \quad (152)$$

The above relation will be normalized to eliminate dependence on T_o . Define the variables

$$\sigma \equiv \kappa \frac{T_o}{1 + T_o} \quad (153)$$

$$\sigma_l \equiv \frac{\alpha \Delta t P_I}{2 - \alpha \Delta t P_I} < \sigma < \frac{\alpha \Delta t P_I}{1 - \alpha \Delta t P_I} \equiv \sigma_u$$

where σ_l and σ_u denote the lower and upper bounds on σ obtained from (152). These bounds are illustrated in Figure 12 as a function of the loop parameter $\alpha \Delta t P_I$. τ depends on the eigenvalues of K_x . If

$$c = \sum_{i=1}^m \frac{\alpha \Delta t \lambda_i}{2 - \alpha \Delta t \lambda_i} \cong \frac{\alpha \Delta t \lambda_k}{2 - \alpha \Delta t \lambda_k} \quad (154)$$

for some λ_k , then σ is near its upper bound. This situation occurs when λ_k approximates the total input power, i.e., the signal environment contains one very high level interfering signal. σ is near its lower bound when the eigenvalues are approximately equal, for example, when the thermal noise power is high.

Since the eigenvalues are assumed unknown, the upper bound in Figure 12 must generally be used to determine a value for α which insures an acceptable excess noise level when the weights are near their steady-state solutions. This upper bound increases rapidly as $\alpha \Delta t P_I$ is increased in the interval $[0.5, 1.0]$. Thus, it is advisable to set $\alpha \Delta t P_I < 0.5$ to obtain acceptable steady-state performance; the resulting penalty in transient response will be relatively minimal (say, a factor of two decrease in the convergence rate).

The preceding results apply to the DLMS algorithm when $R_{\Delta} \neq 0$ (Equation (54)). When R_{x_d} is known a priori, the weight equation can be modified as in Equation (58) and thus the term

R_{Δ} in Equation (101) vanishes (denoted as the $R_{\Delta} = [0]$ case). Upon setting $R_{\Delta} = [0]$, Equation (116) reduces to

$$\begin{aligned}
 E(C_j C_{\ell}^*) &= E\left\{ (\phi P^{-1} y_{\Delta})_j (\phi P^{-1} y_{\Delta})_{\ell}^* \right. \\
 &\quad \left. + (\phi w_{\text{opt}})_j (\phi w_{\text{opt}})_{\ell}^* \right\} \\
 &= E(y_{\Delta}^{\dagger} \Lambda y_{\Delta}) K_{x_{j\ell}} - E(y_{\Delta}^{\dagger} P \underline{s} \underline{s}^{\dagger} P^{-1} y_{\Delta}) s_j s_{\ell}^* + w_{\text{opt}}^{\dagger} K_{x_{\text{opt}}} K_{x_{j\ell}} \\
 &\quad - w_{\text{opt}}^{\dagger} \underline{s} \underline{s}^{\dagger} w_{\text{opt}} s_j s_{\ell}^* .
 \end{aligned} \tag{155}$$

The matrix EBB^{\dagger} may thus be expressed as

$$\begin{aligned}
 E(\underline{BB}^{\dagger}) &= E(y_{\Delta}^{\dagger} \Lambda y_{\Delta}) \Lambda - E(y_{\Delta}^{\dagger} P \underline{s} \underline{s}^{\dagger} P^{-1} y_{\Delta}) \underline{s} \underline{s}^{\dagger} \\
 &\quad + |\tilde{r}|^2 \frac{T_0}{1+T_0} \Lambda - |\tilde{r}|^2 \frac{T_0}{1+T_0} P \underline{s} \underline{s}^{\dagger} P^{-1}
 \end{aligned} \tag{156}$$

Again assuming the input desired signal power is much smaller than the total input power (see Equations (127) and (128)), Equation (156) is approximated by

$$E(\underline{BB}^{\dagger}) \approx |\tilde{r}|^2 \frac{T_0}{1+T_0} \Lambda + E y_{\Delta}^{\dagger} \Lambda y_{\Delta} \Lambda \tag{157}$$

Employing the same steps used to derive Equation (133), the excess output noise can be shown to be

$$\begin{aligned}
 E(y_{\Delta}^{\dagger} \Lambda y_{\Delta}) \Big|_{R_{\Delta}=[0]} &\approx |\tilde{r}|^2 \frac{T_0}{1+T_0} \frac{C}{1-C} \\
 &= T_0 E(y_{\Delta}^{\dagger} \Lambda y_{\Delta}) \Big|_{R_{\Delta} \neq [0]} .
 \end{aligned} \tag{158}$$

A comparison of Equations (133) and (158) indicates that when the optimum output signal-to-noise ratio (T_0) is greater than one, excess noise due to weight jitter is smaller if $\tilde{r}(t)$ is inserted into the loop to form an error feedback voltage ($R_{\Delta} \neq [0]$ case shown in Figure 7). If $T_0 < 1$, then the effects of weight jitter can be

reduced by replacing $\hat{x}(t_{k-1})\hat{r}^+(t_{k-1})$ in Equation (54) by the cross-correlation vector R_{xd} (Equation (58)). Equation (54) provides better performance when $T_0 > 1$ due to the correlation properties of $R_{\Delta}(t)$ and $\phi(t)w(t)$; that is, the mean square of $[(R_{\Delta})_i - (\phi\hat{w})_i]$ is smaller than the mean square of $[(\phi\hat{w})_i]$.

That better performance is obtained using Equation (58) for $T_0 < 1$ apparently is due to a higher noise level in R_{Δ} , i.e., the estimate of R_{xd} is too noisy. This conjecture is supported by results given in Chapter V where the effects of estimating R_{xd} are analyzed, and by the experimental results presented in Chapter VI.

The bounds on σ given in Figure 12 are related to the performance measure κ by

$$\sigma_{\ell} < \kappa \left| R_{\Delta} \neq [0] \right. \frac{T_0}{1+T_0} < \sigma_u \quad (159)$$

These same upper bounds can be used to determine κ for $R_{\Delta} = [0]$ as follows:

$$\sigma_{\ell} < \kappa \left| R_{\Delta} = [0] \right. \frac{1}{1+T_0} < \sigma_u \quad (160)$$

2. Analog LMS Algorithm

In an ALMS algorithm implementation, weights are updated in a continuous manner according to the vector differential equation

$$\frac{dw(t)}{dt} = \alpha [\hat{x}(t)\hat{r}^+(t) - \hat{x}(t)\hat{x}^+(t)w(t)] \quad (161)$$

This expression can be obtained from the DLMS algorithm equation by letting $\Delta t \rightarrow 0$. Clearly, Δt can no longer be considered the interval between independent samples.

In section B, it was shown that Equation (161) could be approximated by the ideal ALMS equation

$$\frac{d\bar{w}(t)}{dt} = \alpha (R_{xd} - K_x \bar{w}(t)) \quad (162)$$

provided the level of correlation between $w(t)$ and $\hat{x}(t)\hat{x}^+(t)$ was sufficiently small, i.e., $\alpha \Delta t \lambda_{\max} < 1$. The purpose in this section will be to determine a first order correction to the solution of

Equation (162) which takes into account correlation between $w(t)$ and $\underline{x}(t)\underline{x}^T(t)$ for higher loop bandwidths. Performance will be evaluated in terms of excess noise which appears at the array output due to weight jitter. Undesired signals are assumed sample functions from zero-mean Gaussian processes and the desired signal is assumed to have a constant envelope. To simplify the analysis, the input signals and the thermal noise processes are modeled as ideal bandpass processes with a (double-sided) bandwidth of B Hz. That is (see Equations (5 and 6)),

$$R_i(\tau) = \frac{\sin \pi B \tau}{\pi B \tau} \quad i = 1, 2, \dots, p \quad (163)$$

$$R_\sigma(\tau) = \frac{\sin \pi B \tau}{\pi B \tau}$$

The basic technique used to evaluate the effects of weight jitter is similar to that of the previous section in that the difference between the instantaneous and optimum weight vector will be studied when the mean weights are near their steady-state condition. As opposed to the DLMS algorithm case, however, the mean of Equation (161) does not necessarily converge to w_{opt} . To show this, the difference vector is defined as

$$\hat{z}(t) \equiv w(t) - \bar{w}(t) \quad (164)$$

where $\bar{w}(t)$ is the solution to the ideal ALMS equation (Equation (162)). It is important to note that $\bar{w}(t)$ is not the mean of the solution to the instantaneous ALMS equation (Equation (161)). Subtracting Equation (162) from Equation (161) yields the differential equation for $\hat{z}(t)$;

$$\frac{d\hat{z}(t)}{dt} = \alpha [R_\Delta(t) - K_X \hat{z}(t) - \phi(t) w(t)] \quad (165)$$

The random variables $R_\Delta(t)$ and $\phi(t)$ are defined in Equation (102) with t_{k-1} replaced by t . Let P be a unitary transformation which diagonalizes K_X . Multiplying both sides of Equation (165) by P , one obtains

$$\frac{dy_\Delta(t)}{dt} = \alpha [PR_\Delta(t) - \Lambda y_\Delta(t) - P\phi(t)\bar{w}(t) - P\phi(t)P^{-1}y_\Delta(t)] \quad (166)$$

where

$$y_\Delta(t) \equiv P\hat{z}(t) = P(w(t) - \bar{w}(t))$$

Equation (166) represents m differential equations of the form

$$\frac{dy_{i\Delta}(t)}{dt} = \alpha \{ [PR_{\Delta}(t)]_i - \lambda_i y_{i\Delta}(t) - [P\phi(t) \bar{w}(t)]_i - [P\phi(t) P^{-1} y_{\Delta}(t)]_i \} ; \quad i = 1, 2, \dots, m \quad (167)$$

In this expression, $y_{i\Delta}(t)$ represents the i^{th} component of vector $y_{\Delta}(t)$.

A solution to the homogeneous equation

$$\frac{dy_{i\Delta}^H(t)}{dt} + \alpha \lambda_i y_{i\Delta}^H(t) = 0$$

is given by

$$y_{i\Delta}^H(t) = y_{i\Delta}^H(t_0) e^{-\alpha \lambda_i (t-t_0)} \quad t \geq t_0 \quad (168)$$

The forced response is found by multiplying Equation (167) by $\exp[\alpha \lambda_i t]$ and integrating the result with respect to t :

$$y_{i\Delta}^F(t) = \alpha \int_{t_0}^t [PR_{\Delta}(\tau) - P\phi(\tau) \bar{w}(\tau) - P\phi(\tau) P^{-1} y_{\Delta}^F(\tau)]_i e^{-\alpha \lambda_i (t-\tau)} d\tau \quad (169)$$

For sufficiently long adaption times, the mean weight vector will be near its steady-state solution. The corresponding case for $y_{i\Delta}(t)$ is found by letting $t_0 \rightarrow \infty$. Thus, when the mean weight vector $y_{i\Delta}$ is near steady-state, $y_{i\Delta}(t)$ becomes

$$\lim_{t_0 \rightarrow \infty} y_{i\Delta}(t) = \lim_{t_0 \rightarrow \infty} y_{i\Delta}^H(t) + y_{i\Delta}^F(t) \quad (170)$$

or

$$y_{i\Delta}(t) = \alpha \int_{-\infty}^t [PR_{\Delta}(\tau) - P\phi(\tau) \bar{w}(\tau) - P\phi(\tau) P^{-1} y_{\Delta}(\tau)]_i e^{-\alpha \lambda_i (t-\tau)} d\tau \quad (171)$$

The ensemble average of Equation (171), provided it is stationary, may be expressed in vector form as

$$\bar{y}_\Delta \equiv E y_\Delta(t) = -\alpha E \int_{-\infty}^t e^{-\alpha\Lambda(t-\tau)} P\phi(\tau) P^{-1} y_\Delta(\tau) d\tau \quad (172)$$

which shows that the difference between the mean weights and the optimum weights are generally non-zero (even in steady-state). To find a first order approximation for Equation (172), assume $y_\Delta(\tau)$ is approximated by

$$y_\Delta(\tau) \triangleq -\alpha \int_{-\infty}^{\tau} e^{-\alpha\Lambda(\tau-\tau_1)} [PR_\Delta(\tau_1) - P\phi(\tau_1)\bar{w}] d\tau_1 \quad (173)$$

Employing this assumption, Equation (172) becomes

$$\begin{aligned} \bar{y}_\Delta \triangleq & -\alpha^2 \int_{-\infty}^t \int_{-\infty}^{\tau} e^{-\alpha\Lambda(t-\tau)} E \{ P\phi(\tau)P^{-1} e^{-\alpha\Lambda(\tau-\tau_1)} PR_\Delta(\tau_1) \} d\tau d\tau_1 \\ & + \alpha^2 \int_{-\infty}^t \int_{-\infty}^{\tau} e^{-\alpha\Lambda(t-\tau)} E \{ P\phi(\tau)P^{-1} e^{-\alpha\Lambda(\tau-\tau_1)} P\phi(\tau_1)\bar{w} \} d\tau d\tau_1 \end{aligned} \quad (174)$$

Following the steps used in deriving Equation (122), the second matrix enclosed by brackets in Equation (174) can be shown to have the ij th component

$$\begin{aligned} E [\phi(\tau) A\phi(\tau_1)]_{ij} &= TR [A(\gamma) K_x(-\gamma)] K_{x_{ij}}(\gamma) \\ &- TR [A(\gamma) \underline{s} \underline{s}^\dagger(-\gamma)] [\underline{s} \underline{s}^\dagger(\gamma)]_{ij} \end{aligned} \quad (175)$$

where $\gamma = \tau - \tau_1$ (176)

$$\begin{aligned} K_x(\gamma) &= E[\underline{\tilde{x}}(\tau) \underline{\tilde{x}}^\dagger(\tau_1)] = K_x^\dagger(-\gamma) \\ \underline{s} \underline{s}^\dagger(\gamma) &= E[\underline{\tilde{s}}(\tau) \underline{\tilde{s}}^\dagger(\tau_1)] = [\underline{s} \underline{s}^\dagger(-\gamma)]^\dagger \end{aligned}$$

The second term in Equation (174) is evaluated by letting

$$A(\gamma) = P^{-1} e^{-\alpha\Lambda(\tau-\tau_1)} P \quad (177)$$

and substituting Equation (175) into the kernel of the integral. The result is expressed by the m -dimensional vector

(178)

$$\begin{aligned}
D(t) &= \alpha^2 \int_{-\infty}^t \int_{-\infty}^{\tau} e^{-\alpha\Lambda(t-\tau)} E \{ P\phi(\tau)P^{-1} e^{-\alpha\Lambda(\tau-\tau_1)} P\phi(\tau_1)\bar{w} \} d\tau_1 d\tau \\
&= \alpha^2 \int_{-\infty}^t \int_{-\infty}^{\tau} e^{-\alpha\Lambda(t-\tau)} \text{TR}[P^{-1} e^{-\alpha\Lambda(\tau-\tau_1)} PK_X(\tau-\tau_1)] \\
&\quad \cdot PK_X(\tau_1-\tau)\bar{w} d\tau_1 d\tau - \alpha^2 \int_{-\infty}^t \int_{-\infty}^{\tau} e^{-\alpha\Lambda(t-\tau)} \\
&\quad \cdot \text{TR}[P^{-1} e^{-\alpha\Lambda(\tau-\tau_1)} P \underline{s} \underline{s}^\dagger(\tau-\tau_1)] P \underline{s} \underline{s}^\dagger(\tau_1-\tau)\bar{w} d\tau_1 d\tau
\end{aligned}$$

The first term in Equation (174) is evaluated in a similar manner. Adding the two results, rearranging terms, and transforming variables where appropriate yields

(179)

$$\begin{aligned}
\bar{y} &= \alpha^2 \int_{-\infty}^t \int_{-\infty}^{\tau} e^{-\alpha\Lambda(t-\tau)} P \{ \text{TR}[e^{-\alpha K_X(\tau-\tau_1)} K_X(\tau-\tau_1)] \\
&\quad \cdot K_X(\tau_1-\tau) K_X^{-1} R_{xd} - \text{TR}[e^{-\alpha K_X(\tau-\tau_1)} M(\tau_1-\tau)] R_{xd}(\tau-\tau_1) \\
&\quad - \text{TR}[e^{-\alpha K_X(\tau-\tau_1)} \underline{s} \underline{s}^\dagger(\tau_1-\tau)] \underline{s} \underline{s}^\dagger(\tau_1-\tau) K_X^{-1} R_{xd} \} d\tau_1 d\tau
\end{aligned}$$

where

$$\begin{aligned}
K_X &\equiv K_X(0) \\
R_{xd} &\equiv R_{xd}(0) \\
\underline{s} \underline{s}^\dagger &= \underline{s} \underline{s}^\dagger(0) \\
M &\equiv M(0)
\end{aligned}$$

Using Equation (163) and the identity $\bar{w} = K_X^{-1} R_{xd}$, Equation (179) reduces to

$$\bar{y}_\Delta = \frac{\alpha^2}{T+T_0} \int_{-\infty}^t \int_{-\infty}^{\tau} f(\tau-\tau_1) e^{-\alpha\Lambda(t-\tau)} P R_{xd} d\tau d\tau_1 \quad (180)$$

where

$$f(\tau-\tau_1) = \underline{s}^+ P^{-1} e^{-\alpha\Lambda(\tau-\tau_1)} P \underline{s} \frac{\sin^2_{\pi} B(\tau-\tau_1)}{[\pi B(\tau-\tau_1)]^2} \quad (181)$$

The function $f(\tau-\tau_1)$ is real and positive and has the upper bound

$$f(\tau-\tau_1) \leq P_s \frac{\sin^2_{\pi} B(\tau-\tau_1)}{[\pi B(\tau-\tau_1)]^2}$$

Thus,

$$\begin{aligned} \bar{y} &= g \frac{\alpha^2}{1+T_0} \int_{-\infty}^t \int_{-\infty}^{\tau} P_s \frac{\sin^2_{\pi} B(\tau-\tau_1)}{[\pi B(\tau-\tau_1)]^2} e^{-\alpha\Omega(t-\tau)} PR_{xd} \cdot d\tau d\tau_1 \quad (182) \\ &= g \frac{\alpha}{2B} P_s \frac{1}{1+T_0} \Omega^{-1} PR_{xd} \\ &= g \frac{\alpha}{2B} P_s \frac{1}{1+T_0} Pw_{opt} \end{aligned}$$

where g is a real number less than one. By the sampling theorem, B^{-1} is the interval between independent samples of the input process. Equation (182) may therefore be expressed in terms of the interval (Δt) between independent samples as

$$\bar{y}_{\Delta} = \beta Pw_{opt} \quad (183)$$

where $\beta = g \frac{\alpha\Delta t}{2} \frac{P_s}{1+T_0}$

The mean of the solution to the instantaneous weight equation [Equation (161)] is approximated by

$$Ew(t) \Big|_{t \rightarrow \infty} = (\tilde{z}(t) + w_{opt}) \Big|_{t \rightarrow \infty} = (\beta + 1)w_{opt} \quad (184)$$

Consequently, the output signal-to-noise ratio is unaffected even though the difference between $Ew(t)$ (in steady-state) and w_{opt} is non-zero. Note that the magnitude of \bar{y}_Δ is small compared to the magnitude of w_{opt} for $\alpha\Delta t P_s \ll 1$.

When $R_{\Delta d}$ is given ($R_\Delta = [0]$ case), Equation (179) becomes

$$\bar{y} = \alpha^2 \int_{-\infty}^t \int_{-\infty}^{\tau} e^{-\alpha\Lambda(t-\tau)} \frac{\sin^2 \pi B(\tau-\tau_1)}{[\pi B(\tau-\tau_1)]^2} \quad (185)$$

$$\cdot \sum_{i=1}^m e^{-\alpha\lambda_i(\tau-\tau_1)} \lambda_i P K_x w_{opt} - \underline{s}^\dagger P^{-1} e^{-\alpha\Lambda(\tau-\tau_1)} P \underline{s}$$

$$\cdot P \underline{s} \underline{s}^\dagger w_{opt} \quad d\tau d\tau_1$$

By employing the same procedure used to derive Equation (184), it can be shown that Equation (185) reduces to

$$\bar{y}_\Delta \approx g \frac{\alpha\Delta t}{2} P_I - \frac{T_0}{1+T_0} P_s P w_{opt} ; \quad R_\Delta = [0]$$

Again, directional properties of \bar{y}_Δ are such that the output SNR remains unaffected, although the magnitude of \bar{y}_Δ is much larger than in the $R_\Delta \neq [0]$ case.

Equations (182) and (186) represent first order approximations for the difference between the mean weight vector and the optimum weight vector; thus, they are accurate only for small values of $\alpha\Delta t P_I$ ($\ll 1$). An expression for \bar{y}_Δ which is accurate for larger values of $\alpha\Delta t P_I$ can be obtained by employing a second order correction to Equation (173), i.e.,

$$y_\Delta(\tau) = \alpha \int_{-\infty}^{\tau} e^{-\alpha\Lambda(\tau-\tau_1)} [P R_\Delta(\tau_1) - P\phi(\tau_1)\bar{w} - P\phi(\tau_1)P^{-1} y_\Delta(\tau_1)] d\tau$$

where $y_\Delta(\tau_1)$ is approximated as in Equation (173). Approximate expressions for \bar{y}_Δ , derived using this second order correction, are given by

$$\bar{y}_\Delta \Big|_{R_\Delta \neq [0]} \triangleq \frac{\alpha \Delta t}{2} \frac{P_s}{1 + T_0} - \frac{(\alpha \Delta t)^2}{2} P_s^2 P_{w_{opt}} \quad (187)$$

$$- \frac{(\alpha \Delta t)^2}{2} [\Lambda^{-1} P_{ss}^\dagger M R_{xd} + P_{ss}^\dagger R_{xd}]$$

$$\bar{y}_\Delta \Big|_{R_\Delta = [0]} \triangleq \left[\frac{\alpha \Delta t}{2} \left(P_I - \frac{T_0}{1 + T_0} P_s \right) - \frac{(\alpha \Delta t)^2}{2} P_I^2 \right] P_{w_{opt}}$$

$$- \frac{(\alpha \Delta t)^2}{2} \Lambda P R_{xd}$$

The above results indicate that the output signal-to-noise ratio of the filter $E w(t)$ degrades as $\alpha \Delta t P_I$ is increased, since \bar{y}_Δ is no longer co-linear with w_{opt} . Moreover, the extent of degradation is dependent upon the covariance matrix and the arrival angles of the signal sources. To simplify subsequent analyses of the effects of weight jitter, any deviation of $w(t)$ from w_{opt} is assumed to degrade the output signal-to-noise ratio. Since \bar{y}_Δ in Equation (187) or (188) has a component directed along w_{opt} , the expression to be obtained for excess noise power at the array output due to weight jitter will represent an upper bound.

Evaluation of the total output power is more difficult compared to the DLMS case since the processes $w(t)$ and $x(t)$ can no longer be assumed independent. In particular, cross-terms in the expression for the output power (Equation (138)) must be retained:

$$P_T = w_{opt}^\dagger K_x w_{opt} + E \left\{ \hat{z}^\dagger(t) \tilde{x}(t) \tilde{x}^\dagger(t) w_{opt} \right. \quad (189)$$

$$\left. + w_{opt}^\dagger \tilde{x}(t) \tilde{x}^\dagger(t) \hat{z}(t) + \hat{z}^\dagger(t) \tilde{x}(t) \tilde{x}^\dagger(t) \hat{z}(t) \right\}$$

Substituting $\phi(t) = \tilde{x}(t) \tilde{x}^\dagger(t) - K_x$ and $y(t) = P \hat{z}(t)$, and performing the indicated ensemble averages, Equation (189) reduces to

(190)

$$\begin{aligned}
P_T = & w_{opt}^\dagger K_x w_{opt} + E[y_\Delta^\dagger(t) P_\phi(t) w_{opt}] + E[w_{opt}^\dagger \phi(t) P^{-1} y_\Delta(t)] \\
& + E[y_\Delta^\dagger(t) P_\phi(t) P^{-1} y_\Delta(t)] + E[y_\Delta^\dagger(t) \Lambda y_\Delta(t)] \\
& + E[y_\Delta^\dagger(t) P K_x w_{opt}] + E[w_{opt}^\dagger K_x P^{-1} y_\Delta(t)]
\end{aligned}$$

Terms in Equation (190) containing w_{opt} can be further reduced using techniques established in the derivation of Equations (183) and (186). It can be shown that the cross-terms in Equation (190) cancel, so that

$$\begin{aligned}
P_T = & |r|^2 \frac{T_o}{T + T_o} + E[y_\Delta^\dagger(t) P_\phi(t) P^{-1} y_\Delta(t)] \\
& + E[y_\Delta^\dagger(t) \Lambda y_\Delta(t)]
\end{aligned} \tag{191}$$

Since evaluation of the middle term in Equation (191) is the most difficult, the steps involved will be given in reasonable detail; procedures for evaluating the last term are similar (though less involved) and will not be repeated. To simplify the analysis, $y_{i\Delta}(t)$ in Equation (171) will be approximated by the components of the vector in Equation (173). A first order correction to results obtained under this assumption will then be given.

For the $R_\Delta \neq [0]$ case, the middle term in Equation (191) may be expressed as

$$\begin{aligned}
E y^\dagger(t) P_\phi(t) P^{-1} y_\Delta(t) = & \alpha^2 E \int_{-\infty}^t \int_{-\infty}^{\tau_1} \left\{ [R_\Delta^\dagger(\tau_1) P^{-1} \right. \\
& - w_{opt}^\dagger \phi(\tau_1) P^{-1}] \exp[-\alpha\Lambda(t-\tau_1)] P_\phi(t) P^{-1} \\
& \left. \cdot \exp[-\alpha\Lambda(t-\tau_2)] [P R_\Delta(\tau_2) - P\phi(\tau_2) w_{opt}] \right\} d\tau_1 d\tau_2
\end{aligned} \tag{192}$$

Equation (192) contains the third order moments of the process $\phi(t)$. After very tedious algebraic manipulation, it can be shown that

$$E \phi_{ij}^*(\tau_1) \phi_{k\ell}(t) \phi_{mn}(\tau_2) = \quad (193)$$

$$\begin{aligned} & K_{X_{j\ell}}(\tau_1-t) K_{X_{kn}}(t-\tau_2) K_{X_{mi}}(\tau_2-\tau_1) \\ & + K_{X_{jn}}(\tau_1-\tau_2) K_{X_{ki}}(t-\tau_1) K_{X_{m\ell}}(\tau_2-t) \\ & - s_i^*(\tau_1) s_k(t) K_{X_{jn}}(\tau_1-\tau_2) s_m(\tau_2) s_\ell^*(t) \\ & - s_n^*(\tau_2) s_k(t) s_j(\tau_1) s_\ell^*(t) K_{X_{mi}}(\tau_2-\tau_1) \\ & - s_n^*(\tau_2) s_k(t) K_{X_{j\ell}}(\tau_1-t) s_m(\tau_2) s_i^*(\tau_1) \\ & - K_{X_{kn}}(t-\tau_2) s_j(\tau_1) s_\ell^*(t) s_m(\tau_2) s_i^*(\tau_1) \\ & - s_i^*(\tau_1) s_k(t) s_j(\tau_1) s_n^*(\tau_2) K_{X_{m\ell}}(\tau_2-t) \\ & - s_\ell^*(t) s_m(\tau_2) s_j(\tau_1) s_n^*(\tau_2) K_{X_{ki}}(t-\tau_1) \end{aligned}$$

Now

$$E w_{opt}^\dagger \phi^\dagger(\tau_1) A_1^{(1)} \phi(t) A_2^{(2)} \phi(\tau_2) w_{opt} = \quad (194)$$

$$\sum_i \sum_j \sum_k \sum_\ell \sum_m \sum_n \bar{w}_i^* \beta_{ji}^*(\tau_1) A_{jk}^{(1)} \phi_{k\ell}(t) A_{\ell m}^{(2)} \phi_{mn}(\tau_2) \bar{w}_n$$

Substituting Equation (193) into (194) yields the result

$$E w_{opt}^\dagger \phi^\dagger(\tau_1) A^{(1)} \phi(t) A^{(2)} \phi(\tau_2) w_{opt} = \quad (195)$$

$$\begin{aligned} & w_{opt}^\dagger K_X(\tau_1-t) \exp[-\alpha K_X(t-\tau_2)] K_X(\tau_2-\tau_1) \\ & \cdot \exp[-\alpha K_X(t-\tau_1)] K_X(t-\tau_2) w_{opt} + w_{opt}^\dagger K_X(\tau_1-\tau_2) w_{opt} \end{aligned}$$

$$\cdot \text{TR}[\exp[-\alpha K_x(t-\tau_1)]] \text{TR}[\exp[-\alpha K_x(t-\tau_2)]] K_x(\tau_2-t)]$$

+ Terms in $s_k(\gamma)$ where $k = 1, 2, \dots, m$ and $\gamma = t, \tau_1, \text{ or } \tau_2$

where

$$A^{(1)} = p^{-1} e^{-\alpha\Lambda(t-\tau_1)} p$$

$$A^{(2)} = p^{-1} e^{-\alpha\Lambda(t-\tau_2)} p$$

Assuming that the input desired signal power is much smaller than the total input power, the terms in $S_k(\gamma)$ can be neglected. Also, by assuming the same input signal structure employed in deriving y , Equation (195) reduces to

$$E w_{\text{opt}}^\dagger \phi^\dagger(\tau_1) A^{(1)} \phi(t) A^{(2)} \phi(\tau_2) w_{\text{opt}} \doteq \quad (196)$$

$$\left\{ R_{\text{Xd}}^\dagger p^{-1} \Lambda e^{-\alpha\Lambda(t-\tau_1)} e^{-\alpha\Lambda(t-\tau_2)} p R_{\text{Xd}} \right.$$

$$+ R_{\text{Xd}}^\dagger K_x^{-1} R_{\text{Xd}} \left[\sum_{i=1}^m \lambda_i e^{-\alpha\lambda_i(t-\tau_1)} \right]$$

$$\cdot \left. \left[\sum_{j=1}^m \lambda_j e^{-\alpha\lambda_j(t-\tau_2)} \right] \right\}$$

$$\cdot \frac{\sin \pi B(\tau_2-\tau_1)}{\pi B(\tau_2-\tau_1)} \frac{\sin \pi B(t-\tau_1)}{\pi B(t-\tau_1)} \frac{\sin \pi B(t-\tau_2)}{\pi B(t-\tau_2)}$$

To simplify the double integral of Equation (196) contained in Equation (192), each integral will be approximated by a double sum. That is,

$$D(t) \doteq \int_{-\infty}^t \int_{-\infty}^{\tau} w_{\text{opt}}^\dagger \phi^\dagger(\tau_1) A^{(1)} \phi(t) A^{(2)} \phi(\tau_2) w_{\text{opt}} d\tau_1 d\tau_2 \quad (197)$$

$$\doteq (\Delta t)^2 \sum_{i=-\infty}^{t/\Delta t} \sum_{j=-\infty}^{t/\Delta t} w_{\text{opt}}^\dagger \phi^\dagger(i\Delta t) A^{(1)} \phi(t) A^{(2)} \phi(j\Delta t) w_{\text{opt}}$$

$$\begin{aligned}
& \text{(197) (continued)} \\
& = (\Delta t)^2 \sum_{i=-\infty}^{t/\Delta t} \sum_{j=-\infty}^{t/\Delta t} \left\{ R_{xd}^+ P^{-1} \Lambda e^{-\alpha\Lambda(t-i\Delta t)} e^{-\alpha\Lambda(t-j\Delta t)} P R_{xd} \right. \\
& \quad + R_{xd}^+ K_x^{-1} R_{xd} \left[\sum_{k=1}^m \lambda_k e^{-\alpha\lambda_k(t-i\Delta t)} \right] \\
& \quad \cdot \left. \left[\sum_{j=1}^m \lambda_j e^{-\alpha\lambda_j(t-j\Delta t)} \right] \right\} \\
& \quad \cdot \frac{\sin \pi B[(j-i)\Delta t]}{\pi B[(j-i)\Delta t]} \frac{\sin \pi B(t-i\Delta t)}{\pi B(t-i\Delta t)} \frac{\sin \pi B(t-j\Delta t)}{\pi B(t-j\Delta t)}
\end{aligned}$$

Next, let Δt equal the interval between independent samples of the input signals ($= B^{-1}$). For this case, the double sum in Equation (197) reduces to

$$\begin{aligned}
& \text{(198)} \\
D(t) & \approx (\Delta t)^2 \sum_{i=-\infty}^{t/\Delta t} \left\{ R_{xd}^+ P^{-1} \Lambda e^{-2\alpha\Lambda(t-i\Delta t)} P R_{xd} \right. \\
& \quad + R_{xd}^+ K_x^{-1} R_{xd} \left[\sum_{k=1}^m \lambda_k e^{-\alpha\lambda_k(t-i\Delta t)} \right]^2 \left. \right\} \frac{\sin^2 \pi B(t-i\Delta t)}{[\pi B(t-i\Delta t)]^2} \\
& \approx \Delta t \int_{-\infty}^t \left\{ R_{xd}^+ P^{-1} \Lambda e^{-2\alpha\Lambda(t-\tau)} P R_{xd} \right. \\
& \quad + R_{xd}^+ K_x^{-1} R_{xd} \left[\sum_{k=1}^m \lambda_k e^{-\alpha\lambda_k(t-\tau)} \right]^2 \left. \right\} \\
& \quad \cdot \frac{\sin^2 \pi B(t-\tau)}{[\pi B(t-\tau)]^2} d\tau \\
& = g_1 \Delta t \int_{-\infty}^t \left\{ R_{xd}^+ P^{-1} \Lambda P R_{xd} + R_{xd}^+ K_x^{-1} R_{xd} \left[\sum_{k=1}^m \lambda_k \right]^2 \right\} \\
& \quad \cdot \frac{\sin^2 \pi B(t-\tau)}{[\pi B(t-\tau)]^2} d\tau \\
& = g_1 \frac{\Delta t}{2B} |\tilde{r}|^2 \left[\underline{s} P^{-1} \Lambda P \underline{s} + \frac{T_o}{T+T_o} P I^2 \right]
\end{aligned}$$

where g_1 is a real constant less than or equal to one. When $\alpha \Delta t P_I \ll 1$, $g_1 \approx 1$. Thus, $D(t)$ has the upper bound

$$D(t) \leq \frac{1}{2} (\Delta t)^2 |\tilde{r}|^2 \left[\underline{s}^\dagger P^{-1} \Delta P \underline{s} + \frac{T_0}{1+T_0} P_I^2 \right]$$

where B^{-1} in Equation (196) was set to equal to Δt . Remaining terms in Equation (192) are evaluated in a similar manner. The result may be written

$$E[y_\Delta^\dagger(t) P_\phi(t) P^{-1} y_\Delta(t)] \approx \quad (199)$$

$$\frac{\alpha^2 (\Delta t)^2}{2} |\tilde{r}|^2 \left\{ P_N^2 \frac{1}{1+T_0} + \underline{s}^\dagger P^{-1} \Delta P \underline{s} + \frac{T_0}{1+T_0} P_N P_S + P_S^2 \right\}$$

where P_N and P_S denote the input undesired and desired signal powers, respectively. Note that P_N^2 is the dominant term for $P_N^2 \gg (1+T_0)P_S^2$.

The steps required to evaluate the remaining term in Equation (191) is similar to the procedure outlined above; thus only the result will be given:

$$E[y_\Delta^\dagger(t) \Delta y_\Delta(t)] \approx \frac{\alpha \Delta t}{2} |\tilde{r}|^2 \left[P_N \frac{1}{1+T_0} + P_S \frac{T_0}{(1+T_0)^2} \right] \quad (200)$$

Consequently, for $R_\Delta \neq 0$,

$$P_T \approx |\tilde{r}|^2 \left\{ \frac{T_0}{1+T_0} + \frac{1}{2} \frac{\alpha \Delta t P_N}{1+T_0} + \frac{\alpha \Delta t P_S T_0}{(1+T_0)^2} \right. \\ \left. + \frac{(\alpha \Delta t P_N)^2}{2(1+T_0)} + \frac{1}{2} (\alpha \Delta t)^2 \underline{s}^\dagger P^{-1} \Delta P \underline{s} \right. \\ \left. + \frac{(\alpha \Delta t)^2 P_N P_S T_0}{2(1+T_0)} + \frac{(\alpha \Delta t P_S)^2}{2} \right\} \quad (201)$$

The approximation in Equation (201) was derived assuming the last term in Equation (171) negligible. Also, accuracy depends on the assumption $\alpha \lambda_{\max} \ll B$. To obtain a first order correction to Equation (201) which applies for higher loop bandwidths, let

$$y_{\Delta}(t) = \alpha \int_{-\infty}^t e^{-\alpha\Lambda(t-\tau)} [PR_{\Delta}(\tau) - P\phi(\tau)\bar{w} - P\phi(\tau)P^{-1}y_{\Delta}(\tau)] d\tau \quad (202)$$

where $y_{\Delta}(\tau)$ in Equation (202) is approximated by Equation (173). In this case, additional terms appear on the right side of Equation (200):

$$\begin{aligned} E y_{\Delta}^{\dagger}(t) \Lambda y_{\Delta}(t) &\approx \frac{\alpha \Delta t}{2} |r|^2 \frac{P_N}{1 + T_0} + \frac{T_0 P_S}{(1 + T_0)^2} \\ &- \frac{\alpha \Delta t}{2} E y_{\Delta}^{\dagger} P \phi^{\dagger} [R_{\Delta} - \phi \bar{w}] - \frac{\alpha \Delta t}{2} E [R_{\Delta}^{\dagger} - \bar{w}^{\dagger} \phi^{\dagger}] \phi P^{-1} y_{\Delta} \\ &+ \frac{\alpha \Delta t}{2} E [y_{\Delta}^{\dagger} P \phi^{\dagger} \phi P^{-1} y_{\Delta}] + E (y_{\Delta}^{\dagger} P \phi^{\dagger} P^{-1}) \Lambda E P \phi P^{-1} y_{\Delta} \end{aligned} \quad (203)$$

where

$$\phi = \phi(t), R_{\Delta} = R_{\Delta}(t), \text{ and } y_{\Delta} = y_{\Delta}(t).$$

Calculation of each of these expectations show that all terms are small compared to the term $\alpha \Delta t E [y_{\Delta}^{\dagger} P \phi \phi^{\dagger} P^{-1} y_{\Delta}]$ when $P_S \ll P_N$. Its value is approximated by

$$\begin{aligned} E y_{\Delta}^{\dagger} P \phi^{\dagger} \phi P^{-1} y_{\Delta} &\approx E y_{\Delta}^{\dagger} \Lambda y_{\Delta} P_I - E y_{\Delta}^{\dagger} P \underline{\underline{P}} P^{-1} y_{\Delta} P_S \\ &\approx E y_{\Delta}^{\dagger} \Lambda y_{\Delta} P_I \end{aligned}$$

Thus, after a first order correction, $E y_{\Delta}^{\dagger} \Lambda y_{\Delta}$ is approximated by

$$E y_{\Delta}^{\dagger} \Lambda y_{\Delta} \approx \frac{\alpha \Delta t}{2 - \alpha \Delta t P_I} |r|^2 P_N \frac{1}{1 + T_0} + \frac{T_0 P_S}{(1 + T_0)^2} \quad (204)$$

First order corrections to Equation (192) yield terms in $(\alpha \Delta t P_I)^n$, where $n \geq 3$. These terms can be neglected for $\alpha \Delta t P_i \ll 0.5$.

In summary, if (1) $\alpha\Delta t P_I \approx 0.5$, (2) $P_S \ll P_N$, (3) noise and interference approximate sample functions from zero-mean Gaussian processes, and (4) the spectrum of $\tilde{x}(t)$ approximates an ideal bandpass characteristic, then the total array output power is approximated (bounded above) by

$$P_T \approx |\tilde{r}|^2 \left\{ \frac{T_0}{1+T_0} + \frac{\alpha\Delta t}{2 - \alpha\Delta t P_I} \frac{P_N}{1+T_0} + \frac{T_0 P_S}{(1+T_0)^2} \right. \\ \left. + \frac{(\alpha\Delta t)^2 P_N^2}{2(1+T_0)} + \frac{(\alpha\Delta t)^2}{2} \underline{P^{-1} \Lambda P} + \frac{(\alpha\Delta t)^2 P_N P_S T_0}{2(1+T_0)} \right. \\ \left. + \frac{\alpha\Delta t P_S^2}{2} \right\} \quad (205)$$

Since $P_S \ll P_N$, the approximation in Equation (205) can be further simplified to

$$P_T \approx |\tilde{r}|^2 \frac{T_0}{1+T_0} + \frac{\alpha\Delta t P_I}{2 - \alpha\Delta t P_I} \frac{|\tilde{r}|^2}{1+T_0} + \frac{(\alpha\Delta t P_N)^2 |\tilde{r}|^2}{2(1+T_0)} \quad (206)$$

The second term in Equation (206) represents excess noise power due to weight jitter:

$$P_{EN} \approx \frac{\alpha\Delta t |\tilde{r}|^2}{2 - \alpha\Delta t P_I} \frac{P_I}{1+T_0} + \frac{(\alpha\Delta t P_N)^2}{2} \frac{|\tilde{r}|^2}{1+T_0} \quad (207)$$

The last two terms in Equation (191) were also evaluated for the $R_\Delta = [0]$ case. The resulting expression for the excess noise power due to weight jitter was found to be approximated by the product of Equation (207) and the optimum output signal-to-noise ratio (T_0); this is the same relationship between the $R_\Delta = [0]$ and $R_\Delta \neq [0]$ cases obtained for the digital LMS algorithm.

A comparison of Equations (133) and (207) indicates a similarity between the expressions for excess noise power derived for the digital and analog LMS control loops. For $\alpha\Delta t P_I \ll 1$, the parameter $\alpha\Delta t C$ in Equation (133) is approximated by $\alpha\Delta t P_I / 2$. Thus, the excess noise power at the array output due to jitter is nearly the same for both the ALMS and DLMS configurations when the loop bandwidth is much smaller than the input signal bandwidth. For larger values of $\alpha\Delta t P_I$ (up to a value of one), the excess noise power in Equation (207) (normalized to $T_0^{-1} (1+T_0) \|\mathbf{u}_{opt}\|^2$) remains between the bounds σ_ℓ and σ_u derived for the DLMS case (see Figure 12). This similarity is not

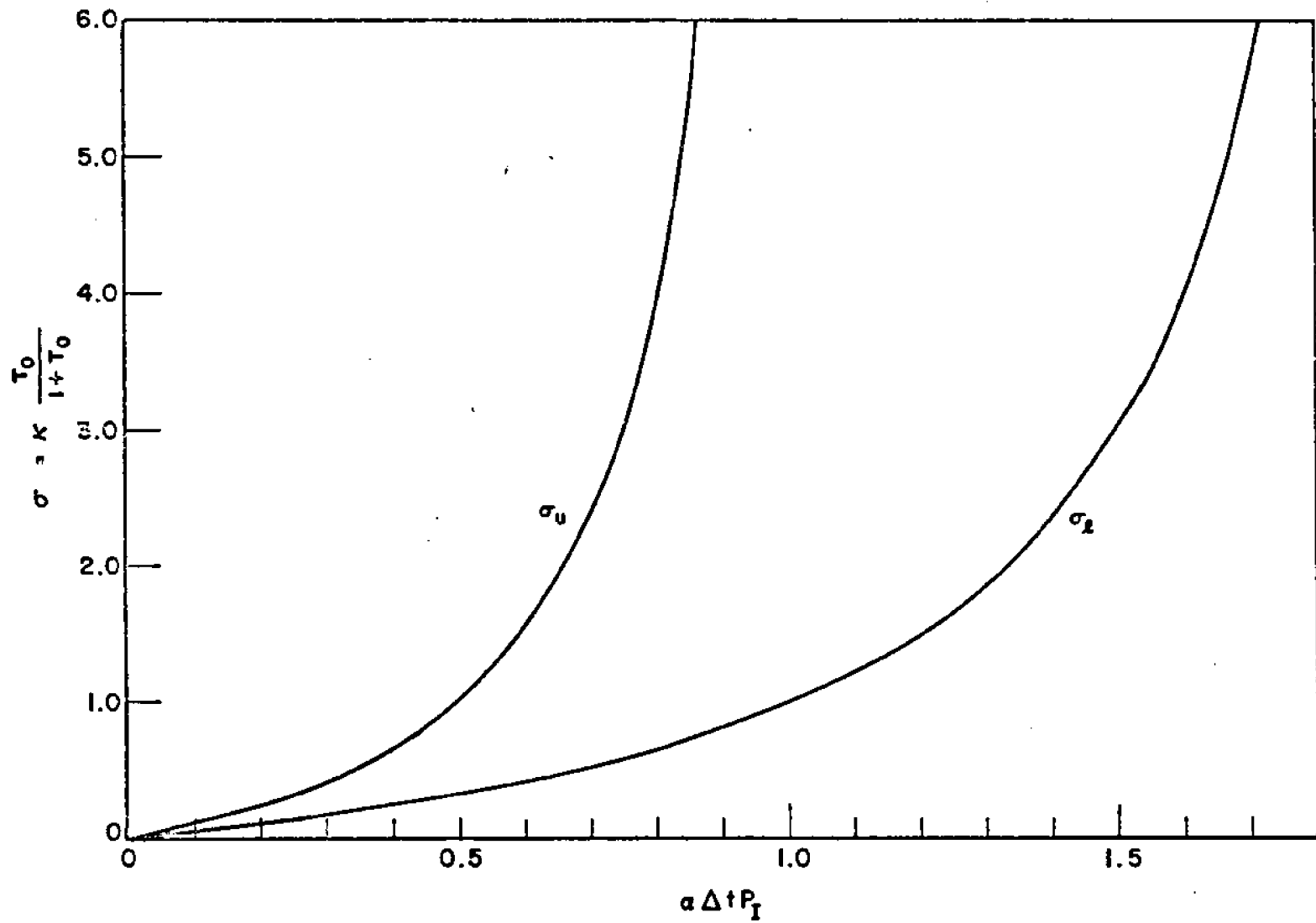


Figure 12--Upper and lower bounds on the (normalized) ratio of the excess noise power to the noise power without jitter.

surprising, since the two derivations were based on similar assumptions regarding independent samples. It also follows from the sampling theorem that the performance of the LMS loop would not change significantly by simply reducing the interval between weight updates to zero (analog case). It is important to note, however, that a fundamental difference exists between the analog and digital control loops under high loop bandwidth conditions. The digital loop was shown to become unstable when the loop bandwidth exceeds a certain value, whereas the analog loop remains "stable" for all values of α . For α sufficiently large, the analog loop will respond to minimize the instantaneous error between the array output and the reference signal, i.e., the array output signal can equal the reference signal even though the desired signal power at the array output is small relative to the total output power. This points out one of the difficulties encountered when analyzing the effects of weight jitter on ALMS loop performance. The purpose of the adaptive array is to optimize the array output by forming an appropriate pattern rather than to "modulate" the input signals so that they match the temporal structure of the reference signal. Clearly, the latter phenomenon cannot be tolerated when the reference signal is generated from the array output via waveform processing (which is the case of interest). For this reason, the excess noise (Equation (207)) is considered to be additive system noise, even though the excess noise is correlated with the reference signal (and thus the desired signal). This assumption is further discussed in Chapter VI.

E. The Effects of Weight Jitter on Desired Signal Coherence

1. Introduction

In preceding sections of this chapter, the effects of weight jitter have been evaluated by determining the excess noise power it generates at the array output. Results obtained can be used as general guidelines for system design. However, the power measure provides little information regarding the effects of weight jitter on the phase of the desired signal. Such information is important in many systems, particularly those employing coherent or partially coherent phase detectors to demodulate the received signal.

In the following two sections, the effects of weight jitter on coherence of the desired signal will be evaluated for systems employing the DLMS algorithm. These results can be used to approximate the ALMS algorithm with appropriate assumptions. As in previous sections of this chapter, the signal environment is

assumed to consist of zero-mean, Gaussian, undesired signals and a PN-coded desired signal. In the following section, an expression for the variance of the output signal phase is derived which applies when the desired signal phase fluctuations are small. Then, in the last section, a specific example is considered in which the effects of weight jitter on the average output signal-to-noise ratio of a coherent detector are determined.

2. Desired Signal Amplitude and Phase Jitter

Weight jitter not only causes excess noise to appear at the array output, but also randomly phase modulates the desired signal. The resulting phase jitter tends to decohere the desired signal at the array output, thus further degrading system performance. Desired signal phase jitter can be viewed as resulting from pattern fluctuations in the desired signal DOA, which is equal to a complex multiple of the cross-correlation vector R_{xd} . Thus, the array output in response to a cw signal arriving at the array input from this direction is proportional to [see Equation (46)]

$$\begin{aligned}\hat{w}^\dagger(t)R_{xd} &= \hat{z}^\dagger(t)R_{xd} + w_{opt}^\dagger R_{xd} \\ &= y_\Delta^\dagger P R_{xd} + |\tilde{r}|^2 \frac{T_o}{T + T_o}\end{aligned}\quad (208)$$

The expression in Equation (208) is, in general, a complex number and thus can be written

$$w^\dagger R_{xd} = \left| \hat{w}^\dagger R_{xd} \right| e^{j\theta} \quad (209)$$

where

$$\theta = \tan^{-1} \left[\frac{\text{Im} \{ y_\Delta^\dagger P R_{xd} \}}{|\tilde{r}|^2 \frac{T_o}{T + T_o} + \text{Re} \{ y_\Delta^\dagger P R_{xd} \}} \right] \quad (210)$$

Here $\text{Im} \{ \}$ and $\text{Re} \{ \}$ denote the real and imaginary parts of the expression enclosed by parentheses. To linearize Equation (210), it is assumed that

$$\left| y_\Delta^\dagger P R_{xd} \right| \approx \frac{1}{3} |\tilde{r}|^2 \frac{T_o}{T + T_o} \quad (211)$$

In other words, the absolute value of θ is assumed smaller than about one-half radian. In this case, Equation (210) is bounded by

$$|\theta| < |\theta_\ell| < \left| \tan^{-1} \left[\frac{3}{2} \frac{\text{Im}\{y_{\Delta}^{\dagger} P_{R_{xd}}\}}{|\tilde{r}|^2 \frac{T_0}{1+T_0}} \right] \right| \quad (212)$$

where

$$\theta_\ell = \sqrt{2} \frac{\text{Im}\{y_{\Delta}^{\dagger} P_{R_{xd}}\}}{|\tilde{r}|^2 \frac{T_0}{1+T_0}}$$

The first and second moments of θ_ℓ are given by

$$E \theta_\ell = 0 \quad (213)$$

and

$$E \theta_\ell^2 = 2 \frac{(1+T_0)^2}{T_0^2 r^4} E[\text{Im}\{y_{\Delta}^{\dagger} P_{\underline{s}}\}]^2 = \text{Var}(\theta_\ell).$$

Since

$$\begin{aligned} E[\text{Im}\{y_{\Delta}^{\dagger} P_{\underline{s}}\}]^2 &= \frac{1}{2} E[(\text{Re}\{y_{\Delta}^{\dagger} P_{\underline{s}}\})^2 + (\text{Im}\{y_{\Delta}^{\dagger} P_{\underline{s}}\})^2] \\ &\leq E y_{\Delta}^{\dagger} P_{\underline{s}} \underline{s} \underline{s}^{\dagger} P^{-1} y_{\Delta} \end{aligned} \quad (214)$$

an upper bound on $E \theta_\ell^2$ is given by

$$E \theta_\ell^2 \leq \frac{(1+T_0)^2}{T_0^2 |\tilde{r}|^2} E y_{\Delta}^{\dagger} P_{\underline{s}} \underline{s} \underline{s}^{\dagger} P^{-1} y_{\Delta} \quad (215)$$

From Equations (116) and (126)

$$\begin{aligned} E y_{\ell\Delta} y_{j\Delta}^* &= \frac{\alpha\Delta t}{\lambda_{\ell\ell} + \lambda_j - \alpha\Delta t \lambda_{\ell} \lambda_j} \\ &- |\tilde{r}|^2 \frac{1}{(1+T_0)^2} (P_{\underline{s}}) (P_{\underline{s}})_j^* + |\tilde{r}|^2 \frac{1}{1+T_0} \Lambda_{\ell j} \\ &- E(y_{\Delta}^{\dagger} P_{\underline{s}} \underline{s} \underline{s}^{\dagger} P^{-1} y_{\Delta}) (P_{\underline{s}})_\ell (P_{\underline{s}})_j^* ; R_{\Delta} \neq [0] \end{aligned} \quad (216)$$

and, by Equation (158)

$$\begin{aligned}
 E y_{\ell \Delta} y_{j \Delta}^* &= \frac{\alpha \Delta t}{\lambda_i + \lambda_j - \alpha \Delta t \lambda_i \lambda_j} \left[|\tilde{r}|^2 \frac{T_0}{1 + T_0} \frac{1}{1 - C} \Lambda_{\ell j} \right. \\
 &\quad \left. - |\tilde{r}|^2 \frac{T_0}{1 + T_0} (P \underline{s})_{\ell} (P \underline{s})_{j}^* - E(y_{\Delta}^{\dagger} P \underline{s} \underline{s}^{\dagger} P^{-1} y_{\Delta}) \right. \\
 &\quad \left. \cdot (P \underline{s})_{\ell} (P \underline{s})_{j}^* \right] ; R_{\Delta} = [0]
 \end{aligned} \tag{217}$$

Thus,

$$\begin{aligned}
 E(y_{\Delta}^{\dagger} P \underline{s} \underline{s}^{\dagger} P^{-1} y_{\Delta}) &= \sum_{j=1}^m \sum_{\ell=1}^m (y_{\ell \Delta} y_{j \Delta}^*) (P \underline{s})_j (P \underline{s})_{\ell}^* \\
 &= \sum_{\ell=1}^m \sum_{j=1}^m \frac{\alpha \Delta t |(P \underline{s})_{\ell}|^2 |(P \underline{s})_j|^2}{\lambda_{\ell} + \lambda_j - \alpha \Delta t \lambda_j \lambda_{\ell}} \\
 &\quad - \left[|\tilde{r}|^2 \frac{1}{(1 + T_0)^2} - E(y_{\Delta}^{\dagger} P \underline{s} \underline{s}^{\dagger} P^{-1} y_{\Delta}) \right] \\
 &\quad + |\tilde{r}|^2 \frac{\alpha \Delta t}{1 + T_0} \frac{1}{1 - C} \sum_{\ell=1}^m \frac{|(P \underline{s})_{\ell}|^2}{2 - \alpha \Delta t \lambda_{\ell}} ; R_{\Delta} \neq [0]
 \end{aligned} \tag{218}$$

or $E(y_{\Delta}^{\dagger} P \underline{s} \underline{s}^{\dagger} P^{-1} y_{\Delta})$

$$\begin{aligned}
 &= \sum_{\ell=1}^m \sum_{j=1}^m \frac{\alpha \Delta t |(P \underline{s})_{\ell}|^2 |(P \underline{s})_j|^2}{\lambda_{\ell} + \lambda_j - \alpha \Delta t \lambda_j \lambda_{\ell}} \\
 &\quad - \left[|\tilde{r}|^2 \frac{T_0}{1 + T_0} - E(y_{\Delta}^{\dagger} P \underline{s} \underline{s}^{\dagger} P^{-1} y_{\Delta}) \right] \\
 &\quad + |\tilde{r}|^2 \frac{\alpha \Delta t T_0}{1 + T_0} \frac{1}{1 - C} \sum_{\ell=1}^m \frac{|(P \underline{s})_{\ell}|^2}{2 - \alpha \Delta t \lambda_{\ell}} ; R_{\Delta} = [0]
 \end{aligned}$$

In terms of the real, positive number h , defined by

$$h = \sum_{\ell=1}^m \sum_{j=1}^m \frac{\alpha \Delta t |(P \underline{s})_{\ell}|^2 |(P \underline{s})_j|^2}{\lambda_{\ell} + \lambda_j - \alpha \Delta t \lambda_{\ell} \lambda_j} > 0 \quad (219)$$

Equation (218) may be expressed as

$$\begin{aligned} E(y_{\Delta}^{\dagger} P \underline{s} \underline{s}^{\dagger} P^{-1} y_{\Delta}) &= - \frac{h |\tilde{r}|^2}{1+h} \frac{1}{(1+T_0)^2} \quad (220) \\ &+ \frac{\alpha \Delta t}{1+h} \frac{|\tilde{r}|^2}{1+T_0} \frac{1}{1-C} \sum_{\ell=1}^m \frac{|(P \underline{s})_{\ell}|^2}{2 - \alpha \Delta t \lambda_{\ell}} ; R_{\Delta} \neq [0] \\ &= - \frac{h |\tilde{r}|^2}{1+h} \frac{T_0}{1+T_0} \frac{\alpha \Delta t}{1+h} \frac{T_0 |\tilde{r}|^2}{1+T_0} \frac{1}{1-C} \\ &\cdot \sum_{\ell=1}^m \frac{|(P \underline{s})_{\ell}|^2}{2 - \alpha \Delta t \lambda_{\ell}} ; R_{\Delta} = [0] \end{aligned}$$

Clearly

$$h < \alpha \Delta t P_s \frac{T_0}{1+T_0} \ll 1 \quad (221)$$

and thus

$$\begin{aligned} E(y_{\Delta}^{\dagger} P \underline{s} \underline{s}^{\dagger} P^{-1} y_{\Delta}) & \quad (222) \\ & \doteq - h |\tilde{r}|^2 \frac{1}{(1+T_0)^2} + \frac{\alpha \Delta t |\tilde{r}|^2}{1+T_0} \frac{1}{1-C} \\ & \cdot \sum_{\ell=1}^m \frac{|(P \underline{s})_{\ell}|^2}{2 - \alpha \Delta t \lambda_{\ell}} ; R_{\Delta} \neq [0] \\ & \doteq - h |\tilde{r}|^2 \frac{T_0}{1+T_0} + \frac{\alpha \Delta t T_0 |\tilde{r}|^2}{1+T_0} \frac{1}{1-C} \sum_{\ell=1}^m \frac{|(P \underline{s})_{\ell}|^2}{2 - \alpha \Delta t \lambda_{\ell}} ; R_{\Delta} = [0]. \end{aligned}$$

From Equation (215)

$$E\theta_{\ell}^2 \leq \begin{cases} 2 \frac{1 + T_0}{T_0} \left[\frac{\alpha \Delta t}{1 - C} \sum_{\ell=1}^m \frac{|(P \underline{s})_{\ell}|^2}{2 - \alpha \Delta t \lambda_{\ell}} - \frac{h}{1 + T_0} \right]; & R_{\Delta} \neq [0] \\ 2 \frac{1 + T_0}{T_0} \left[\frac{\alpha \Delta t}{1 - C} \sum_{\ell=1}^m \frac{|(P \underline{s})_{\ell}|^2}{2 - \alpha \Delta t \lambda_{\ell}} - h \right]; & R_{\Delta} = [0]. \end{cases} \quad (223)$$

provided Equation (211) is satisfied, i.e.,

$$y_{\Delta}^{\dagger} P \underline{s} \underline{s}^{\dagger} P^{-1} y_{\Delta} \lesssim \frac{1}{9} |\tilde{r}|^2 \frac{T_0^4}{(1 + T_0)^2}$$

This relation places an upper bound on instantaneous functions of θ_{ℓ} . Since y_{Δ} is a zero-mean random vector generated from Gaussian processes, it is reasonable to assume that, with high probability,

$$y_{\Delta}^{\dagger} P \underline{s} \underline{s}^{\dagger} P^{-1} y_{\Delta} \approx 3 E(y_{\Delta}^{\dagger} P \underline{s} \underline{s}^{\dagger} P^{-1} y_{\Delta})$$

In this case, the condition on the validity of Equation (222) reduces to

$$E \theta_{\ell}^2 \approx \frac{1}{12} (\text{radian})^2 \quad (224)$$

In order to evaluate Equation (223), eigenvalues of K_x must be determined for the specific signal environment. However, certain bounds can be established if P_s and P_I are known. Since

$$\sum_{\ell=1}^m \frac{|(P \underline{s})_{\ell}|^2}{2 - \alpha \Delta t \lambda_{\ell}} < P_s$$

Equation (222) has the upper bound (for $\alpha \Delta t P_I \approx 0.5$)

$$E(y_{\Delta}^{\dagger} P \underline{s} \underline{s}^{\dagger} P^{-1} y_{\Delta}) < \begin{cases} \frac{\alpha \Delta t |\tilde{r}|^2 P_s}{(1 + T_0)(1 - C)} \ll \frac{1}{1 + T_0}; & R_{\Delta} \neq [0] \\ \frac{\alpha \Delta t |\tilde{r}|^2 P_s T_0}{(1 + T_0)(1 - C)} \ll \frac{T_0}{1 + T_0}; & R_{\Delta} = [0] \end{cases} \quad (225)$$

which implies

$$E\theta^2 < E\theta_e^2 \begin{cases} 2 \frac{1 + T_0}{T_0^2} \frac{\alpha\Delta t P_s}{1 - C} ; R_\Delta \neq [0] \\ 2 \frac{1 + T_0}{T_0} \frac{\alpha\Delta t P_s}{1 - C} ; R_\Delta = [0] \end{cases} \quad (226)$$

The relation in (226) shows that an upper bound on desired signal phase jitter is proportional to the input desired signal power and has an inverse relationship with the optimum output SNR.

By the relation in (224), Equation (223) remains a good approximation if

$$\alpha\Delta t P_s < \frac{T_0^2}{12(1 + T_0)} (1 - C) \quad ; R_\Delta \neq [0] \quad (227)$$

or

$$\alpha\Delta t P_s < \frac{T_0}{12(1 + T_0)} (1 - C) \quad ; R_\Delta = [0]$$

i.e., when $\alpha\Delta t P_s \ll 1$ and T_0 is sufficiently large. These requirements will be satisfied in a wide variety of signal environments of interest.

To illustrate the level of phase jitter encountered in a practical environment, Equations (223) were evaluated numerically for the example given in section II b; Table II displays results obtained when the loop gain parameter is set to a moderately high value ($\alpha\Delta t P_I \cong 0.5$, $\alpha\Delta t C \cong 0.25$). As is expected, phase jitter is very small for all cases, with the largest jitter occurring when the separation between the interference and desired signal arrival angles is smallest.

The output desired signal power is determined from the ensemble average

$$E[\underline{w}^\dagger \underline{s} \underline{s}^\dagger \underline{w}] = E[\underline{y}_\Delta^\dagger \underline{P} \underline{s} \underline{s}^\dagger \underline{P}^{-1} \underline{y}_\Delta] + \underline{w}_{\text{opt}}^\dagger \underline{s} \underline{s}^\dagger \underline{w}_{\text{opt}} \quad (228)$$

Table II. An Upper Bound on the Variance of the Desired Signal Phase at the Array Output for $R_{\Delta}=[0]$ and $R_{\Delta} \neq [0]$ for Several Values of the Angular Separation Parameter ψ .

ψ	λ_1	λ_2	λ_k	$(PS)_1$	$(PS)_2$	$(PS)_k$	T_0	$E_{\theta_e}^2$	$E_{\theta_e}^2$
								$R_{\Delta} \neq 0$	$R_{\Delta} = 0$
90°	5	4001	1	2	0	0	4	8.2×10^{-5}	1.5×10^{-4}
60°	4.25	4002	1	1.802	0.866	0	3.244	1.1×10^{-4}	2.3×10^{-4}
45°	3.29	4003	1	1.514	1.306	0	2.295	1.9×10^{-4}	3.5×10^{-4}
30°	2.2	4004	1	1.09	1.673	0	1.20	5.1×10^{-4}	5.8×10^{-4}
15°	1.33	4005	1	0.575	1.915	0	0.331	4.4×10^{-3}	1.4×10^{-3}

$\alpha \Delta t P_I = 0.4$

(228) (continued)

$$= E[y_{\Delta}^{\dagger} P \underline{s} \underline{s}^{\dagger} P^{-1} y_{\Delta}] + \frac{\tau_o^2 |\tilde{r}|^2}{(1 + \tau_o)^2}$$

From Equation (225), an upper bound on the variance of the output desired signal due to weight jitter, normalized to $w_{opt}^{\dagger} \underline{s} \underline{s}^{\dagger} w_{opt}$, may be expressed as

$$\frac{1 + \tau_o}{\tau_o^2} \frac{\alpha \Delta t P_s}{1 - C} \quad ; \quad R_{\Delta} \neq [0]$$

$$\frac{1 + \tau_o}{\tau_o} \frac{\alpha \Delta t P_s}{1 - C} \quad ; \quad R_{\Delta} = [0]$$

The output desired signal power is negligibly affected by weight jitter if these ratios are small (for example, when the relations given in (227) are satisfied).

3. Effects of Weight Jitter on Coherent Detection

In this section, the effects of weight jitter on system performance will be determined for a specific desired signal waveform. Since one of the primary goals of this study has been to determine performance of a jointly operational TDMA-adaptive array (TDMA/AA) implementation, desired signal modulation and demodulation will be modeled to closely resemble TDMA modulation and demodulation techniques outlined in Chapter II.

The complex envelope of the desired signal is assumed to be expressible as

$$\tilde{s}(t) = \frac{\beta}{\sqrt{2}} \exp [j(\phi_1(t) + \theta_1)] \quad (229)$$

where β and θ_1 represent constant amplitude and phase factors, respectively, and $\phi_1(t)$ represents the time-varying component of $\tilde{s}(t)$. Biphase (antipodal) modulation is employed to convey data at a rate of b_1 bits per second, and the random PN code is used to spread the signal spectrum by a factor* of n , where n is

*The code and data bit streams are added modulo two and are then used to biphase modulate a cw signal to generate the desired signal.

an integer. Defining $\Delta\tau$ as the inverse of the code rate, T as the inverse of the data rate, $D(t)$ as the data bit stream, and $c(t)$ as the code bit stream, one obtains the following relations:

$$\begin{aligned}
 D(t) &= \pm 1 && \text{constant for } T \text{ seconds} && (230) \\
 c(t) &= \pm 1 && \text{constant for } \Delta\tau \text{ seconds} \\
 \phi_1(t) &= c(t) D(t) \frac{\pi}{2} = \pm\pi/2 && \text{constant for } \Delta\tau \text{ seconds} \\
 T &= n \Delta\tau && n \geq 1 \\
 E\phi_1(t) \phi_1(t + \tau) &= 0 && \tau > \Delta\tau
 \end{aligned}$$

The TDMA modems employ a differential phase-shift keyed (DPSK) receiver for signal detection; that is, decisions are based on the difference in phase between adjacent bits. Owing to certain difficulties encountered in analyzing the effects of weight jitter on DPSK receiver performance, however, coherent detection (PSK) will be assumed. As will be shown, the results obtained for the coherent detector will provide a general guide to DPSK receiver performance.

In ideal coherent detection, the carrier phase is assumed known a priori at the receiver. In order to apply this requirement to a system containing an adaptive array, it is necessary to assume that the time average phase of the desired signal is known or has been accurately estimated. The signal $r'(t)$ available at the receiver is assumed to have the following property when the mean weights (\bar{w}) are near their steady-state solution:

$$\begin{aligned}
 E\hat{\gamma}(t) \hat{r}'^\dagger(t) &= E w^\dagger(t) \underline{\hat{x}}(t) r'^*(t) && (231) \\
 &= \bar{w}^\dagger(t) \underline{\hat{x}}(t) r'^*(t) \\
 &= w_{\text{opt}}^\dagger L
 \end{aligned}$$

where $\hat{\gamma}(t)$ represents the array output signal, \bar{w} is the ensemble average of $w(t)$, and L is an m -dimensional vector assumed constant during a given data bit interval. To simplify the notation, assume this interval is $[0, T]$. In arriving at the result in Equation (231), it was assumed that the desired signal carrier frequency and the code $c(t)$ are known at the receiver. Note that the ensemble average given in Equation (231) is real valued.

The receiver is assumed to employ matched filter detection. At baseband, this is equivalent to the operation

$$\begin{aligned} v(T) &= \frac{1}{T} \int_0^T [\tilde{y}(t) r'^{\dagger}(t)] dt \\ &= \frac{1}{T} \int_0^T [w^{\dagger} \tilde{x}(t) r'^{\dagger}(t)] dt \end{aligned} \quad (232)$$

where $v(T)$ represents the detector output voltage at time T . Noise in the propagation medium between the array output and the receiver input has been assumed negligible to focus attention exclusively on the effects of weight jitter.

When \bar{w} is near steady-state, the ensemble mean of $v(T)$ is given by

$$\begin{aligned} E v(T) &= E \left\{ \frac{1}{T} \int_0^T [w^{\dagger} \tilde{u}(t) r'^{\dagger}(t) + w^{\dagger} \tilde{s}(t) r'^{\dagger}(t)] dt \right\} \\ &= E[\tilde{y}(t) r'^{\dagger}(t)] \\ &= w_{\text{opt}}^{\dagger} L \end{aligned} \quad (233)$$

where $\tilde{x}(t) = \tilde{u}(t) + \tilde{s}(t)$.

The above result follows from the assumption that $w(t)$ is independent* of $\tilde{x}(t) r'^{\dagger}(t)$. The variance of $v(T)$ is expressed as

$$\begin{aligned} \text{Var}(v(T)) &= E \{ [v(T) - w_{\text{opt}}^{\dagger} L] [v(T) - w_{\text{opt}}^{\dagger} L] \} \\ &= E \frac{1}{T^2} \int_0^T \int_0^T \{ w_0^{\dagger} \tilde{u}(\tau_1) r'^{\dagger}(\tau_1) \\ &\quad + \hat{z}^{\dagger}(\tau_1) [\tilde{u}(\tau_1) r'^{\dagger}(\tau_1) + L] \} (\tilde{u}^{\dagger}(\tau_2) w_0 r'(\tau_2) \\ &\quad + [\tilde{u}^{\dagger}(\tau_2) r'(\tau_2) + L^{\dagger}] \hat{z}(\tau_2) \} d\tau_1 d\tau_2 \end{aligned} \quad (234)$$

*This applies to the DLMS algorithm only.

where $w_0 = w_{opt}$
and $\hat{z}(t) = w(t) - w_0$.

The weights are assumed updated according to the DLMS algorithm (Equations (54) and (58)). For the purposes of analysis, the interval Δt is taken as the interval between independent samples of the product $\hat{x}(t) r^{\dagger}(t)$. In the digital algorithm, $\hat{z}(\tau_1)$ is constant for Δt seconds, so that Equation (234) becomes

$$\begin{aligned} \text{var}(v(T)) = E \frac{1}{T^2} \int_0^T \int_0^T & \left\{ w_0^{\dagger} \underline{\hat{u}}(\tau_1) \hat{r}^{\dagger}(\tau_1) \right. \\ & + \hat{z}^{\dagger}(i\Delta t) [\underline{\hat{u}}(\tau_1) \hat{r}^{\dagger}(\tau_1) + L] \left. \right\} \left\{ \underline{\hat{u}}^{\dagger}(\tau_2) w_0 \hat{r}^{\dagger}(\tau_2) \right. \\ & + [\underline{\hat{u}}^{\dagger}(\tau_2) \hat{r}^{\dagger}(\tau_2) + L^{\dagger}] \hat{z}(j\Delta t) \left. \right\} d\tau_1 d\tau_2 \end{aligned} \quad (235)$$

where $\tau_1 \leq i\Delta t < \tau_1 + \Delta t$
and $\tau_2 \leq j\Delta t < \tau_2 + \Delta t$; $i, j = 0, 1, 2, \dots, n$.

When $\hat{z}(i\Delta t) \equiv 0$, $\text{var}(v(T))$ equals the minimum output noise power, given by

$$\begin{aligned} N_{\min} = E \frac{1}{T^2} \int_0^T \int_0^T & w_0^{\dagger} \underline{\hat{u}}(\tau_1) \hat{r}^{\dagger}(\tau_1) \hat{r}^{\dagger}(\tau_2) \\ & \cdot \underline{\hat{u}}^{\dagger}(\tau_2) w_0 d\tau_1 d\tau_2 \end{aligned} \quad (236)$$

The variance of the excess noise voltage at the detector output, caused by weight jitter, may be defined by

$$\begin{aligned} \text{var}(v_e(T)) = \text{var}(v(T)) - N_{\min} \quad (237) \\ = E \frac{1}{T^2} \int_0^T \int_0^T & \left\{ w_0^{\dagger} \underline{\hat{u}}(\tau_1) \hat{r}^{\dagger}(\tau_1) [\underline{\hat{u}}^{\dagger}(\tau_2) \hat{r}^{\dagger}(\tau_2) + L^{\dagger}] \hat{z}(j\Delta t) \right. \\ & + \hat{z}^{\dagger}(i\Delta t) [\underline{\hat{u}}(\tau_1) \hat{r}^{\dagger}(\tau_1) + L] \hat{r}^{\dagger}(\tau_2) \underline{\hat{u}}^{\dagger}(\tau_2) w_0 \\ & + \hat{z}^{\dagger}(i\Delta t) [\underline{\hat{u}}(\tau_1) \hat{r}^{\dagger}(\tau_1) + L] [\underline{\hat{u}}^{\dagger}(\tau_2) \hat{r}^{\dagger}(\tau_2) + L^{\dagger}] \\ & \left. \cdot \hat{z}(j\Delta t) \right\} d\tau_1 d\tau_2 \end{aligned}$$

To simplify the analysis, the double integral in Equation (237) is approximated by the double sum

$$\begin{aligned}
 \text{var}(v_e(T)) \doteq E & \frac{(\Delta t)^2}{T^2} \sum_{i=0}^{n-1} \sum_{j=0}^{n-1} \left\{ w_0^+ \underline{\hat{u}}(i\Delta t) \tilde{r}'^*(i\Delta t) \right. \\
 & \cdot [\underline{\hat{u}}^+(j\Delta t) \tilde{r}'(j\Delta t) + L^+] z(j\Delta t) + \hat{z}^+(i\Delta t) \\
 & \cdot [\underline{\hat{u}}(i\Delta t) \tilde{r}'^*(i\Delta t) + L] r'(j\Delta t) \underline{\hat{u}}^+(j\Delta t) w_0 \\
 & + \hat{z}^+(i\Delta t) [\underline{\hat{u}}(i\Delta t) \tilde{r}'^*(i\Delta t) + L] \\
 & \left. \cdot [\underline{\hat{u}}^+(j\Delta t) \tilde{r}'(j\Delta t) + L^+] \hat{z}(j\Delta t) \right\} .
 \end{aligned} \tag{238}$$

By Equation (230) and the independence of $\underline{\hat{u}}^+(j\Delta t)$, $r'(j\Delta t)$ and $z(i\Delta t)$ for $j \geq i$, Equation (238) reduces to

$$\begin{aligned}
 \text{var}(v_e(T)) \doteq 2 & \frac{(\Delta t)^2}{T^2} \sum_{i=0}^{n-1} \sum_{j=0}^{j-1} \\
 & \cdot E[w_0^+ \underline{\hat{u}}(i\Delta t) \tilde{r}'^+(i\Delta t) L^+ \hat{z}(j\Delta t)] \\
 & + \frac{(\Delta t)^2}{T^2} \sum_{i=1}^{n-1} \sum_{j=0}^{i-1} E[\hat{z}^+(i\Delta t) L \tilde{r}'(j\Delta t) \underline{\hat{u}}^+(j\Delta t) w_0 \\
 & + R \frac{(\Delta t)^2}{T^2} \sum_{i=0}^{n-1} E[\hat{z}^+(i\Delta t) M \hat{z}(j\Delta t)] \\
 & + \sum_{i=0}^{n-1} \sum_{j=0}^{n-1} E[\hat{z}^+(i\Delta t) L L^+ \hat{z}(j\Delta t)]
 \end{aligned} \tag{239}$$

where $R = |\tilde{r}'|^2$.

The above result applies when $\bar{w} = w_{opt}$. When $\bar{w} = w_{opt}$, the vector $z(i\Delta t)$ can be expressed in the eigenvector space as [see Equation (112)]

$$y_\Delta(i\Delta t) = \alpha \Delta t \sum_{j=0}^{\infty} [I - \alpha \Delta t \Lambda]^j \underline{B}^{i-j-1} \tag{240}$$

where $\hat{z}(i\Delta t) = P^{-1} y_{\Delta}(i\Delta t)$

and

$$\underline{B}^{\xi} = PR_{\Delta}(\xi\Delta t) - P\phi(\xi\Delta t) P^{-1} y_{\Delta}(\xi\Delta t) - P\phi(\xi\Delta t) w_0 \quad .$$

The following result will also be required:

$$E[y_{\Delta}(i\Delta t) y_{\Delta}^{\dagger}(j\Delta t)] = \begin{cases} [I - \alpha\Delta t\Lambda]^{i-j} E[y_{\Delta}(j\Delta t) y_{\Delta}^{\dagger}(j\Delta t)] & i \geq j \\ E[y_{\Delta}(i\Delta t) y_{\Delta}^{\dagger}(i\Delta t)] [I - \alpha\Delta t\Lambda]^{j-i} & i \leq j \end{cases} \quad (241)$$

The m^2 components of the matrix $E(y_{\Delta}y_{\Delta}^{\dagger})$ can be evaluated using the procedure outlined in section IV D 2. The ij^{th} component is given by

$$E(y_{i\Delta} y_{j\Delta}^*) = \frac{\alpha\Delta t}{\lambda_i + \lambda_j - \alpha\Delta t\lambda_i\lambda_j} \quad (242)$$

$$\cdot \left\{ \frac{|\tilde{r}|^2}{1 + T_0} \Lambda_{ij} - \frac{|\tilde{r}|^2}{(1 + T_0)^2} (P \underline{s})_i (P \underline{s})_j^* \right.$$

$$\left. + E[y_{\Delta}^{\dagger} \Lambda y_{\Delta}] - \underline{s}^{\dagger} P^{-1} E y_{\Delta} y_{\Delta}^{\dagger} P \underline{s} (P \underline{s})_i (P \underline{s})_j^* \right\} ; i, j = 1, 2, \dots, m.$$

A complete solution to Equation (242) requires evaluation of the as yet undetermined expectations appearing on the right side. By iterative application of Equation (242)

$$E(y_{\Delta}^{\dagger} \Lambda y_{\Delta}) = \frac{\alpha\Delta t |\tilde{r}|^2}{T - \alpha\Delta t c} \sum_{i=1}^m \left\{ \frac{\lambda_i}{2 - \alpha\Delta t\lambda_i} \frac{1}{1 + T_0} \right.$$

$$\left. - \frac{|(P \underline{s})_i|^2}{2 - \alpha\Delta t\lambda_i} \frac{1}{(1 + T_0)^2} - \frac{1}{|\tilde{r}|^2} \underline{s}^{\dagger} P^{-1} E y_{\Delta} y_{\Delta}^{\dagger} P \underline{s} \right.$$

$$\left. \cdot \frac{|(P \underline{s})_i|^2}{2 - \alpha\Delta t\lambda_i} \right\} \quad (243)$$

From Equation (133), and the assumption $P_s \ll P_I$,

$$E(y_{\Delta}^{\dagger} \Lambda y_{\Delta}) \approx \frac{\alpha \Delta t |r|^2}{1 - \alpha \Delta t c} \frac{1}{1 + \tau_0} \quad (244)$$

Thus

$$E y_{i\Delta} y_{j\Delta}^* \approx \frac{\alpha \Delta t |r|^2}{\lambda_i + \lambda_j - \alpha \Delta t \lambda_i \lambda_j} \left[\frac{1}{1 + \tau_0} - \frac{1}{1 - \alpha \Delta t c} \Lambda_{ij} \right] \quad (245)$$

provided $\alpha \Delta t c \approx 0.5$. Although evaluation of the first two terms in Equation (239) is tedious, the procedure is straightforward and thus will not be detailed here. Employing Equation (241), the results are

$$E[w_0^{\dagger} \underline{\tilde{u}}(i\Delta t) \tilde{r}'^*(i\Delta t) L^{\dagger} z(j\Delta t)] = \quad (246)$$

$$- \alpha \Delta t w_0^{\dagger} M w_0 L^{\dagger} P^{-1} [I - \alpha \Delta t \Lambda]^{j-i-1} P L \quad ; i < j$$

$$E[z^{\dagger}(j\Delta t) L \tilde{r}'(i\Delta t) \underline{\tilde{u}}^{\dagger}(i\Delta t) w_0] = \quad (247)$$

$$- \alpha \Delta t w_0^{\dagger} M w_0 L^{\dagger} P^{-1} [I - \alpha \Delta t \Lambda]^{i-j-1} \quad ; i > j.$$

Equation (239) can thus be written as

$$\text{var}(v_e(T)) \approx -2R \frac{\Delta t}{T} \sum_{j=1}^{n-1} \sum_{i=0}^{j-1} \quad (248)$$

$$\cdot \alpha \Delta t w_0^{\dagger} M w_0 \underline{s}^{\dagger} P^{-1} [I - \alpha \Delta t \Lambda]^{j-i-1} P \underline{s}$$

$$+ R \left(\frac{\Delta t}{T} \right)^2 \sum_{j=0}^{n-1} \sum_{i=0}^j \underline{s}^{\dagger} P^{-1} [I - \alpha \Delta t \Lambda]^{j-i}$$

$$\cdot E[y_{\Delta}(i\Delta t) y_{\Delta}^{\dagger}(i\Delta t)] P \underline{s}$$

$$+ R \left(\frac{\Delta t}{T} \right)^2 \sum_{j=0}^{n-2} \sum_{i=j+1}^{n-1} \underline{s}^{\dagger} P^{-1} E[y_{\Delta}(j\Delta t) y_{\Delta}^{\dagger}(j\Delta t)] [I - \alpha \Delta t \Lambda]^{i-j} P \underline{s}$$

$$+ R \frac{\Delta t}{T} \left\{ E y_{\Delta}^{\dagger} \Lambda y_{\Delta} - E \underline{s}^{\dagger} P^{-1} y_{\Delta} y_{\Delta}^{\dagger} P^{-1} \underline{s} \right\} .$$

Since $E(\underline{s}^T \underline{p}^{-1} y y^T \underline{p}^{-1} \underline{s})$ has been shown to be much smaller than $E(y^T \underline{\Lambda} y)$, it can be neglected in Equation (248). Substituting Equations (244) and (245) into Equation (248) and rearranging terms yields

$$\begin{aligned}
 \text{var}(v_e(T)) &\doteq 2 R \left(\frac{\Delta t}{T}\right)^2 \sum_{j=1}^{n-1} \sum_{i=0}^{j-1} \sum_{k=1}^m \quad (249) \\
 &\cdot \frac{\alpha \Delta t |\tilde{r}|^2}{T + T_0} (1 - \alpha \Delta t \lambda_k)^{j-i} (P \underline{s})_k^2 \\
 &\cdot \left\{ \frac{1}{(2 - \alpha \Delta t \lambda_k)(T - \alpha \Delta t c)} - \frac{T_0}{T + T_0} \frac{1}{T - \alpha \Delta t \lambda_k} \right. \\
 &\left. - \frac{1}{T + T_0} \sum_{\ell=1}^m \frac{|(P \underline{s})_\ell|^2}{\lambda_k + \lambda_\ell - \alpha \Delta t \lambda_k \lambda_\ell} \right\} \\
 &+ R \frac{\Delta t}{T} \sum_{k=1}^m |(P \underline{s})_k|^2 \frac{\alpha \Delta t |\tilde{r}|^2}{T + T_0} \frac{1}{(2 - \alpha \Delta t \lambda_k)(T - \alpha \Delta t c)} \\
 &- \frac{1}{T + T_0} \sum_{\ell=1}^m \frac{|(P \underline{s})_\ell|^2}{\lambda_k + \lambda_\ell - \alpha \Delta t \lambda_k \lambda_\ell} + R \frac{\Delta t}{T} \frac{\alpha \Delta t c}{T - \alpha \Delta t c} \frac{|\tilde{r}|^2}{T + T_0} .
 \end{aligned}$$

Again applying the assumption that $P_s \ll P_I$, it is easily shown that

$$\sum_{\ell=1}^m \frac{|(P \underline{s})_\ell|^2}{\lambda_k + \lambda_\ell - \alpha \Delta t \lambda_k \lambda_\ell} < \frac{T_0}{T + T_0} ,$$

that the first term in Equation (249) has the upper bound

$$R \frac{\alpha \Delta t |\tilde{r}|^2 P_s}{T + T_0} ,$$

and that the second term has the upper bound

$$R \frac{\Delta t}{T} \frac{\alpha \Delta t |\tilde{r}|^2 P_s}{T + T_0} \frac{1}{T + T_0} .$$

Thus, by making the additional assumption

$$2 n P_s \ll c \quad (250)$$

Equation (249) can be approximated by

$$\text{var}(v_e(T)) \approx R \frac{\Delta t}{T} \frac{\alpha \Delta t c |\tilde{r}|^2}{1 - \alpha \Delta t c} \frac{1}{1 + T_0} \quad (251)$$

Equation (251) gives an approximation for the variance of the excess noise at the detector output due to jitter, provided n is large and that

$$(a) \quad 2 n P_s \ll c = \sum_{i=1}^m \frac{\lambda_i}{2 - \alpha \Delta t \lambda_i} \quad (252)$$

$$(b) \quad \alpha \Delta t P_s \ll \frac{1}{1 + T_0}$$

$$(c) \quad \alpha \Delta t c < 1$$

Since Equation (237) was approximated by the double sum in Equation (238), Equation (251) best approximates the excess noise variance when the input signal $\tilde{x}(t)$ approximates an ideal bandpass process with $\Delta t = B^{-1}$, where B represents the double-sided bandwidth. When $B > (\Delta t)^{-1}$, Equation (251) gives an upper bound on the variance.

Although assumptions given in Equation (252) permitted the expression for $\text{var}(v_e(T))$ to be greatly simplified, they are valid in a wide variety of high-level interfering signal environments. Equation (252)(a) is the most restrictive condition, since it requires that the product of the waveform processing gain and the input desired signal power be much smaller than the total input power. When this requirement is not met, then past history of $z(i\Delta t)$ for $i\Delta t$ in $[0, T]$ may significantly affect the value of $\text{var}(v_e(T))$, thereby causing inaccuracies in Equation (251). In this case, Equation (241) should be used, provided $P_s \ll P_I$.

The expression for the output noise power when $w(t) = w_{\text{opt}}(t)$ (Equation (236)) can also be estimated by approximating the double integral by a double sum and performing the indicated ensemble average:

$$N_{\text{min}} \approx |\tilde{r}|^2 |\tilde{r}|^2 \frac{\Delta t}{T} \frac{T_0}{(1 + T_0)^2} \quad (253)$$

The variance of $v(T)$ is obtained by summing Equation (251) with Equation (253):

$$\text{var}[v(T)] \approx |\tilde{r}|^2 |\tilde{r}'|^2 \frac{1}{T + T_0} \frac{\Delta t}{T} \left[\frac{\alpha \Delta t c}{T - \alpha \Delta t c} + \frac{T_0}{T + T_0} \right] \quad (254)$$

The output signal-to-noise ratio D will be used as a measure of detector performance, where

$$D \equiv \frac{|E v(T)|^2}{\text{var}[v(T)]} \quad (255)$$

Note that although D is a classical definition for the output signal-to-noise ratio, it does not necessarily equal the average output signal-to-noise ratio, since $v(T)$ is generally not stationary in the interval $[0, T]$. Equation (255) is meaningful in that (1) it normalizes the square of the mean (of $v(T)$) to the mean square and (2) it approximates the average output signal-to-noise ratio when $v(T)$ is near its mean (for example, when $D \gg 1$). Using Equations (233) and (254), Equation (255) becomes

$$D = \frac{T}{\Delta t} T_0 \left[\frac{1}{1 + \frac{\alpha \Delta t c}{T - \alpha \Delta t c} \frac{T + T_0}{T_0}} \right] \quad (256)$$

This result shows that weight jitter reduces the detector's output signal-to-noise ratio by the same factor (in brackets) that the processor's output signal-to-noise ratio is reduced (see Equation (143)). In other words, the waveform processing gain of the coherent detector is (about) equal to the spectrum spreading ratio, even when the excess noise power is large relative to the quiescent (no jitter) noise power. For a given set of loop parameters (α , Δt , and c), system performance can be improved by increasing the integration time T assuming the relations given in Equation (252) are satisfied.

The analysis to this point applies to the DLMS algorithm for $R_\Delta \neq [0]$. When the desired signal DOA is known, the variance of $v(T)$ can be evaluated by setting $R_\Delta = [0]$ in each step used to derive Equation (249). The result is approximated by

$$\text{var}(v_e(T)) \Big|_{R_\Delta = [0]} \approx 2 |\tilde{r}'|^2 \left(\frac{\Delta t}{T} \right)^2 \sum_{j=1}^{n-1} \sum_{i=0}^{j-1} \sum_{k=1}^m \quad (257)$$

$$\begin{aligned}
& \cdot \alpha \Delta t |\tilde{r}|^2 (1 - \alpha \Delta t \lambda_k)^{j-1} |(P \underline{s})_k|^2 \\
& \cdot \left\{ \frac{T_o}{(2 - \alpha \Delta t \lambda_k)(1 + T_o)(1 - \alpha \Delta t c)} - \frac{T_o^2}{(1 + T_o)^2} \sum_{\ell=1}^m \right. \\
& \cdot \left. \frac{|(P \underline{s})_\ell|^2}{\lambda_k + \lambda_\ell - \alpha \Delta t \lambda_k \lambda_\ell} - \frac{T_o}{(1 + T_o)^2} \frac{1}{1 - \alpha \Delta t \lambda_k} \right\} \\
& + |\tilde{r}'|^2 \frac{\Delta t}{T} \sum_{k=1}^m |(P \underline{s})_k|^2 \frac{\alpha \Delta t |\tilde{r}|^2}{1 + T_o} \left\{ \frac{T_o}{(2 - \alpha \Delta t \lambda_k)(1 - \alpha \Delta t c)} \right. \\
& \left. - \frac{T_o^2}{(1 + T_o)^2} \sum_{\ell=1}^m \frac{|(P \underline{s})_\ell|^2}{\lambda_k + \lambda_\ell - \alpha \Delta t \lambda_k \lambda_\ell} \right\} + |\tilde{r}'|^2 \frac{\Delta t}{T} \\
& \cdot \frac{\alpha \Delta t c}{1 - \alpha \Delta t c} \frac{T_o}{1 + T_o} .
\end{aligned}$$

If the assumptions in Equation (252) are satisfied and if

$$\alpha \Delta t P_s \ll \frac{T_o}{1 + T_o}$$

then Equation (257) may be approximated by

$$\text{var}(v_e(T)) \Big|_{R_\Delta = [0]} = T_o \text{var}(v_e(T)) \Big|_{R_\Delta \neq [0]} . \quad (258)$$

Thus, the performance measure D for the $R_\Delta = [0]$ case becomes

$$D \Big|_{R_\Delta = [0]} = \frac{T}{\Delta t} T_o \left\{ \frac{1}{1 + \frac{\alpha \Delta t c}{1 - \alpha \Delta t c} (1 + T_o)} \right\} \quad (259)$$

The minimum signal-to-noise ratio required at the processor output, as a function of the normalized parameter

$$g = \frac{D}{2} \frac{\Delta t}{T} \quad (260)$$

is shown in Figures 13 and 14 for two different values of the loop parameter $\alpha\Delta t c$. Figure 13 applies to the $R_{\Delta} \neq [0]$ case and Figure 14 applies to the $R_{\Delta} = [0]$ case. In a given signal environment, the transient response (or convergence rate) is ten times faster for $\alpha\Delta t c = 0.5$ than for $\alpha\Delta t c = 0.05$. For the $R_{\Delta} = [0]$ case, weight jitter causes the largest degradation in performance when g is small, i.e., for $g = 0.01$, T_{omin} must be increased by more than 8 dB when $\alpha\Delta t c = 0.5$ to obtain the same performance as a system with negligible weight jitter. For larger values of g , the relative performance degradation due to weight jitter decreases. For the $R_{\Delta} = [0]$ case, the effects of weight jitter are most pronounced for large values of g . For fixed values of input signal power and D , the minimum required output signal-to-noise ratio can be reduced in both the $R_{\Delta} = [0]$ and $R_{\Delta} \neq [0]$ cases by reducing the convergence rate (proportional to α) or by increasing the spectrum spreading ratio ($T/\Delta t$).

Under appropriate assumptions, the previous results can be used to approximate the effects of weight jitter on the performance of a DPSK detector. In coherent detection, decisions (at $t = T$) are based on the matched filter output voltage $v(T)$. In differential detection, decisions (at $t = 2T$) are based on the parameter

$$z(2T) = u(T) u^{\dagger}(2T) \quad (261)$$

where

$$u(T) = \frac{1}{T} \int_0^T \tilde{\gamma}(t) \tilde{r}'^{\dagger}(t) dt \quad (262)$$

and

$$u(2T) = \frac{1}{T} \int_T^{2T} \tilde{\gamma}(t) \tilde{r}'^{\dagger}(t) dt$$

In ideal differential detection, it is assumed (1) that the desired signal carrier frequency and the data bit arrival times are known at the receiver and (2) that $u(T)$ and $u(2T)$ are statistically independent random processes. Consequently, $\tilde{r}'^{\dagger}(t)$ and $\tilde{r}'(t)$ differ only by a constant phase angle. The performance measure D derived for coherent detection can therefore be used to approximate the signal-to-noise ratio of $u(T)$ and $u(2T)$:

$$D \Big|_{\text{DPSK}} = \frac{|E u(T)|^2}{\text{var}[u(T)]} = \frac{|E u(2T)|^2}{\text{var}[u(2T)]} = \frac{|E v(T)|^2}{\text{var}[v(T)]} \quad (263)$$

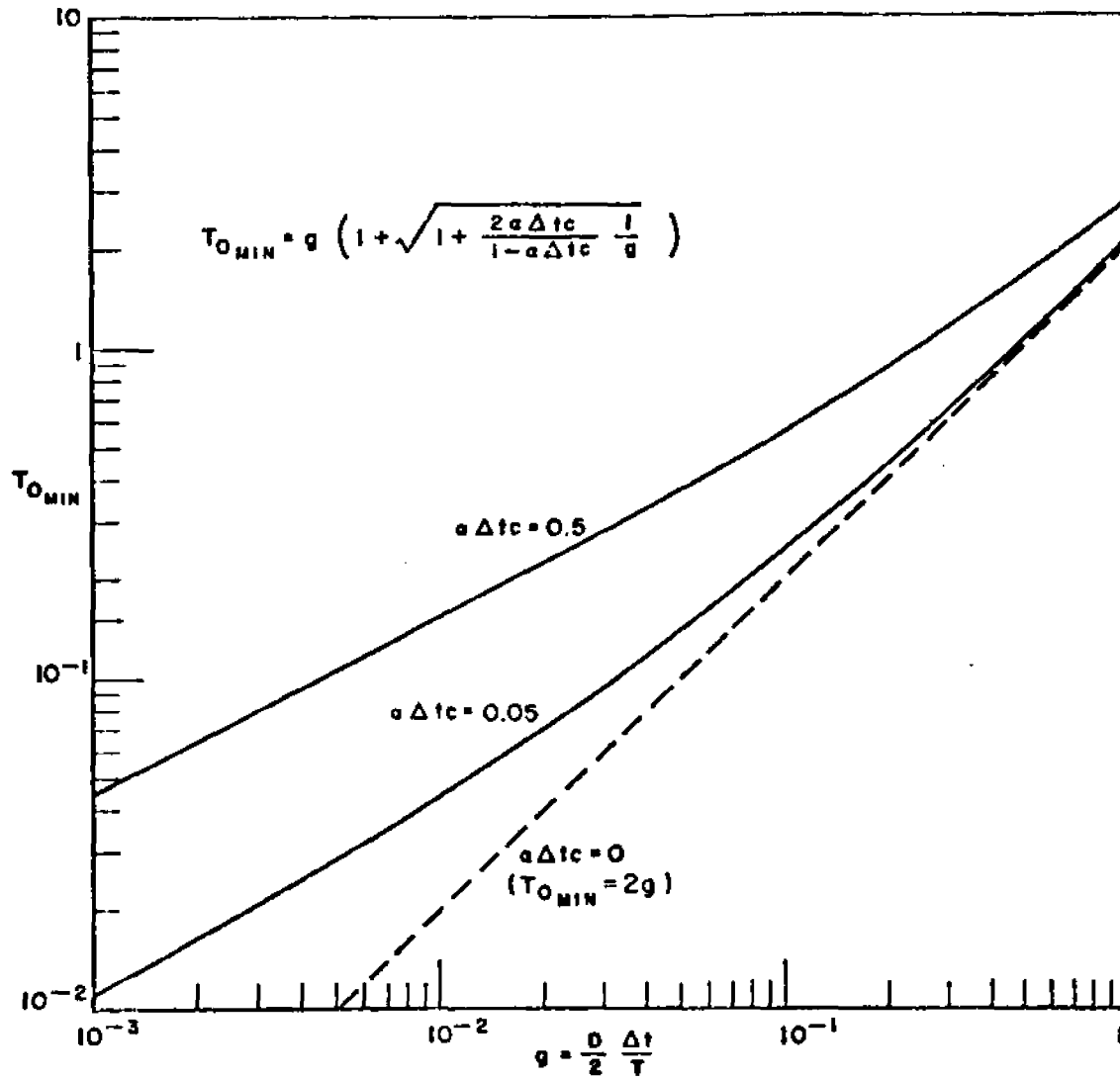


Figure 13. The minimum output signal-to-noise ratio required to obtain the performance level g ; $R_{\Delta} \neq [0]$.

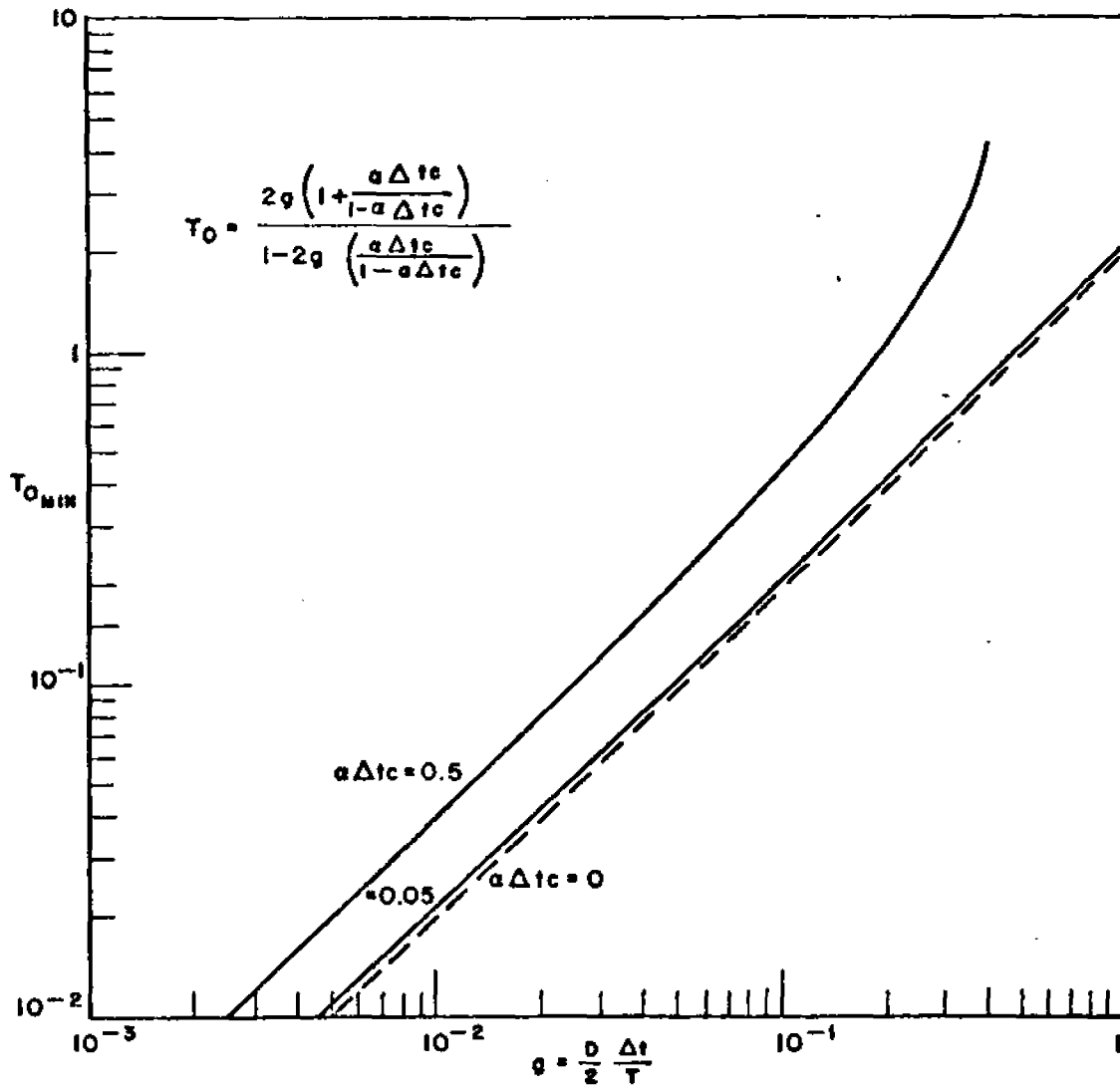


Figure 14--The minimum output signal-to-noise ratio required to obtain the performance level g ; $R_{\Delta} = [0]$.

CHAPTER V

TRANSIENT RESPONSE AND SIGNAL ESTIMATION

A. Introduction

Physical implementations of the spatial filter represented by $w_{opt} = K_x^{-1} R_{xd}$ require accurate estimates of K_x (or M) and R_{xd} based on noisy input data. The accuracy of these estimates, of course, depends on the method used to average the data. The LMS algorithm relies on averaging in the control loop to perform these estimates, which gives rise to two opposing system objectives; rapid response time and small control loop noise. Large control loop noise results when the weights are allowed to respond rapidly to instantaneous fluctuations of the input covariance matrix and the cross-correlation vector. The loop noise can be reduced by lowering the loop gain (and thus increasing the response time) since the instantaneous fluctuations are averaged over a longer period of time.

In this chapter, the separate effects of estimating K_x and R_{xd} in a finite observation interval will be determined. The primary objective will be to compare the relative performance of the LMS algorithm with an algorithm in which the spatial filter w is calculated directly by inverting an estimate of the covariance matrix and multiplying the result by an estimate of the cross-correlation vector. The estimates of K_x or R_{xd} are based on the maximum likelihood (ML) principle, which is optimal in that it yields an unbiased estimate with minimum variance [26]. Although an algorithm based on these estimates will be shown, in theory, to converge more rapidly than the LMS algorithm, it is considerably more difficult to implement circuits which estimate each element of K_x and then invert the result, since this operation requires m^2 estimates and an $m \times m$ matrix inversion. Moreover, finite circuit speeds preclude the possibility for achieving the theoretical convergence rate except when the input signals are very narrowband and the array size is small (see discussion in Chapter II). The comparison of the LMS and optimum estimator algorithms to be presented will thus be based on theoretical rather than practical considerations. The results of the analysis will be useful in determining (1) requirements for accurately estimating R_{xd} , (2) the effectiveness of control loop averaging relative to optimum estimation, and (3) an upper bound on LMS algorithm performance. The performance measure employed will be the output signal-to-noise ratio versus time (or observation interval). In order to isolate the effects of estimating R_{xd} from the effects of estimating K_x (or M when the desired signal is absent), analysis performed in section B assumes K_x (or M) is known a priori and the analysis in section C

assumes R_{xd} is known a priori. A method for approximating the response time when both K_x and R_{xd} are estimated is presented at the end of section C. Section D compares these results with the transient and steady-state performance of the LMS algorithm.

B. Estimating the Desired Signal Direction of Arrival Vector

Two spatial filters which optimize the array output signal-to-noise ratio (see Chapter III) are given by

$$w_1 = K_x^{-1} R_{xd}$$

and

$$w_2 = M^{-1} R_{xd} \quad . \quad (265)$$

In this section, the array output signal-to-noise ratio will be determined when R_{xd} in Equations (264) and (265) is replaced by its estimate \hat{R}_{xd} as follows:

$$\hat{w}_1 = K_x^{-1} \hat{R}_{xd} \quad (266)$$

$$\hat{w}_2 = M^{-1} \hat{R}_{xd} \quad . \quad (267)$$

To focus attention exclusively on the effects of errors in this estimate due to noise, K_x or M will be assumed given. In a practical system, this assumption implies that a sufficiently accurate estimate of one of these matrices is available when \hat{w}_1 or \hat{w}_2 is implemented. Equation (267) applies when the input covariance matrix is estimated in the absence of the desired signal, as would be the case prior to the TDMA preamble interval*, whereas Equation (266) applies when the desired signal is present at the array input, e.g., during the preamble interval. In the latter case, the estimates of K_x and R_{xd} may well be performed simultaneously. The validity of any performance measure of filter \hat{w}_1 would thus require the unrealistic assumption that the input covariance matrix estimate converges much more rapidly than the cross-correlation vector estimate. For this reason, emphasis will be placed on determining the performance of filter \hat{w}_2 .

*If another user's signal is present, it is treated as an interfering source.

The output signal-to-noise ratio, given w_2 , was shown in Chapter III to be given by

$$\left[\left(\frac{S}{N} \right)_0 \middle| w_2 \right] = \frac{\hat{w}_2^\dagger \underline{s} \underline{s}^\dagger \hat{w}_2}{\hat{w}_2^\dagger M \hat{w}_2} \quad (268)$$

which, in terms of \hat{R}_{xd} , may be written

$$\left[\left(\frac{S}{N} \right)_0 \middle| \hat{w}_2 \right] = \frac{\hat{R}_{xd}^\dagger M^{-1} \underline{s} \underline{s}^\dagger M^{-1} \hat{R}_{xd}}{\hat{R}_{xd}^\dagger M^{-1} \hat{R}_{xd}} \quad (269)$$

Equations (268) and (269) apply at any instant of time after filter \hat{w}_2 has been implemented.

The output SNR defined in Equation (269) is a function of the random vector \hat{R}_{xd} and thus is a (real) random variable. If Equation (268) [or (269)] is considered a function of \hat{w}_2 , then [see Equation (33)] it is bounded above by the optimum output SNR:

$$\left[\left(\frac{S}{N} \right)_0 \middle| \hat{w}_2 \right] \leq \frac{w_{opt}^\dagger \underline{s} \underline{s}^\dagger w_{opt}}{w_{opt}^\dagger M w_{opt}} = \underline{s}^\dagger M^{-1} \underline{s} \geq T_0 \quad (270)$$

where

$$w_{opt} = \beta M^{-1} R_{xd}$$

and β is an arbitrary constant. The performance of filter \hat{w}_2 will be determined by evaluating the mean output signal-to-noise ratio. To do this, it is convenient to normalize Equation (269) to its upper bound. That is, let

$$\rho_2 \equiv \frac{1}{T_0} \left[\left(\frac{S}{N_0} \right) \middle| \hat{w}_2 \right] = \frac{\hat{R}_{xd}^\dagger M^{-1} \underline{s} \underline{s}^\dagger M^{-1} \hat{R}_{xd}}{\hat{R}_{xd}^\dagger M^{-1} \hat{R}_{xd} \underline{s}^\dagger M^{-1} \underline{s}} \quad (271)$$

The mean and variance of the real random variable ρ_2 will be found by first determining its probability density function under the assumption that R_{xd} is a Gaussian random vector. Before proceeding, several additional assumptions will be made regarding the input signal statistics.

For the TDMA application being addressed, the desired signals are generated by quadrature (or biphase) modulating a constant envelope c.w. signal. It is therefore assumed that the desired signal $\tilde{s}(t)$ has a constant amplitude. The instantaneous cross-correlation vector is defined as

$$R_{xd}^I(t) = \tilde{x}(t) \tilde{r}^+(t) \quad (272)$$

where $\tilde{r}^+(t)$ represents the reference signal. It is assumed that the receive code timing and the desired signal carrier frequency are known a priori and that no data* is conveyed by $\tilde{s}(t)$. It therefore follows that

$$\tilde{r}(t) = A \tilde{s}(t) e^{j\theta} \quad (273)$$

where A and θ are assumed unknown real constants; e.g., signal phase and amplitude are not assumed known (or estimated). The mean cross-correlation vector, averaged over all signals present, thus becomes

$$\begin{aligned} R_{xd} &= E \tilde{x}(t) \tilde{r}^+(t) & (274) \\ &= E[\tilde{u}(t) + \tilde{s}(t)] \tilde{r}^+(t) \\ &= E \tilde{s}(t) \tilde{r}^+(t) \\ &= \tilde{s}(t) \tilde{r}^+(t) \end{aligned}$$

The above steps follow from the assumption that $\underline{u}(t)$ and $\underline{s}(t)$ are uncorrelated.

*This is the case during the preamble, for example.

Next, define $R_{\Delta}(t)$ as the difference between the instantaneous and average cross-correlation vector.

$$R_{\Delta}(t) = R_{xd}^I(t) - R_{xd} \quad . \quad (275)$$

Clearly, the ensemble average of each of the m components of $R_{\Delta}(t)$ equals zero:

$$E R_{\Delta}(t) = [0] \quad . \quad (276)$$

In the analysis, the random vector $R_{\Delta}(t)$ is modeled as a sample function from an m -variate Gaussian process. R_{xd} will be estimated by averaging k samples of $\underline{\hat{x}}(t) \hat{r}^T(t)$:

$$\begin{aligned} \hat{R}_{xd} &= \frac{1}{k} \sum_{i=1}^k \underline{\hat{x}}(t_i) \hat{r}^T(t_i) \quad t_1 < t_2 < \dots < t_k \quad (277) \\ &= \frac{1}{k} \sum_{i=1}^k R_{\Delta}(t_i) + R_{xd} \quad . \end{aligned}$$

It follows that \hat{R}_{xd} is unbiased, since

$$E \hat{R}_{xd} = R_{xd} \quad (278)$$

To simplify the analysis, $\Delta t = t_j - t_{j-1}$ ($j = 2, 3, \dots, m$) will be assumed constant and equal to the interval (Δt) between independent samples of $R_{\Delta}(t)$. In this case, it is easily shown that Equation (277) is the maximum likelihood estimate of R_{xd} [26]. Note that any Δt greater than the code chip duration results in (approximately) independent samples (assuming PN code modulation). Care must be exercised at this point in applying the Gaussian assumption. If the input noise signals ($\underline{u}(t)$) are assumed sample functions from independently distributed zero-mean Gaussian processes, then R_{xd} is m -variate Gaussian when t equals the interval between independent samples of $\underline{\hat{u}}(t)$. In more general noise situations, e.g., when narrowband interferences are present, the random vector R_{xd} only approximates a Gaussian process* [see Chapter VI]. As in Chapter IV, the difference between R_{xd} and its estimate \hat{R}_{xd} is defined as

*By the central limit theorem [28], this approximation generally improves as the number of samples grows larger.

$$\hat{R}_\Delta \equiv \hat{R}_{xd} - R_{xd} = \frac{1}{k} \sum_{i=1}^k R_\Delta(t_i) \quad ; \quad t_i - t_{i-1} = \Delta t \quad (279)$$

Again, it follows that

$$E \hat{R}_\Delta = [0] \quad . \quad (280)$$

The density function for ρ_2 is determined by first evaluating the density of R_Δ . The density function for the complex m -dimensional random vector \hat{R}_Δ is completely determined by its covariance matrix [27]:

$$\begin{aligned} \text{cov}(\hat{R}_\Delta) &= E \hat{R}_\Delta \hat{R}_\Delta^\dagger \quad (281) \\ &= E \left[\frac{1}{k} \sum_{i=1}^k \tilde{x}(t_i) \tilde{r}^\dagger(t_i) - R_{xd} \right] \\ &\quad \cdot \left[\frac{1}{k} \sum_{j=1}^k \tilde{x}^\dagger(t_j) \tilde{r}(t_j) - R_{xd}^\dagger \right] \\ &= E V - R_{xd} R_{xd}^\dagger \end{aligned}$$

where

$$E V = E \frac{1}{k^2} \sum_{i=1}^k \sum_{j=1}^k \tilde{x}(t_i) \tilde{r}^\dagger(t_i) \tilde{r}(t_j) \tilde{x}^\dagger(t_j) \quad . \quad (282)$$

Fourth order moments contained in Equation (282) can be evaluated by first separating $\tilde{x}(t)$ into desired signal and interference components, substituting the results into Equation (282), and then applying the assumption that $\tilde{x}(t_i) \tilde{r}^\dagger(t_i)$ and $\tilde{x}(t_j) \tilde{r}^\dagger(t_j)$ [$i \neq j$] are statistically independent. This procedure yields

$$E V = \frac{k-1}{k} R_{xd} R_{xd}^\dagger + \frac{1}{k} |\tilde{r}|^2 M + \frac{1}{k} R_{xd} R_{xd}^\dagger \quad . \quad (283)$$

Combining Equation (281) and Equation (283) generates the desired result

$$\text{cov}(\hat{R}_\Delta) = \frac{|r|^2}{k} M \quad . \quad (284)$$

The vector R_Δ is therefore characterized by the Gaussian probability density

$$P(R_\Delta) = (\pi)^{-m} \left| \frac{|r|^2}{k} M \right|^{-1} \exp \left[- \frac{k}{|r|^2} R_\Delta^\dagger M^{-1} R_\Delta \right] \quad (285)$$

where $|(\)|^{-1}$ represents the reciprocal of the determinant of the enclosed matrix and m represents the number of complex weights. The probability density of ρ_2 , in terms of the variables k , m , and T_0 , will be determined by performing a series of linear transformations on R_Δ .

For notational convenience, Equation (271) is rewritten in the form

$$\rho_2 = \frac{\hat{R}_{xd}^\dagger M^{-1} R_{xd} R_{xd}^\dagger M^{-1} \hat{R}_{xd}}{\hat{R}_{xd}^\dagger M^{-1} \hat{R}_{xd} R_{xd}^\dagger M^{-1} R_{xd}} \quad . \quad (286)$$

To put Equation (286) into a form which is more directly solvable, let x be an m -dimensional vector defined by the linear transformation

$$x = M^{-1/2} R_{xd} \quad . \quad (287)$$

A definition for $M^{-1/2}$ is given in Appendix II. Combining (286) and (287), yields

$$\begin{aligned} \rho_2 &= \frac{\hat{R}_{xd}^\dagger M^{-1/2} M^{-1/2} R_{xd} R_{xd}^\dagger M^{-1/2} M^{-1/2} \hat{R}_{xd}}{\hat{R}_{xd}^\dagger M^{-1} \hat{R}_{xd} R_{xd}^\dagger M^{-1/2} M^{-1/2} R_{xd}} \quad (288) \\ &= \frac{\hat{R}_{xd}^\dagger M^{-1/2} \underline{x} \underline{x}^\dagger M^{-1/2} \hat{R}_{xd}}{\hat{R}_{xd}^\dagger M^{-1} \hat{R}_{xd} \underline{x}^\dagger \underline{x}} \quad . \end{aligned} \quad (288)$$

The $m \times m$ matrix M is positive definite and Hermitian. Therefore, the scalar $R_{xd}^\dagger M^{-1} R_{xd}$ is a positive real number. In particular, its square root is defined. Next, define the vector \underline{y} as \underline{x} normalized to one:

$$\underline{y} = (R_{xd}^\dagger M^{-1} R_{xd})^{-1/2} \underline{x} \quad (289)$$

Computing

$$\begin{aligned} \underline{y}^\dagger \underline{y} &= \underline{x}^\dagger (R_{xd}^\dagger M^{-1} R_{xd})^{-1/2} (R_{xd}^\dagger M^{-1} R_{xd})^{-1/2} \underline{x} \\ &= (R_{xd}^\dagger M^{-1} R_{xd})^{-1} \underline{x}^\dagger \underline{x} \\ &= 1 \end{aligned}$$

verifies the normalization. Thus, in terms of \underline{y} , the normalized output signal-to-noise ratio has the form

$$\hat{\rho}_2 = \frac{\hat{R}_{xd}^\dagger M^{-1/2} \underline{y} \underline{y}^\dagger M^{-1/2} \hat{R}_{xd}}{\hat{R}_{xd}^\dagger M^{-1} \hat{R}_{xd}} \quad (290)$$

Since \underline{y} is a unit vector, there exists a unitary matrix U such that

$$\underline{y} = U \underline{g} \quad (291)$$

where

$$\underline{g}^\dagger = (1, 0, 0, \dots, 0) \quad (292)$$

and

$$U^\dagger U = U^{-1} U = I$$

Thus,

$$\rho_2 = \frac{\hat{R}_{xd}^+ M^{-1/2} U \underline{G} \underline{G}^+ U^{-1} M^{-1/2} \hat{R}_{xd}}{\hat{R}_{xd}^+ M^{-1/2} U U^{-1} M^{-1/2} R_{xd}^+} \quad (293)$$

Now define an m-dimensional random vector \hat{c} by the following linear transformation:

$$\hat{c} = U^{-1} M^{-1/2} \hat{R}_{xd} \quad (294)$$

In terms of \hat{c} , Equation (293) reduces to

$$\rho_2 = \frac{\hat{c}^+ \underline{G} \underline{G}^+ \hat{c}}{\hat{c}^+ \hat{c}} \quad (295)$$

Further simplification is possible by noting that $\hat{c}^+ \underline{G}$, $\underline{G}^+ \hat{c}$, and $\hat{c}^+ \hat{c}$ are scalars.

$$\underline{G}^+ \hat{c} = \hat{c}_1$$

$$\hat{c}^+ \underline{G} = \hat{c}_1^*$$

$$\hat{c}^+ \hat{c} = \sum_{i=1}^m |\hat{c}_i|^2$$

where \hat{c}_j denotes the j^{th} component of \hat{c} .

$\hat{\rho}_2$ expressed in terms of the components c_i ($i = 1, 2, \dots, m$) of the vector \hat{c} , is given by

$$\begin{aligned} \hat{\rho}_2 &= \frac{|\hat{c}_1|^2}{\sum_{i=1}^m |\hat{c}_i|^2} \\ &= \frac{1}{1 + \frac{1}{|\hat{c}_1|^2} (|\hat{c}_2|^2 + |\hat{c}_3|^2 + \dots + |\hat{c}_m|^2)} \end{aligned} \quad (296)$$

The joint probability density function of $|\hat{c}_1|^2$ and $\sum_{i=1}^m |c_i|^2$ is found by appropriately transforming the density of \hat{R}_{xd} . \hat{c} is related to the random vector \hat{R}_{xd} by

$$\hat{c} = U^{-1} M^{-1/2} \hat{R}_{xd}, \quad (297)$$

which can be written in the form

$$\hat{c} = H \hat{R}_{xd}$$

where $H = U^{-1} M^{-1/2}$.

Each \hat{c}_i is a linear combination of the components of the vector \hat{R}_{xd} . That is,

$$\hat{c}_i = \sum_{j=1}^m H_{ij} (\hat{R}_{xd})_j$$

where $(\hat{R}_{xd})_j$ denotes the j^{th} component of \hat{R}_{xd} . Since the components of \hat{R}_{xd} are jointly Gaussian, the components of \hat{c} are also jointly Gaussian [27]. The joint density of the \hat{c}_i is thus determined by the mean and covariance of \hat{c} . The desired result is obtained by performing the following series of inverse transformations:

$$\begin{aligned} E \hat{c} &= U^{-1} M^{-1/2} R_{xd} \\ &= U^{-1} \underline{x} \\ &= U^{-1} (R_{xd}^+ M^{-1} R_{xd})^{1/2} \underline{y} \\ &= (R_{xd}^+ M^{-1} R_{xd})^{1/2} \underline{g} \end{aligned}$$

Thus

$$E \hat{\underline{c}} = \begin{bmatrix} (R_{xd}^+ M^{-1} R_{xd})^{1/2} \\ 0 \\ 0 \\ \vdots \\ 0 \end{bmatrix} \quad (298)$$

and

$$\begin{aligned} \text{cov}(\hat{\underline{c}}) &= E U^{-1} M^{-1/2} \hat{R}_{\Delta} \hat{R}_{\Delta}^+ M^{-1/2} U \quad (299) \\ &= U^{-1} M^{-1/2} E \hat{R}_{\Delta} \hat{R}_{\Delta}^+ M^{-1/2} U \\ &= \frac{|\tilde{r}|^2}{k} U^{-1} M^{-1/2} M M^{-1/2} U \\ &= \frac{|\tilde{r}|^2}{k} I \end{aligned}$$

As a result, the set of random variables \hat{c}_j , $j = 1, 2, \dots, m$, are mutually stochastically independent Gaussian processes, each with variance $|\tilde{r}|^2/k$. The components \hat{c}_j , $j \neq 1$, are zero mean, whereas the mean of \hat{c}_1 equals $(R_{xd}^+ M^{-1} R_{xd})^{1/2}$. Let

$$\hat{Q}_1 = \frac{2k}{|\tilde{r}|^2} |c_1|^2 \quad (300)$$

$$\hat{Q}_2 = \frac{2k}{|\tilde{r}|^2} (|c_2|^2 + |c_3|^2 + \dots + |c_m|^2) \quad (301)$$

It can be shown [29] that the random variable \hat{Q}_1 has a non-central chi-square distribution with two degrees of freedom and non-centrality parameter $2 T_0 k$ and that \hat{Q}_2 has a chi-square distribution with $2m-2$ degrees of freedom. Therefore,

$$\hat{\rho}_2 = \frac{Q_1}{Q_1 + Q_2} = \frac{2 F'}{2 F' + 2m-2} \quad (302)$$

where the random variable F' , defined by

$$F' = \frac{(2m-2) Q_1}{2 Q_2} \quad ; \quad m = 2 \quad (303)$$

is non-central F distributed with parameters

$$r_1 = 2, \quad r_2 = 2m-2, \quad \theta = 2 T_0 k \quad .$$

The distribution function of $\hat{\rho}_2$ is an infinite sum of incomplete beta functions (e.g., [30]). The probability that $\hat{\rho}_2$ is less than the real number z is given by

$$P_r(\hat{\rho}_2 < z) = \sum_{j=0}^{\infty} e^{-kT_0} \frac{(kT_0)^j}{j!} I_z(1+j, m-1) \quad ; \quad (304)$$

$$0 < z < 1, \quad m \geq 2$$

where $I_z(1+j, m-1)$ is defined as the incomplete beta function

$$I_z(1+J, m-1) = \frac{1}{B(1+J, m-1)} \int_0^z t^J (1-t)^{m-2} dt$$

$$B(1+J, m-1) = \frac{j! (m-2)!}{(m+j-1)!} \quad .$$

Equation (304) gives the probability distribution function of the normalized output SNR $\hat{\rho}_2$, which is the desired result.

The performance provided by filter w_1 can be evaluated in a similar manner. When the weights are determined according to Equation (266), then the expression for the output signal-to-noise ratio, given w_1 , becomes

$$\left[\left(\frac{S}{N} \right)_0 \mid \hat{w}_1 \right] = \frac{\hat{R}_{xd}^+ K_x^{-1} \underline{s} \underline{s}^+ K_x^{-1} \hat{R}_{xd}}{\hat{R}_{xd}^+ K_x^{-1} M K_x^{-1} \hat{R}_{xd}} \quad . \quad (305)$$

As before, define $\hat{\rho}_1$ as Equation (305) normalized to the optimum T_0 :

$$\hat{\rho}_1 = \frac{1}{T_0} \left[\begin{pmatrix} \underline{S} \\ \underline{N} \end{pmatrix}_0 \mid \hat{w}_1 \right] = \frac{\hat{R}_{xd}^+ K_x^{-1} R_{xd} R_{xd}^+ K_x^{-1} \hat{R}_{xd}}{\hat{R}_{xd}^+ K_x^{-1} M K_x^{-1} \hat{R}_{xd} R_{xd}^+ M^{-1} R_{xd}} \quad (306)$$

By the matrix inversion lemma,

$$K_x^{-1} \hat{R}_{xd} = M^{-1} Q \hat{R}_{xd}$$

where

$$Q = I - \frac{\underline{s} \underline{s}^+ M^{-1}}{1 + \underline{s}^+ M^{-1} \underline{s}}$$

Thus

$$\hat{\rho}_1 = \frac{\hat{R}_{xd}^+ Q^+ M^{-1} R_{xd} R_{xd}^+ M^{-1} Q \hat{R}_{xd}}{\hat{R}_{xd}^+ Q^+ M^{-1} Q \hat{R}_{xd} R_{xd}^+ M^{-1} R_{xd}} \quad (307)$$

Employing steps similar to the analysis on \hat{w}_2 , Equation (307) can be reduced to the form

$$\hat{\rho}_1 = \frac{|\hat{d}_1|^2}{|\hat{d}_1|^2 + |\hat{d}_2|^2 + \dots + |\hat{d}_m|^2} \quad (308)$$

The vector

$$\underline{\hat{d}} = [\hat{d}_1, \hat{d}_2, \dots, \hat{d}_m]$$

is an m-variate Gaussian random vector with mean and covariance matrix

$$E \underline{\hat{d}}^+ = [f, 0, 0, \dots, 0]$$

$$\text{cov}(\hat{\underline{d}}) = \frac{|\tilde{r}|^2}{k} \begin{bmatrix} \frac{1}{(1 + T_0)^2} & 0 & 0 & \dots & 0 \\ 0 & 1 & 0 & \dots & 0 \\ 0 & 0 & 1 & \dots & 0 \\ \vdots & & & & \vdots \\ 0 & 0 & 0 & \dots & 1 \end{bmatrix}$$

where $f = |\tilde{r}| \frac{T_0}{1 + T_0}$.

Thus the \hat{d}_i , $i = 1, 2, \dots, m$, are statistically independent Gaussian random variables. Now define the random variables

$$\hat{Q}_3 = \frac{2k}{|\tilde{r}|^2} (1 + T_0)^2 |\hat{d}_1|^2 \quad (309)$$

$$\hat{Q}_4 = \frac{2k}{|\tilde{r}|^2} \sum_{i=2}^m |\hat{d}_i|^2$$

\hat{Q}_3 has a non-central chi-square distribution with two degrees of freedom and non-centrality parameter $2 T_0 k$ [29] and \hat{Q}_4 has a chi-square distribution with $2 m - 2$ degrees of freedom. The random variable

$$F' = \frac{(2m - 2) \hat{Q}_3}{2 \hat{Q}_4} = \frac{(2m - 2) (1 + T_0)^2 |\hat{d}_1|^2}{2 \sum_{i=2}^m |\hat{d}_i|^2} \quad (310)$$

therefore has a non-central F distribution with two and $2 m - 2$ degrees of freedom and with non-centrality parameter $2 T_0 k$. ρ_1 , expressed in terms of F' , is obtained by substituting Equation (310) in Equation (309):

$$\hat{\rho}_1 = \frac{2 F'}{2 F' + (1 + T_0)^2 (2 m - 2)} \quad 0 < F' < \infty, \quad m \geq 2 \quad (311)$$

The density function of $\hat{\rho}_1$ is difficult to evaluate since it cannot be expressed in terms of known functions. However, it is useful to note that F' defined in Equation (310) has the same distribution as F' defined in Equation (303), which permits direct comparison of the performance measures $\hat{\rho}_1$ and $\hat{\rho}_2$. Assuming F' given, it can be shown that

$$(a) \quad \hat{\rho}_1 = \frac{\hat{\rho}_2}{\hat{\rho}_2 + (1 + T_0)^2 (1 - \rho_2)} \quad (312)$$

$$(b) \quad \hat{\rho}_1 < \hat{\rho}_2 < 1 \quad ; \quad T_0 > 0$$

$$(c) \quad \hat{\rho}_1 \doteq \frac{\rho_2}{1 - \hat{\rho}_2} \frac{1}{(1 + T_0)^2} \quad ; \quad \frac{\hat{\rho}_2}{1 - \hat{\rho}_2} \ll (1 + T_0)^2$$

or $\hat{\rho}_1 \ll 1$

$$(d) \quad \lim_{T_0 \rightarrow 0} \hat{\rho}_1 = \hat{\rho}_2$$

and, when F' is viewed as a random variable, that

$$(e) \quad \lim_{k \rightarrow \infty} \hat{\rho}_1 = \lim_{k \rightarrow \infty} \hat{\rho}_2$$

Relations given in (312(a)) and (312(b)) indicate that the output signal-to-noise ratio obtained from $w_1 = K_x^{-1} \hat{R}_{xd}$ is less* than that obtained from $w_2 = M^{-1} \hat{R}_{xd}$. The performance difference is greatest when T_0 is large and k is small [Equation (312(c))]. The decrease in the rate of convergence is apparently

*Both w_1 and w_2 converge to w_{opt} as $k \rightarrow \infty$.

due to the presence of terms in the covariance matrix due to desired signal which are not required in implementing the optimum filter. Relations (312(d)) and (312(e)) show that in many cases of interest, i.e., when T_0 is small and the sample size (k) is large, the performance provided by filters \hat{w}_1 and \hat{w}_2 are nearly the same.

The distribution function for $\hat{\rho}_2$, given in Equation (304), is a function of the number of elements (m) and the product T_0k , where k represents the number of independent samples and T_0 represents the optimum output SNR. Array performance is therefore directly proportional to k and T_0 .

Two measures of the normalized output signal-to-noise ratio $\hat{\rho}_2$ have been evaluated numerically. One measure employed is the probability that the output SNR is within 3 dB of its optimum value; e.g.,

$$q = P_r(\hat{\rho}_2 > 0.5) \quad .$$

Figure 15 illustrates the calculated value of q versus T_0k for several different array sizes (m). In the limit as the number of samples approaches infinity, the probability that $\hat{\rho}_2$ is greater than 0.5 approaches one; that is, the estimate of R_{x^d} improves as the averaging time increases. As m increases, a larger value of T_0k is required to obtain the same value for q . This is as expected, since the optimum output signal-to-noise ratio generally increases with m , but the noise in each component of $\tilde{x}(t)$ $\tilde{r}^i(t)$ does not change.

The mean value of $\hat{\rho}_2$ was used as a second measure of performance. The mean of a random variable \tilde{x} which has the beta distribution

$$\tilde{x} \sim I_2(a, b)$$

is given by [30]

$$E \hat{x} = \frac{a}{a + b} \quad .$$

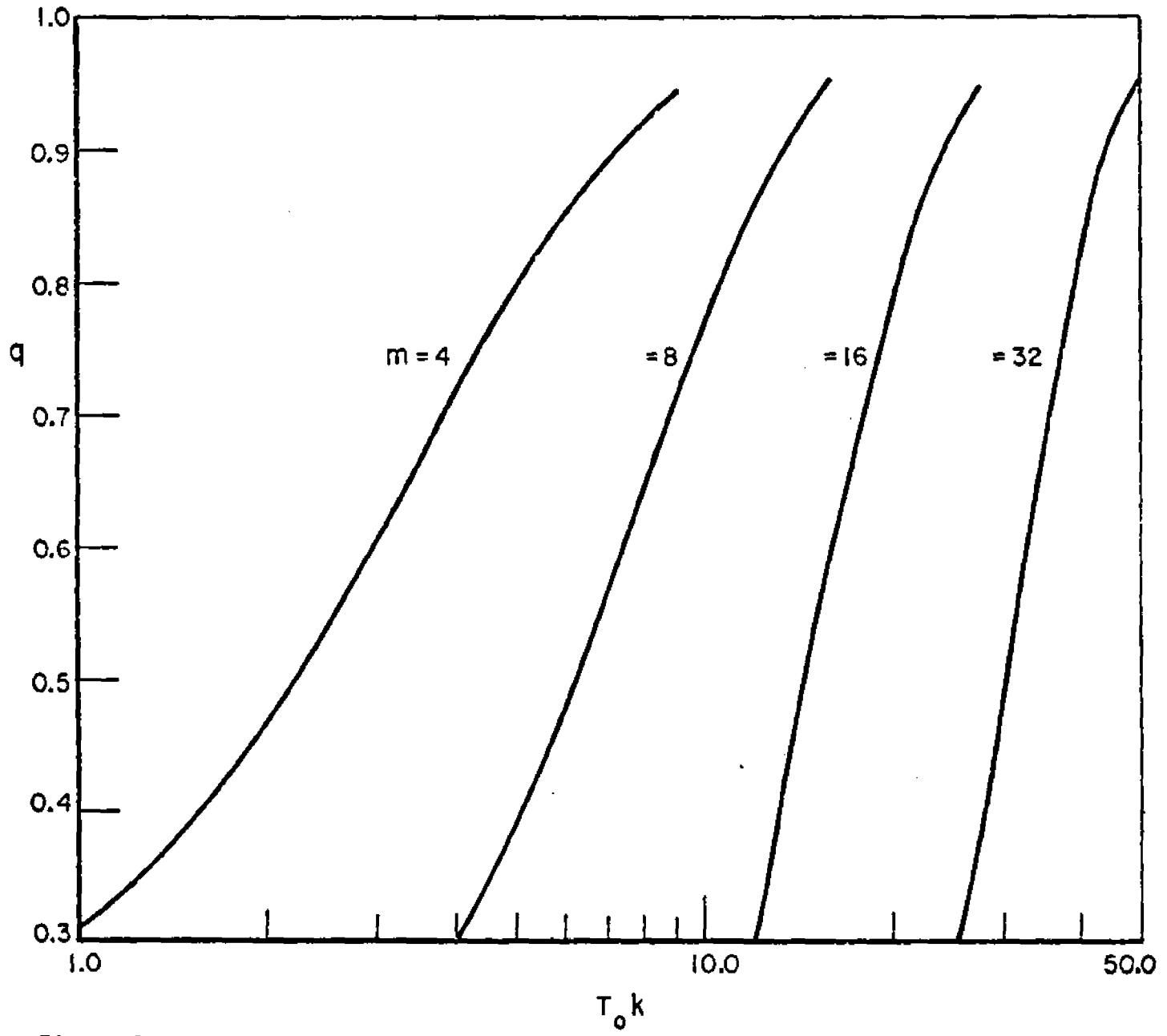


Figure 15--The probability that the average output signal-to-noise ratio, normalized to T_0 , is less than -3 dB versus T_0 and the number of samples (k) for several different array sizes.

Since $\hat{\rho}_2$ is composed of an infinite sum of beta distributions, its mean is obtained by letting $a = j + 1$, $b = m - 1$, and summing as in Equation (304). That is,

$$E \hat{\rho}_2 = \sum_{j=0}^{\infty} e^{-T_0 k} \frac{(T_0 k)^j}{j!} \frac{1+j}{m+j} \quad (313)$$

Similarly, it can be shown that the variance of $\hat{\rho}_2$ is expressed as

$$\begin{aligned} \text{var}(\hat{\rho}_2) &= E \hat{\rho}_2^2 - [E \hat{\rho}_2]^2 \quad (314) \\ &= \sum_{j=0}^{\infty} e^{-T_0 k} \frac{(T_0 k)^j}{j!} \frac{(1+j)(2+j)}{(j+m)(j+m+1)} - [E \hat{\rho}_2]^2 \end{aligned}$$

Figure 16 illustrates the dependence of $E \hat{\rho}_2$ on $T_0 k$ for several values of m . To establish an approximate confidence interval on $E \hat{\rho}_2$, the standard deviation of $\hat{\rho}_2$, normalized to $E \hat{\rho}_2$, has also been graphed in Figure 17. In all cases shown, the mean of the output signal-to-noise ratio is within 3 dB of its optimum value when $T_0 k$ is greater than the number of elements m . Moreover, the (normalized) standard deviation is less than about 0.3 when this criterion is satisfied.

Thus far, the analytical results have shown that (1) the maximum likelihood estimate of the cross-correlation converges to R_{xd} as the number of samples approaches infinity; (2) the mean of the normalized output signal-to-noise ratio of filter w_2 depends only on the product $T_0 k$, e.g., it does not explicitly depend on the signal geometries; and (3) the convergence rate depends on the number of elements (or the number of complex weights). These results were checked by a computer simulation of a four-element linear array with identical, equally spaced elements. The k th sample of the input noise vector applied to the simulated array was generated from independent samples of a zero-mean Gaussian process g as follows:

$$\tilde{u}_k = \sum_{i=1}^P \sqrt{A_i} (g_{i1}^k + j g_{i2}^k) \underline{v}_i + n_t^k \quad (315)$$

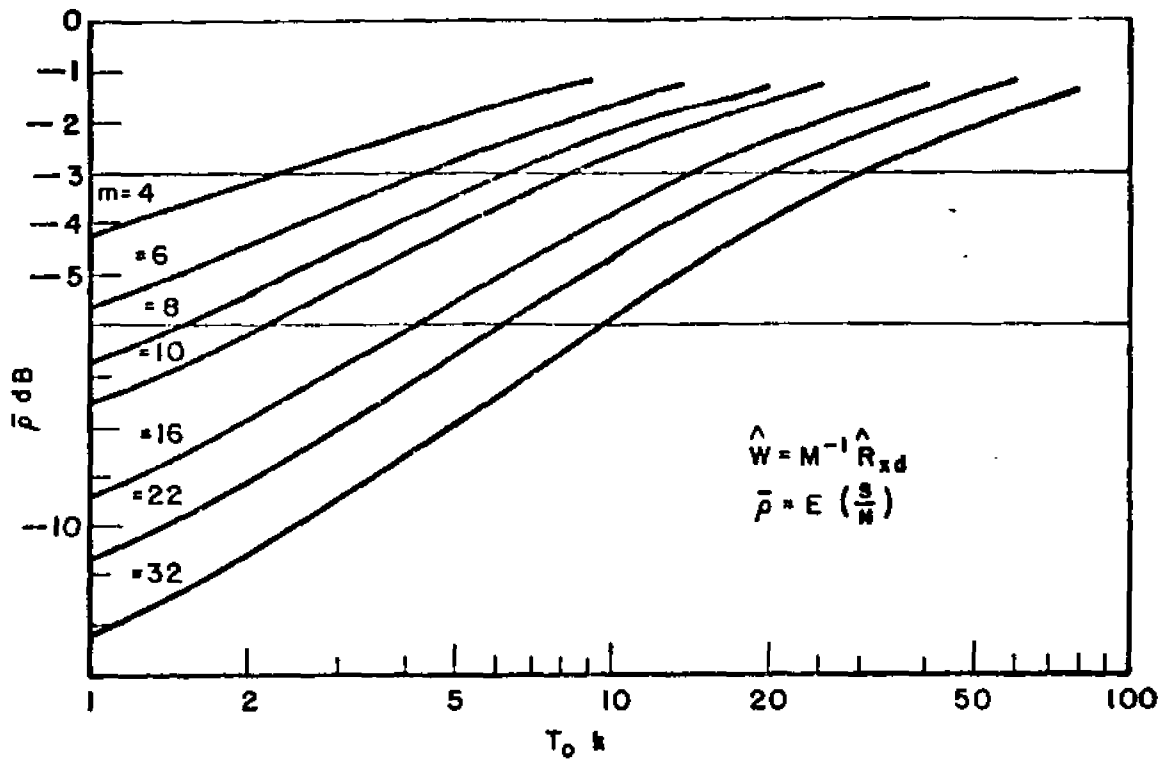


Figure 16--The average normalized output signal-to-noise ratio versus $T_0 k$ for several different array sizes.

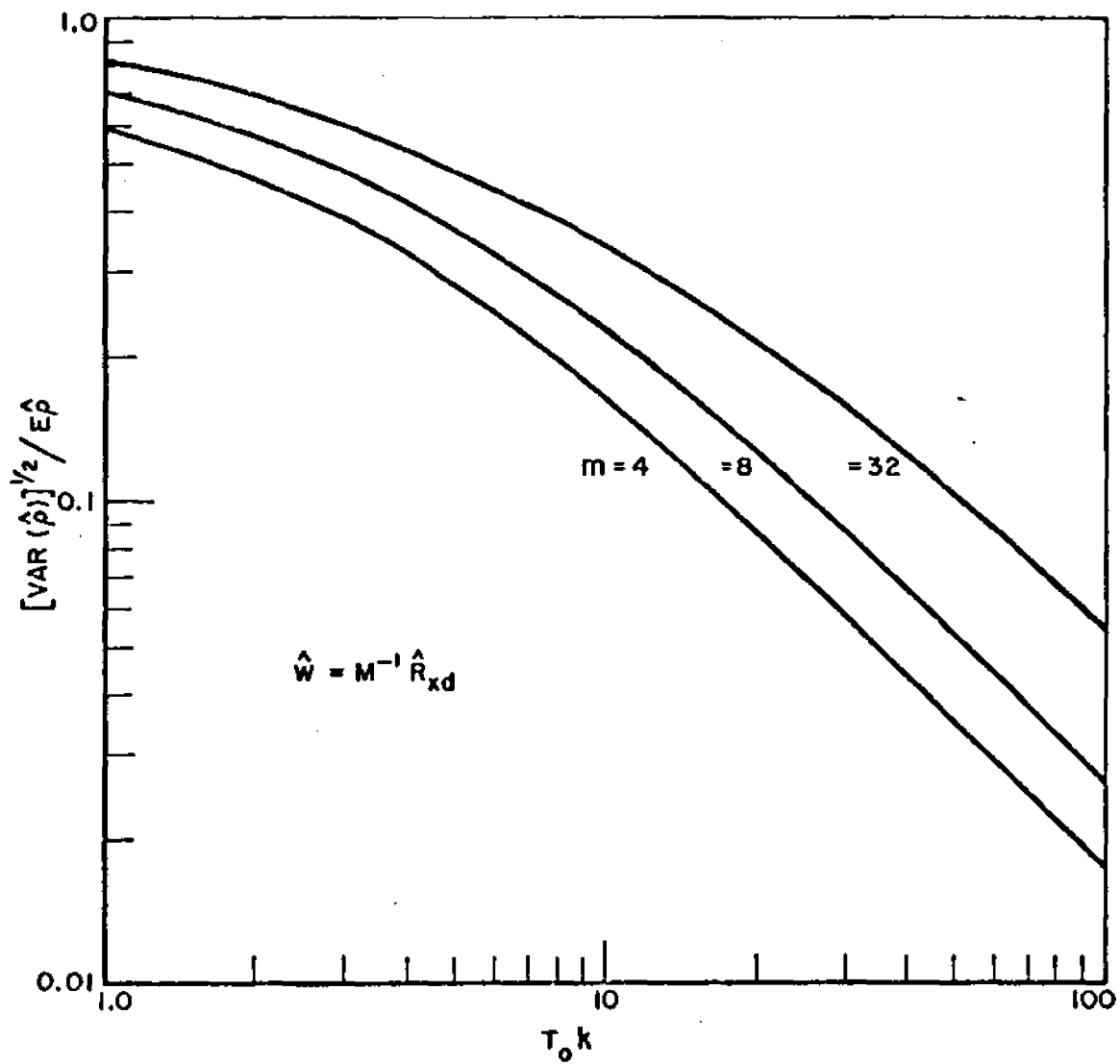


Figure 17--The standard deviation of $\hat{\rho}$ normalized to $\bar{\rho}$.

where

$$n_t^k = \sigma_2 \begin{bmatrix} g_{(p+1)1}^k + j g_{(p+1)2}^k \\ g_{(p+2)1}^k + j g_{(p+2)2}^k \\ \vdots \\ g_{(p+m)1}^k + j g_{(p+m)2}^k \end{bmatrix} .$$

Here, \underline{v}_ℓ represents the direction delay vector of the ℓ^{th} interfering signal and n_t^k represents the k^{th} sample of the element thermal noise vector. The real numbers g_{i1}^k and g_{i2}^k are statistically independent samples from a Gaussian distribution which has variance one. Thus, the i^{th} interfering signal has a per-element input power of A_i watts and the per-element thermal noise power is σ^2 . The k^{th} sample of the desired signal $\tilde{s}(t)$ was generated by sampling the complex envelope of a P-N coded c.w. signal; the number of samples per code bit could be selected equal to any positive integer.

Figures 18-20 compare \hat{E}_2 obtained in the simulation with the theoretical result given in Equation (313) for fixed signal environments; each point in the simulation represents an average of 100 independent trails. The signal environment and sample rate (relative to the code rate) corresponding to each figure is summarized in Table III.

Table III. Conditions Under Which Simulation Results in Figures 18-20 were obtained.

Relative Input Power Per Element and
DOA (in electrical degrees) per element

Desired Signal	Interference No. 1	Interference No. 2	Thermal Noise	T_0	Sample Rate	Figure No.
0 dB/0°	20 dB/30°	10 dB/60°	0 dB	-4.57 dB	10	18
4.57 dB	20 dB/30°	10 dB/60°	0 dB	0 dB	10	19
0 dB	-20 dB/30°	-20 dB/60°	0 dB	5.87 dB	10	20

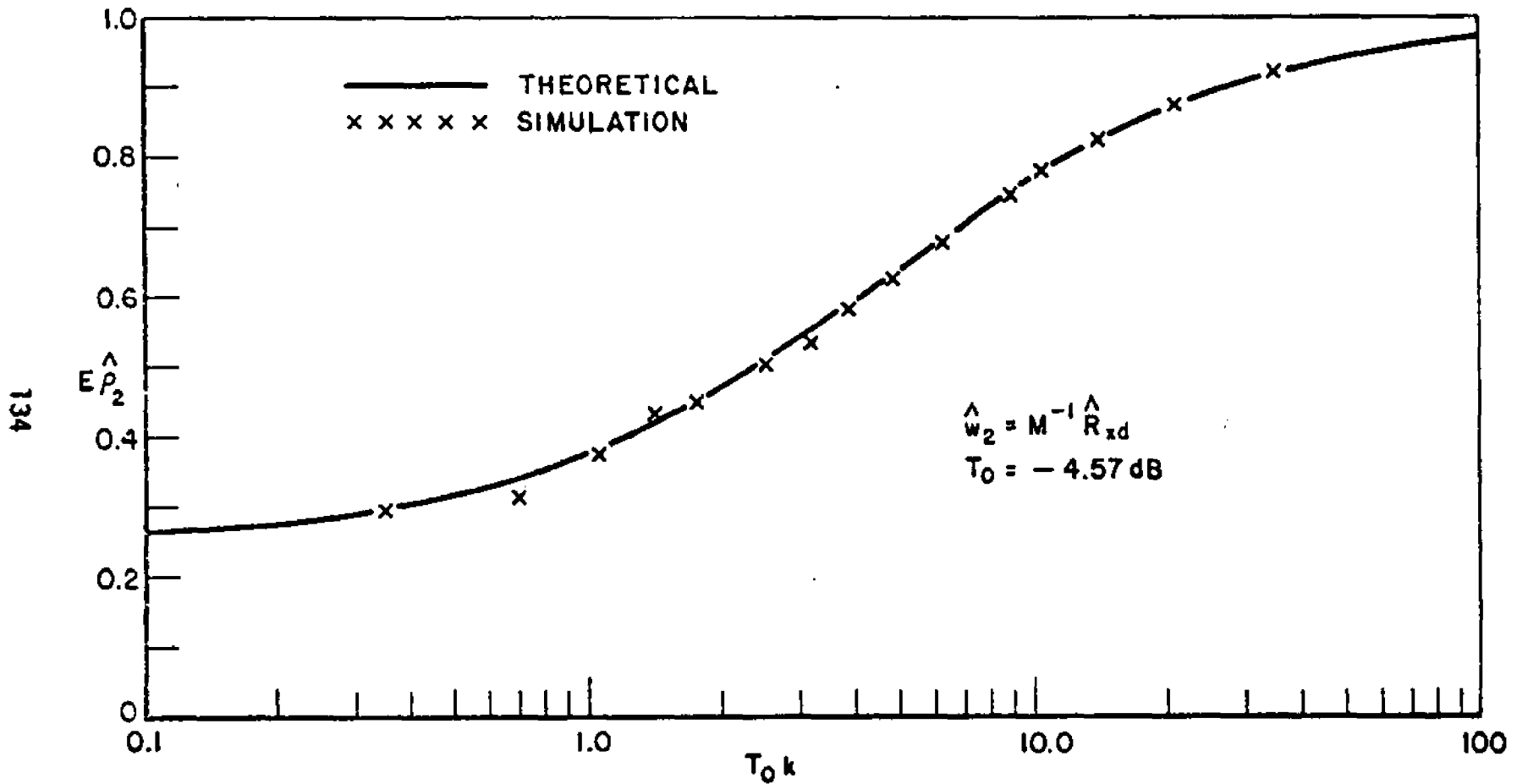


Figure 18--The average normalized output signal-to-noise ratio versus $T_0 k$ for a four-element array. Computer simulation results represent an average of 100 independent trials. $P'_s = 0 \text{ dB} / \underline{0^\circ}$; $\sigma^2 = 10 \text{ dB} / \underline{30^\circ}$; $10 \text{ dB} / \underline{60^\circ}$.

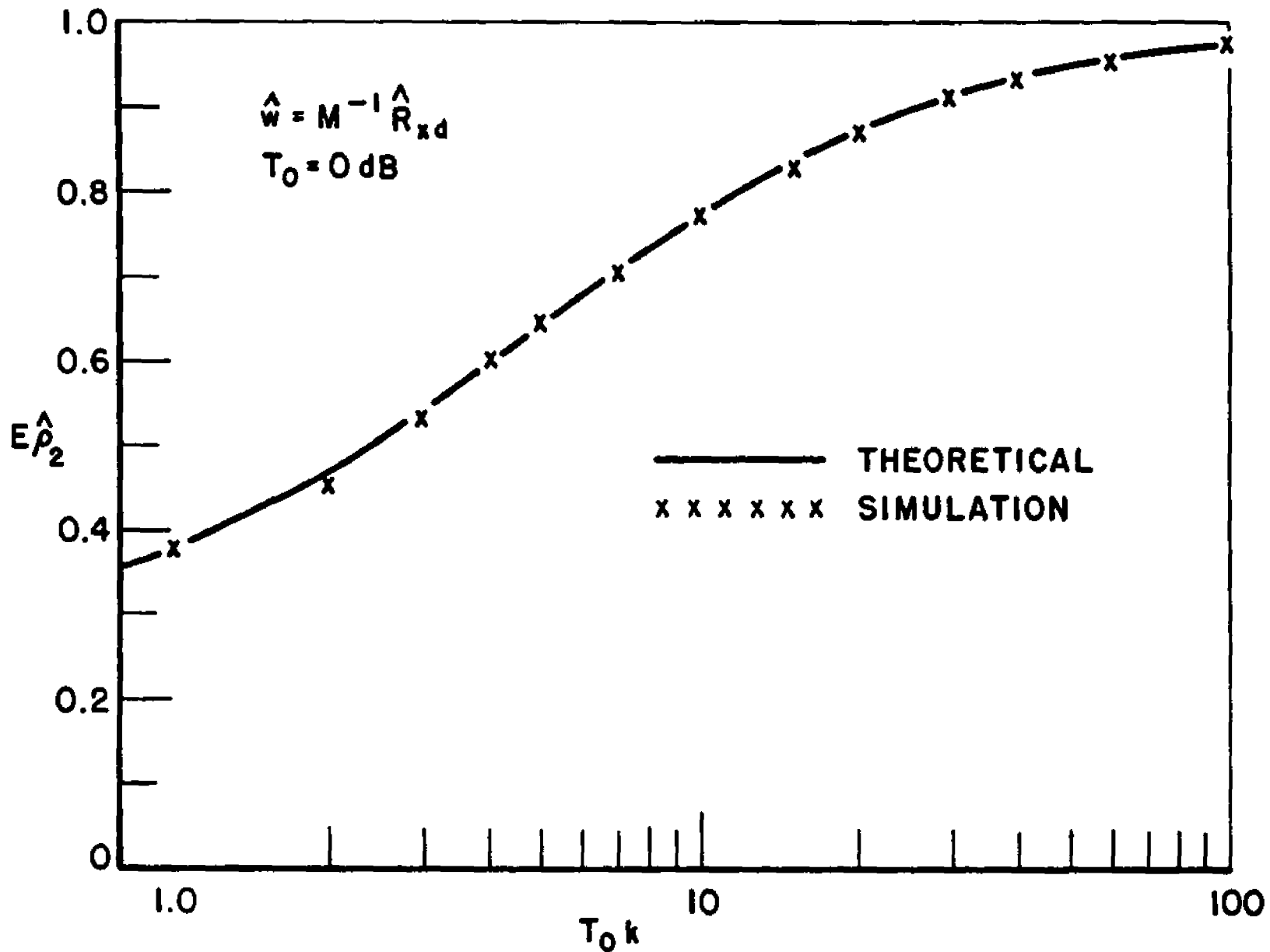


Figure 19--The average normalized output signal-to-noise ratio versus $T_0 k$ for a four-element array. Computer simulation results represent an average of 100 independent trials. $P_s^i = 4.57 \text{ dB} / 0^\circ$; $\sigma^2 = 0 \text{ dB}$. Two interfering signals: $20 \text{ dB} / 30^\circ$; $10 \text{ dB} / 60^\circ$.

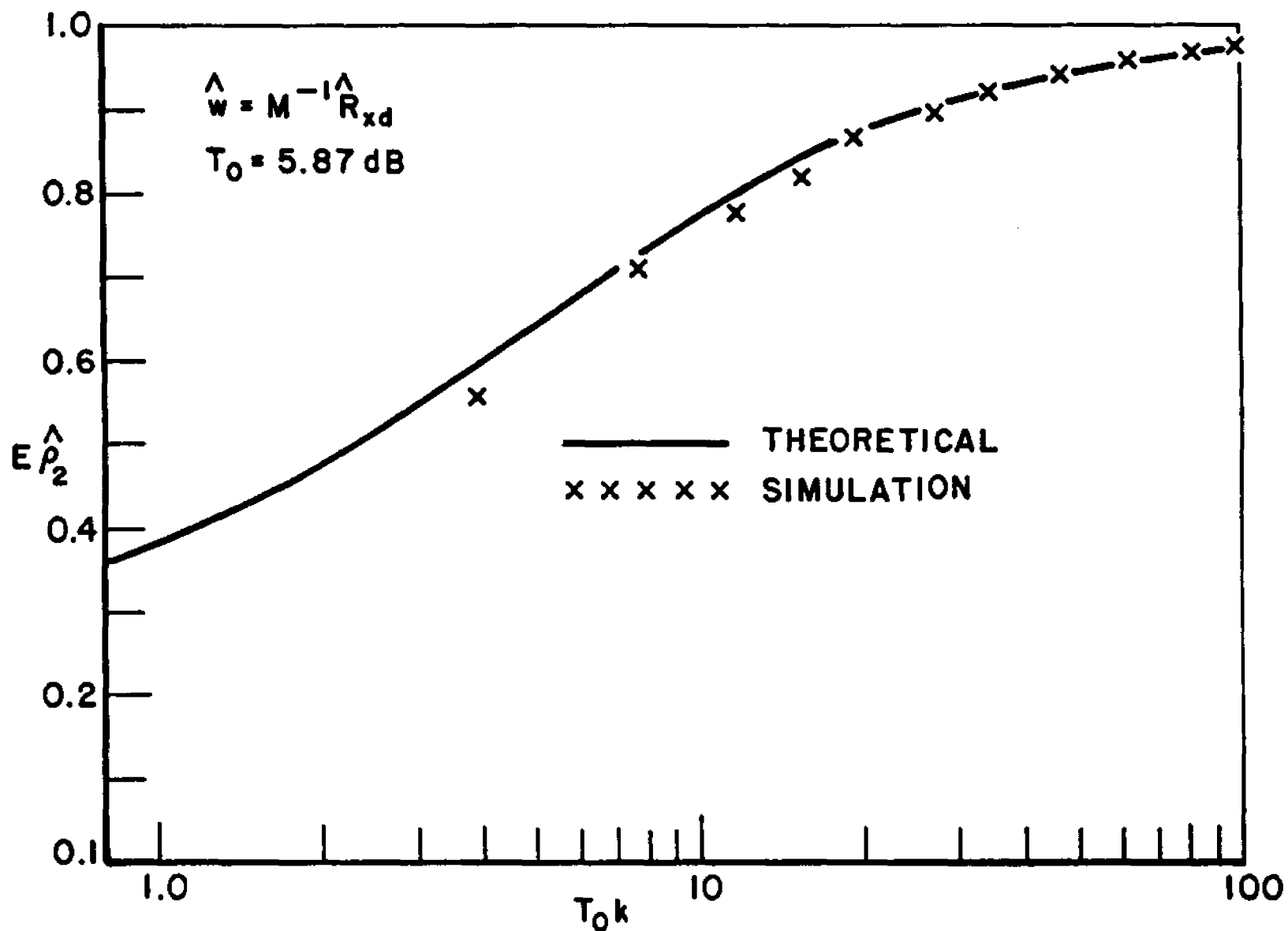


Figure 20--The average normalized output signal-to-noise ratio versus $T_0 k$ for a four-element array. Computer simulation results represent an average of 100 independent trials. $P_s^i = 0 \text{ dB} / 0^\circ$; $\sigma^2 = 0 \text{ dB}$. Two interfering signals: $-20 \text{ dB} / 30^\circ$; $-20 \text{ dB} / 60^\circ$.

In each case, simulation results closely agreed with theoretical results. Although not shown, many other signal environments (with $p \leq 3$) and sampling rates (relative to the code rate) were simulated and compared to the theoretical result; in all cases, similarly close agreement was obtained.

C. Estimating the Input Signal Covariance Matrix

The results presented in part B established guidelines for determining when it is appropriate to assume that an accurate estimate of the input cross-correlation vector (R_{xd}) can be obtained. In this section, R_{xd} is assumed given, and the weights will be determined by inverting an estimate of the input covariance matrix and substituting this result into Equation (264) or Equation (265); this method for implementing w will be denoted as the direct matrix inversion (DMI) technique. The matrix K_x (or M) will be estimated by using k independent samples of the input vector $\hat{X}(t)$ and by employing the maximum likelihood principle. The above procedure will be shown to converge to w_{opt} as k get large and, more importantly, the rate at which the output signal-to-noise ratio converges to T_0 will be established.

Two different methods for implementing the DMI technique will be considered; one assumes that $\hat{X}(t)$ contains the desired signal and the other assumes its presence negligible. Letting \hat{K}_x denote the estimate of K_x and \hat{M} the estimate of M , the weights for each respective technique may be written

$$\hat{w}_3 = \hat{K}_x^{-1} R_{xd} \quad (316)$$

$$\hat{w}_4 = \hat{M}^{-1} R_{xd} \quad (317)$$

The array output signal-to-noise ratio, given \hat{w}_3 or \hat{w}_4 , thus becomes

$$\left(\frac{S}{N}\right)_3 = \frac{R_{xd}^+ \hat{K}_x^{-1} \underline{s} \underline{s}^+ \hat{K}_x^{-1} R_{xd}}{R_{xd}^+ \hat{K}_x^{-1} M \hat{K}_x^{-1} R_{xd}} \quad (318)$$

$$\left(\frac{S}{N}\right)_4 = \frac{R_{xd}^\dagger \hat{M}^{-1} \underline{s} \underline{s}^\dagger \hat{M}^{-1} R_{xd}}{R_{xd}^\dagger \hat{M}^{-1} M \hat{M}^{-1} R_{xd}} \quad (319)$$

In order to find a closed form solution for the rate of convergence of the output SNR defined in Equation (318) or Equation (319), all signals present at the array input are modeled as sample functions from zero-mean Gaussian processes. Results derived under this assumption can be used to approximate performance in cases where the input signals approximate zero-mean Gaussian processes. The results can also be used to approximate performance for large sample sizes (k) when the input signals are random, zero-mean processes but not Gaussian. The approach adopted to accommodate the presence of a "deterministic" signal (i.e., the constant envelope desired signal) is to approximate performance by assuming a zero-mean Gaussian process in the derivation. The theoretical results obtained in this manner are then compared with computer simulation results to determine the validity of this approximation in realistic signal environments.

It is also assumed that the signals are independently distributed. Thus, the input signal vector $\underline{\tilde{x}}(t)$ is an m -variate complex Gaussian process with probability density

$$p(\underline{\tilde{x}}(t_i)) = (\pi)^{-m} |K_x|^{-1} \exp [-\underline{\tilde{x}}^\dagger(t_i) K_x^{-1} \underline{\tilde{x}}(t_i)] \quad (320)$$

where $K_x = E \underline{\tilde{x}}(t) \underline{\tilde{x}}^\dagger(t)$

The estimate of K_x will be based on k samples

$$\underline{\tilde{x}}(t_0 + \Delta t), \underline{\tilde{x}}(t_0 + 2 \Delta t), \dots, \underline{\tilde{x}}(t_0 + k \Delta t) \quad (321)$$

where Δt represents the interval between independent samples. The joint probability density of this set of observations is thus expressed as

$$p(\underline{\tilde{x}}(\Delta t), \underline{\tilde{x}}(2 \Delta t), \dots, \underline{\tilde{x}}(k \Delta t)) \quad (322)$$

$$= (\pi)^{-mk} |K_x|^{-k} \exp \left[- \sum_{i=1}^K \underline{\tilde{x}}^\dagger(i \Delta t) K_x^{-1} \underline{\tilde{x}}(i \Delta t) \right]$$

where t_0 has been set to zero for notational convenience. It has been shown that the maximum likelihood estimate of K_x , based on K independent samples of the process with density (322) is given by [6]

$$\hat{K}_x = \frac{1}{K} \sum_{i=1}^K \underline{\tilde{x}}(i \Delta t) \underline{\tilde{x}}^\dagger(i \Delta t) \quad (323)$$

Clearly,

$$E \hat{K}_x = K_x$$

Since each element of the $m \times m$ matrix \hat{K}_x is a random variable, the output signal-to-noise ratio in Equation (318) is also a random variable. The statistical properties of $(S/N)_3$ may be determined by deriving a probability density for the normalized output SNR, defined by

$$\hat{\rho}_3 \equiv \frac{\left(\frac{S}{N}\right)_3}{T_0} = \frac{R_{xd}^\dagger \hat{K}_x^{-1} \underline{s} \underline{s}^\dagger \hat{K}_x^{-1} R_{xd}}{R_{xd}^\dagger \hat{K}_x^{-1} M \hat{K}_x^{-1} R_{xd} \underline{s}^\dagger M^{-1} \underline{s}} \quad (324)$$

When $\underline{\hat{x}}(t)$ does not contain the desired signal $\underline{\tilde{s}}(t)$, then the expression for the normalized output SNR becomes

$$\hat{\rho}_4 = \frac{\left(\frac{S}{N}\right)_4}{T_0} = \frac{R_{xd}^\dagger \hat{M}^{-1} \underline{s} \underline{s}^\dagger \hat{M}^{-1} R_{xd}}{R_{xd}^\dagger \hat{M}^{-1} M \hat{M}^{-1} R_{xd} \underline{s}^\dagger M^{-1} \underline{s}} \quad (325)$$

The real variables $\hat{\rho}_3$ and $\hat{\rho}_4$ are random with the property

$$p_r(0 \leq \rho_j \leq 1) = 1 \quad ; \quad j = 3, 4$$

Reed, et al., [6] along with Goodman, have shown that the joint distribution of the estimated noise covariance matrix M is given by the central complex Wishart distribution. Via a series of variable transformations, they were then able to show that the random variable $\hat{\rho}_4$ defined in Equation (325) has a beta function distribution with parameters $k-m+2$ and $m-1$. That is,

$$p(\rho_4) = \frac{k!}{(m-2)!(k+1-m)!} (1-\rho_4)^{m-2} \rho_4^{k+1-m} \quad (326)$$

The expected value of ρ_4 was found to be

$$E \hat{\rho}_4 = \frac{k+2-m}{k+1} \quad (327)$$

and its variance

$$\text{var}(\hat{\rho}_4) = \frac{(k-m+2)(m-1)}{(k+1)^2(k+2)} \quad (328)$$

By Equations (327) and (328), $\hat{\rho}_4$ converges in the mean to one. Therefore, the weight vector w_4 [Equation (317)] generates a spatial filter which, on the average, converges to the optimum filter as k approaches infinity.

The measure $\hat{\rho}_4$ was intended for radar applications where it is appropriate to assume that input signal contains no desired signal components. However, in TDMA and other communication systems applications, the desired signal is generally assumed present in all data samples; in this case, the measure ρ_3 is appropriate.

Since the desired signal is also assumed to be a sample function from a zero-mean Gaussian process, the random variable

$$\hat{\rho}_3 = \frac{R_{xd}^+ \hat{K}_x^{-1} \underline{s} \underline{s}^+ \hat{K}_x^{-1} R_{xd}}{R_{xd}^+ \hat{K}_x^{-1} K_x \hat{K}_x^{-1} R_{xd} \underline{s}^+ K_x^{-1} \underline{s}} \leq 1 \quad (329)$$

has the same type of density as $\hat{\rho}_4$. Statistical properties of $\hat{\rho}_3$ will be determined by relating Equation (324) to Equation (329).

R_{yd} is a complex scalar multiple of \underline{s} ; thus, to simplify the notation, let

$$\rho_3' = \frac{\underline{s}^\dagger \hat{K}_x^{-1} \underline{s} \underline{s}^\dagger \hat{K}_x^{-1} \underline{s}}{\underline{s}^\dagger \hat{K}_x^{-1} K_x \hat{K}_x^{-1} \underline{s} + \underline{s}^\dagger K_x^{-1} \underline{s}} \quad (330)$$

and

$$\hat{\rho}_3 = \frac{\underline{s}^\dagger \hat{K}_x^{-1} \underline{s} \underline{s}^\dagger \hat{K}_x^{-1} \underline{s}}{\underline{s}^\dagger \hat{K}_x^{-1} M \hat{K}_x^{-1} \underline{s} + \underline{s}^\dagger M^{-1} \underline{s}} \quad (331)$$

Now

$$K_x = M + \underline{s} \underline{s}^\dagger$$

so that, by the matrix inversion lemma,

$$K_x^{-1} \underline{s} = \frac{1}{1 + T_0} M^{-1} \underline{s} \quad (332)$$

and

$$\underline{s}^\dagger K_x^{-1} \underline{s} = \frac{T_0}{1 + T_0} \quad (334)$$

Substituting Equations (332) and (334) into Equation (330) and rearranging terms yields

$$\begin{aligned} \rho_3' &= \frac{1 + T_0}{T_0} \frac{\underline{s}^\dagger \hat{K}_x^{-1} \underline{s} \underline{s}^\dagger \hat{K}_x^{-1} \underline{s}}{\underline{s}^\dagger \hat{K}_x^{-1} M \hat{K}_x^{-1} \underline{s} + \underline{s}^\dagger \hat{K}_x^{-1} \underline{s} \underline{s}^\dagger \hat{K}_x^{-1} \underline{s}} \quad (335) \\ &= \frac{1 + T_0}{T_0} \frac{1}{\frac{1}{T_0 \rho_3} + 1} \end{aligned}$$

Solving Equation (335) for $\hat{\rho}_3$ in terms of ρ_3' yields the expression

$$\hat{\rho}_3 = \frac{\hat{\rho}_3'}{T_0(1 - \hat{\rho}_3') + 1} \quad (336)$$

where $\hat{\rho}_3'$ has the probability density of Equation (326). It follows that

$$E \hat{\rho}_3 < E \hat{\rho}_4 \quad (337)$$

$$\lim_{T_0 \rightarrow 0} E \hat{\rho}_3 = E \hat{\rho}_4 \quad (338)$$

$$(T_0 + \Delta T_0) E \hat{\rho}_3(T_0 + \Delta T_0) > T_0 E \hat{\rho}_3(T_0) \quad (339)$$

where $\hat{\rho}_3(T_0 + \Delta T_0)$ represents the random variable $\hat{\rho}_3$ for the case in which the optimum output SNR is $T_0 + \Delta T_0$ ($\Delta T_0 > 0$).

The inequality in Equation (337) implies that, on the average, the output signal-to-noise ratio achieved by calculating $\hat{w} = \hat{K}_x^{-1} R_{xd}$ is less than that achieved by calculating $\hat{w} = \hat{M}^{-1} R_{xd}$ (except in the limit as $k \rightarrow \infty$). This behavior is a consequence of the fact that the matrix required for implementing the optimum weight vector can be determined from the thermal noise and interfering signals and that the presence of the desired signal can only degrade the estimate of this matrix (i.e., the desired signal provides no additional information of value in estimating M). The limit in (338) indicates that the difference in performance obtained using \hat{w}_3 or \hat{w}_4 becomes small for $T_0 < 1$. The last inequality (339) shows that the average output SNR (unnormalized) obtained using \hat{w}_3 increases as T_0 increases. Thus, the presence of desired signal in the estimate of the covariance matrix slows down the rate of convergence with respect to the convergence rate obtained with the signal absent, but the absolute output SNR increases (for a given value of k) as T_0 increases.

The probability density of $\hat{\rho}_3$ can be evaluated by noting that

$$\hat{\rho}_3 = \frac{1}{1 + (1 + T_0) \frac{m-1}{k-m+2} \hat{Q}}$$

where \hat{Q} is a random variable having an F distribution with $2(m-2)$ and $2(K-m+2)$ degrees of freedom. However, its distribution will not be evaluated since the moments of $\hat{\rho}_3$ can be determined from the distribution of $\hat{\rho}_4$ [Equation (326)]. The mean of $\hat{\rho}_3$ can be expressed in the form of an infinite series as follows:

$$E \hat{\rho}_3 = \frac{a}{a+b} \left\{ 1 + \sum_{i=1}^{\infty} (-T_0)^i \left(\frac{b}{a+b+1} \right) \cdot \left(\frac{b+1}{a+b+2} \right) \cdots \left(\frac{i+b-1}{i+a+b} \right) \right\} \quad (340)$$

where $a = k - m + 2$

and $b = m - 1$.

The dependence of $E \hat{\rho}_3$ on T_0 is illustrated in Figures 21-23 for $m = 4$, $m = 8$, and $m = 16$, respectively, where m represents the number of antenna elements; each curve corresponds to a fixed value for k . These results show that $E \hat{\rho}_3$ increases monotonically with k and that the number of samples required to achieve the same performance with respect to optimum increases as T_0 or m increase. Constant (absolute) output signal-to-noise ratio curves, for $(S/N)_3 = -10$ dB, 0 dB, and 10 dB, are superimposed on each graph for comparison purposes. Since the slope of these curves is always more negative than the slope of the constant k curves, $(S/N)_3$ increases with T_0 , which is in agreement with inequality (339).

Note that \hat{w}_4 significantly outperforms \hat{w}_3 when $T_0 \gg 1$. In this case, it would be advantageous to remove the components of \hat{K}_x due to the desired signal. Unfortunately, this can only be done if $\underline{s}(t)$ is known or if it can be accurately estimated. In other words, a priori knowledge of R_{xd} or even \underline{s} does not provide sufficient information for improving the convergence rate of \hat{w}_3 . To show this, let

$$\hat{D} = \frac{1}{K} \sum_{i=1}^K \hat{x}(t_i) \hat{x}^\dagger(t_i) - \underline{s} \underline{s}^\dagger$$

Then

$$\hat{D} = \hat{K}_x - \underline{s} \underline{s}^\dagger$$

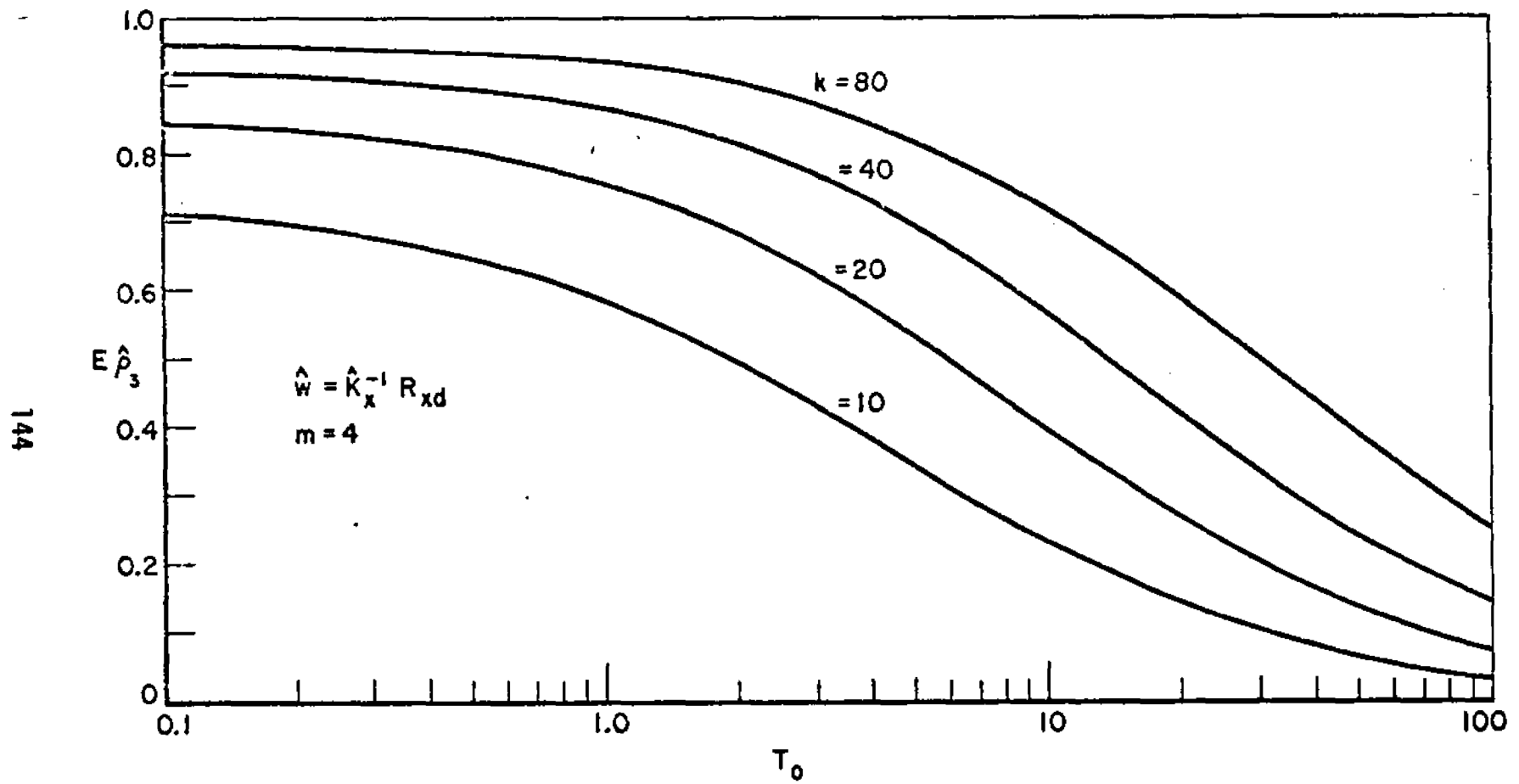


Figure 21--The average normalized output signal-to-noise ratio versus the optimum output signal-to-noise ratio for several different sample sizes (k).

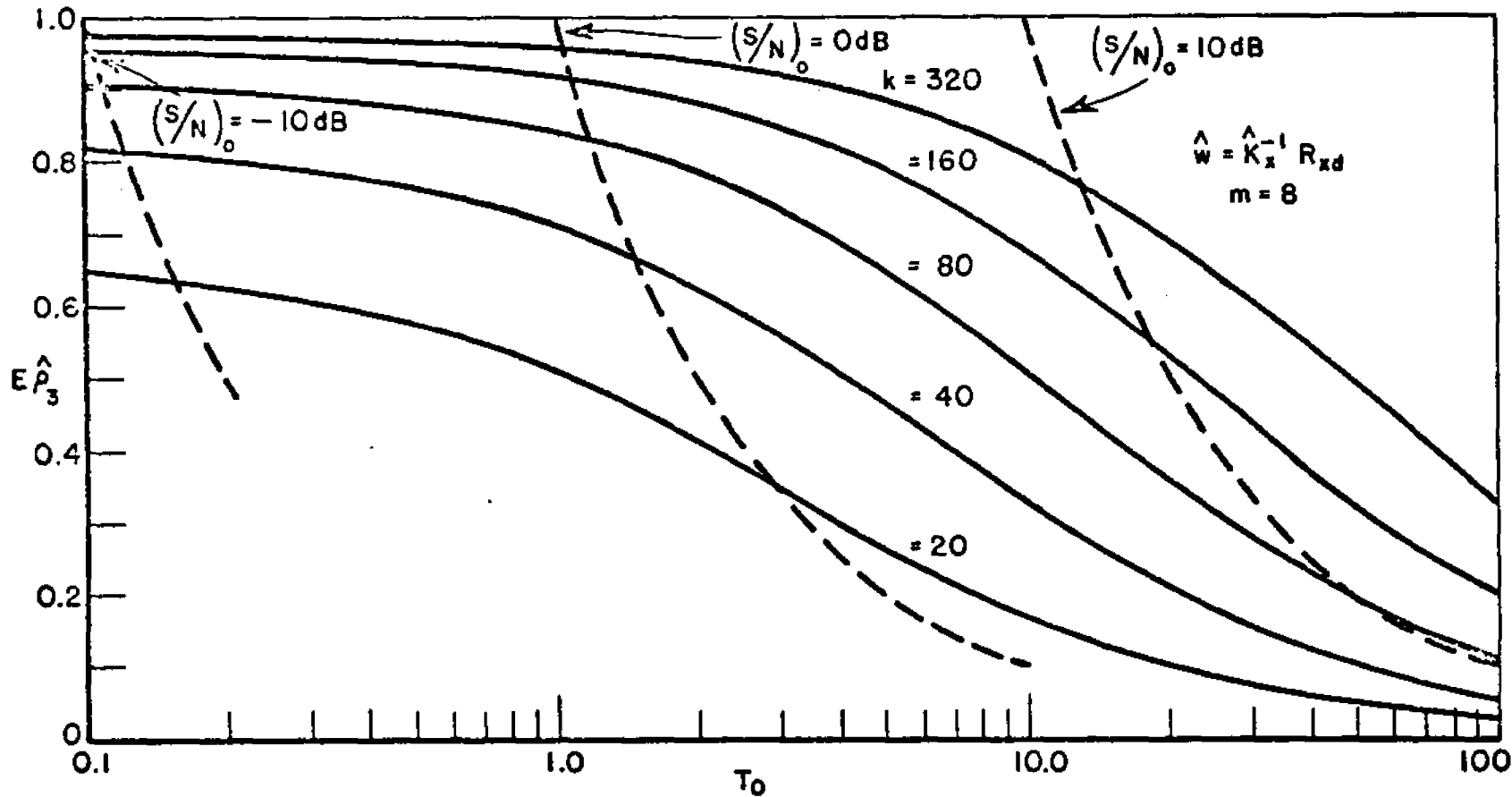


Figure 22--The average normalized output signal-to-noise ratio versus the optimum output signal-to-noise ratio for several different sample sizes (k).

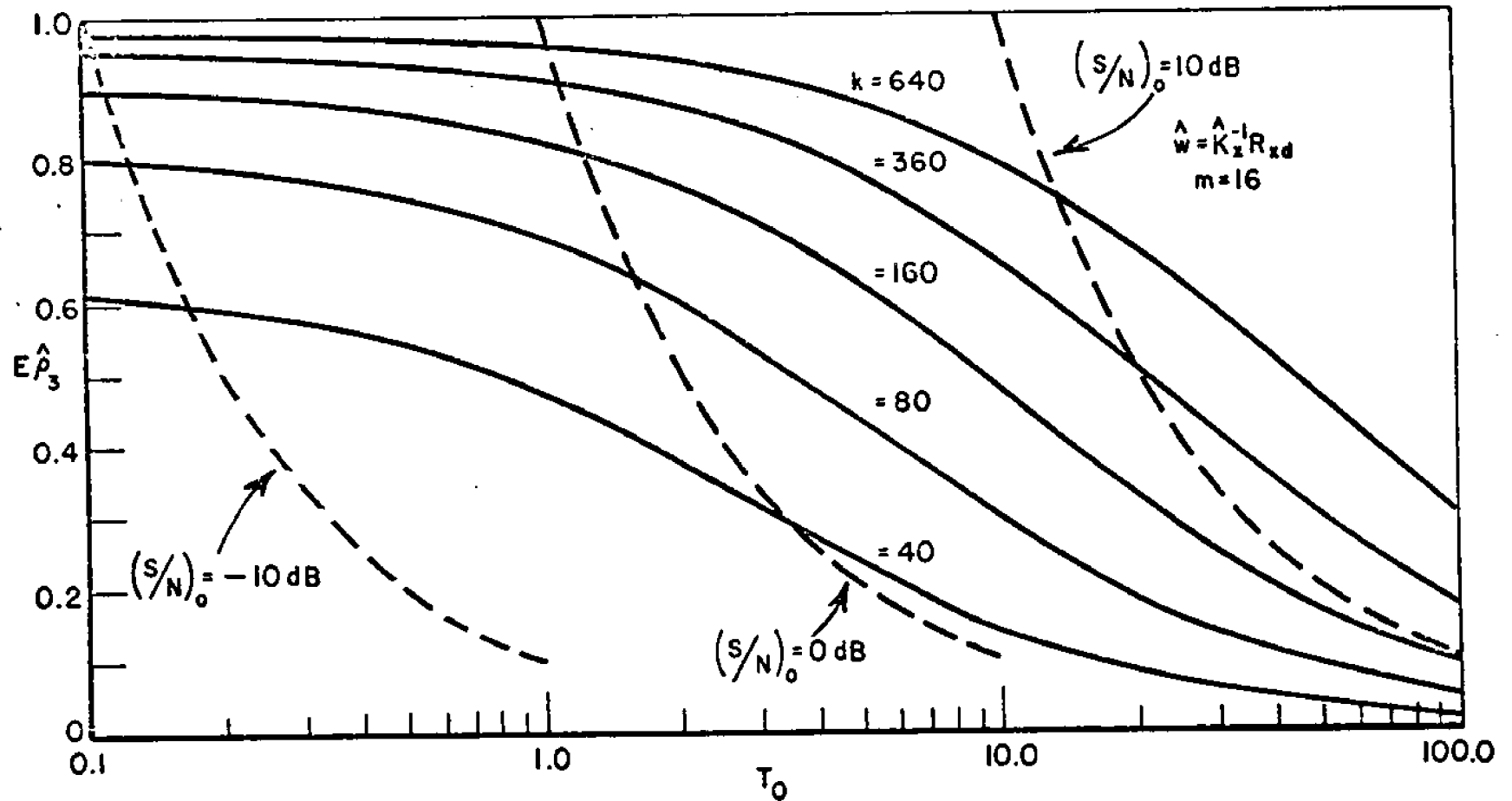


Figure 23--The average normalized output signal-to-noise ratio versus the optimum output signal-to-noise ratio for several different sample sizes (k).

and $E \hat{D} = M$.

Define

$$\begin{aligned} \hat{w}_s &= \hat{D}^{-1} \underline{s} & (341) \\ &= (\hat{K}_x - \underline{s} \underline{s}^\dagger)^{-1} \underline{s} \\ &= \frac{1}{1 + \underline{s}^\dagger \hat{K}_x^{-1} \underline{s}} \hat{K}_x^{-1} \underline{s} \end{aligned}$$

Although the coefficient of $\hat{K}_x^{-1} \underline{s}$ in Equation (341) is a random variable, the output SNR obtained by using w_5 is identical to that obtained from \hat{w}_3 and thus no improvement is achieved. Of course, in most communication systems applications, $\underline{s}(t)$ contains random data and fluctuates in phase and/or amplitude; for these cases it is unrealistic to assume that $\underline{s}(t)$ is known or even that it can be estimated with an adequate degree of accuracy.

Most communications systems are designed to meet performance criteria under worst case conditions. For example, one performance criterion could be the minimum acceptable signal-to-noise ratio at some point in the system. An adaptive array is then implemented to provide the desired performance criterion based on expected worst case interference and noise situations; that is, it is designed such that its worst case output signal-to-noise ratio is above some minimum, say T_{\min} . The curves shown in Figures 21-23 indicate that if T_{\min} is small, e.g., less than 0 dB or -3 dB, the impact of the presence of desired signal on convergence rates is minimal.

Computer simulations of the DMI technique were performed for the case of a linear four-element array. The array elements were assumed identical and equally spaced. The thermal noise and interfering signals were generated from independent samples of a zero-mean Gaussian process as in part B of this chapter. Also, a PN coded constant envelope signal was generated in the simulation to more accurately simulate signals encountered in the TDMA application under investigation (note that the analysis assumes the desired signal is zero mean Gaussian). The average normalized output signal-to-noise ratio ($E \hat{\rho}_3$) versus the number of samples (k) was used as the performance measure.* Figures 24-29 show that

*Each point in the simulation represents an average of 100 independent trials.

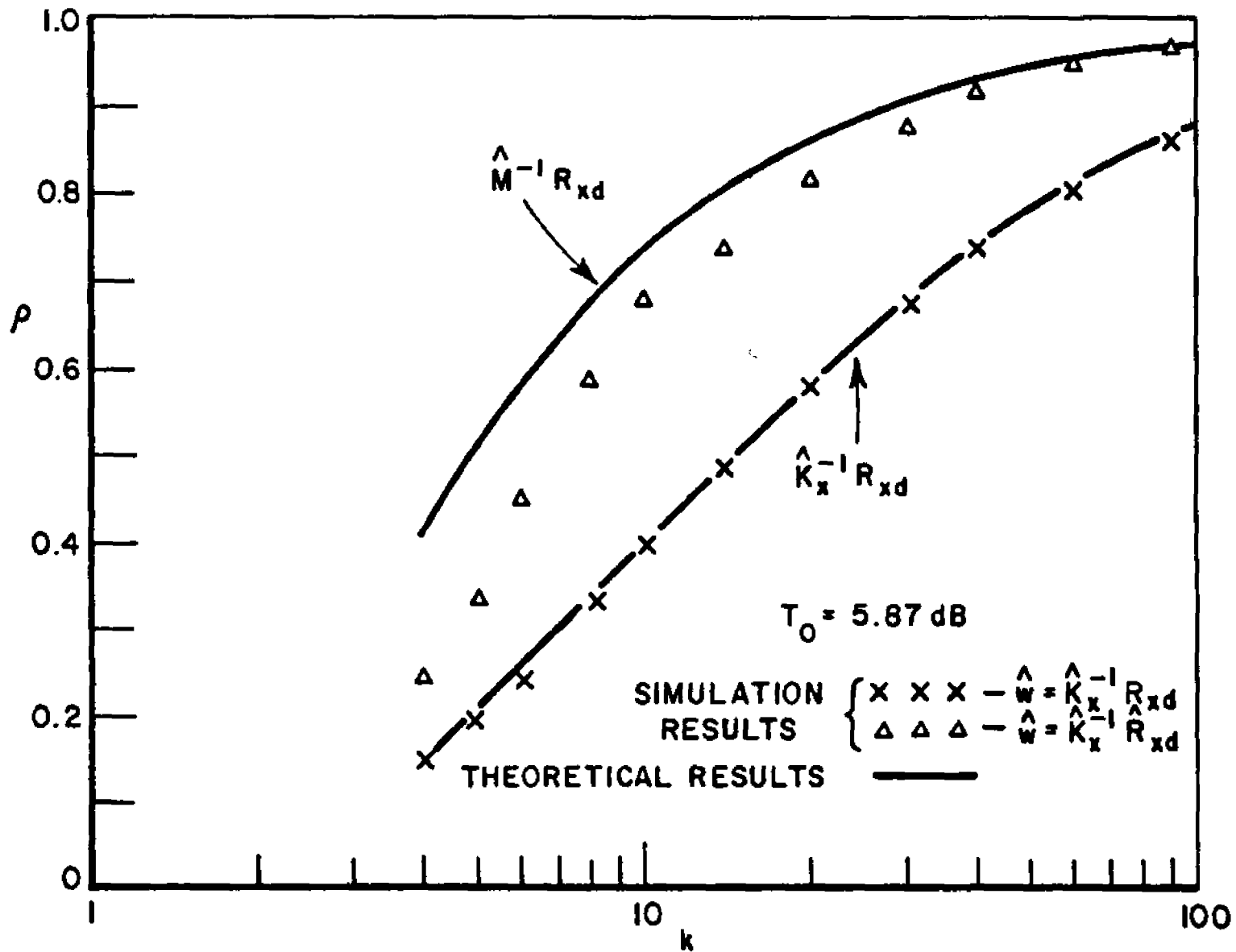


Figure 24--The average normalized output signal-to-noise ratio versus the number of samples for a four-element array. Computer simulation results represent an average of 100 runs. Input signals same as in Figure 20.

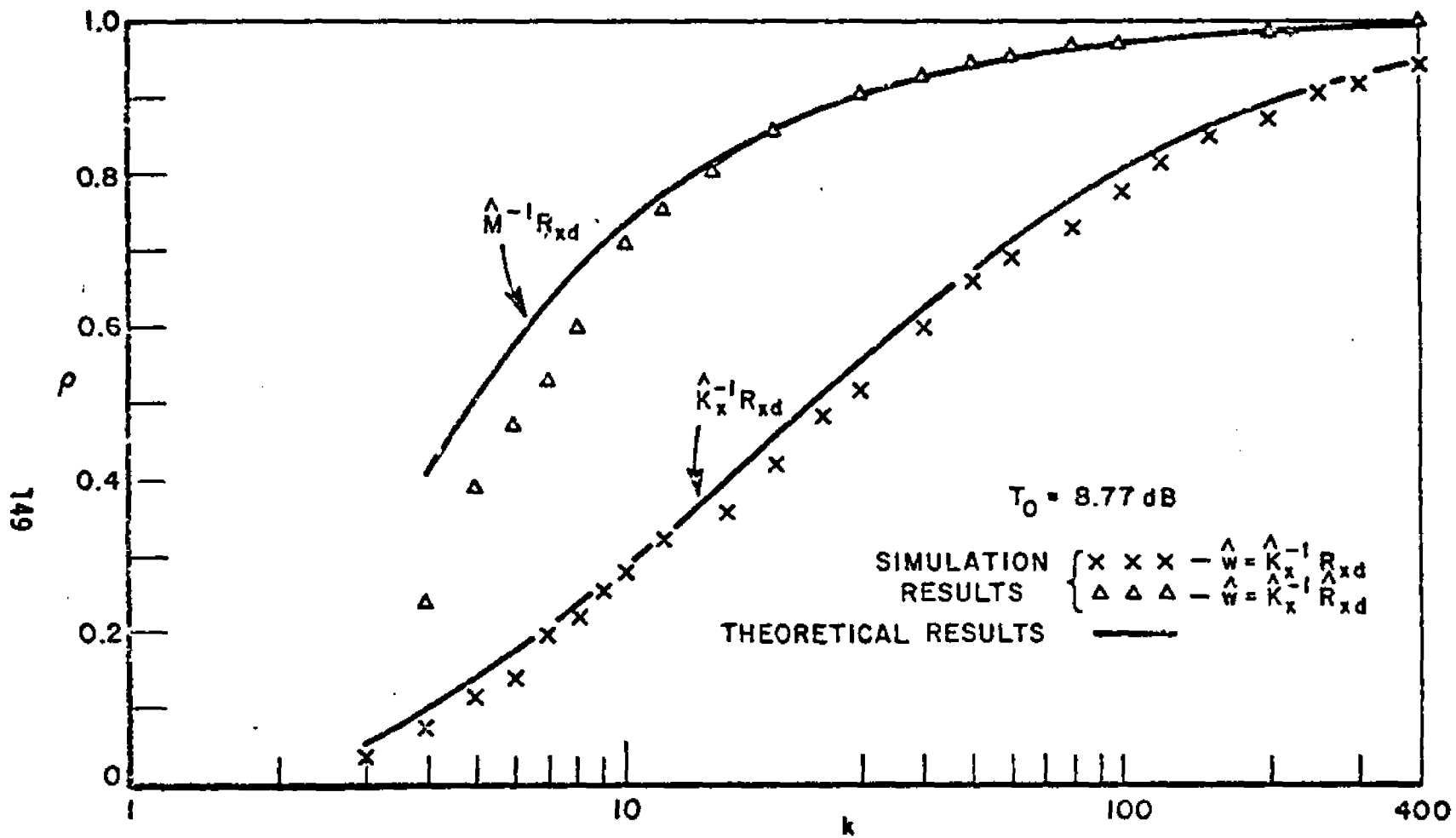


Figure 25--The average normalized output signal-to-noise ratio versus the number of samples for a four-element array. Computer simulation results represent an average of 100 runs. $P_s^i = 14.6 \text{ dB } / 0^\circ$; $\sigma^2 = 0 \text{ dB}$. Two interfering signals: $30 \text{ dB } / 30^\circ$; $20 \text{ dB } / 60^\circ$.

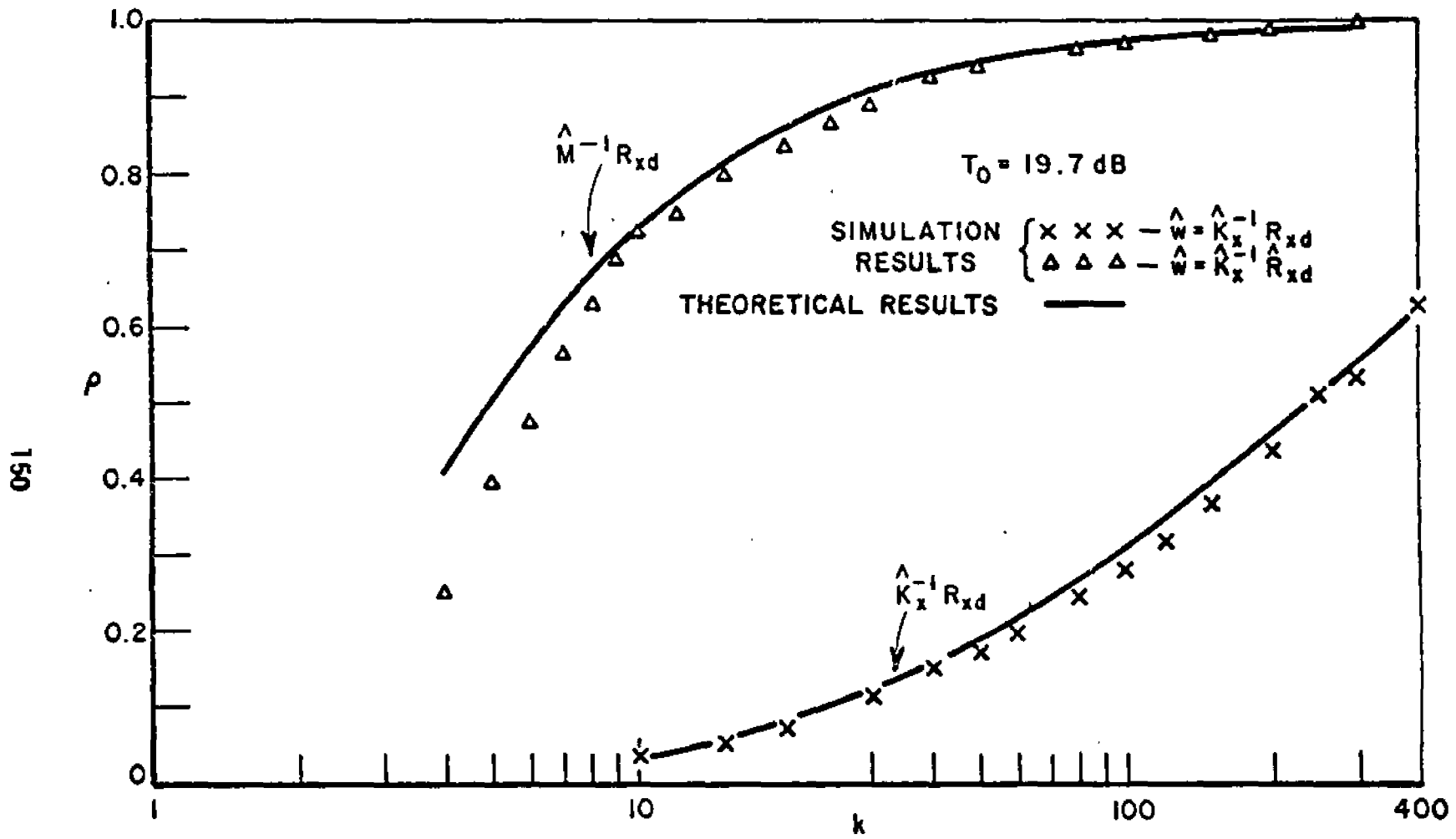


Figure 26--The average normalized output signal-to-noise ratio versus the number of samples for a four-element array. Computer simulation results represent an average of 100 runs.

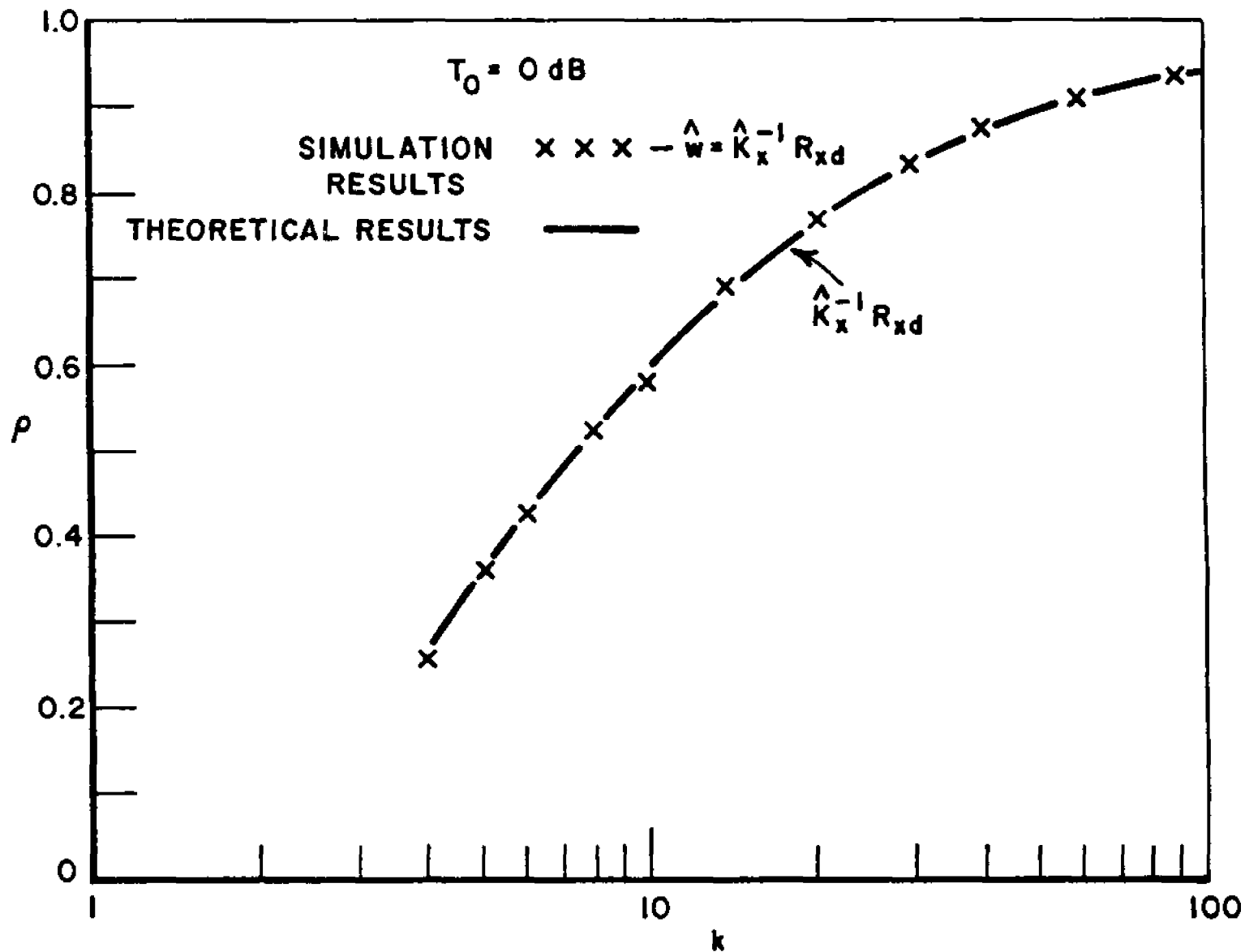


Figure 27--The average normalized output signal-to-noise ratio versus the number of samples for a four-element array. Computer simulation results represent an average of 100 runs. Input signals same as in Figure 19.

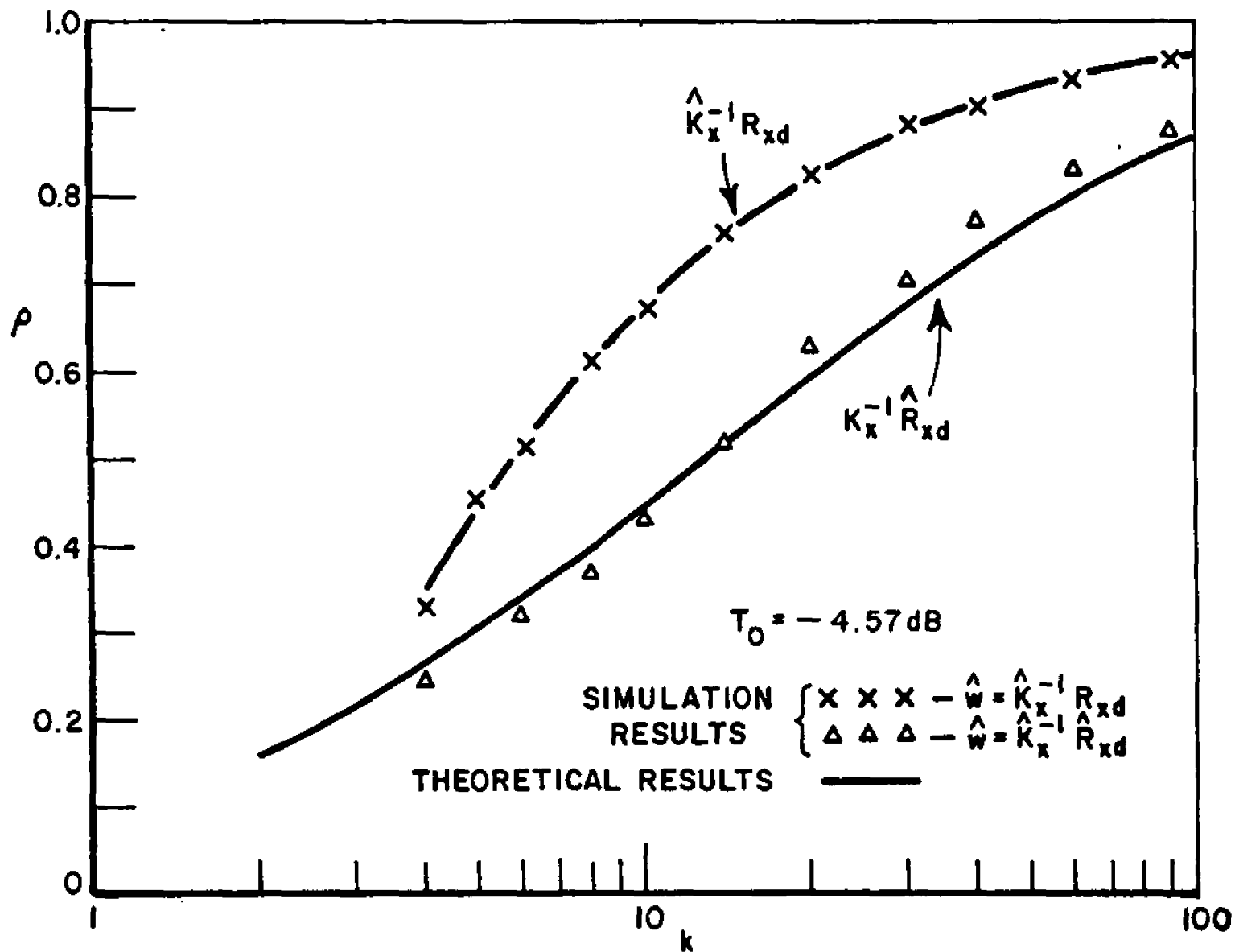


Figure 28--The average normalized output signal-to-noise ratio versus the number of samples for a four-element array. Computer simulation results represent an average of 100 runs. Input signals same as in Figure 18.

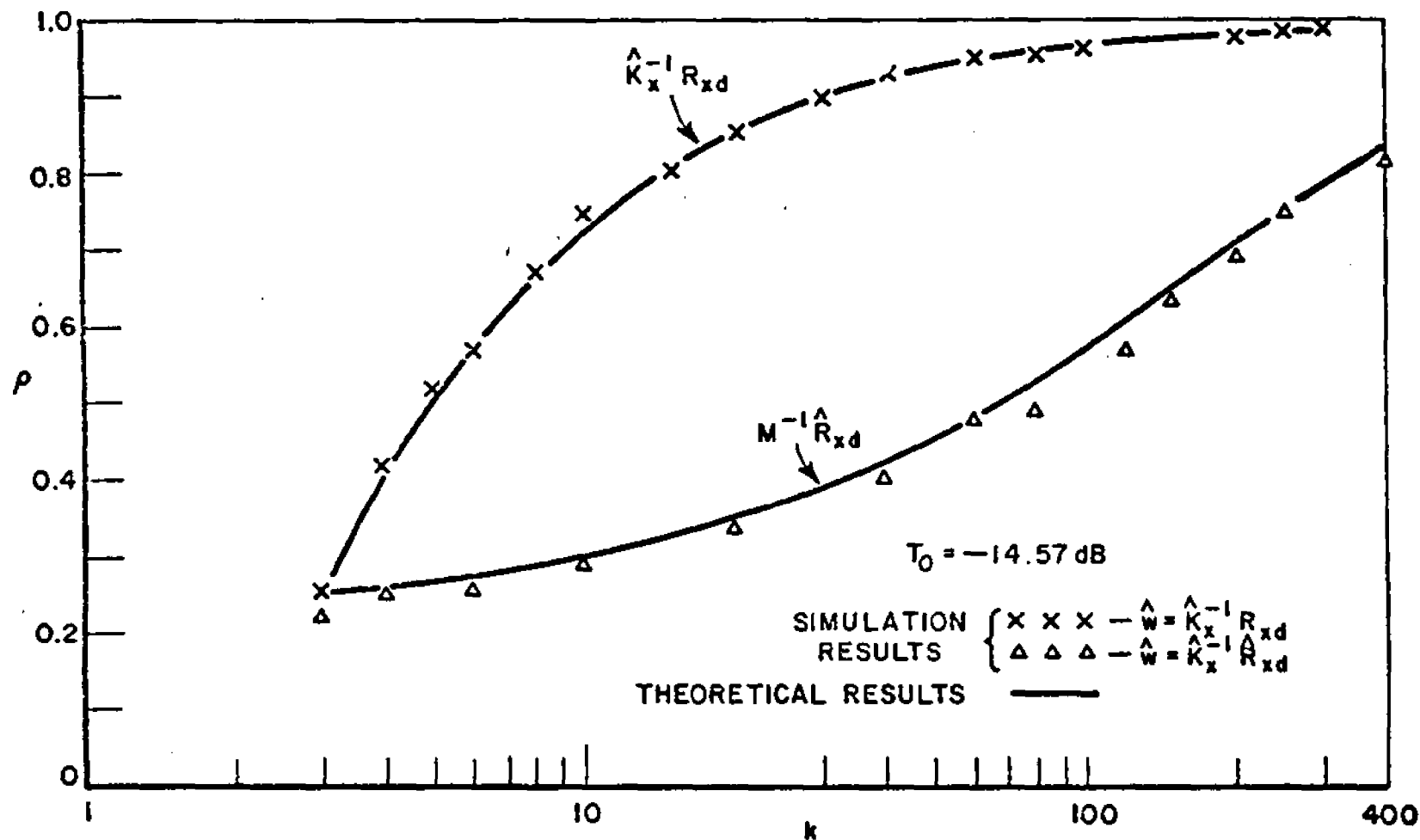


Figure 29--The average normalized output signal-to-noise ratio versus the number of samples for a four-element array. Computer simulation results represent an average of 100 runs. Input signals same as in Figure 18 except $P_s' = -10 \text{ dB}$.

the simulation results agree very closely with the theoretical result for a number of different input signal environments. The results also indicate that the Gaussian assumption on the desired signal gives a good approximation to the deterministic case, at least for the signal environments tested.

For the purposes of comparison, the average normalized output SNR ρ_6 afforded by the weight vector $\hat{w}_6 = \hat{K}_x^{-1} \hat{R}_{xd}$ -- an algorithm in which the weights are determined from concurrent* estimates of K_x and R_{xd} -- is also shown in Figures 24-29. Several important observations should be made about these results.

1. When $T_0 > 1$ (Figures 24-26), the output SNR converges more rapidly if the exact vector R_{xd} is replaced by its concurrent estimate

$$\hat{R}_{xd} = \frac{1}{k} \sum_{i=1}^k \underline{\tilde{x}}(i\Delta t) \underline{\tilde{x}}^{\dagger}(i\Delta t)$$

and vice-versa for $T_0 < 1$ (Figures 28 and 29). When $T_0 = 1$ (Figure 27), the two spatial filters produced nearly identical output signal-to-noise ratios for all values of k . These results are similar to the relationship between T_0 and the effects of weight jitter encountered in Chapter IV. Again, it appears that the better performance obtained using the estimated cross-correlation vector at high signal-to-noise ratios is due to correlation of the estimate \hat{R}_{xd} with the estimate \hat{K}_x .

2. When T_0 was large, the mean output signal-to-noise ratio of the filter $\hat{w}_6 = \hat{K}_x^{-1} \hat{R}_{xd}$ (determined by simulation) was approximated by the theoretical response filter $w_4 = M^{-1} R_{xd}$ [see Equation (327)]. Agreement was best for $k \gtrsim 10$. Note that the average output signal-to-noise ratio of filter \hat{w}_6 must be less than w_4 , since w_4 is optimum.
3. When T_0 was small ($\ll 1$) (see Figures 28 and 29), the output signal-to-noise ratio of filter $\hat{w}_6 = \hat{K}_x^{-1} \hat{R}_{xd}$ was approximated by the theoretical response of filter $w_1 = K_x^{-1} R_{xd}$ [and thus $w_2 = M^{-1} \hat{R}_{xd}$; see Equation (312)(d)]. This result was expected, since the algorithm $\hat{K}_x^{-1} \hat{R}_{xd}$ converges much faster than $K_x^{-1} R_{xd}$ for T_0 small, i.e., the dominant source of the slower response of $\hat{K}_x^{-1} \hat{R}_{xd}$ was caused by an insufficiently accurate estimate of R_{xd} .

*

$$\hat{K}_x = \frac{1}{k} \sum_{i=1}^k \underline{\tilde{x}}(i t) \underline{\tilde{x}}^{\dagger}(i\Delta t) \text{ and } \hat{R}_{xd} = \frac{1}{k} \sum_{i=1}^k \underline{\tilde{x}}(i\Delta t) \underline{\tilde{r}}^{\dagger}(i\Delta t)$$

The results in this section have shown that the mean output SNR of the filter $\hat{w}_4 = \hat{M}^{-1} R_{xd}$ converges more rapidly than the filter $\hat{w}_5 = \hat{K}_x^{-1} R_{xd}$, with the greatest disparity in the convergence rate occurring when the optimum output signal-to-noise ratio is large. Based on simulation results, it was found that replacing R_{xd} by the estimate \hat{R}_{xd} (obtained concurrently with the estimate \hat{K}_x) significantly improved the response of filter \hat{w}_5 when T_0 was large; for sufficiently large values of T_0 and k , the responses of $\hat{w}_6 = \hat{K}_x^{-1} \hat{R}_{xd}$ and \hat{w}_4 were nearly the same. When $T_0 = 1$ (0 dB), the responses of \hat{w}_5 and \hat{w}_6 were found to be nearly identical. When $T_0 < 1$, \hat{w}_5 provided a better response relative to \hat{w}_6 . Finally, for $T_0 \ll 1$, it was found that the response of \hat{w}_6 was approximated by the response of

$$\hat{w}_1 = K_x^{-1} \hat{R}_{xd} \text{ and } \hat{w}_2 = M^{-1} \hat{R}_{xd}.$$

D. Comparison with LMS Algorithm Transient Response

In this section, the digital LMS algorithm is compared with the two weight algorithms \hat{w}_5 and \hat{w}_6 to determine their relative transient responses. Results illustrating the time dependence of the average output signal-to-noise ratio are obtained by computer simulation of a linear array of four identical, equally-spaced elements immersed in an environment which is assumed to contain a P-N code (biphase) modulated desired signal and noise and interfering sources which are sample functions from uncorrelated zero-mean Gaussian processes. These results are compared to theoretical results derived in Chapters IV and V.

The mean output SNR normalized to T_0 , denoted by ρ , versus the number of independent samples k (time), is used as the performance measure. The mean is determined by averaging the results of 50 independent adaptations for each data point; in most cases, this provides sufficient smoothing of instantaneous fluctuations in ρ .

The two techniques studied for inserting desired signal information are considered; R_{xd} given and \hat{R}_{xd} estimated (by averaging $\hat{x}(t) r^*(t)$). The respective weight equations which apply are as follows:

$$\begin{array}{l}
 \left. \begin{array}{l}
 \text{(a) } w((k+1)\Delta t) = w(k\Delta t) + \alpha\Delta t [R_{xd} - \underline{\hat{x}}(k\Delta t) \\
 \quad \cdot \underline{\hat{x}}^\dagger(k\Delta t) w(k\Delta t)] \\
 \text{(b) } \hat{w}_5((k+1)\Delta t) = \hat{K}_x^{-1} R_{xd}
 \end{array} \right\} R_{xd} \text{ given} \\
 \\
 \left. \begin{array}{l}
 \text{(c) } w((k+1)\Delta t) = w(k\Delta t) + \alpha\Delta t [\underline{\hat{x}}(k\Delta t) \underline{\hat{r}}^\dagger(k\Delta t) \\
 \quad - \underline{\hat{x}}(k\Delta t) \underline{\hat{x}}^\dagger(k\Delta t) w(k\Delta t)] \\
 \text{and} \\
 \text{(d) } \hat{w}_6((k+1)\Delta t) = \hat{K}_x^{-1} \hat{R}_{xd}
 \end{array} \right\} r(t) \text{ given}
 \end{array}$$

In the above expressions, Δt represents the interval between independent samples of the input noise signals and k represents the total number of samples taken. The number of samples per code chip was arbitrarily set equal to four.*

Before comparing transient response, several factors regarding the LMS algorithm must be considered. First, an appropriate loop gain constant (α) must be selected. An approximation to the excess noise at the array output caused by weight jitter when the weights are near their steady-state solution was derived in Chapter IV for the two cases $R_\Delta = [0]$ [Equation (158)] and $R_\Delta \neq [0]$ [Equation (133)]. If the inequality given by Equation (227) is satisfied, then the output SNR is negligibly affected by desired signal modulation caused by weight jitter. Note that the presence of the desired signal is not neglected under this assumption. Assuming the inequality is satisfied, the mean of the steady-state output SNR, normalized to T_0 , may be approximated by

*Any integer greater than or equal to one yields (nearly) the same transient response if $P_S \ll P_I$.

$$(a) \quad \rho_{LMS} \Big|_{R=[0]} \doteq \frac{1-c}{1+T_0 c} \quad (343)$$

$$(b) \quad \rho_{LMS} \Big|_{R \neq [0]} \doteq \frac{1-c}{1+c/T_0}$$

where

$$c = \alpha \Delta t \sum_{i=1}^m \frac{\lambda_i}{2 - \alpha \Delta t \lambda_i}$$

The asymptotic value to which the output SNR converges may be determined from Equations (343) for a fixed value of α and a known signal environment. When the signal environment is unknown (a priori), as assumed in applications under consideration, c can be approximated by $\alpha \Delta t P_I$ (see Figure 12), and the range of T_0 can be approximated from expected worst case signal environments. Once these parameters have been determined (or approximated), α can be chosen so that ρ_{LMS} is greater than the desired minimum. In the computer simulations, the loop gain was set to the relatively large value of

$$\alpha = \frac{0.4}{\Delta t P_I}$$

to obtain rapid response times and to illustrate the penalty incurred due to weight jitter in various signal situations. Note that this value for α is only 2.5 times smaller than the maximum value $(\Delta t P_I)^{-1}$ (see Equations (136) and (137)).

Weight initialization is a second factor which must be considered, since it can have a great impact on transient response. Results in parts B and C of this chapter were derived assuming that "initial" weights were zero to eliminate biasing effects. However, in certain environments, biasing the initial weights in the desired signal direction (for example) may increase response time [see Chapter IV, C]. In what follows, initial conditions on the weights derived by estimating K_x or R_{Xd} are assumed zero. In the case of the LMS algorithm, three different initial weights are employed:

$$(a) \quad w^\dagger(t_0) = [0, 0, 0, 0] \equiv [0] \quad (344)$$

$$(b) \quad w^\dagger(t_0) = [a, 0, 0, 0]$$

and

$$(c) \quad w(t_0) = \lambda_{\min}^{-1} R_{xd}$$

where a is a complex type scalar constant and λ_{\min} is the minimum eigenvalue of K_x . Equations (344)(a) and (344)(b) do not utilize a priori parameters; in this respect, they are similar to the estimation algorithms. The LMS weights are initialized to the desired signal DOA vector [Equation (344)(c)] to illustrate the improved transient response noted in Chapter IV, C. The amplitude of $w(t_0)$ in (344)(c) has been scaled so that initial weight error is removed or reduced along eigenvectors associated with λ_{\min} ; note that $\lambda_{\min} = \sigma^2$ if $p \leq 3$ where p is the number of directional interference sources and σ^2 represents the per-element thermal noise power.

A third consideration involves the reference signal amplitude and phase, which affects LMS algorithm transient response when the initial pattern is omnidirectional (response is unaffected by these parameters when $w(t_0) = [0]$ or $w(t_0) = R_{xd}$). When the reference amplitude and phase are fixed, the resulting transient response is highly dependent on a [see Equation (344)(b)] as well as the signal environment. In particular, the output SNR may not be a monotonic function of time during weight transients. This behavior is to be illustrated in the simulation by setting

$$a = 4$$

$$\text{and } s(t) r^\dagger(t) = 2\sqrt{P_S} \underline{-45^\circ}$$

Figures 30-34 illustrate the convergence rate of each algorithm in Equations (342) and each initial condition in Equations (344). The curves are numbered in each graph as follows:

Curve Number	Algorithm	$w(t_0)$
①	Equation (342)(a)	$= R_{xd}^+$
②	Equation (342)(c)	$= R_{xd}^+$
③	Equation (342)(a)	$= [a, 0, 0, 0]$
④	Equation (342)(c)	$= [a, 0, 0, 0]$
⑤	Equation (342)(a)	$= [0, 0, 0, 0]$
⑥	Equation (342)(c)	$= [0, 0, 0, 0]$
⑦	$\hat{w} = \hat{K}_x^{-1} R_{xd}$	---
⑧	$\hat{w} = \hat{K}_x^{-1} \hat{R}_{xd}$	---

To focus attention on the general trend of the results, data for $k \leq 10$ are connected by a series of straight lines. For $k \geq 10$, the lines indicate average values and are not intended to show instantaneous fluctuations. Each figure illustrates results obtained in the fixed signal environment described in Table IV.

Figure 30 illustrates the mean output SNR response for an input interference-to-signal ratio of 14 dB and an input signal to thermal noise ratio of 0 dB. Since the angular separation between signal and interference is relatively large in this case, the presence of the interfering source does not significantly affect T_0 . That is, the filter w is nearly co-phased to the designed signal in steady-state. The longest time constant in the LMS algorithm for this case is determined by the relation

$$\tau_{\max} \doteq \frac{1}{\alpha \Delta t \sigma^2} = \frac{P_I}{0.4 \sigma^2} = 270 \text{ samples} \quad (345)$$

Consequently, all curves should be near their steady-state value after about 540 samples (two time constants).

The most important aspect of the results shown in Figure 30 is that, apart from curve 6, the time constant associated with convergence of the output SNR is shorter than τ_{\max} . The most rapid response is obtained when the weights are initialized to R_{xd} or when the initial weights are zero with $R = [0]$. In all three of these cases (curves 1, 2, and 5), initial response is faster than the

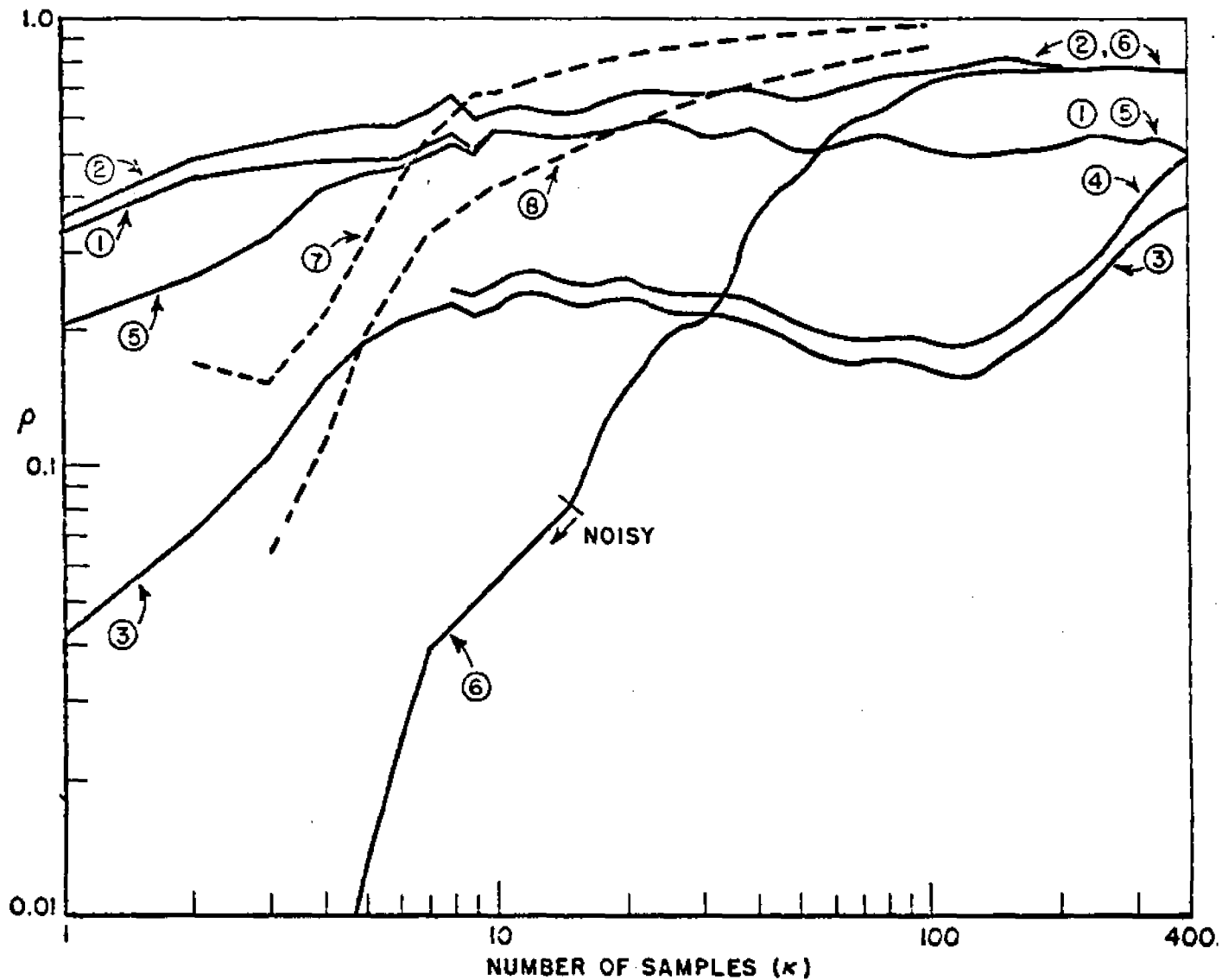


Figure 30--The average normalized output signal-to-noise ratio versus the number of samples for six different algorithms. The curves represent computer simulation results averaged over 50 runs. See Table II.

two estimation algorithms (curves 7 and 8), since (1) their initial conditions are biased toward the desired signal DOA (this biasing occurs in curve 5 since the first non-zero weight vector is $\alpha \Delta t R_{Xd}$) and (2) the initial bias happens to provide an initially high output SNR (not necessarily true, in general). Curves 1, 2, and 5 increase monotonically until the effects of weight jitter become significant.

Curve 6, which corresponds to the $w(t_0) = [0]$, $R_{\Delta} \neq [0]$ case, provides the poorest performance for $k < 30$. As discussed later in this section, the convergence rate of the output SNR is proportional to λ_1 , where λ_1 is the eigenvalue associated with the convergence of the output desired signal power to its optimum value. In the present example,

$$\lambda_1 \approx 4$$

$$\langle e_1, \underline{s} \rangle = (P_s)_1 \approx 2$$

$$\langle e_k, \underline{s} \rangle = (P_s)_k \approx 0 \quad k = 2, 3, 4$$

Since $w(t_0)=[0]$, the output desired signal power remains small until the array responds along the eigenvector associated with λ_1 . The time constant associated with the output desired signal power response is approximately

$$\tau_1 \approx \frac{1}{\alpha \Delta t \lambda_1} \approx 67 \text{ samples}$$

which roughly agrees with the simulation result (curve 6).

For $K > 30$, the convergence was better in all cases compared to the $w(t_0) = [1, 0, 0, 0]$ case. Whereas the initial response of curves 3 and 4 show the output SNR increasing with k , this trend reverses when the algorithm begins to respond to the desired signal [along e_1], since any decrease in the dot product of w and e_1 without corresponding decreases in the dot product of w and the thermal noise eigenvectors causes the output signal to thermal noise ratio (and thus ρ) to decrease. When the array begins to respond along the thermal noise eigenvectors, ρ again begins to increase. The phenomenon of ρ passing through a minimum is undesirable, since it generally occurs just prior to the onset of response to thermal noise and the minimum value depends on the

Table IV. Conditions Under Which Simulation Results in Figures 30-34 Were Obtained. Average values of the normalized output signal-to-noise ratio are also given.

Figure Number	Input Power and Arrival Angles				T_0	$\alpha\Delta t$	P_I	c (approx)	$\bar{\rho}_{LMS}$ $R_{\Delta}=0$	$\bar{\rho}_{LMS}$ $R_{\Delta}\neq 0$	a	Angle of	
	Desired Signal	Interfering No. 1	Signals No. 2	Thermal Noise								$\hat{s}(t)$	$\hat{r}^T(t)$
30	1.0/ <u>0°</u>	25./ <u>-75°</u>	0	1.0	3.80	0.4	0.243	0.39	0.73	4/ <u>0°</u>	-45		
31	1.0/ <u>0°</u>	25./ <u>30°</u>	0	1.0	1.218	0.4	0.25	0.58	0.62	4/ <u>0°</u>	-45°		
32	1.0/ <u>0°</u>	25./ <u>30°</u>	10./ <u>60°</u>	1.0	0.4158	0.4	0.237	0.70	0.49	4/ <u>0°</u>	-45°		
33	1.0/ <u>0°</u>	25./ <u>30°</u>	10./ <u>60°</u>	1.0	0.4158	0.4	0.237	0.70	0.49	4/ <u>0°</u>	0°		
34	1.0/ <u>0°</u>	1000./ <u>30°</u>	10./ <u>60°</u>	1.0	0.3282	0.4	0.25	0.693	0.43	4/ <u>0°</u>	-45°		

signal environment (see Figure 32, for example). This minimum may occur when the desired signal component of the array output is initially (1) larger than $\hat{r}(t)$ or (2) out of phase with respect to $\hat{r}(t)$. The second cause is eliminated if the reference signal is derived from the array output. The first cause can be avoided by choosing a such that

$$|a|^2 < \frac{|\hat{r}|^2}{p_s} .$$

However, to avoid slow response to thermal noise, a must be zero.

Although not shown for all cases, curves 2, 4, and 6 converge to $\rho = 0.74$ and curves 1, 3, and 5 converge to $\rho = 0.44$. These values are very close to those predicted in Equations (343) [see Table IV]. Curves 1 and 5 momentarily exceed the steady-state signal-to-noise ratio since the full influence of weight jitter requires averaging over all time constants*. Note that \hat{w}_5 and \hat{w}_6 achieve normalized output SNR's of $\rho = 0.44$ and $\rho = 0.74$, respectively, for $k \approx 11$. This implies that the LMS control loop performs a running time average over about 11 samples of the input data for $\alpha \Delta t P_I = 0.4$.

Figure 31 illustrates array performance when the angular separation between the desired and interfering signals is reduced to 30° per element. In this example, T_0 is reduced by 5 dB (compared to T_0 in Figure 30) to 1.218 (numeric). Since T_0 is near one, the two estimation algorithms (shown as one curve) yield nearly identical results and the LMS algorithms converge to about the same steady-state values. The LMS algorithm continues to provide excellent performance when $w(t_0) = R_{xd}$, responding at about the same rate as \hat{w}_5 and \hat{w}_6 . The response of curve 5, as well as curves 1 and 2, are slower than those of Figure 1 since the advantage of initializing w to $\lambda_{\min}^{-1} R_{xd}$ is diminished by the proximity of the interfering source. The second longest time constant (the time constant associated with transforming to the desired signal in this case) increases to

$$\tau_1 \doteq 123 \text{ samples} ,$$

which accounts for the increased response time of curve 6. The response obtained when the array pattern is initially omnidirectional is nearly the same, i.e., it has a minimum for $k \approx 130$.

*Note that Equations (343) were derived assuming the mean weights were near their steady-state solution. See Chapter VI for further discussion of the effects of jitter during transient conditions.

Figure 32 displays the relative responses when a second interfering source is added. In this case, $T_0 < 1$. Consequently, w_5 outperforms w_6 and $\rho_{\text{LMS}}|_{R_{\Delta}=0} > \rho_{\text{LMS}}|_{R_{\Delta} \neq 0}$. Also, performance differences between the LMS and estimation algorithms are more pronounced, the latter providing superior convergence rates. The most striking difference between Figures 31 and 32 is exhibited in the response of curves 3 and 4. In Figure 32, ρ undergoes a sharp minimum for $k \approx 200$ which is primarily caused by the initial phase difference between $\tilde{r}(t)$ and the desired signal component of the array output. Figure 4 shows the response when their relative phases are initially aligned.

Less apparent in Figure 32 is a temporary "leveling-off" effect caused by the presence of the second interfering source. This effect is far more pronounced in Figure 33, which illustrates a portion of the LMS algorithm response when the highest level interfering signal is increased 16 dB relative to its level in Figure 32. Since T_0 drops only about 1 dB, the response of the estimation algorithms remain (essentially) unchanged relative to Figure 3. On the other hand, the wider spread in eigenvalues causes the LMS algorithms to converge at a much slower rate. In particular, the ratio P_1/λ_1 is 40 times larger, and thus τ_1 is 40 times greater as displayed in the response of curve 6. Performance is improved when the weights are initialized to $\lambda_{\min}^{-1} R_{\text{xd}}$. Response in this case is rapid for $k < 10$, but "levels off" after the high-level interference source is nulled and before response has commenced along the eigenvector associated with the next largest eigenvalue λ_2 ($\neq 12$). Setting $w(t_0)$ approximately equal to $\lambda_1^{-1} R_{\text{xd}}$ has the advantage in that ρ will be near its asymptotic value if the adaption time exceeds $\alpha\lambda_2$, as opposed to $\alpha\lambda_1$ when $w(t_0) = [0]$. In this particular example, a factor of (about) ten increase in the convergence rate can be achieved in this manner. Note that if $w(t_0) = \lambda_2^{-1} R_{\text{xd}}$, then the effective time constant equals $(\alpha\lambda_{\max})^{-1}$. The "catch" here is that λ_2 must be known precisely, since even a small difference between $w(t_0)$ and $\lambda_2^{-1} R_{\text{xd}}$ can cause the output SNR to "level off" well below T_0 .

The average output signal to noise ratio in the case of curve 6 ($w(t_0)=[0]$, $R_{\Delta} \neq [0]$) is shown in Figures 30-34 to converge at a much slower rate compared to the other configurations, yet the expression describing ideal LMS algorithm transmit behavior indicates the response of curve 6 should be nearly the same as the response of curve 5 ($R_{\Delta}=[0]$ case). The difference between curves 5 and 6 stems from the fact that the excess noise to output desired signal ratio is much higher during weight transient when an ideal reference, rather than R_{xd} , is used to distinguish the desired signal from interference sources within the LMS algorithm feedback loop.

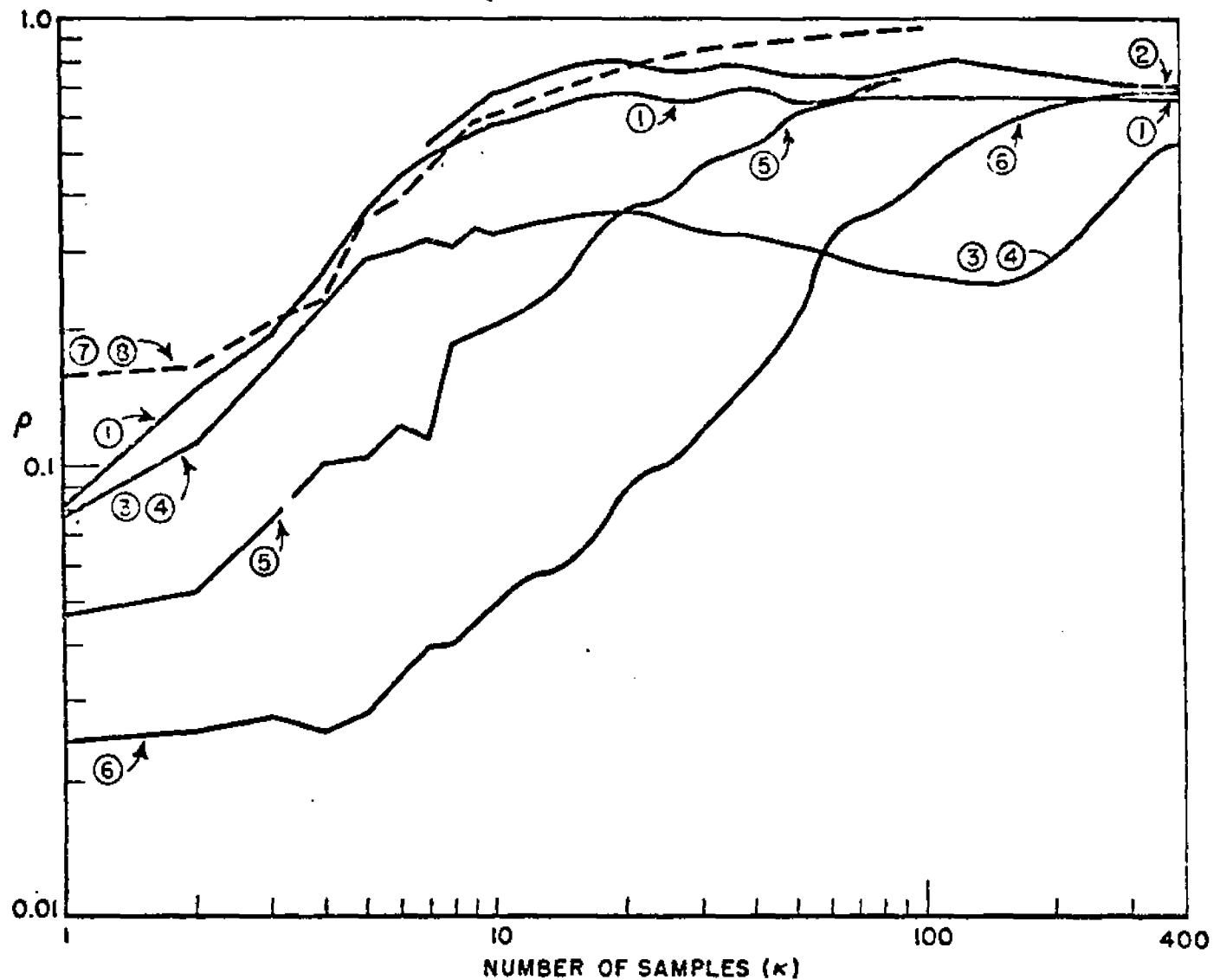


Figure 31--The average normalized output signal-to-noise ratio versus the number of samples for six different algorithms. The curves represent computer simulation results averaged over 50 runs. See Table II.

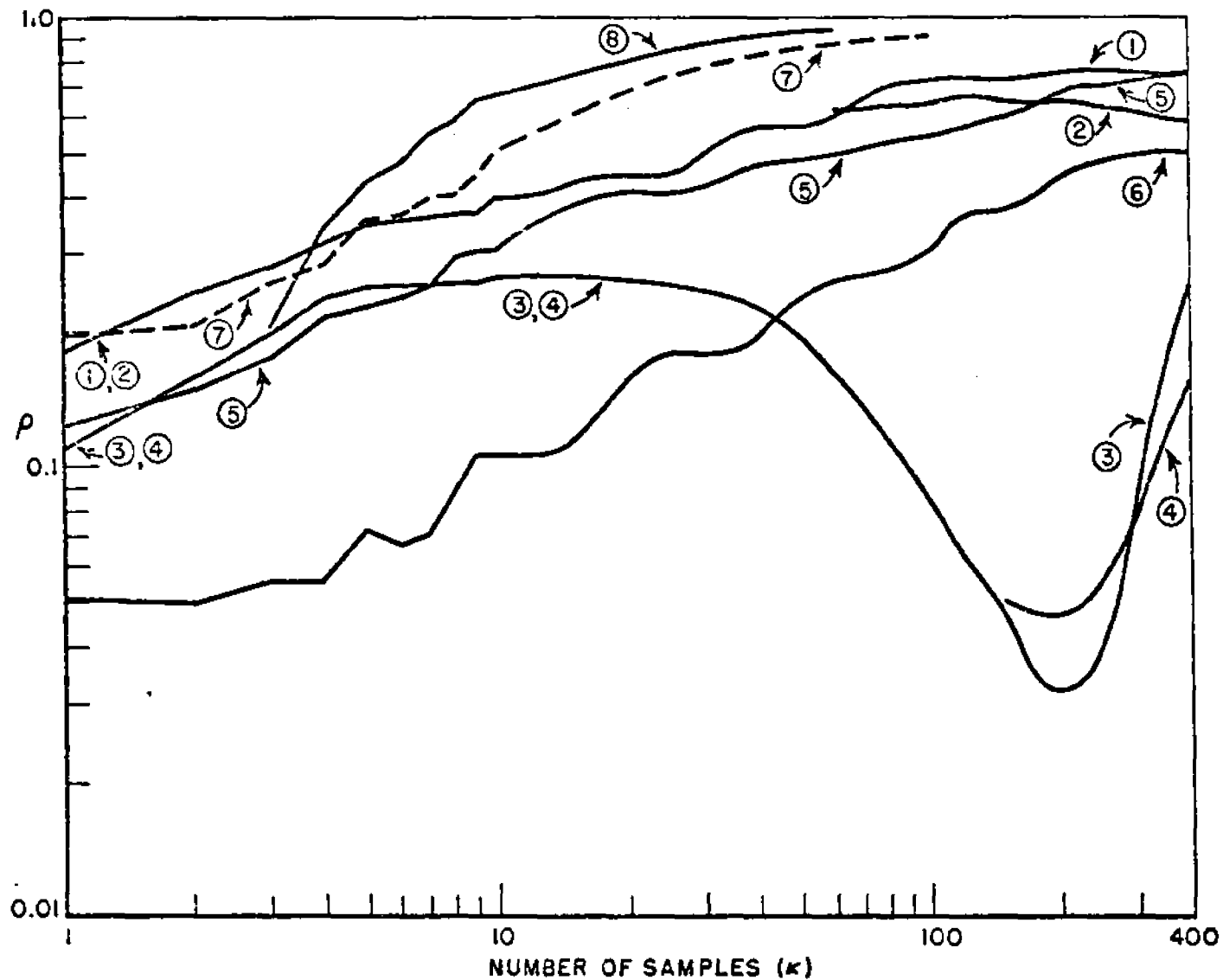


Figure 32--The average normalized output signal-to-noise ratio versus the number of samples for six different algorithm. The curves represent computer simulation results averaged over 50 runs. See Table II.

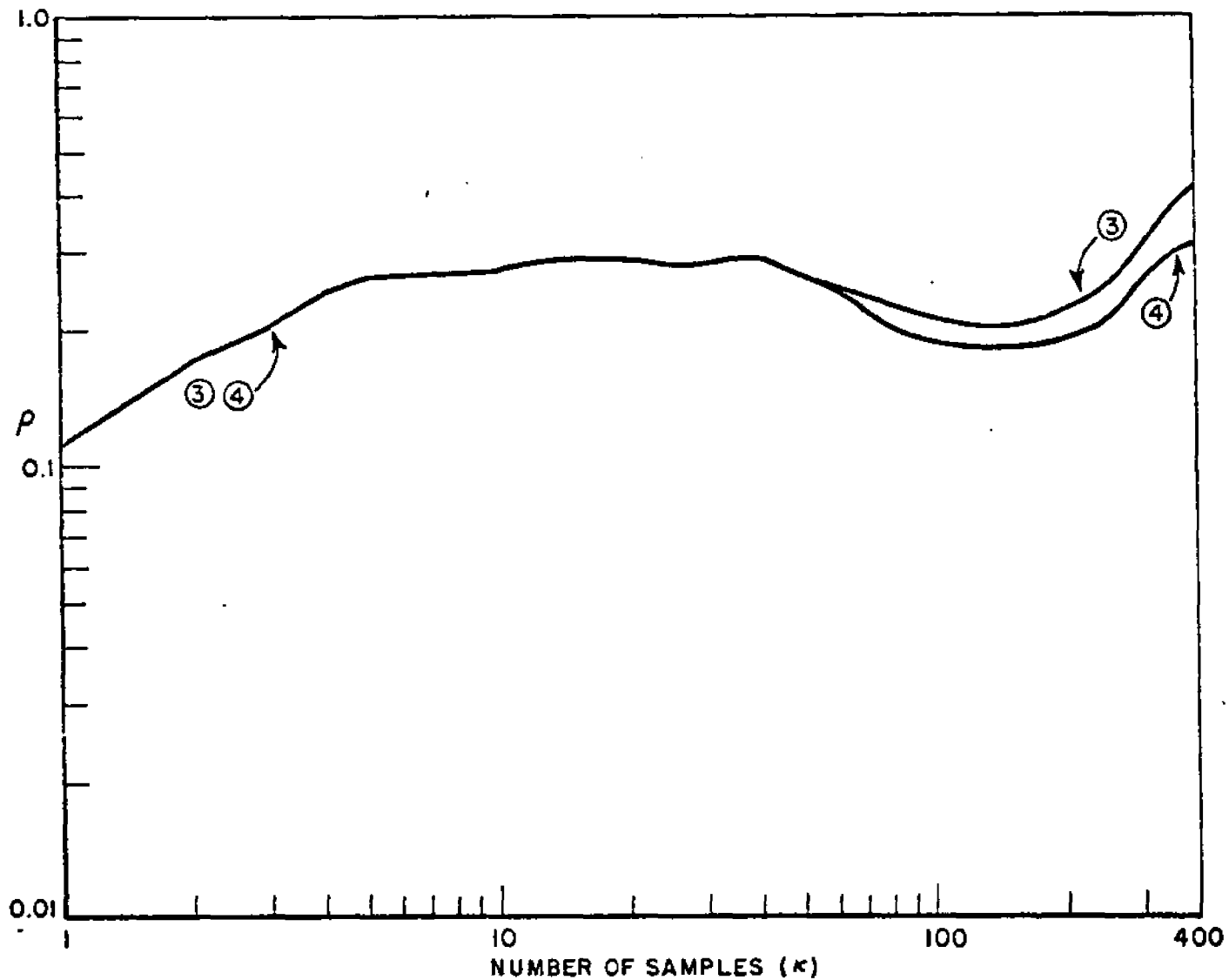


Figure 33--The average normalized output signal-to-noise ratio versus the number of samples for six different algorithms. The curves represent computer simulation results averaged over 50 runs. See Table II.

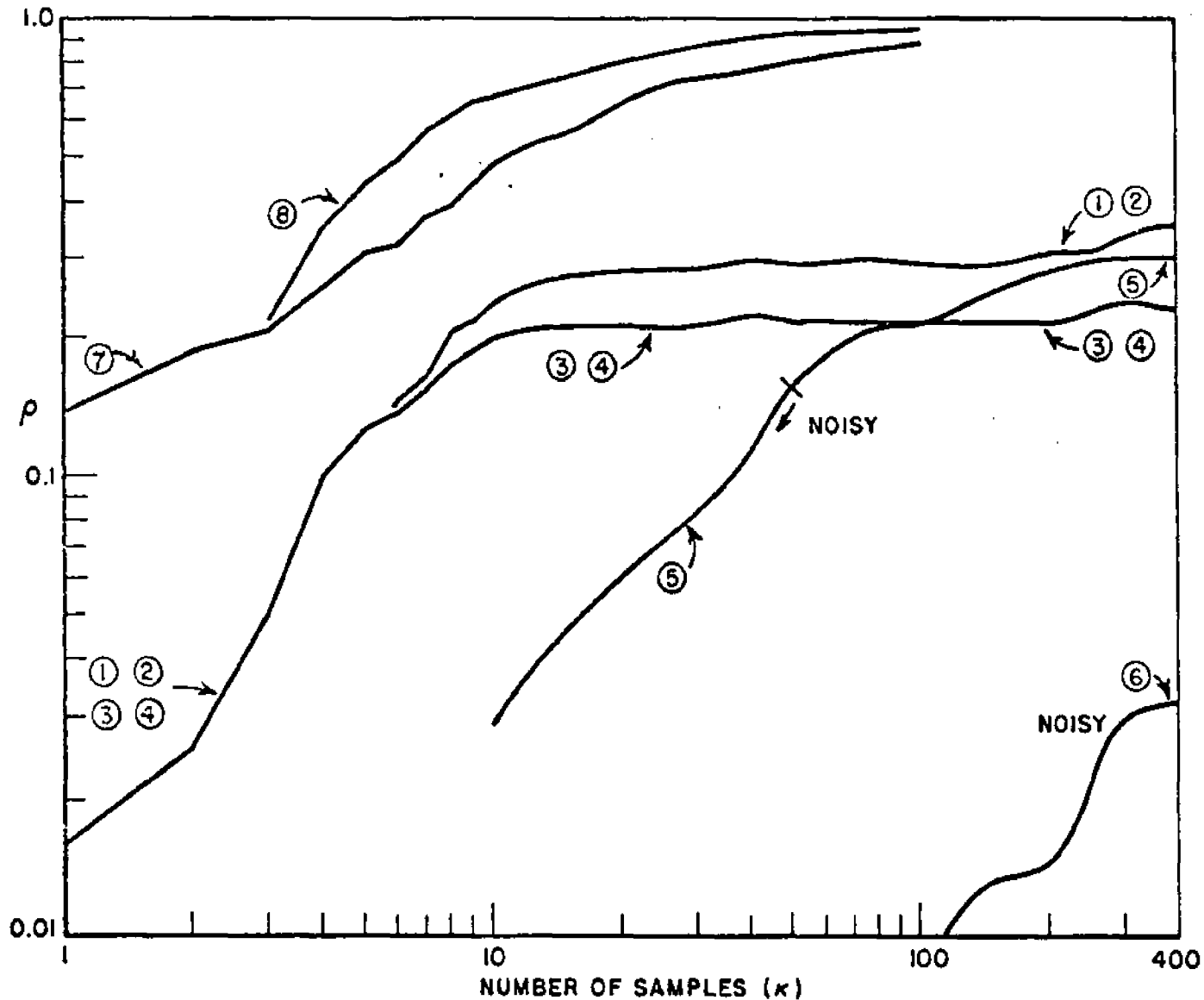


Figure 34--The average normalized output signal-to-noise ratio versus the number of samples for six different algorithms. The curves represent computer simulation results average over 50 runs. See Table II.

The output desired signal power is initially very small in both cases since the magnitude of the initial weight vector is zero. The excess noise due to jitter in the case of curve 5 is also initially small since the array output signal is the only source of control loop noise. When $R_{\Delta} \neq [0]$, however, the reference signal by input signal cross-terms which appear at the error multiplier outputs introduce a fixed level of noise within the feedback loop, thereby causing a significant degradation in the output SNR when the output desired signal level is small relative to the reference signal. The convergence rate of the output desired signal power to its optimum value was proportional to $(\alpha \Delta t \lambda)^{-1}$ in Figures 30-34, which accounts for the relatively poor performance obtained when the adaption interval was less than $(\alpha \lambda \eta)^{-1}$.

CHAPTER VI

AN EXPERIMENTAL TDMA - ADAPTIVE ARRAY SYSTEM

A. Introduction

The analytical results presented in Chapters IV and V have demonstrated in theory that an adaptive array processor can be utilized to suppress high level interfering signals incident on an array of antenna elements. These results, however, were derived under generalized assumptions regarding the input signal structure and the reference signal. Also, the effects of circuit imperfections within the array processor were neglected. In order to demonstrate that an adaptive spatial processor (ASP) can be effectively implemented in practice and to augment the theoretical results with practical design information, an experimental four-element ASP was constructed and tested. The ASP was designed to be compatible with the TDMA system described in Chapter II and Reference [20] to the extent practicable. The performance of this experimental TDMA/adaptive spatial processor (TDMA/ASP) is addressed in this chapter.

In accord with the TDMA/ASP system design requirements delineated in Chapter II, the ASP was implemented using the LMS algorithm. Since analysis has shown that the ALMS and DLMS algorithms provide comparable performance, at least in terms of the mean weight response and the excess noise power caused by weight jitter, the analog (ALMS) approach was selected instead of the digital (DLMS) approach to (1) minimize circuit complexity and (2) focus attention on the relation between loop bandwidth and input signal bandwidth rather than on the interval between weight updates (recall that the desired signal bandwidth increases by a factor of eight when the system is operated in the higher-rate format (HRF)).

The results to be presented were obtained by bench-testing the TDMA/ASP system in conjunction with other equipments which collectively simulated an ASP located at a hard-limiting satellite repeater and a TDMA modem located at a ground station. The bench-test approach permitted close control of signal parameters and eliminated from consideration the effects of antenna element patterns and mutual coupling; as previously noted, these results can be extended to include performance characteristics of the antenna subsystem by appropriately modifying the (processor) input signal representations. The general theory of operation and a brief description of the bench-test configuration are given in the following sub-section. The separate subsystems are described in greater detail in subsequent sub-sections.

Design considerations relevant to implementing the ALMS algorithm are discussed in section C. Included in this discussion are the effects of non-ideal circuit components and dynamic range considerations. The experimental results begin in section D with measurements of performance under small loop gain conditions (i.e., negligible weight jitter) with the weights near their steady-state solutions. BEP measurements under higher loop gain conditions are presented in the last part of section D. The measured BEP performance when the system is operated in the pulsed signal TDMA format is then presented in section E.

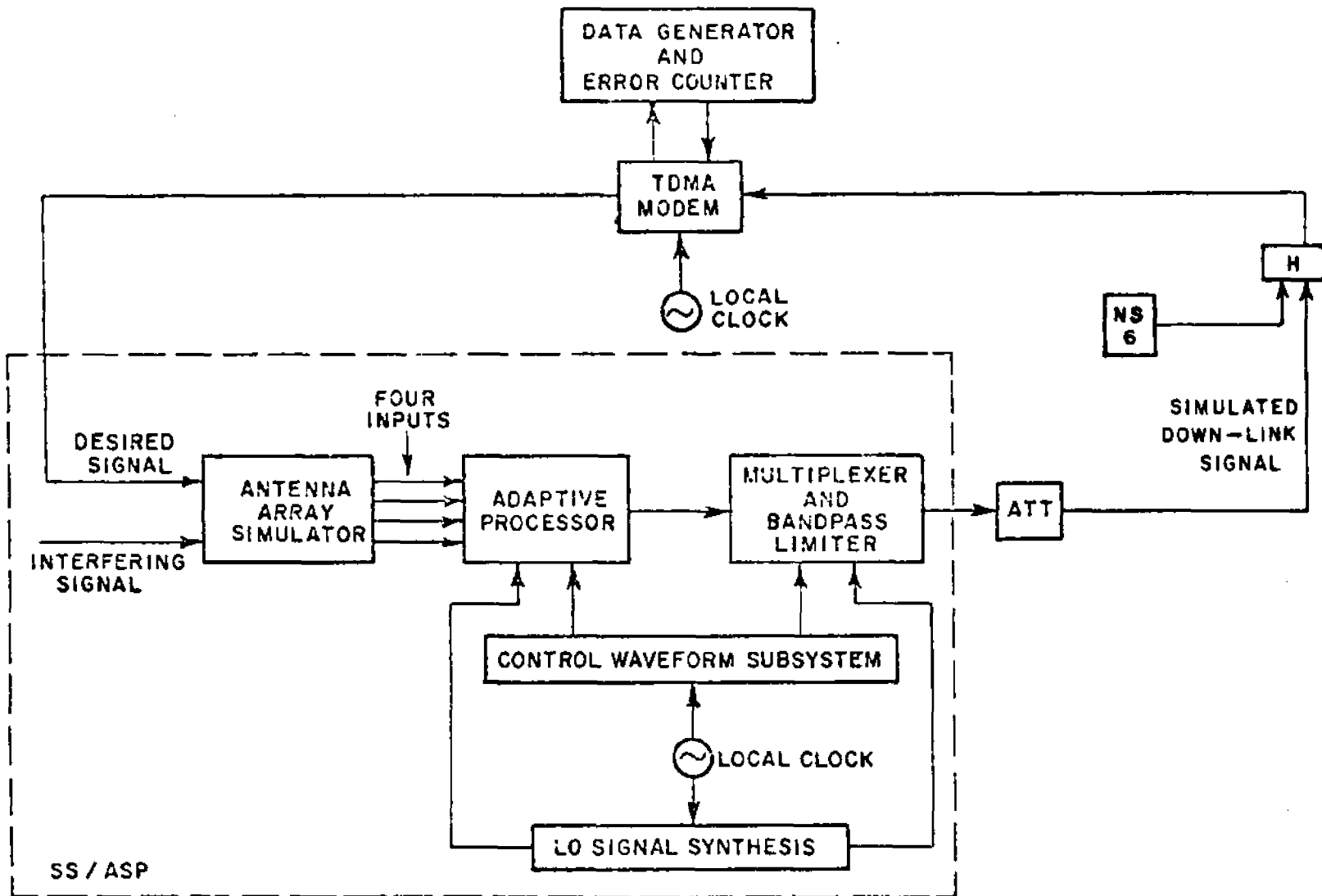
B. Description of the Experimental System

1. Description of Bench-Test Configuration and General Operating Principles

A functional block diagram of the bench-test configuration is shown in Figure 35. The satellite simulator/adaptive spatial processor (SS/ASP) subsystem contains (1) an antenna array simulator for simulating up-link received signals, (2) a band-pass limiter to simulate the signal transmitted on the down-link, (3) the adaptive spatial processor, and (4) associated locally generated control waveforms.

As noted in Chapter II, two PN code pairs* are generated autonomously within the SS/ASP which are identical in structure to two PN code pairs generated within each TDMA modem. One code pair is used to generate the network clock signal (NCS) and the second pair is used to generate a reference signal. The two codes are generated synchronously within the SS/ASP and signals transmitted by the TDMA modems arrive at the SS/ASP in synchronism with the second code pair (see sub-section 6 and Chapter II). Each user normally conveys data by transmitting a pulsed signal during his assigned time slot(s) from a direction which is assumed unknown. Of course, the output of the array processor will not exhibit a suitably-high desired signal to interference plus thermal noise ratio until after an appropriate pattern is formed. Therefore, all pulses utilized to convey data from a TDMA modem are preceded by the transmission of a preamble to allow the ASP to form an appropriate pattern. The TDMA/ASP has been designed so that each preamble need only span one time slot,

*Each pair is used for generating a single quadrature modulated signal.



N.S. \sim 70 MHz NOISE SOURCE, $BW_{3dB} \cong$ 8 MHz
 ATT \sim ATTENUATOR

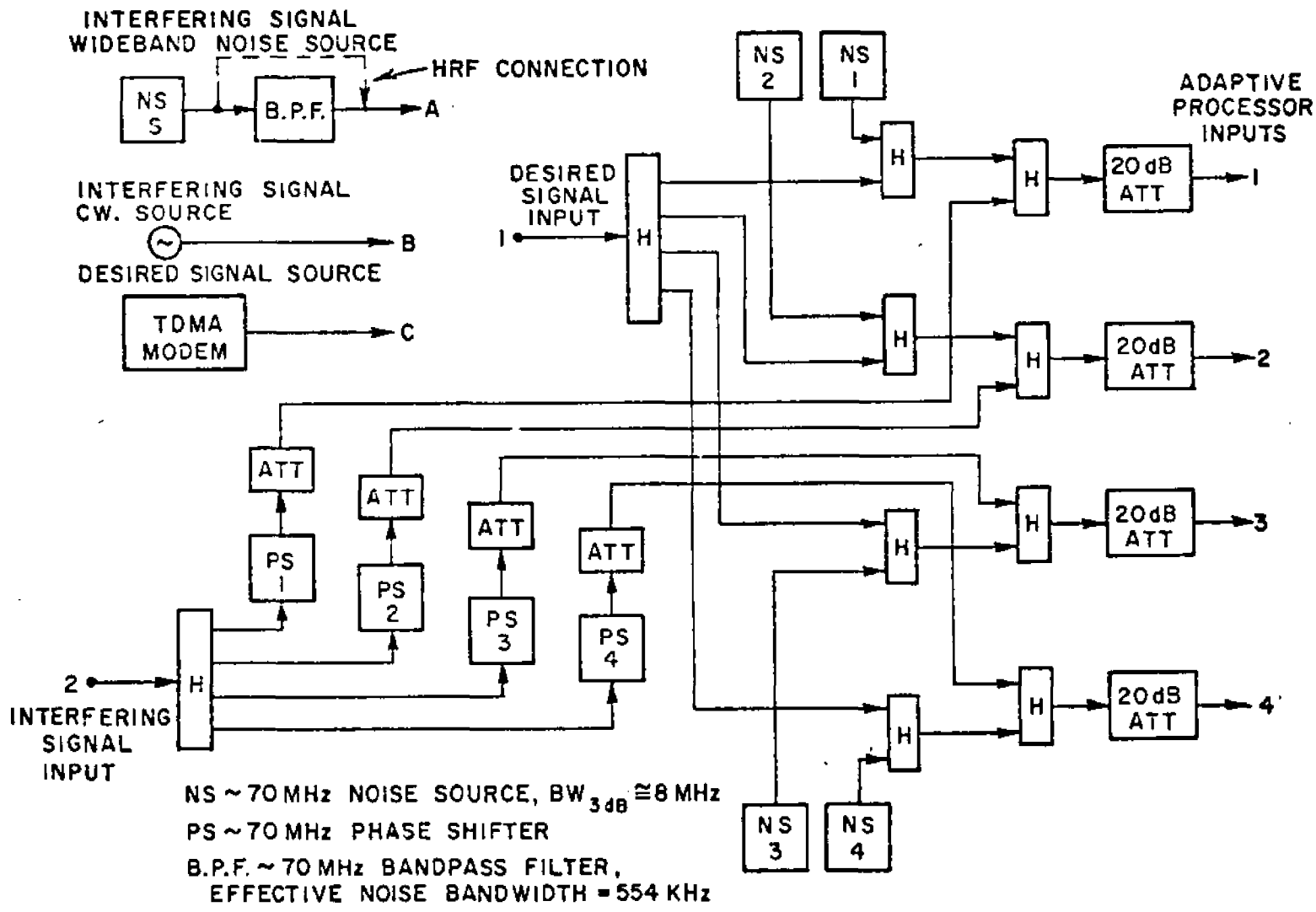
Figure 35--A functional block diagram of the satellite simulator/adaptive spatial processor bench-test.

although the duration of this interval was extended in cases where steady-state performance was being measured (Chapter VI D). The signal transmitted during a preamble contained PN code modulation only (no data). Consequently, a scaled replica* of the desired signal could have been generated locally within the SS/ASP. However, in all results to be presented, the reference signal was estimated by temporally processing the array output signal in order to focus attention on the effectiveness of this approach. To permit continued adaptation when data was to be conveyed (i.e., during the data or overhead slots), it was necessary to estimate the reference signal using the temporal processing approach since the data modulation was not known a priori. Since any practical filter introduces non-zero envelope delay, the phase of the reference signal generated by temporal processing was incorrect following transitions in the desired signal's phase resulting from the impression of data on the coded carrier until phase transitions had "propagated through" the filter. The LMS control loop was prevented from responding improperly during the intervals of time when the phase of the reference signal was incorrect by forcing the error signal to zero or holding the weights constant during an appropriate portion of each data bit interval. Adaptation was performed on a continuous basis during the preamble, since no data were conveyed in this case.

2. Input Signal Synthesis

The method used to simulate four antenna element outputs is illustrated in Figure 36. For most experiments, the desired signal was generated within one of the prototype TDMA modems configured to operate in either the HRF or LRF mode. Biphasic data were transmitted at an instantaneous rate of 10.95 Kbps in the LRF and at 87.6 Kbps in the HRF; the PN code rate was 16 times the data rate in each case. Three different types of interfering signals were generated. A noise source having a 3 dB bandwidth of about 8 MHz, centered about 70 MHz, was used to generate wideband interference. In the LRF mode of operation, the noise was first applied to one of two 70 MHz bandpass filters to establish an effective noise bandwidth of 560 KHz or 1.7 MHz. The interfering source was also a c.w. signal generator. The interfering signals were progressively phased using manually adjustable phase-shifters to simulate off-broadside incidence of interference on a linear array of equally spaced elements. These phase-shifters were 30 percent bandwidth (21 MHz bandwidth) devices and thus exhibited reasonably constant parameters over

*A small frequency offset between the desired signal and the reference signal negligibly affected the results to be presented. Reinhard [15] evaluated the effects of larger frequency offsets.



174

Figure 36--Input signal synthesis.

the 10 MHz IF bandwidth. The desired and interfering signals associated with a given element were summed in wideband hybrids with the output of a (simulated element) noise source having a 3 dB bandwidth of 8 MHz centered on 70 MHz. In this configuration, the desired signal source was simulated to arrive broadside with respect to the linear array, and the phase-shifter adjustments determined relative arrival angles between interference and desired signal; the phase shifters could be adjusted to obtain per-element phase shifts ranging from zero to 70° (electrical). The broadside pattern of an equally spaced (1.5 wavelengths per element spacing) four-element linear array is shown in Figure 37. For an angular separation of desired signal and interference of 4.35 degrees - one-half the beamwidth - the value of ψ is 41 electrical degrees per element.

3. Adaptive Processor Configuration

A functional diagram of the experimental adaptive processor is shown in Figure 4. This configuration incorporates a noteworthy design improvement over the conventional analog LMS algorithm configured in accord with Figure 2. Prior to generating the error by input signal product, the error signal is down-converted to a second i.f. frequency. In this case, only one wideband quadrature hybrid and four error multipliers are required as opposed to the four wideband quadrature hybrids and eight error signal multipliers required to implement the configuration in Figure 2. More importantly, offset voltages generated by the input signal by down-converted error signal multipliers do not affect the dynamic range of the control loops since the product components of interest are i.f. signals. These i.f. signals are transformed into in-phase and quadrature baseband signals which are integrated to generate in-phase and quadrature weights, respectively. Of course, offset voltages still exist at the input to the integrators. However, the magnitudes of the d.c. offsets are considerably reduced since the baseband signals are generated by passive mixers each of which has a constant envelope, narrowband, high-level signal at one input port and, under steady-state conditions, a low-level signal at the other port. Moreover, it is possible to minimize the effects of d.c. offsets at the integrator input by appropriately selecting gain parameters as outlined in section C.

A more detailed functional diagram of the adaptive processor is illustrated in Figure 38. The simulated antenna output signals were applied to four 70 MHz i.f. amplifiers. Each amplifier was (manually) gain adjustable over a 30 dB to 70 dB range and had a nominal 10 MHz bandwidth. Relative phase and amplitude characteristics of each of these amplifiers are shown in Figure 39.

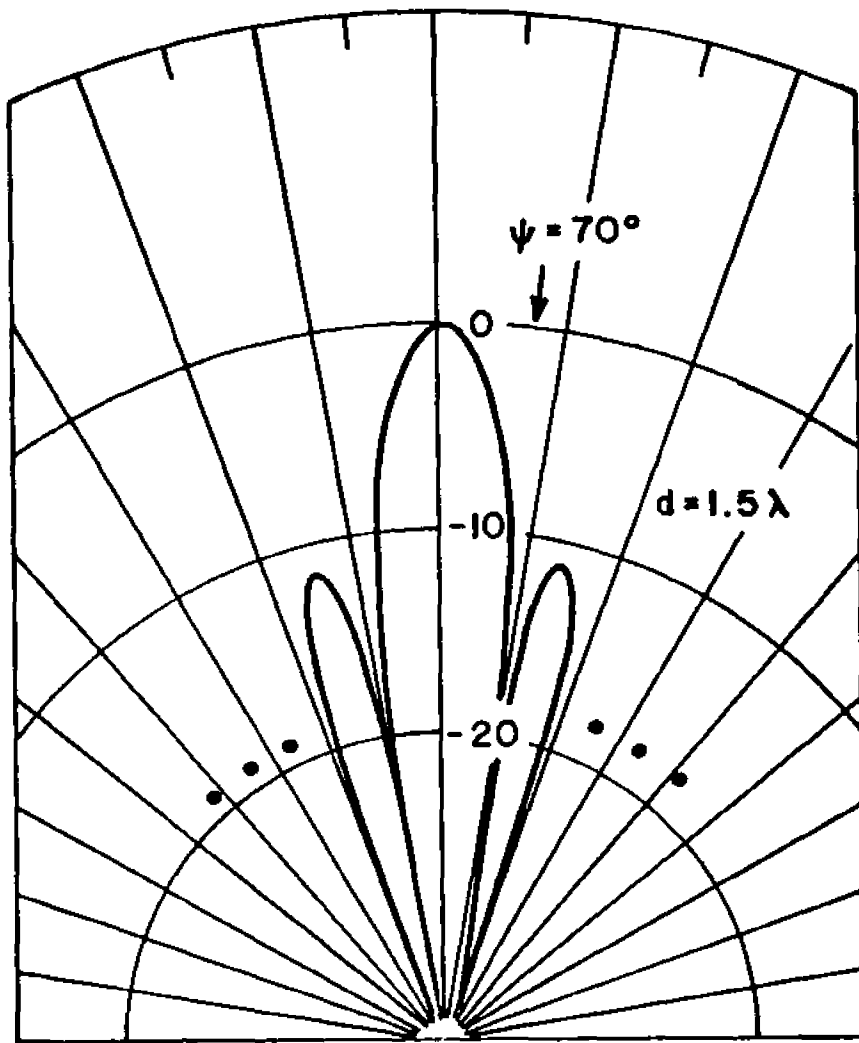


Figure 37--Normalized broadside pattern of a four-element, 1.5λ -spaced linear array.

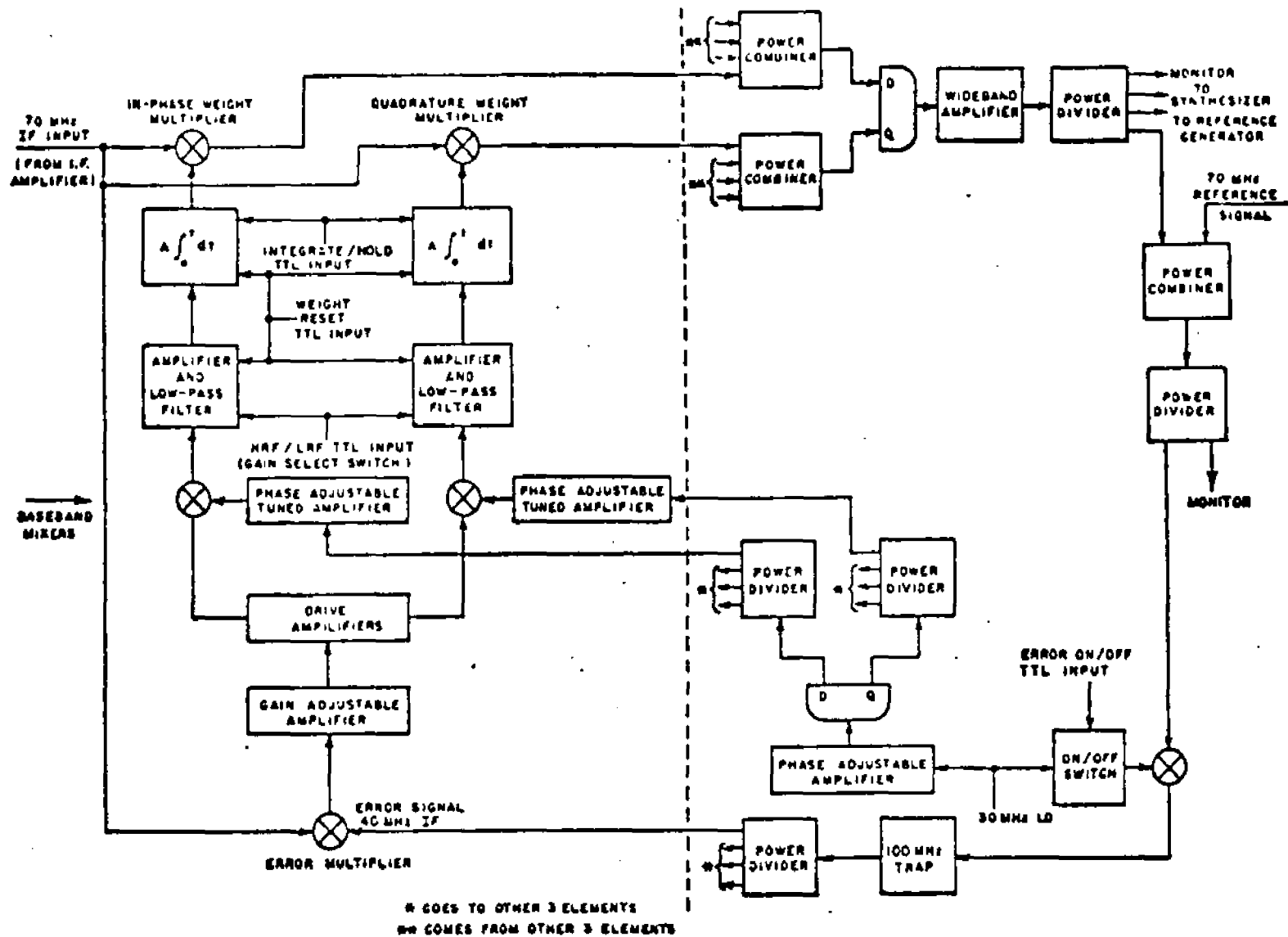


Figure 38--Functional diagram of the present LMS algorithm implementation showing greater detail.

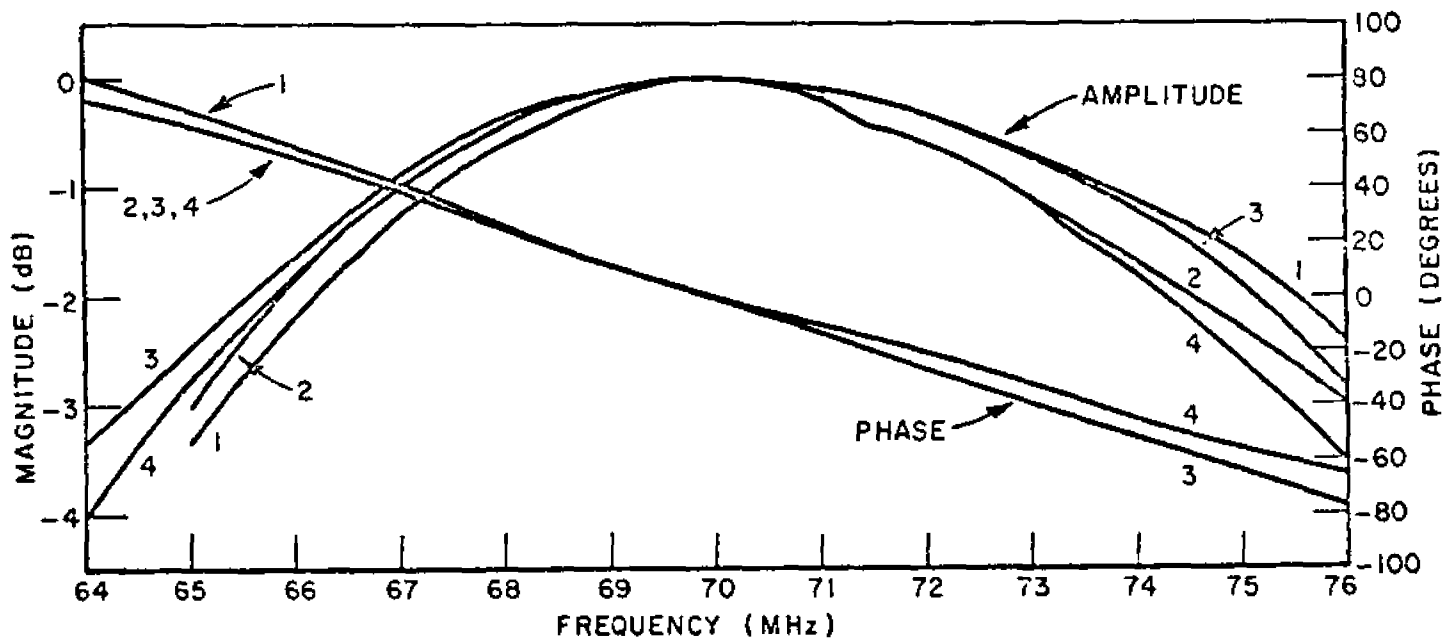


Figure 39--Relative phase and amplitude characteristics of the 70 MHz i.f. bandpass amplifier. Absolute phase and amplitude are not shown.

Four quadrant, variable transconductance multipliers were employed to implement both the signal weighting and error-by-signal multiplication functions, and wideband hybrid combiners/splitters were employed to combine or split signals within the feedback loop in order to minimize delays and impedance mismatches. The quadrature hybrid used to generate the array output was specified to maintain phase quadrature to within two degrees over a 30 percent bandwidth; the remaining hybrids (in the signal path) were 10-100 MHz devices. In addition to the integrator, filters were inserted at various points within the feedback path. One filter was employed to eliminate the upper side-band resulting from the 70 MHz to 40 MHz i.f. down-conversion and a second filter was employed to eliminate the upper side-band generated in each of the four error-by-input signal multipliers. Again, to minimize the effects of feedback delay, both filters were designed to have much wider bandwidths than the i.f. bandwidths. Provision was also made for inserting a low-pass filter prior to each integrator to reduce the adverse effects of weight jitter (see section C). Subsequent tests have shown, however, inserting low-pass filters at these points in the feedback loop can cause loop instability due to an accumulation of delays (even though the delays are relatively small) in other circuits within the loop. For this reason, results to be presented were obtained with the low-pass filter removed. A total phase shift of 180 degrees around the feedback loop at the 70 MHz operating frequency was established by adjusting the relative phase of the LO signals applied to the baseband mixers and the 70 to 40 MHz i.f. down-converter. Of course, the phase shift differed from 180 degrees at other frequencies due to the circuit and cable delays. In the present implementation, circuit and cable delays within the feedback loop resulted in a phase error (at frequencies different from the center frequencies) between the two signals applied to the input signal by error signal multipliers. The effect of this phase error was to "decorrelate" the feedback and input signals, as reflected by the dependence of the d.c. output voltage of the baseband amplifier* versus the input (c.w.) frequency shown in Figure 40. At frequencies corresponding to a phase shift of $\pm 90^\circ$ with respect to the phase shift at 70 MHz, the d.c. output was zero. These two frequencies are shown to be separated by 13.1 MHz, indicating that the loop delay was approximately equal to the reciprocal of 26.2 MHz, or about 38 nsec. Delay within the bandwidth of the input signals (65 to 75 MHz) was slightly less at about 29 nsec. The effects of the decorrelation, and a method for compensating for these effects, is discussed in section C.

*This result was obtained by setting all but one of the weight control voltages equal to zero and applying a c.w. signal to the i.f. input of the non-zero weight.

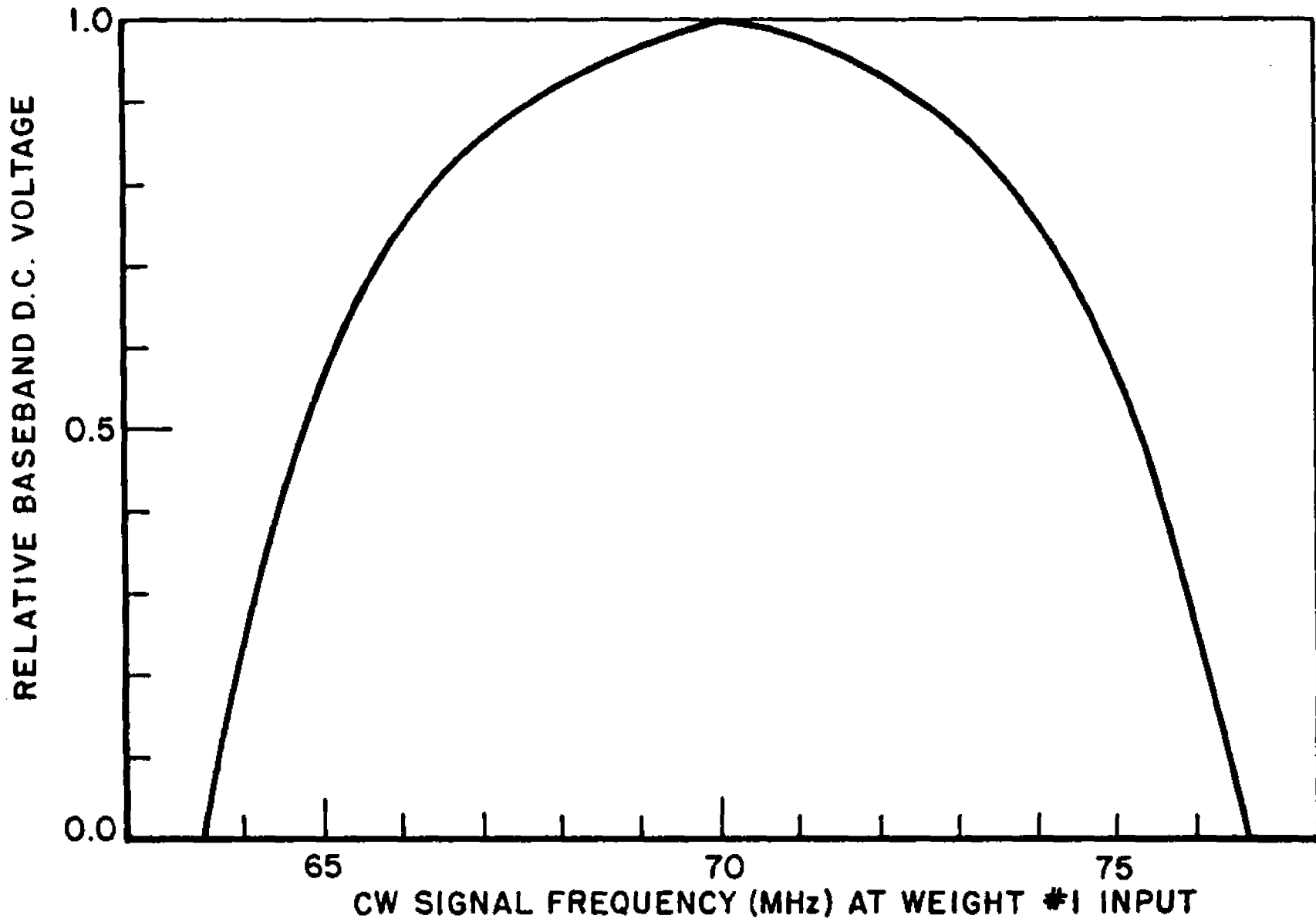


Figure 40--D.C. voltage measured at the baseband amplifier output versus the array input signal frequency.

Additional delays occurred between the error multiplier output and the weight control input due primarily to the presence of "stray" poles in the non-ideal components used to implement the integrator and baseband circuits. As delineated in section C, these poles place a lower limit on loop response time required for stable operation; the experimental processor was capable of providing stable operation for time constants $[(\alpha\lambda_{\max})^{-1}]$ as small as 100 nsec, which was much smaller than the time constants encountered in the experiments.

Means were provided in the present ASP implementation for switching off the LO used to drive the 70 MHz to 40 MHz i.f. down-converter when the appropriate TTL control signal was applied to the LO driver, thereby opening the feedback loop. Also, the integrator in each channel could be operated in one of three modes -- initial conditions set,* integrate, or hold -- depending on the states of two TTL control signals. All eight integrators were in a common operating mode at any given instant of time. Details regarding the purpose of these functions are given in sub-section 6.

Measurements were conducted to determine the circuit parameters of experimental ASP. These measurements are summarized in Appendix III. The circuit parameters and operating principles of the ASP implementation are described in greater detail in Reference [20].

4. Reference Signal Processor Description

The purpose of the reference signal processor was to estimate the desired signal waveform (denoted "70 MHz reference signal" in Figure 38) via temporal processing. To distinguish the desired signal from interference or noise, each user transmitted quadrature**signal on which a specified code had been impressed. The ratio of the code rate to the data rate determines the ultimate gain which can be achieved by waveform processing. The TDMA-adaptive array system employed a maximal length (127 bit) pseudo-noise (PN) code with a code rate 16 times the data rate, which provided an optimum processing gain in a wideband Gaussian noise environment of about 12 dB. Clearly, when one considers interfering signals 20 dB to 30 dB stronger than desired signal levels, waveform processing alone would not provide an adequate estimate

*Initial weight settings are adjusted manually.

**A biphasic option is also available.

of the desired signal. For this reason, the adaptive array output was used as the reference signal processor input to take advantage of an additional processing gain provided by nulling of high-level interfering signals by the adaptive array.

A functional diagram of the waveform processor is shown in Figure 41. Starting in the upper left, the array output was down-converted to a 10 MHz i.f. by mixing it with a 60 MHz LO signal on which the appropriate quadrature code modulation had been impressed. The signal was next bandpass filtered to remove a major portion of the interferences while retaining almost all of the desired signal; thus, its bandwidth had to be wide enough to pass desired signal data but narrow enough to provide processing gain to provide processing gain. This required two separate waveform processing filters, one for the HRF and the other for the LRF. Both filters were double pole (12 dB per octave roll-off). The first bandpass filter, labelled HRF in Figure 41, had a 6 dB bandwidth equal to approximately one-sixth the HRF code rate; the processing gain to HRF signals exceeded 8 dB. The envelope insertion delay of this filter was about 2.5μ sec or approximately one-fifth of a data bit. Processing gain in the LRF was achieved by down-converting the output of the first filter to a 2 MHz IF and then bandpass filtering the result. The second filter bandwidth was equal to approximately one-sixth the LRF code rate and the input-to-output envelope delay was approximately one-fifth of a data bit interval. The LRF filter output was reconverted to a 10 MHz i.f. signal which was then multiplexed with the HRF filter output. The mux selected the signal according to the format being used. Following the mux was a hard-limiter which rendered the waveform processor output independent of input amplitude. The quadrature code was next reimpressed on the hard-limiter output by mixing it with the same 60 MHz LO signal (except for a constant phase angle) employed in the 70 MHz to 10 MHz down-conversion. This operation also up-converts the signal back to 70 MHz i.f. The resulting signal was applied to a gain adjustable amplifier and an analog switch. The analog switch was used to shut off the reference when an appropriate TTL control signal was applied (see Section 6).

When the array processor is near its optimum steady-state condition, the error is reduced to a small value* so that the array output (approximately) matches $r(t)$ in amplitude and phase.

*The error is small except during the reference delay interval.

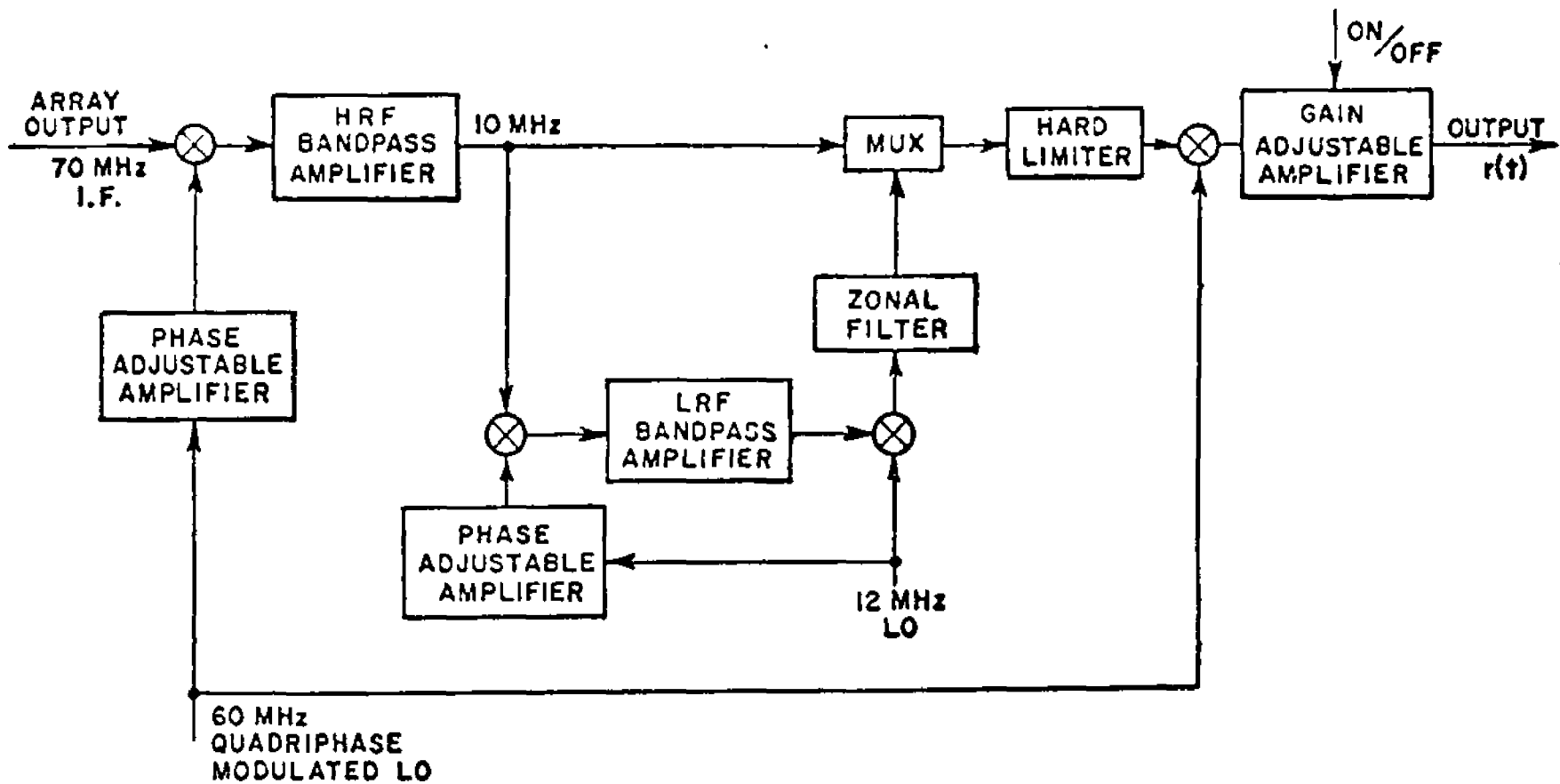


Figure 41--Functional diagram of the waveform processor.

More precisely, for constant envelope desired signals (assume an ideal processor),

$$\begin{aligned}\tilde{\varepsilon}_{SS}(t) &= \tilde{r}(t) - w_{\text{opt}}^{\dagger} \tilde{s}(t) \\ &= -\frac{1}{1 + T_0} \tilde{r}(t)\end{aligned}$$

where $\tilde{\varepsilon}_{SS}(t)$ represents the difference between the desired signal component of the array output and the (in this case, ideal) reference signal. A preferred output level was established by the hard-limiter in Figure 41. A stable phase, on the other hand, is more difficult to achieve since the waveform processor input must be antiphase with its output; any deviation from a 180° phase shift causes a frequency offset at the array output [15]. In practice, it is not possible to entirely eliminate this frequency offset, since the insertion phase of the hard-limiter has a slight dependence on signal level applied at its input. However, it was possible in the present implementation to reduce the offset to the point where it negligibly affected system performance (i.e., the offset was much smaller than the inverse of the longest array processor time constant).

The effects of envelope delay and frequency offset are clearly illustrated by the oscilloscope traces in Figure 42. Figure 42(a) displays the error monitor output (see Figure 42(b)) during the first portion of a data bit when (1) the array was in initial conditions set mode, (2) the desired signal applied at the array processor's input underwent a data bit transition, and (3) the array output amplitude was set equal to the reference signal amplitude. Under these conditions, the reference signal was antiphase with respect to the array output until the data transition had "propagated through" the reference signal processor. Thus, the error signal level was twice the reference signal level for the duration of the reference delay (about 20 μ sec for this example) and was nearly zero during the remainder of the data bit interval. The method used to compensate for the reference delay interval is detailed in sub-section 6. Figure 42(b) shows the frequency offset on one of the weights caused by a reference signal phase error.

5. Multiplexer and Limiter Subsystem

In order to model a TDMA-adaptive array system operating with a hard-limiting repeater satellite, the signal at the adaptive array processor output was applied to the multiplexer and limiter subsystem shown in Figure 43. The multi-

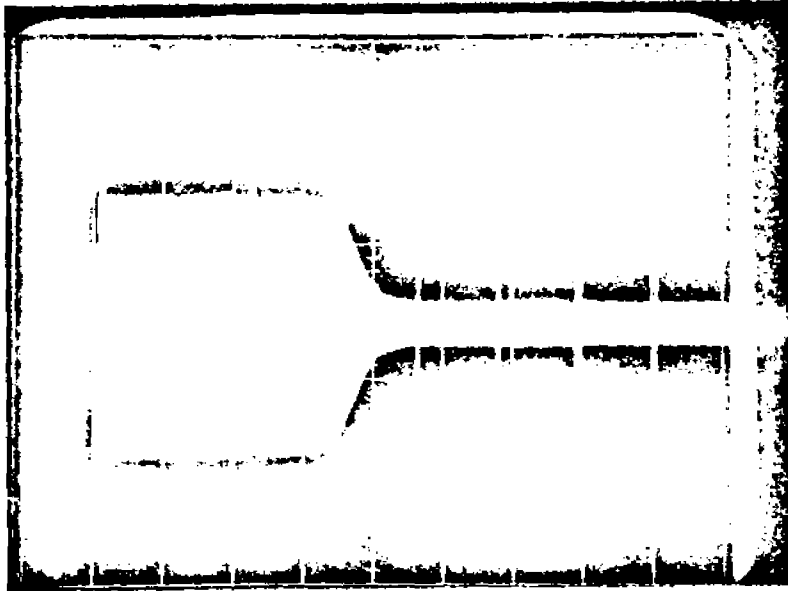


Figure 42(a)--Error monitor output signal (LRF) initial conditions set. Horizontal: 5 μ sec/div.

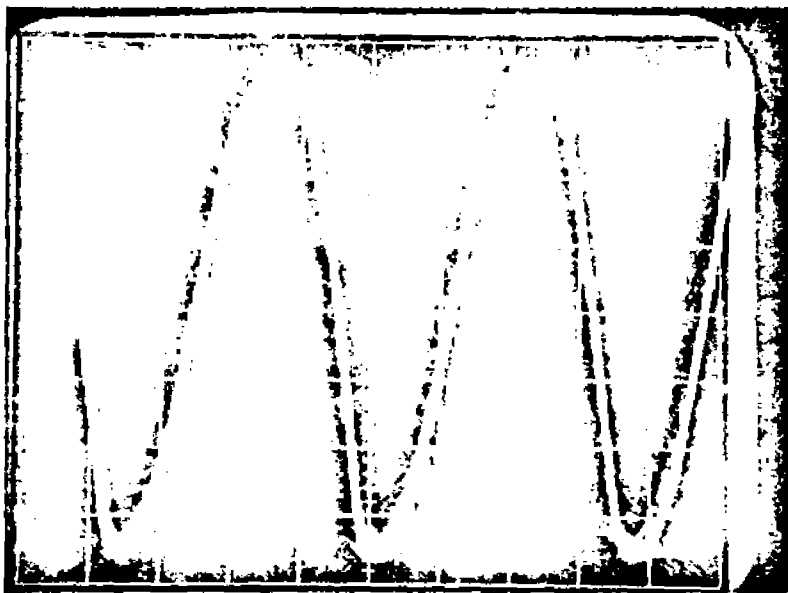


Figure 42(b)--Weight #2 control voltage, continuous adaption. Vertical: 1.0 v/div. Horizontal: 100 μ sec/div.

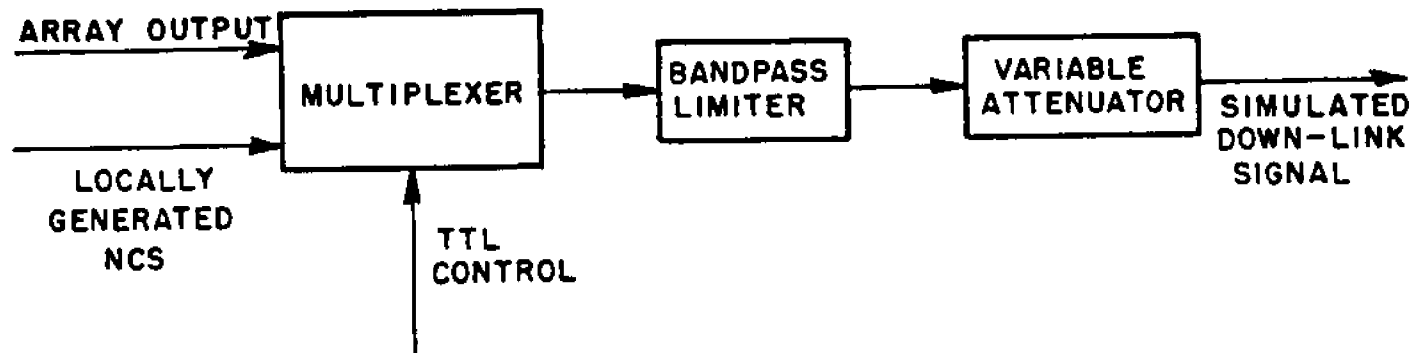


Figure 43--Functional diagram of the multiplexer and limiter subsystem.

plexer selected either the locally generated NCS or the array output signal for transmission depending on the state of a TTL control signal (see sub-section 6). The simulated down-link signal was generated by applying the mux output signal to a bandpass limiter and a variable attenuator.

The limiter suppression characteristics were determined by measuring the relative output signal voltage as a function of the input signal-to-noise ratio. The waveform applied to the limiter's input was generated by adding noise having an 8 MHz spectral width on 70 MHz to a PN code modulated signal (code rate = 175 Kbps); the input signal-to-noise ratio was varied by attenuating the signal level (noise power fixed). The measured results were in close agreement with a well-known theoretical result for the limiter suppression factor [31] as shown in Figure 44. These results will be used in later sections to transform theoretical performance of the TDMA-adaptive array system to measured performance.

6. Control Waveform Subsystem

Since the NCS was generated autonomously within the satellite, a number of additional timing functions required in structuring TDMA/ASP compatibility was performed at the satellite. In addition to generating the two PN code-pairs described previously, these functions included the generation of TTL signals to control the state or operating mode of (1) the integrators, (2) the error signal on/off switch, and (3) the reference signal on/off switch. The state of each of these binary control signals could be set manually or placed under "program" control. Figure 45 illustrates programmed timing relationships between the NCS pulse (labelled "format"), the integrator mode, and the error signal on/off function. The reference on/off control signal is not shown but was identical to the error on/off control waveform. During data and link/range slots, data were added modulo-two to the PN codes at each user terminal (e.g., at the TDMA modem). To circumvent the adverse effects of reference signal processor delay encountered when data were present, adaption was inhibited for the first quarter (slightly greater than the reference signal delay) of each data bit by switching off the error signal and holding the weights (i.e., the integrator output). Note that these functions redundantly disabled the feedback loop. Moreover, the reference signal was disabled at the same time. Subsequent tests have shown that either technique for disabling the feedback loop is equally effective in removing incorrect feedback which occurs during the reference delay, but that merely removing the reference signal during this interval (and not disabling the loop) in some instances resulted in poor steady-state performance. In obtaining results to be presented, only the error

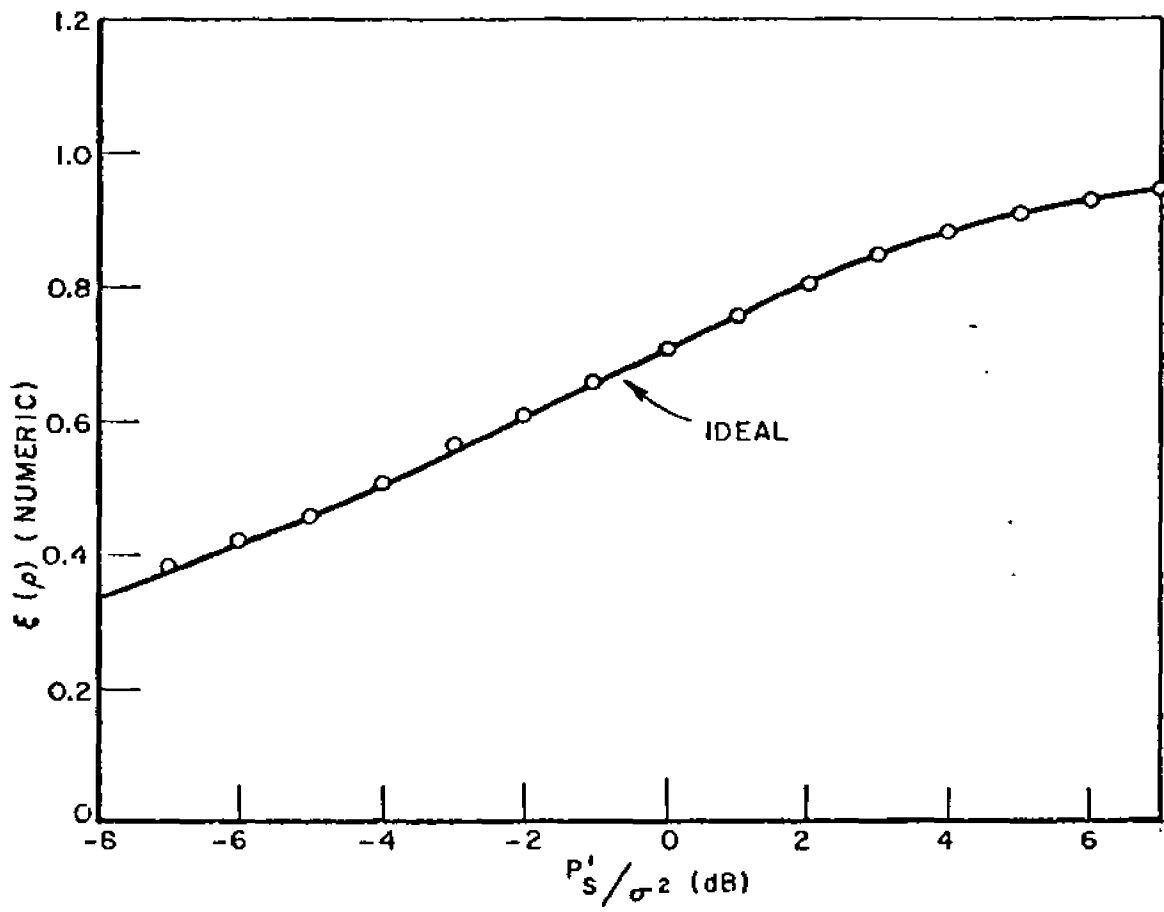


Figure 44--The suppression characteristic of the bandpass limiter versus the input signal-to-noise ratio.

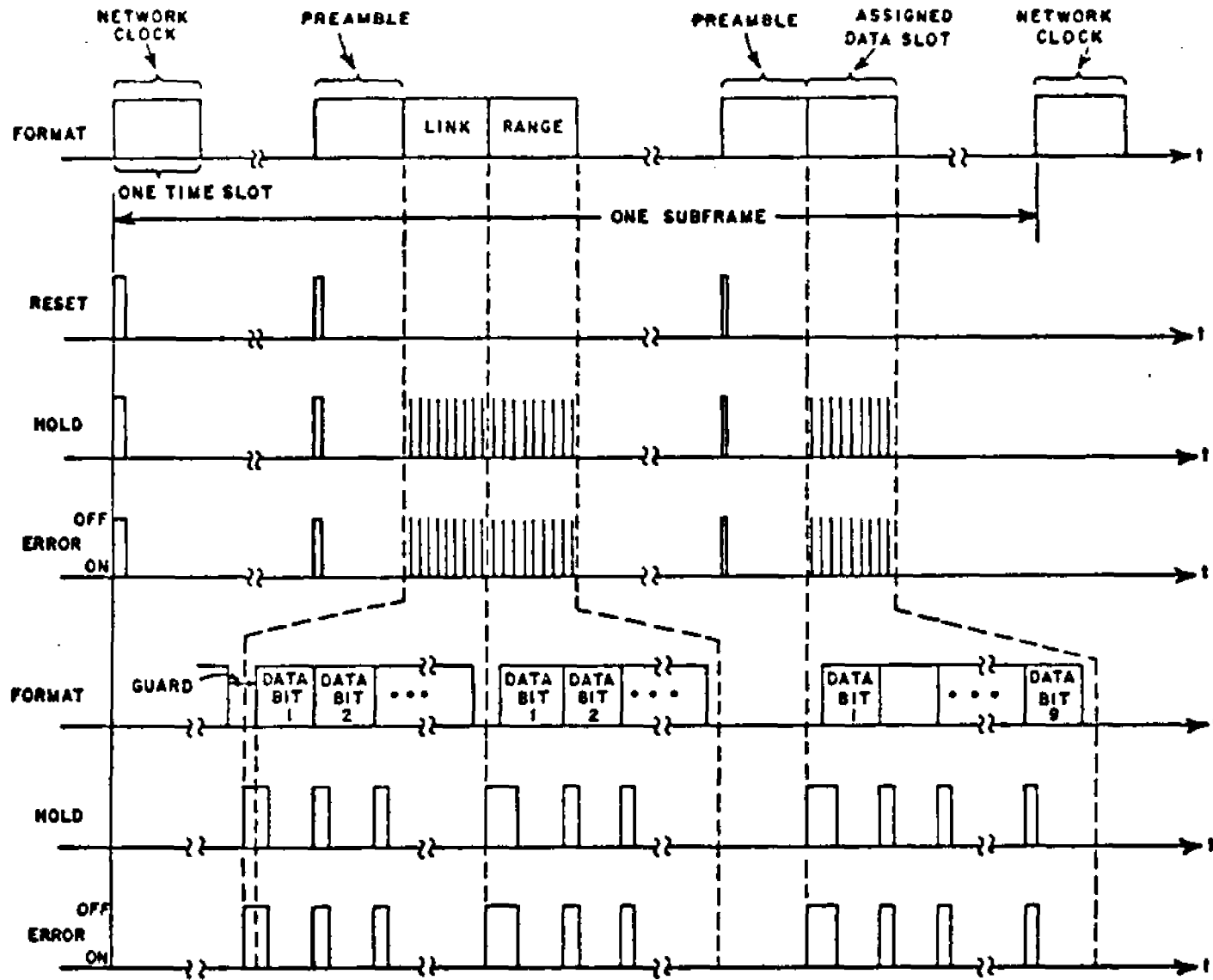


Figure 45--Relationships of the control waveforms to the TDMA format.

signal was placed under "program" control; the reference signal was "on" continuously and the integrator hold mode was disabled.

7. The Bit Error Probability Measure

The TDMA modem incorporated a differential detector to detect biphase data conveyed by the desired signal. The bit error probability (BEP) performance of the detector was used as a measure of SS/TDMA performance under a wide variety of signal environments. As discussed in Chapter V, ideal DPSK detector performance in a Gaussian noise environment is obtained if (1) the circuits used to implement the matched filter/detector are ideal, (2) the channel bandwidth is wide with respect to the code rate, and (3) the locally generated code modulation is synchronized with the code modulation contained on the desired signal. The degree to which these requirements were satisfied by the experimental DPSK receiver and associated time base synchronization subsystems was determined earlier from measurements performed on the TDMA modem. Three different sets of measurements are shown in Figure 46. The data points closest to the ideal curve illustrates detector performance (LRF mode) for the case where the bit timing error was set equal to zero and the bit energy-to-noise density ratio of the signal applied to the detector's input was varied. The deviation from the ideal curve can be attributed to non-ideal circuits used in implementing the detector and to the finite (1.4 MHz double-sided) bandwidth of a filter which preceded the detector. The remaining two sets of data points show detector performance when the sampled-data delay-locked loops (SDDL) were used to maintain desired timing relationships between the transmit or receive clock signals and the NCS. Basically, these loops relied on the correlation properties of the PN code modulation to measure received signal times of arrival. The correlation operation was performed by collapsing the received signal spectra and then bandpass filtering the result -- this operation is functionally represented by the diagram of Figure 47. As presently implemented, the bandpass filters have a 3 dB bandwidth of about 2 KHz (15 KHz in the HRF). Since the received signal upon which these timing estimates are based contain additive noise, the controlled time bases "jitter" with respect to the true time of arrival; consequently, detector performance degrades. The data points shown in Figure 46 corresponding to the highest BEP were measured with both the transmit and receive timing loops enabled,* and the data points corresponding to the next highest BEP were measured with the receive timing loop enabled and the transmit timing error held fixed at zero. These measurements are approximately in accord with the results of previous analytical and experimental studies

*When the TDMA modems are configured for normal operation, both loops are enabled.

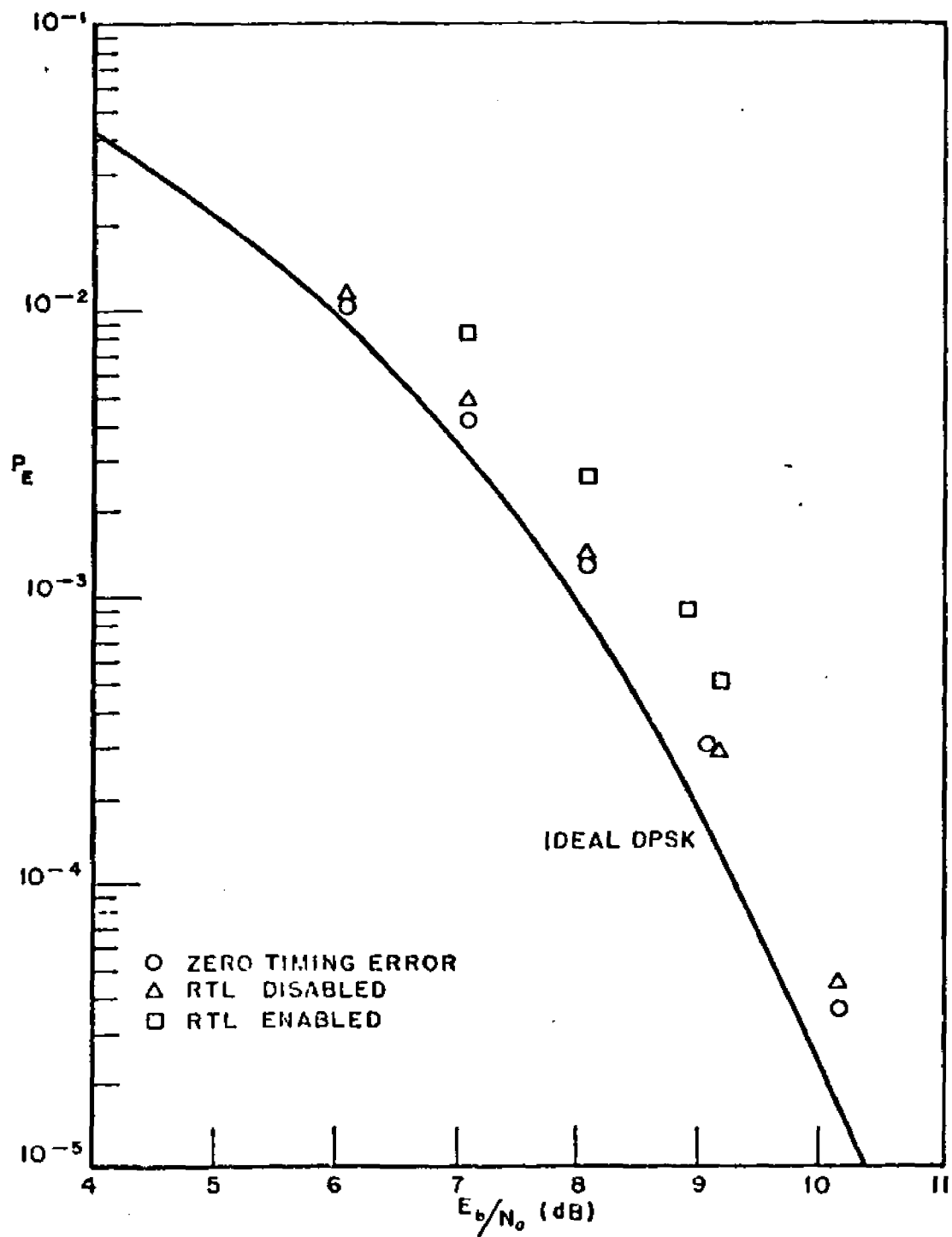


Figure 46--Performance of the differential detector/bit timing synchronization subsystem versus the input bit energy to noise density ratio (LRF).

of SDDL performance [32] and the effects of timing jitter on DPSK receiver performance [33].

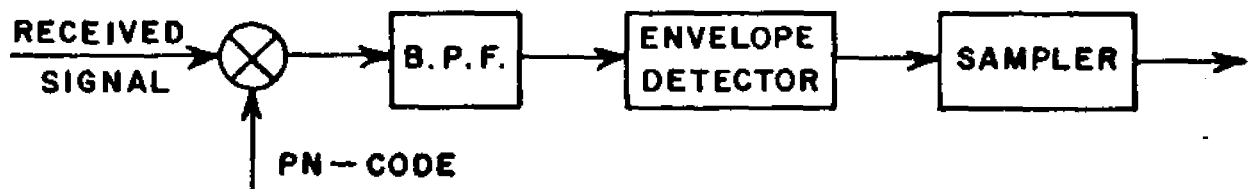


Figure 47--A functional representation of the waveform processing used in the sampled-data delay-locked loops.

Note that for the system in Figure 35, noise added to the signal on the down-link affects the performance of both the receive and transmit timing loops. However, since the NCS is generated within the SS, up-link interference and noise affects only the transmit timing loop (range tracking loop). This distinction will be of importance in later sections where weight jitter and inadequate signal-to-noise ratios at the output of the ASP affect the performance of the range tracking loop.

C. Practical Design Considerations Relevant to the Implementation of the Analog LMS Algorithm

1. Introduction

A brief discussion and analysis of the effects of non-ideal circuit components used to implement the LMS algorithm configured in accord with Figure 38 are presented in this section. In order to simplify the presentation, the effects of weight jitter are neglected.

2. Delays in the Feedback Loop

Since the LMS algorithm relies on negative feedback, transient and steady-state performance can be adversely affected by time delays in circuits used to implement the control loop. In this section, the effects of circuit delays at various points within the feedback loop are evaluated. Circuit delays are assumed constant over the frequency bands of interest and are assumed to be phase-compensated so as to introduce zero phase-shift at the array center frequency. For this case, loop time delays may be lumped into factors identifiable with components of the physical processor as shown in Figure 48. In particular,

(346)

$$\underline{D}_w = \begin{bmatrix} D_{w_1} \\ D_{w_2} \\ \vdots \\ D_{w_m} \end{bmatrix} = \text{delay associated with each weight multiplier (B to C)}$$

$$\underline{D}_e = \begin{bmatrix} D_{e_1} \\ D_{e_2} \\ \vdots \\ D_{e_m} \end{bmatrix} = \text{delay associated with the input leg of each error multiplier (B to H)}$$

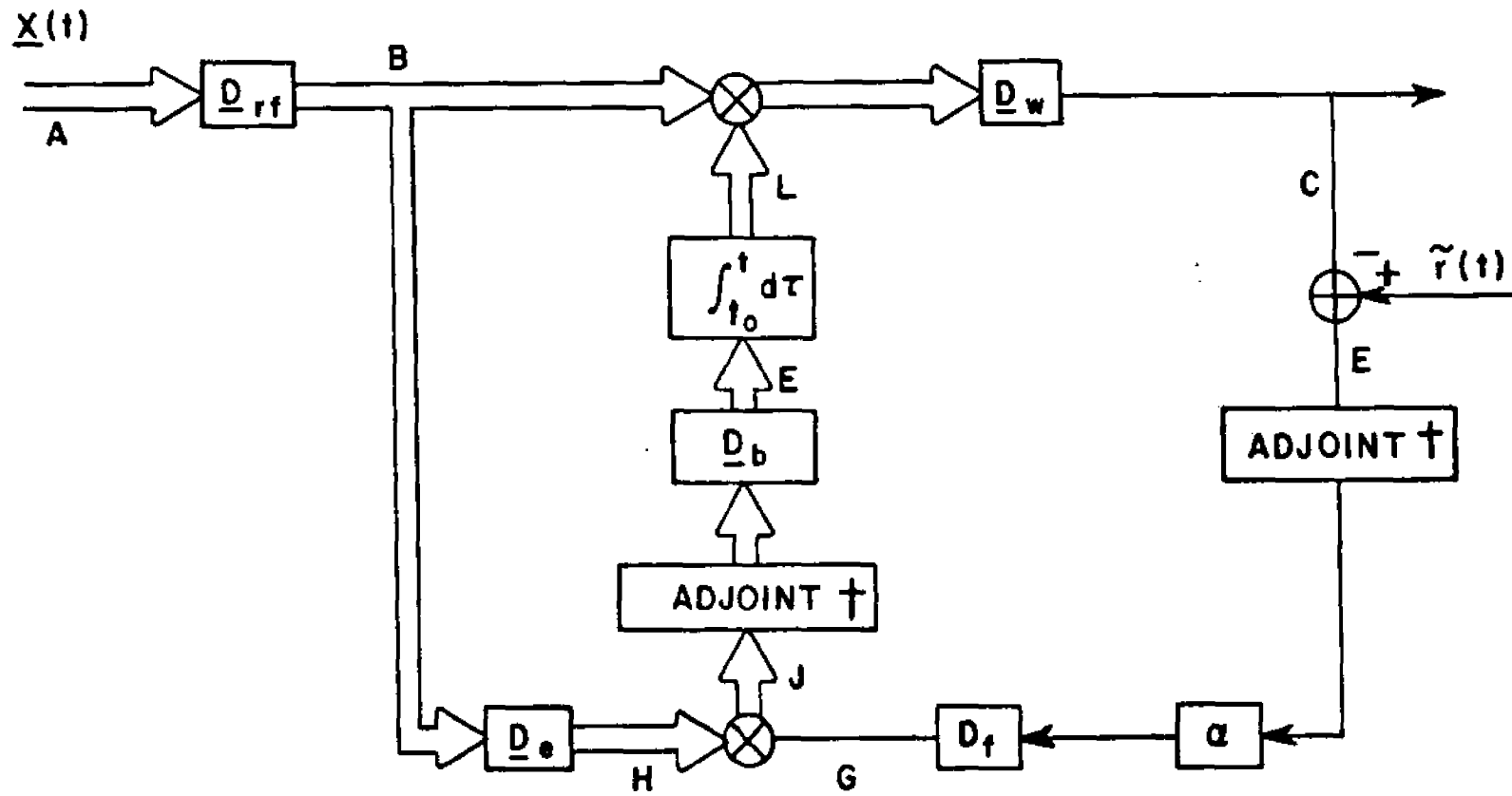


Figure 48--Adaptive processor model with feedback delays.

$$\underline{D}_{r.f.} = \begin{bmatrix} D_{r.f.1} \\ D_{r.f.2} \\ \vdots \\ D_{r.f.m} \end{bmatrix} = \text{delay in r.f. amplifiers preceding each input}$$

$$\underline{D}_b = \begin{bmatrix} D_{b1} \\ D_{b2} \\ \vdots \\ D_{bm} \end{bmatrix} = \text{delay associated with the error multiplier and post-correlation circuits (J to L)}$$

$\underline{D}_f =$ delay in the error signal circuits (F to G) .

The vector weight equation described by this model is given by

$$\frac{dw(t)}{dt} = \alpha \tilde{\underline{x}}(t - \underline{D}_e - \underline{D}_{r.f.}) [\tilde{\underline{r}}^\dagger(t - D_f) - \tilde{\underline{x}}^\dagger(t - \underline{D}_w - \underline{D}_{r.f.} - D_f) w(t - \underline{D}_w - \underline{D}_f - D_b)] \quad (347)$$

where

$$\left. \begin{aligned} \tilde{\underline{x}}_i(t - \underline{D}_w - \underline{D}_{r.f.} - D_f) &\equiv \tilde{\underline{x}}_i(t - D_{w_i} - D_{r.f.i} - D_f) \\ \tilde{\underline{x}}_i(t - \underline{D}_e - \underline{D}_{r.f.}) &\equiv \tilde{\underline{x}}_i(t - D_{e_i} - D_{r.f.i}) \\ w_i(t - \underline{D}_w - D_f - D_b) &\equiv w_i(t - D_{w_i} - D_f - D_{b_i}) \end{aligned} \right\} i=1,2,\dots,m$$

With the definitions

(348)

$$K_{x_{ij}}(\tau_1) \equiv E \{ \tilde{x}_i(t - \underline{D}_e - \underline{D}_{r.f.}) \tilde{x}_j^+(t - \underline{D}_w - \underline{D}_{r.f.} - \underline{D}_f) \}$$

$$R_{x_d}(\tau_2) \equiv E \{ \tilde{x}_i(t - \underline{D}_e - \underline{D}_{r.f.}) \tilde{r}^+(t - \underline{D}_f) \}$$

$$\bar{w}_i(\tau_3) \equiv E w_i(t - \underline{D}_w - \underline{D}_f - \underline{D}_b)$$

$$\tau_{1ij} \equiv \underline{D}_{w_j} + \underline{D}_{r.f.j} + \underline{D}_f - \underline{D}_{e_i} - \underline{D}_{r.f.i}$$

$$\tau_{2i} \equiv \underline{D}_f - \underline{D}_{e_i} - \underline{D}_{r.f.i}$$

$$\tau_{3i} \equiv \underline{D}_f + \underline{D}_{b_i} + \underline{D}_{w_i} \quad ; \quad i, j, = 1, 2, \dots, m$$

the ensemble average of Equation (347) reduces to

$$\frac{d\bar{w}(t)}{dt} = \alpha [R_{x_d}(\tau_2) - K_x(\tau_1) \bar{w}(t - \tau_3)] \quad (349)$$

If $K_x(\tau_1)$ is invertible (which is by no means assured), and if the τ_{3i} are sufficiently small with respect to the control loop bandwidth, the steady-state weight vector

$$w(t) |_{t \rightarrow \infty} = K_x^{-1}(\tau_1) R_{x_d}(\tau_2) \quad (350)$$

is likely to differ significantly from w_{opt} unless each of the m^2 components of τ_1 and each of the m components of τ_2 are small relative to B^{-1} , where B represents the input signal bandwidth. Moreover, since the array output is composed of a linear combination of $\tilde{x}_j(t - \underline{D}_w - \underline{D}_{r.f.})$, the delay $(\underline{D}_{w_i} + \underline{D}_{r.f.i} - \underline{D}_{w_j} - \underline{D}_{r.f.j})$ must also be much smaller than B^{-1} to obtain a broadband nulling capability. Thus, proper design requires that

$$(a) D_f - D_{e_i} - D_{r.f.i} \ll B^{-1} \quad (351)$$

$$(b) D_{w_i} + D_f - D_{e_i} \ll B^{-1}$$

$$(c) D_{w_i} + D_{r.f.i} - D_{w_j} - D_{r.f.j} \ll B^{-1} .$$

In practice, it is possible to satisfy these requirements over a given frequency band by (1) inserting an appropriate delay in path B to H, (2) matching the delays D_{w_i} and D_{w_j} , (3) matching the delays $D_{r.f.i}$ and $D_{r.f.j}$, and (4) adjusting the reference signal delay relative to $D_{r.f.} + D_e - D_f$. Techniques (1), (2), and (4) may be implemented using wideband circuits and delay lines. However, the only effective method for matching r.f. delays is to employ filters which have nearly identical passband characteristics. In some cases, this may require filtering at baseband to obtain close tolerances.

The weights converge as in Equation (350) provided the delay τ_{3_i} ($i = 1, 2, \dots, m$) is "sufficiently small." To obtain a more precise relationship between the delay τ_{3_i} and weight convergence, assume

$$\left. \begin{aligned} \tau_{1_{ij}} &= 0 \\ D_{w_i} + D_{r.f.i} &= D_{w_j} + D_{r.f.i} \\ \text{and } \underline{\tau}_2 &= [0] \end{aligned} \right\} \quad i, j = 1, 2, \dots, m \quad (352)$$

By further assuming that the i^{th} initial weight $\bar{w}_i(t_0)$ remains constant during the initial delay interval $t_0 < t < t_0 + \tau_{3_i}$, the Laplace transform of Equation (349) becomes

$$\bar{w}(s) = \alpha \left\{ \frac{1}{s} R_{xd} - K_x w(t_0) \frac{1}{s} [1 - e^{-(\tau_3 s)}] - K_x \bar{w}(s) e^{-(\tau_3 s)} \right\} \quad (353)$$

where

$$\bar{w}(s) = \mathcal{L}\{\bar{w}(t)\} \quad .$$

The Laplace transform of the component of $\bar{w}(t)$ projected onto the n^{th} eigenvector of K_x satisfies the following equation:

$$s y_n(s) = \alpha \left\{ \frac{1}{s} (P R_{xd})_n - \frac{1}{s} \lambda_n [P \bar{w}(t_0) (1 - e^{-\tau_3 s})]_n \right. \quad (354) \\ \left. - \lambda_n [p \bar{w}(s) e^{-\tau_3 s}]_n \right\} \quad ; n = 1, 2, \dots, m$$

where

$$y(s) = p \bar{w}(s) \quad .$$

By Equations (352),

$$\tau_{3_i} = D_{b_i} + D_{e_i} \quad ; i = 1, 2, \dots, m \quad (355)$$

Assuming the delays are equal among elements, i.e.,

$$\tau_3 = \tau_{3_i} = \tau_{3_j} \quad ; j = 1, 2, \dots, m \quad (356)$$

$y_n(s)$ becomes

$$y_n(s) = \frac{1}{s + \alpha \lambda_n e^{-\tau_3 s}} \frac{\alpha}{s} \quad (357)$$

$$\cdot [(P R_{xd})_n - \lambda_n (P \bar{w}(t_0))_n (1 - e^{-\tau_3 s})] \quad ; n = 1, 2, \dots, m$$

which is the transfer function of the loop shown in Figure 49. Employing the Nyquist stability criterion, this loop, and thus $y_n(t)$, is unconditionally stable if

$$\tau_3 = D_{b_i} + D_{e_i} < \frac{\pi}{2 \alpha \lambda_n} \quad i, n = 1, 2, \dots, m \quad (358)$$

or

$$\alpha \lambda_n < \frac{\pi}{2} \frac{1}{\tau_3} .$$

Consequently, the weight equation [Equation (349)] converges if Equations (352), (356), and (358) are satisfied.

Figure 50 illustrates the time response of $y_n(t)$ for a moderate delay of

$$\tau_3 = \frac{0.5}{\alpha \lambda_n}$$

and several different initial weights $w_0 (= w(t_0))$. The component of w_0 projected onto the n th eigenvector $[(pw_0)_n]$ is normalized to the steady-state value of $y_n(t)$ $[= (P R_{xd})_n / \lambda_n]$. Time delay is shown to induce ringing which is most pronounced when $(Pw_0)_n$ is near to or larger than the steady-state value. The magnitude of the ringing decays at a rate proportional to $\alpha \lambda_n$.

3. Amplitude and Phase Error In The Weight Multipliers

Ideally, when the scalar w_k is applied to the k^{th} complex weight multiplier, its output $(\tilde{y}_k(t))$ is given by $w_k * \tilde{x}_k(t)$. In practice, non-ideal circuit components cause an amplitude and phase error which may be characterized by appropriately scaling the ideal multiplier output as follows:

$$\begin{aligned} \tilde{y}_{ek}(t) &= c_k * e^{-j\Delta_k} \tilde{y}_k(t) \\ &= c_k * e^{-j\Delta_k} w_k * \tilde{x}_k(t) \end{aligned} \quad (359)$$

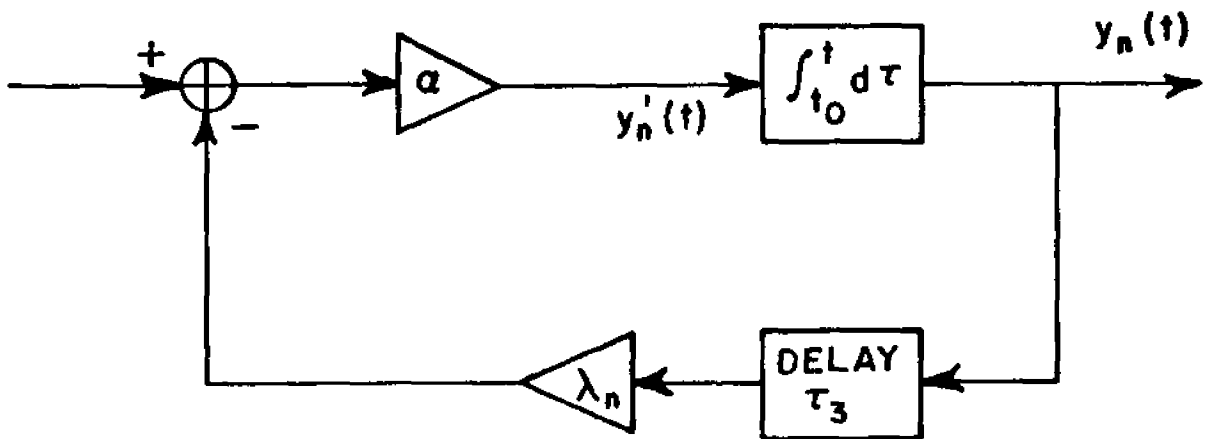


Figure 49--A closed loop representation of the LMS algorithm when $\tau_{1j} = 0$, $\tau_{2j} = 0$, and $\tau_{3j} = \tau_3$ for $i, j = 1, 2, \dots, m$.

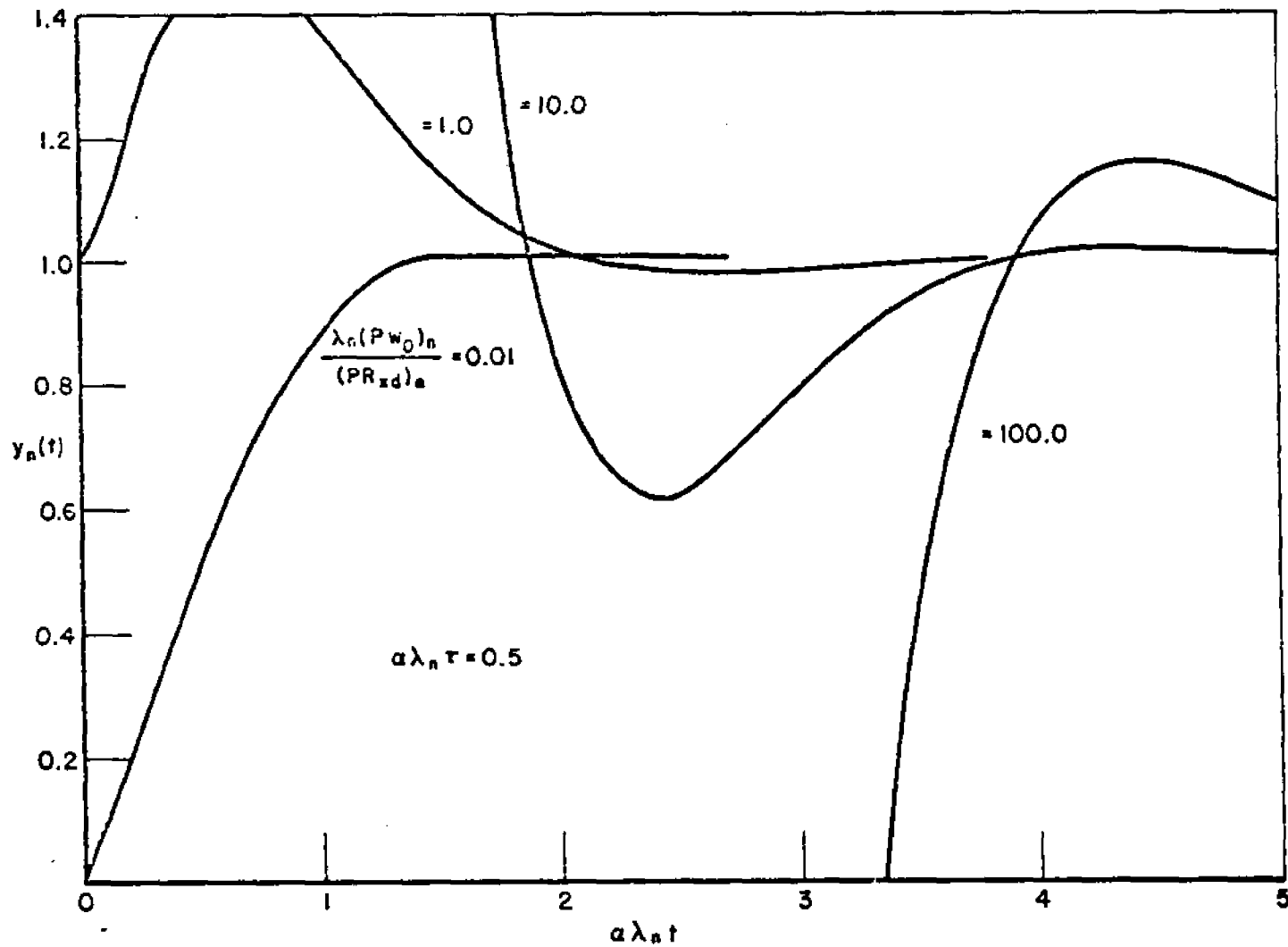


Figure 50--The response of $y_n(t)$ versus adaption time (normalized to the n^{th} time constant) for several different initial weights.
 $\tau_3 = 0.5 (a\lambda_n)^{-1}$.

where $c_k - 1$ and Δ_k represent the amplitude and phase error, respectively, of the k^{th} complex weight. It is assumed that c_k and Δ_k are constant over the input signal bandwidth.

The weight vector is determined by solving the vector differential equation

$$\frac{dw(t)}{dt} = \alpha [R_{xd} - K_x \Omega w(t)] \quad (360)$$

which applies when α is small. Ω is an $m \times m$ diagonal matrix defined by

$$\Omega = \begin{bmatrix} c_1 e^{j\Delta_1} & 0 & \dots & 0 \\ 0 & c_2 e^{j\Delta_2} & \dots & 0 \\ \vdots & & & \vdots \\ 0 & 0 & & c_m e^{j\Delta_m} \end{bmatrix}$$

In general, the elements of Ω depend on the weight vector. Assuming this functional dependence is sufficiently "well-behaved," i.e., c_k and Δ_k are smooth functions of w , then the impact of Ω on the convergence properties of Equation (360) is minimal. Thus,

$$w(t) \Big|_{t \rightarrow \infty} = \Omega^{-1} K_x^{-1} R_{xd} \equiv \bar{w} \quad (361)$$

From Equation (359), the steady-state array output signal is expressed as

$$\begin{aligned} \tilde{y}(t) &= \sum_{k=1}^m \tilde{y}_{ek}(t) = \bar{w}^{\dagger} \tilde{\underline{x}}(t) \\ &= R_{xd}^{\dagger} K_x^{-1} \tilde{\underline{x}}(t) \\ &= w_{\text{opt}}^{\dagger} \tilde{\underline{x}}(t) \end{aligned} \quad (362)$$

which shows that the array output signal-to-noise ratio is unaffected by phase and amplitude imperfections in the weight multiplier circuits (of the type considered).

4. Weight Multiplier Feedthru

Feedthru is the amount of "leakage" between the weight multiplier IF input and IF output ports caused by circuit mismatches and stray capacitances. Its effects on performance may be determined using the model shown in Figure 5]. The complex-type scalars c_{k1} and c_{k2} are assumed constant for a given input signal $x_k(t)$. The output of the k th complex weight can be determined as follows:

$$\begin{aligned}\tilde{y}_k(t) &= w_k^* \tilde{x}_k(t) + (c_{k1} - j c_{k2}^*) \tilde{x}_k(t) \\ &= w_k^* \tilde{x}_k(t) + d_k^* \tilde{x}_k(t)\end{aligned}\quad (363)$$

where

$$d_k = c_{k1} + j c_{k2} \quad (364)$$

Summing the m complex weight outputs yields an expression for the array output

$$\tilde{y}(t) = \sum_{k=1}^m \tilde{y}_k(t) = \underline{w}^{\dagger} \underline{\tilde{x}}(t) = \underline{d}^{\dagger} \underline{\tilde{x}}(t) \quad (365)$$

where

$$\underline{d} = \begin{bmatrix} d_1 \\ d_2 \\ \vdots \\ d_m \end{bmatrix}$$

Thus, for small α ,

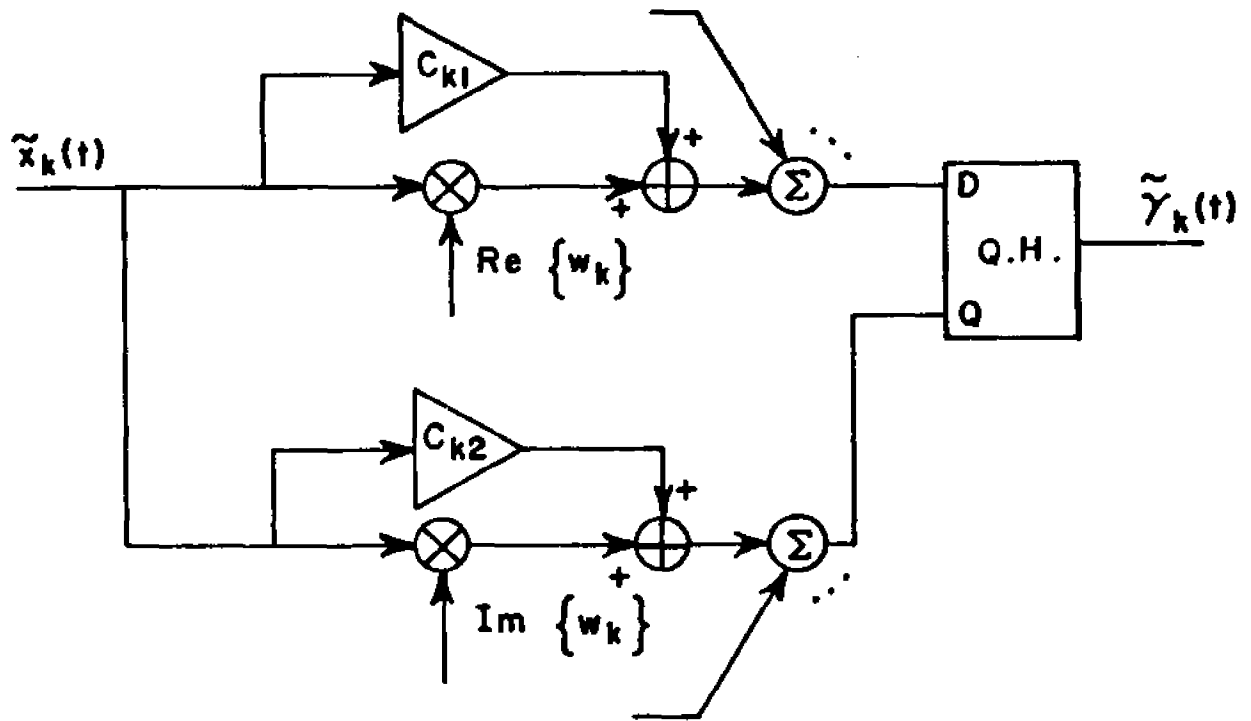


Figure 51--Weight control model with signal feedthru.

$$\frac{dw(t)}{dt} = \alpha(R_{xd} + K_x \underline{d} - K_x w(t)) \quad (366)$$

which converges to the solution

$$w(t)|_{t \rightarrow \infty} = K_x^{-1} R_{xd} + \underline{d} = w_{opt} + \underline{d} \quad (367)$$

The steady-state array output signal, obtained from Equations (365) and (367), is given by

$$\hat{y}(t) = w_{opt}^T \hat{x}(t) \quad (368)$$

Thus, feedthru biases the steady-state weight vector, but does not affect the output signal-to-noise ratio.

5. D.C. Offsets and Dynamic Range Considerations

Preceding results pertaining to array performance were obtained under the assumption that the feedback voltage is zero (on the average) when the output signal-to-noise ratio is optimum. In practice, however, this condition is not satisfied as a result of imperfections in the circuits used to implement the baseband processing functions. In particular, the 30 MHz IF to baseband downconverters, baseband amplifiers, and integrators are not ideal in practice and may be represented as having d.c. offsets at their outputs. To analyze the effects of this error, the loop gain α is separated into the product of the baseband loop gain and the IF loop gain as shown in Figure 52, where

$$\alpha = \beta_1 \beta_2 \beta_3 \beta_4 \quad (369)$$

where

$$\beta_1 = \text{integrator gain constant, (sec)}^{-1}$$

$$\beta_2 = \text{error multiplier gain constant, } \frac{\text{rms - volts}}{(\text{rms - volts})^2}$$

$\beta_3 = \text{IF voltage gain, } \frac{\text{rms - volts}}{\text{rms - volts}}$

$\beta_4 = \text{weight multiplier gain constant (rms - volts)}^{-1}$.

Offset in the i^{th} in-phase (quadrature) weight loop is modeled by adding a constant d.c. error voltage, d_{i1} (d_{i2}), to the base-band mixer output as shown in Figure 52. In this case, the weight equation reduces to*

$$\frac{d\bar{w}(t)}{dt} = \beta_2 R_{xd} - \beta_2 \beta_3 K_x \beta_1 \beta_4 \bar{w} - \underline{d} \quad (370)$$

where

$$\underline{d} = \begin{bmatrix} d_{11} + j d_{12} \\ d_{21} + j d_{22} \\ \vdots \\ d_{m1} + j d_{m2} \end{bmatrix}$$

Equation (370) has the steady-state solution

$$\bar{w}_{ss} \quad \bar{w}(t)|_{t \rightarrow \infty} = \frac{1}{\alpha} (\beta_2 K_x^{-1} R_{xd} - K_x^{-1} \underline{d}) \quad (372)$$

It is apparent from this result that the offset vector \underline{d} changes the cross-correlation vector from its ideal value.

To determine when the effects of d.c. offsets may be neglected, consider the component of \bar{w}_{ss} projected onto the n^{th} eigenvector of K_x :

$$y_{ss_n} = \frac{1}{\alpha \lambda_n} [\beta_2 (P R_{xd})_n - (P \underline{d})_n] \quad (373)$$

*Note that the coefficient of R_{xd} is not α for this case.

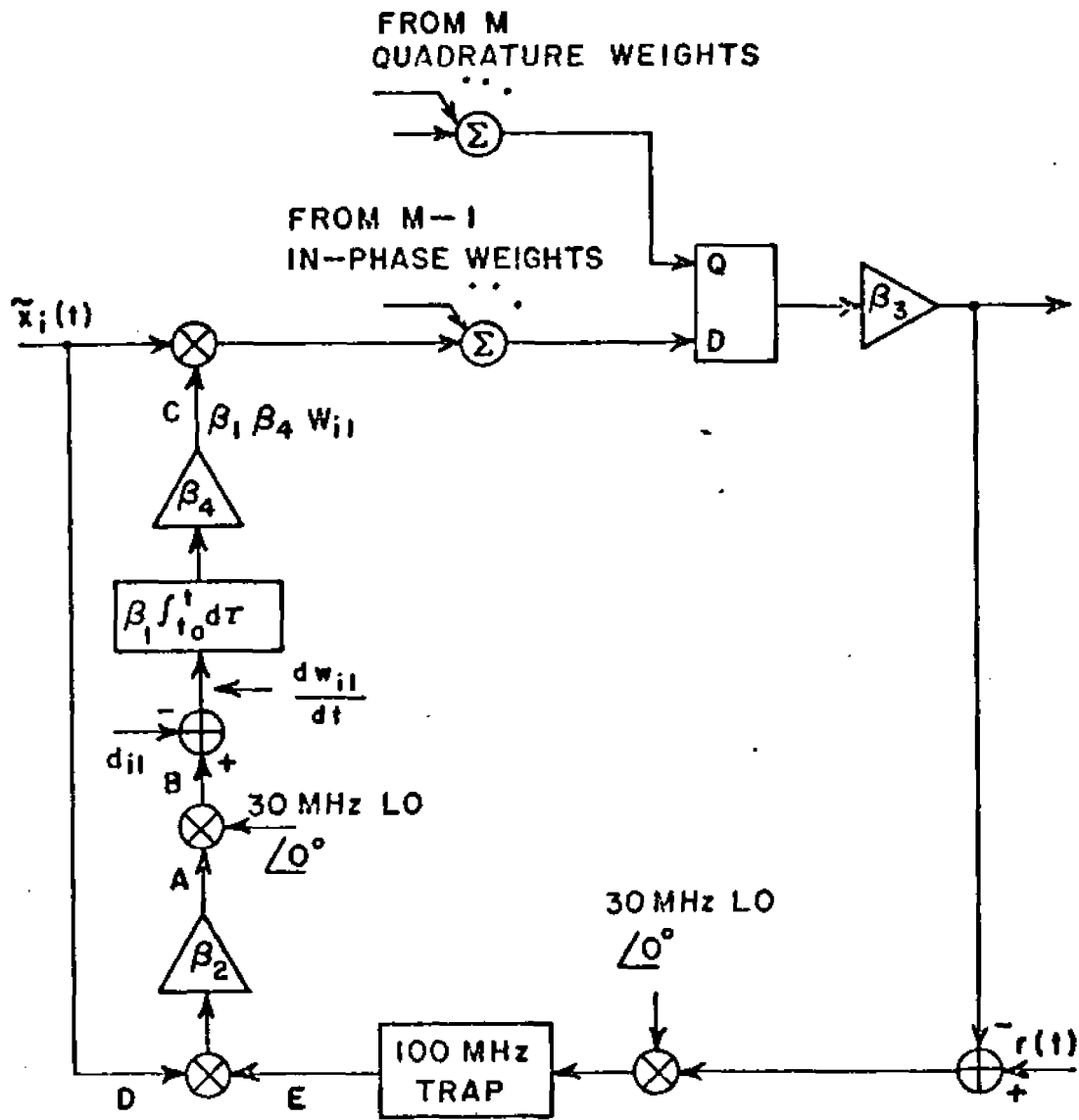


Figure 52--Adaptive processor model with control-loop d.c. offsets. $\alpha = \beta_1 \beta_2 \beta_3 \beta_4$.

The output desired signal power and output noise power are expressed in the eigenspace as

$$S_o = \frac{1}{\alpha^2} \left| \sum_{n=1}^m (P \underline{s})_n^* \frac{1}{\lambda_n} [\beta_2 (P R_{xd})_n - (P \underline{d})_n] \right|^2 \quad (374)$$

$$N_o = \frac{1}{\alpha^2} \sum_{n=1}^m \frac{1}{\lambda_n} |\beta_2 (P R_{xd})_n - (P \underline{d})_n|^2 \quad (375)$$

It is easily shown that S_o and N_o are bounded as follows:

$$S_o > \left[\sqrt{S_{o \text{ opt}}} - \frac{1}{\alpha} \left(\frac{T_o \underline{d}^{\dagger} \underline{d}}{\lambda_{\min} (1 + T_o)} \right)^{1/2} \right]^2 \quad (376)$$

$$N_o > \left[\sqrt{N_{o \text{ opt}}} + \frac{1}{\alpha} \left(\frac{\underline{d}^{\dagger} \underline{d}}{\lambda_{\min}} \right)^{1/2} \right]^2 \quad (377)$$

where

$$S_{o \text{ opt}} \equiv \underline{w}_{\text{opt}}^{\dagger} \underline{s} \underline{s}^{\dagger} \underline{w}_{\text{opt}} = \frac{\beta_2^2}{\alpha^2} |\tilde{r}|^2 \frac{T_o}{1 + T_o}^2$$

$$N_{o \text{ opt}} \equiv \underline{w}_{\text{opt}}^{\dagger} \underline{M} \underline{w}_{\text{opt}} = \frac{\beta_2^2}{\alpha^2} |\tilde{r}|^2 \frac{T_o}{(1 + T_o)^2}$$

$$\lambda_{\min} = \text{minimum eigenvalue* of } K_x \text{ (rms - volts)}^2$$

Consequently, d.c. offsets negligibly affect the output signal-to-noise ratio provided

$$\underline{d}^{\dagger} \underline{d} = \sum_{i=1}^m [|d_{i1}|^2 + |d_{i2}|^2] \ll \lambda_{\min} \beta_2^2 |\tilde{r}|^2 \frac{T_o}{(1 + T_o)^2} \quad (378)$$

*The minimum eigenvalue is equal to the per-element thermal noise power then the array is under-constrained ($p < m$).

Worst case degradation occurs when \underline{d} happens to align with an eigenvector associated with λ_{\min} . By proper assignment of values to the gain factor and the reference signal power, the relation in Equation (378) can be satisfied over the operating range of the input and output signal-to-noise ratios.

To minimize the effects of d.c. offset, system design should initially focus on maximizing the error multiplier gain (β_2). An upper limit on β_2 is imposed in practice by dynamic range limitations in the error multiplier circuits or in the i.f. circuits that follow it. Experimental results indicate that limiting during initial transients, when the error voltage is relatively large, does not adversely affect the convergence rate if the error multiplier is within its linear range when the weights approach their steady-state solution.* When the processor is near steady-state, the average power of the error signal is approximately $|\tilde{r}|^2 (1 + T_0)^{-1}$. Assuming that the maximum peak-to-peak voltage of the error signal is about four times its rms voltage, the maximum peak-to-peak voltage at point B of Figure 52 is approximated by (assuming linear circuit components)

$$\begin{aligned} v_e &\approx 8 \sqrt{\frac{P_I}{m} |\tilde{r}|^2 (1 + T_0)^{-1}} \\ &= 8 \sqrt{P_e |\tilde{r}|^2 (1 + T_0)^{-1}} \end{aligned} \quad (379)$$

where

$$P_e = \frac{P_I}{m} = \text{per-element input signal power (rms - volts)}^2.$$

Thus, linearity is maintained at point B if

$$\beta_2 \approx \frac{v_{e_{\max}}}{v_e} = \frac{1}{8} v_{e_{\max}} \sqrt{\frac{1 + T_0}{|\tilde{r}|^2 P_e}} \quad (380)$$

*Since stability of the LMS loop is phase sensitive, circuits in the feedback path should be designed to maintain a (nearly) constant insertion phase shift when they are driven into limiting.

where $v_{e_{\max}}$ denotes the upper bound on v_e required to maintain linearity.* Assuming Equation (378) is an equality, Equation (378) may be reexpressed as

$$\begin{aligned} \frac{d^+}{d} &<< \lambda_{\min} \beta_2^2 |\tilde{r}|^2 \frac{T_0}{(1+T_0)^2} \\ &= \frac{\lambda_{\min}}{64} \frac{(v_{e_{\max}})^2}{P_{e_{\max}}} \frac{T_0}{1+T_0} \end{aligned} \quad (381)$$

where $P_{e_{\max}}$ denotes the maximum input signal power.* It is apparent from this result that $v_{e_{\max}}$ and β_2 should be as large as possible to minimize the effects of a fixed d.c. offset. The final step in designing a system which minimizes the effects of d.c. offsets involves selecting the appropriate baseband components with d.c. offset characteristics that satisfy the above relation over the expected range of the system parameters λ_{\min} and T_0 .

The relation given in Equation (381) indicates that the effects of d.c. offset are (explicitly) independent of the gain parameters λ_1 , λ_3 , and λ_4 . The selection of λ_3 , however, is governed by other dynamic range considerations. In particular, it is known [15] that performance degrades severely when the weight multiplier circuits are overdriven by excessive input signal power, i.e., the output of each weight multiplier is limited to a certain maximum level. This restriction places a lower bound on λ_3 , since the processor must be capable of (approximately) matching the desired signal component of its output with the reference signal. More precisely,

$$w_{\text{opt}}^+ \tilde{s}(t) = \frac{T_0}{1+T_0} \tilde{r}(t) \quad (382)$$

*It is assumed that the D input (see Figure 52) of the error multiplier is not overdriven.

which implies

$$\beta_3 > |\tilde{r}| \sqrt{\frac{P_{e_{\max}} T_0}{2 \lambda_1 P_{w_{\max}} (1 + T_0)}} \quad (383)$$

where

$P_{w_{\max}}$ = maximum linear output power of each in-phase (or quadrature) weight multiplier (rms - volts)²

λ_1 = smallest non-thermal noise eigenvalue (rms - volts)²

Setting β_3 equal to the minimum in Equation (383) and employing the maximum in Equation (380) yields an expression for the loop gain constant in terms of circuit dynamic range characteristics:

$$\alpha = \frac{\beta_1 \beta_4}{8} v_{e_{\max}} \sqrt{\frac{2}{\lambda_1 P_{w_{\max}}}} \quad (384)$$

where an arbitrary value of 6 dB has been assigned to T_0 . This result shows that α can be selected by choosing an appropriate gain at baseband without effecting processor dynamic range characteristics.

The experimental array described in section B has the following parameter values* in the lower-rate format (LRF):

$$v_{e_{\max}} = 0.7 \quad (\text{p - p volts}) \quad (385)$$

$$P_{e_{\max}} = (m)^{-1} P_{I_{\max}} = 5.2 \times 10^{-2} \quad (\text{rms - volts})^2$$

$$P_{w_{\max}} = 4.5 \quad (\text{rms - volts})^2$$

$$\beta_1 = 1.6 \times 10^5 \quad (\text{sec})^{-1}$$

*Wide band amplifier setting is 50 dB.

$$\beta_2 = 8.52 \frac{\text{rms - volts}}{(\text{rms - volts})^2}$$

$$\beta_3 = 1.7 \frac{\text{rms - volts}}{\text{rms - volts}}$$

$$\beta_5 = 5 (\text{rms - volts})^{-1}$$

$$\alpha = 1.15 \times 10^7 (\text{sec}) (\text{rms - volts})^{-2}$$

$$|\hat{r}| = 0.071 (\text{rms - volts})$$

$$\left. \begin{aligned} |d_{ij}|^2 &\cong 15 \quad \mu\text{V}/^\circ\text{C} \\ \underline{d}^\dagger \underline{d} &= 1.8 \times 10^{-9} \quad [\mu\text{V}/^\circ\text{C}]^2 \end{aligned} \right\} \text{maximum}^*$$

Equation (378) is satisfied if

$$\lambda_{\min} \gg 5 \times 10^{-9} \frac{(1 + T_0)^2}{T_0} \left[\frac{\mu\text{V}}{^\circ\text{C}} \right]^2 \quad (386)$$

and Equation (383) is satisfied if

$$\lambda_1 > 1.0 \times 10^{-5} \frac{T_0}{1 + T_0} \quad (387)$$

Also, β_2 is related to the upper bound of Equation (380) by

$$\beta_2 \doteq \frac{0.2}{1 + T_0} v_{e_{\max}} \frac{(1 + T_0)}{|\hat{r}|^2 p_{e_{\max}}} \quad (388)$$

*Initial d.c. offsets are assumed nulled.

The bound on β_2 is satisfied if $T_0 \gtrsim 1.6$.

Experimental results indicate that d.c. offsets and circuit dynamic range limitations dominate departures from the ideal weight equation [Equation (62)] when the control loop bandwidth is smaller than the input signal and the input signals are narrowband with respect to the 10 MHz IF bandwidth. Thus, the relations in Equations (386) and (387) may be employed to determine the range of input and output parameters over which effective array operation can be expected. If the per-element input power equals $P_{e_{\max}}$ and if the ambient temperature is controlled to within about $\pm 2^\circ$, then the prototype array processor is capable of effectively processing in signal environments with the following properties:

$$T_0 = 1: \quad (389)$$

$$\frac{P_{e_{\max}}}{\lambda_{\min}} \approx 52 \text{ dB}$$

$$\frac{P_{e_{\max}}}{\lambda_1} \approx 42 \text{ dB}$$

$$\beta_2 \doteq 0.14 \text{ C}$$

$$T_0 = 4: \quad (390)$$

$$\frac{P_{e_{\max}}}{\lambda_{\min}} \approx 49 \text{ dB}$$

$$\frac{P_{e_{\max}}}{\lambda_1} \approx 38 \text{ dB} \quad (391)$$

$$\beta_2 \doteq 0.08 C$$

$$T_0 = 10:$$

$$\frac{P_{e_{\max}}}{\lambda_{\min}} \approx 48 \text{ dB}$$

$$\frac{P_{e_{\max}}}{1} \approx 38 \text{ dB}$$

$$\beta_2 \doteq 0.06C$$

where

$$C = v_{e_{\max}} \sqrt{\frac{1 + T_0}{r^2 P_{e_{\max}}}}$$

The bounds in Equations (386) and (387) were derived assuming a worst case signal environment and thus represent minimum capabilities. In particular, when the array is co-phased to desired signal and $T_0 = 4$, an input interference-to-desired signal power of 46 dB can be effectively processed.

The steady-state performance of the experimental adaptive array under high level cw interference conditions is illustrated by the photographs in Figure 53, which were obtained under the following conditions:

$$\frac{P_J}{P_S} = \text{input interference to desired signal ratio} = 43 \text{ dB}$$

$$\frac{P'_S}{\sigma^2} = \frac{P_S}{m\sigma^2} = \text{per element desired signal to thermal noise ratio} = 0 \text{ dB}$$

ψ = angular separation between the desired and interfering signals = 60° per element (electrical).

The interfering signal frequency was offset by 2 MHz from the array center frequency to make it easier to observe the null depth. Figure 53(a) shows the array output spectra before adaption, and Figures 53b, c and d show the spectra of the array output signal, reference signal, and error signal after adaption. The results show that the array completely nulls the interfering signal. The array also improves the output signal to thermal noise ratio, as evidenced by the fact that (1) the output signal level approximates the reference signal level and (2) the desired signal to thermal noise ratio is much higher at the array output (Figure 53b) compared to the error monitor output (Figure 53d). That is, the array has simultaneously formed a beam on the desired signal and nulled an interfering signal 43 dB higher in level.

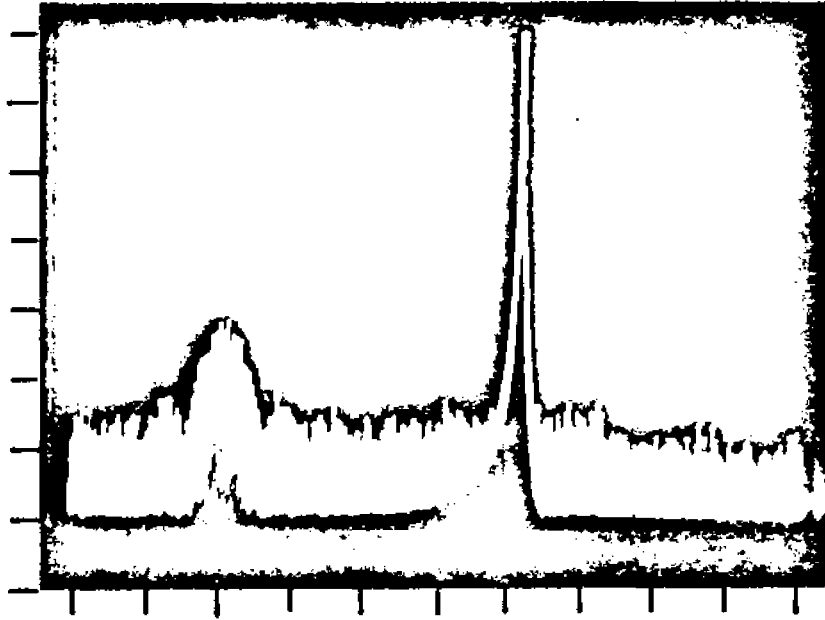
The ratios in Equations (389) and (391) are related to the following system parameters which are easily modified in the present implementation:

$$\lambda_1^{-1} P_{e_{\max}} \sim \begin{cases} \frac{1}{|\tilde{r}|^2} \\ \beta_3^2 \end{cases} \quad (392)$$

$$\lambda_{\min}^{-1} P_{e_{\max}} \sim \begin{cases} \beta_2^2 \\ |\tilde{r}|^2 \\ (\Delta T)^{-2} \end{cases}$$

where

ΔT = maximum change in ambient temperature after d.c. offsets have been nulled.

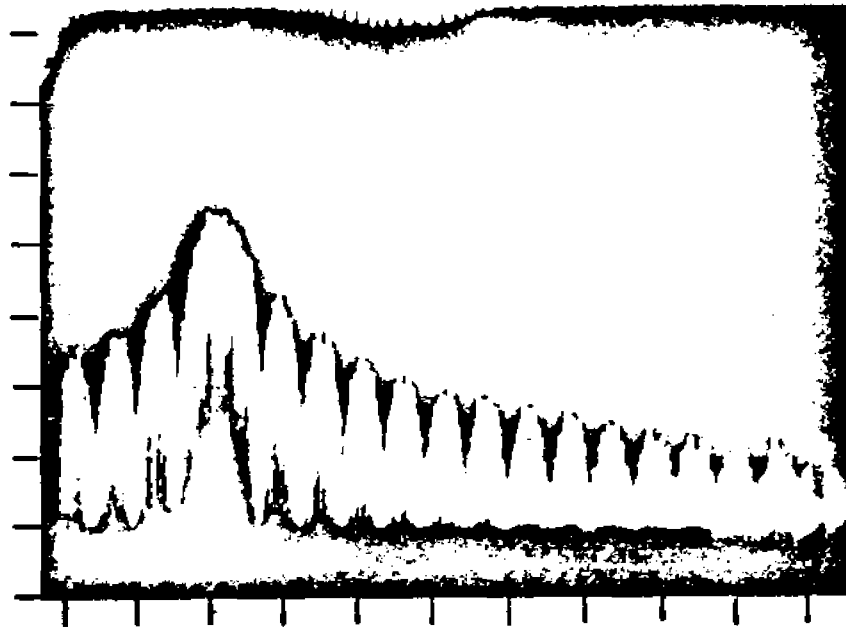


(a) Array output with initial conditions set.

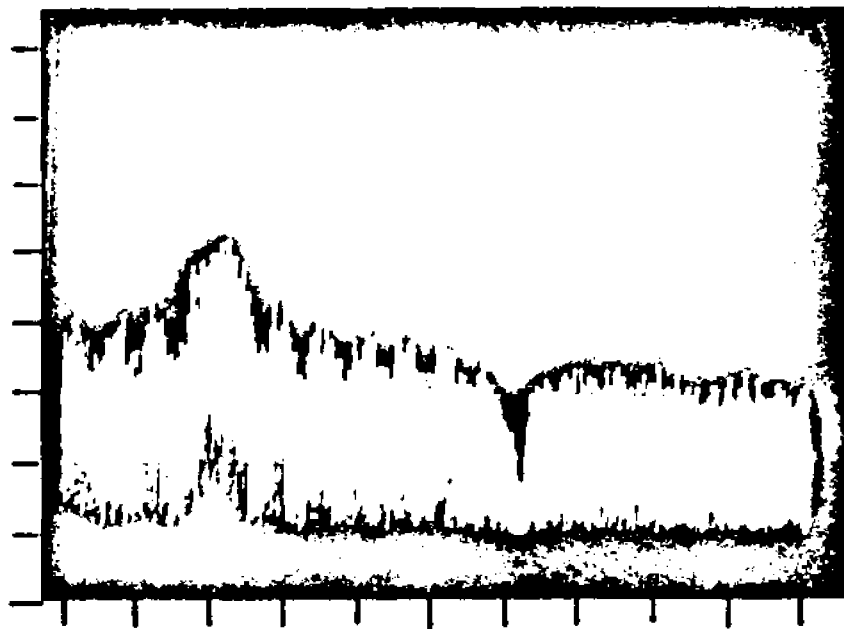


(b) Array output after adaption.

Figure 53--Signal spectra within the LMS control loop.
 $P_j/P_S = 43$ dB; $P_S/\sigma^2 = 0$ dB. Horizontal:
 500 KHz/cm. Vertical: 10 dB/cm.



(c) Reference signal after adaption.



(d) Error signal after adaption.

Figure 53--(cont.)

It is thus possible to optimize the dynamic range by appropriately selecting (or controlling) these parameters. For example, if these parameters are modified as follows,

<u>Parameter Value</u>	<u>Change</u>	(393)
$\beta_3 = 5.287$	+ 10 dB	
$\beta_2 = 27.0$	+ 10 dB	
$ \tilde{r} = 0.018$	- 12 dB	
$(\Delta T) \approx 1^\circ\text{C}$	-12 dB	

then, for $T_0 = 4$ (numeric),

$$\frac{P_{e_{\max}}}{\lambda_{\min}} \approx 59 \text{ dB} \quad (394)$$

$$\frac{P_{e_{\max}}}{\lambda_1} \approx 60 \text{ dB}$$

$$\beta_2 = 0.25 \text{ C} \quad .$$

Note that some clipping in the error multiplier (or i.f. circuits following the error multiplier) may occur for this value of β_2 .

6. The Effects of Higher Order Poles in the Feedback Loop

Ideally, circuits used to implement the LMS control loop would have wide bandwidth and wide dynamic range characteristics. In practice, bandlimited circuits normally result in greater cost effectiveness and improved dynamic range. Moreover, filters are required in the present implementation (see Figure 38) to remove unwanted sidebands generated by the up/down conversions within the loop. The purpose of this section is to determine the effects of narrowband circuit elements on LMS algorithm performance.

Generally, the most stringent dynamic range requirements occur in the weight and error multipliers. In applications which require full dynamic range capabilities, the inputs and outputs of each of these stages should be "tuned" to minimize thermal and stray signal noise which could adversely affect processor performance. As outlined in section 2, delays introduced by these filters should be small relative to the control loop bandwidth and should be accurately matched over the input signal bandwidth. The need for filtering at the input of these devices is alleviated to a certain extent in the present implementation since dynamic range requirements are well within the capabilities of these circuits; thus, input filters were omitted.

Finite component bandwidths are a second source for higher order poles in the feedback loop. In particular, baseband components which must meet wide bandwidth as well as low d.c. drift and high gain requirements can be more costly. Criteria for determining d.c. offset and gain requirements were presented in section 5. Bandwidth requirements will be determined by modeling the feedback loop as shown in Figure 54. Assume the low-pass filter has the following transfer function:

$$G = \frac{a b}{(s + a)(s + b)} \quad (395)$$

The weight equation for this case becomes

$$\begin{aligned} \overset{\cdot\cdot\cdot}{w}(t) &= (a + b) \overset{\cdot\cdot}{w}(t) + a b \overset{\cdot}{w}(t) \\ &= \alpha a b \tilde{x}(t) [\tilde{r}^+(t) - \tilde{x}^+(t) w(t)] \end{aligned} \quad (396)$$

where

$$\overset{\cdot\cdot\cdot}{w}(t) = \frac{d^3 w(t)}{dt^3}, \quad \text{etc.}$$

Taking the ensemble average, Equation (396) reduces to

$$\overset{\cdot\cdot\cdot}{w}(t) + (a + b) \overset{\cdot\cdot}{w}(t) + a b \overset{\cdot}{w}(t) = \alpha a b [R_{xd} - K_x \bar{w}(t)] \quad (397)$$

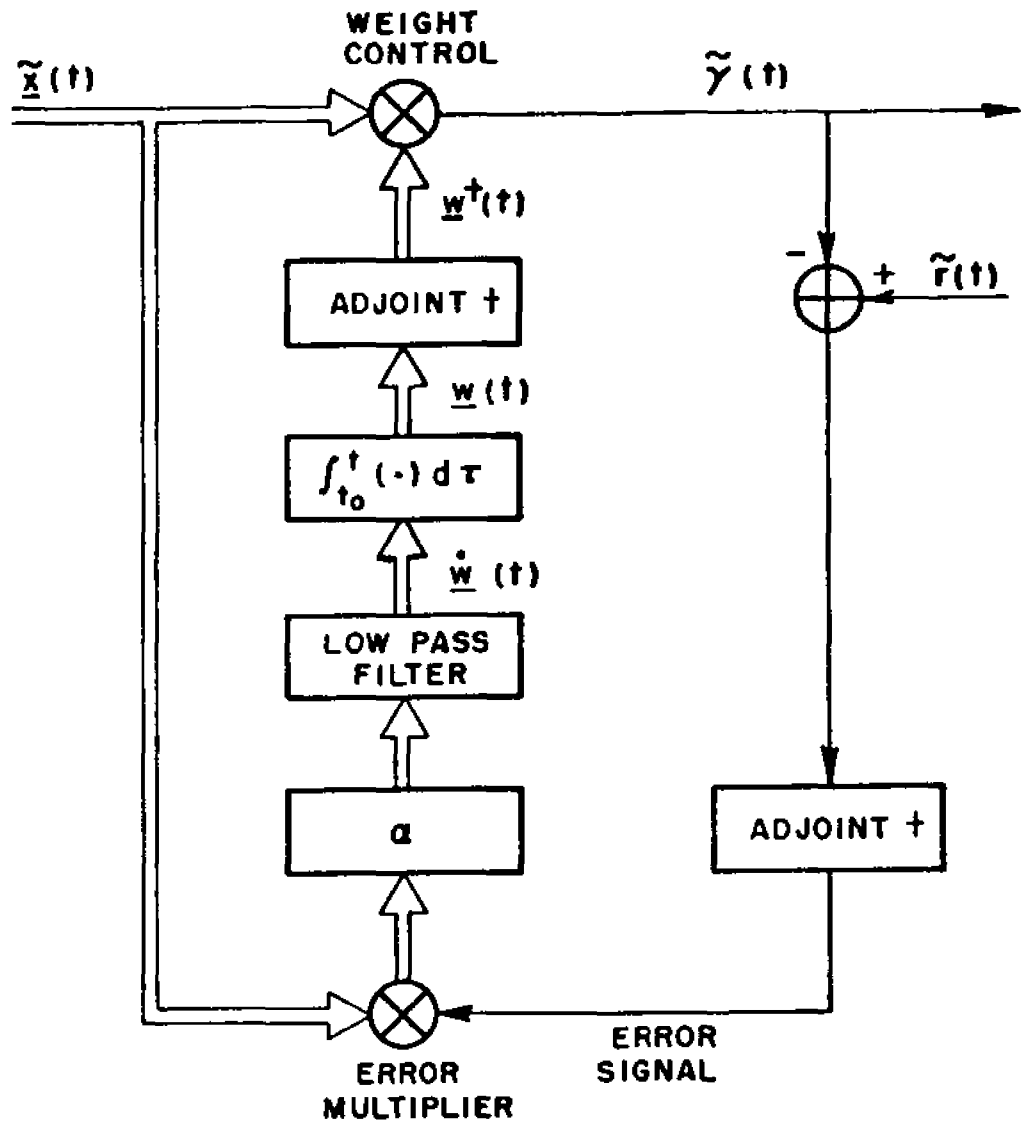


Figure 54--Adaptive processor model with a low-pass filter in the feedback loop.

The component of $\bar{w}(t)$ projected onto the n^{th} eigenvalue is thus described by the equation

$$\begin{aligned} \ddot{y}_n(t) + (a + b) \dot{y}_n(t) + a b y_n(t) + \alpha a b \lambda_n y_n(t) & \quad (398) \\ = \alpha a b (P R_{xd})_n & \quad ; \quad n = 1, 2, \dots, m \end{aligned}$$

By the Routh stability criterion, $y_n(t)$ converges to a finite value if

$$\alpha \lambda_n < a + b \quad (399)$$

The LMS control loop is therefore stable if the above inequality is satisfied for all values of λ_n . Note that well-behaved response normally requires $\alpha \lambda_n < \frac{1}{2}(a + b)$.

Next, suppose that

$$a \gg \alpha \lambda_n \quad (400)$$

In this case, G in Equation (395) represents the transfer function of a single pole low-pass filter and the solution to Equation (398) is approximated by

$$y_n(t) = \frac{(1 - c_n) \left[\frac{(P R_{xd})_n}{\lambda_n} - y_n(t_0) \right]}{2 c_n} \quad (401)$$

$$\cdot \begin{bmatrix} e^{-m_2(t - t_0)} & -e^{-m_1(t - t_0)} \end{bmatrix}$$

$$+ \frac{(P R_{xd})_n}{\lambda_n} \left[1 - e^{-m_1(t - t_0)} \right] + y_n(t_0)$$

$$\cdot e^{-m_1(t - t_0)} \quad ; \quad \dot{y}_n(t_0) = 0$$

where

$$C_n = \sqrt{1 - \frac{4\alpha \lambda_n}{b}}$$

$$m_{1,2n} = -\frac{b}{2} (1 \pm C_n)$$

Figure 55(a) illustrates the dependence of $m_{1,2n}$ on the low-pass filter cutoff frequency (b) and Figure 55(b) illustrates the dependence of $m_{1,2}$ on $\alpha\lambda_n$. If $\alpha\lambda_n \leq b/4$, then the magnitudes of m_{1n} and m_{2n} are greater than $\alpha\lambda_n$, whereas if $\alpha\lambda_n > b/4$, the low-pass filter causes the array to respond more slowly. On the surface, this result seems to imply that α can be increased by a factor of $(\lambda_{\max} b)^{-1}$ to equalize the minimum time constant to the minimum time constant of the ideal LMS algorithm, thereby increasing response time to smaller eigenvalues. However, a detailed analysis has shown that the low-pass filter does not reduce excess noise due to weight jitter for a given set of loop parameters α , Δt , and P_1 . As a result, a single pole low-pass filter can be used to improve the convergence rate by most a factor of two. Further, this improvement can only be realized by selecting $b = 4\alpha \lambda_g$, where λ_g represents the smallest eigenvalue of interest. In general, low-pass filtering should not be employed to obtain improved response to small eigenvalues for the following reasons: (1) the resulting improvement in the convergence rate is relatively small, (2) the required 2 m low-pass filters add to system cost, and (3) excessive "ringing" is induced in the response to large eigenvalues. Also, Equation (401) was derived under the assumption that a is very large and that feedback delay is negligible. Since these two requirements are difficult to achieve in wide-band systems, the addition of a single pole low-pass filter may well cause instability.

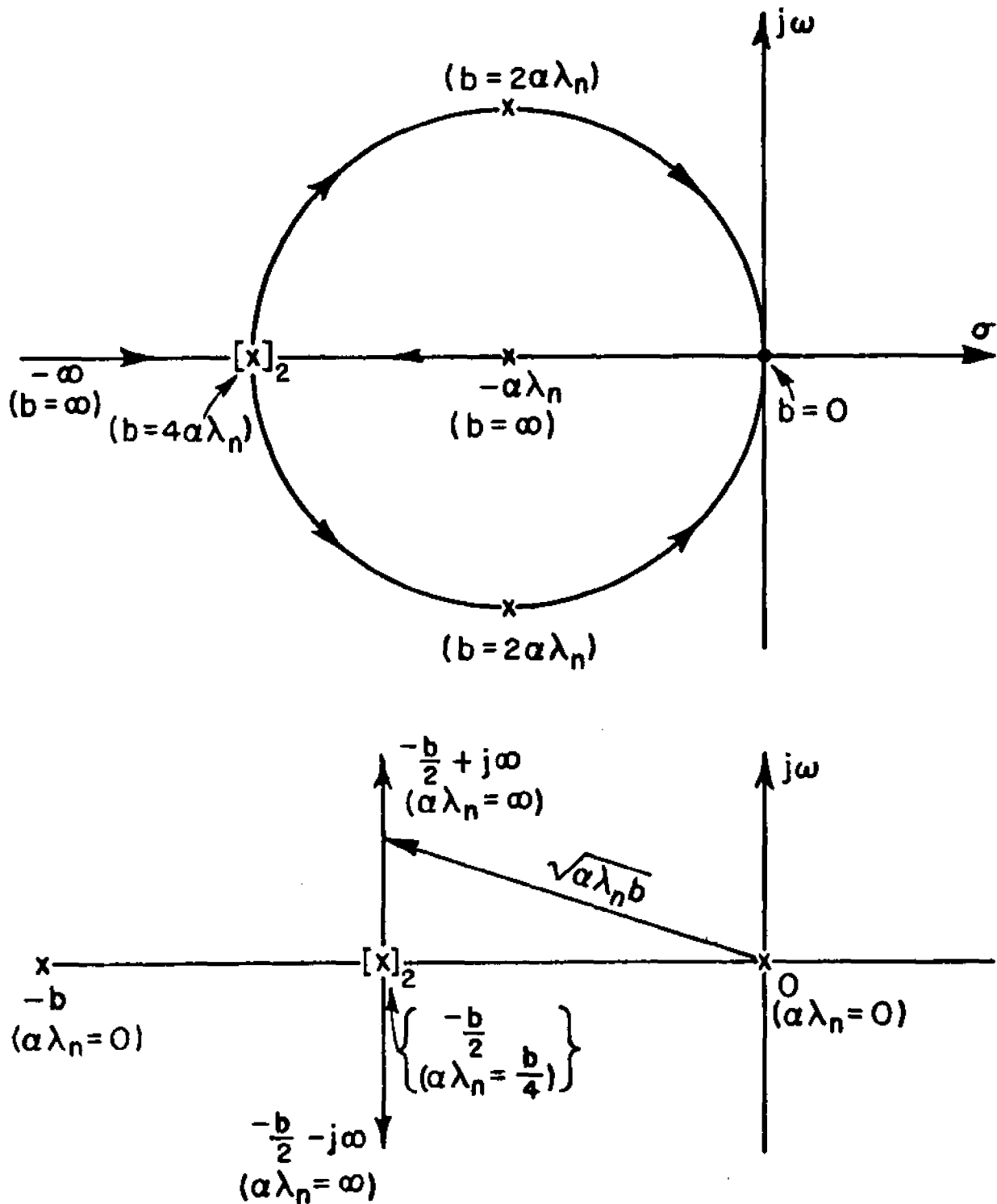


Figure 55--The effect of the low-pass filter cutoff frequency on the poles of the feedback loop.

D. Experimental Performance with a Constant Envelope Signal

1. Introduction

Measurements in this section illustrate basic performance of the system in Figure 35 when the TDMA modem was configured to transmit a PN coded desired signal on a continuous basis. Random data were added to the desired signal during the assigned overhead and data slots. In the following sub-section, the interference protection afforded by waveform processing is evaluated in terms of the measured BEP. In subsequent sub-sections, measurements were performed to evaluate SS/TDMA performance when the mean weights were in the steady-state condition. The steady-state condition was established by allowing the ASP to adapt continuously (except during the reference delay interval) in a stationary environment. The results presented in sub-section 3 show measured performance when the effects of weight jitter were negligible, i.e., when the loop response time was slow with respect to the code rate. The results in sub-section 4 were obtained under higher loop gain conditions, and thus exhibit the effects of weight jitter on system performance.

2. Waveform Processing Gain

The measurements discussed in this section were obtained with the ASP operating in the initial conditions set mode (i.e., constant weight control voltages). In this mode, the array acts simply as a fixed transmission path for input sources of desired signal, interference, and thermal noise. The measurements in Figure 56 indicate the interference immunity afforded by waveform processing at the differential detector. With all but one of the weight control voltages set equal to zero, a fixed level of desired signal and thermal noise and a variable level cw interfering signal was applied to the array input. The input desired signal to thermal noise ratio was set equal to 6 dB and the post-limiter attenuator was fixed at a value corresponding to a detector input energy-to-noise density, E_b/N_0 , of approximately 10.3 dB and a measured BEP of 2.95×10^{-5} (4.3×10^{-5} when the desired signal was quadrature modulated) in the absence of interference. Because the thermal noise bandwidth (8 MHz doubled-sided) was much larger than the data rate, its spectral density was about 15 dB smaller than the spectral density of noise added to the limiter output; therefore its only significant effect on the measurements was to slightly suppress the desired signal power at the bandpass limiter's output. The thermal noise was added to facilitate a comparison between waveform processing gain and adaptive array processing gain in subsequent results to be presented. Three sets of data points are shown in Figure 56.

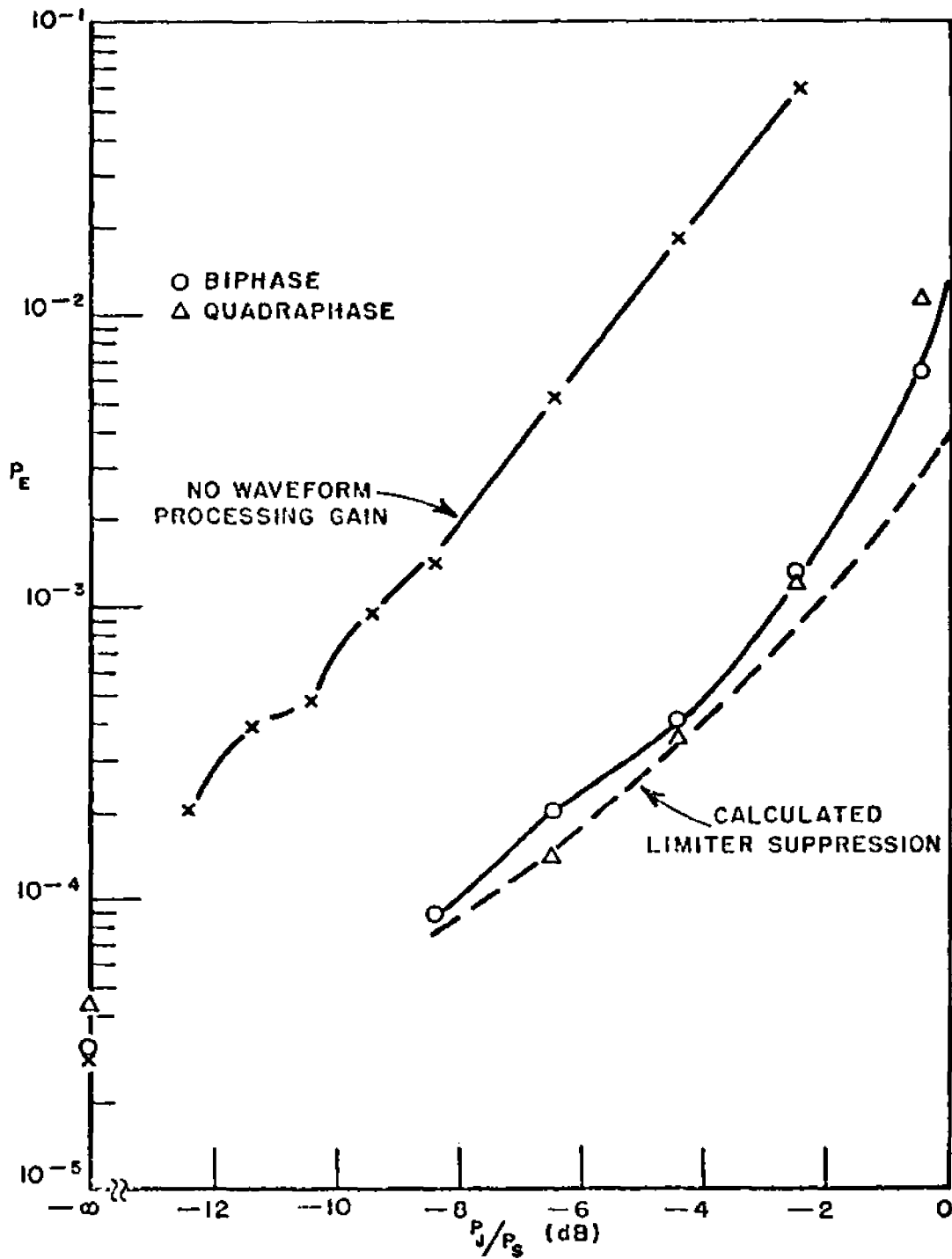


Figure 56--Measurements showing the interference protection afforded by waveform processing at the differential detector for a bandspreading ratio of 16:1. The horizontal scale represents the interference-to-desired signal ratio at the input to the bandpass limiter. Desired signal carrier frequency = 70 MHz. C.W. interference frequency = 70 MHz + 100 Hz.

The set exhibiting the highest measured BEPs represent DPSK detector performance as a function of the input interference to desired signal ratio when the interfering signal was biphase modulated by the same PN code as the desired signal, i.e., the measurements indicate performance without waveform processing gain. The data labelled "biphase" gives performance when the code modulation was removed from the interfering signal. A comparison of these two results indicates that a band-spreading ratio 16 provides only about 5.5 dB of interference protection (the horizontal separation). This amount of waveform processing gain is clearly inadequate when interference to signal ratios of 20 dB to 30 dB are considered since the BEP increased nearly three orders of magnitude as the input ratio was increased to unity (0 dB). It is important to note that the waveform processing gain to cw interference shown in Figure 56 is one factor that determines the closest angular separation between the interfering signal and the desired signal in a given application (e.g., [15]). The reason for this is that the output desired signal to interfering signal ratio of the optimum spatial filter increases as the angular separation decreases. For example, the ratio is as low as -1 dB for the very close angular separation (ψ) of 10° per element when $P_S'/\sigma^2 = 0$ and $P_J/\sigma^2 \approx 7$ dB. (This ratio increases proportionately with P_S'/σ^2). The measured BEP would be very high (above 10^{-2}) in this case regardless of the level of down-link noise added.

In order to minimize this effect, $\psi \geq 30^\circ$ and $P_S'/\sigma^2 \geq 0$ dB in most results to be presented; in this case, the minimum output desired signal to interfering signal ratio of the optimum spatial filter was greater than 8.3 dB regardless of the input interference to desired signal ratio. This minimum occurs for $\psi=30^\circ$ and $P_S'/\sigma^2=0$ dB when $P_J/P_S \approx 0$ dB. For $P_J/P_S=12$ dB, the output desired signal to interference ratio increases to 15 dB due to the power inversion characteristic of the optimum filter. At these relatively low levels of output cw interference, the BEP can be related to the array output SNR with adequate accuracy using the limiter suppression characteristic in Figure 44. A discussion and experimental investigation of performance for closer angular separations was conducted earlier on a similar adaptive array implementation [15]. The interference immunity afforded by quadrature modulation is also shown in Figure 56. The results show that quadrature modulation did not significantly improve performance compared to biphase modulation. The additional expense of utilizing quadrature coded signals for the purpose of providing additional immunity to interference therefore appears unwarranted.

For the purposes of comparison with adaptive array performance presented in later sections, BEP measurements were also conducted using a moderate bandwidth (563 KHz doubled-sided) interfering signal. All other conditions were approximately the same as in the c.w. interference measurements presented in Figure 56.

The predominant source of degradation in the wide-band case, shown in Figure 57, was due to limiter suppression, since the spectral density of the interfering signal was small relative to the spectral density of the post-limiter additive noise. However, the extent of degradation is smaller than that predicted from the limiter suppression characteristic of Figure 44. This difference is apparently due to the fact that the interference was much narrower band relative to the thermal noise bandwidth.

3. Performance with Small Loop Gain

Measurements in this section illustrate the basic performance of the system of Figure 35 when the mean weights are near their steady-state solution and the effects of weight jitter are negligible. The first set of measurements, shown in Figures 58-60, illustrate system performance in the LRF and HRF modes of operation when the input desired signal to thermal noise ratio was 0 dB and no directional interference sources were present. The measured BEP is shown as a function of the (data) bit-energy-to-noise density ratio, which was varied by incrementing the post-limiter attenuator and holding the additive noise level constant. For the purposes of comparison, ideal DPSK detector performance is also shown. Results in Figure 58 were obtained in the LRF mode with the range tracking loop disabled and with zero timing error between the transmit time base and the NCS, and results in Figure 59 were obtained under the same conditions except the range tracking loop was enabled. These two sets of results show that adding quadrature modulation caused a slight increase in the BEP relative to the biphase case. The data closest to the ideal curve in Figures 58 and 59 were taken from the results* in Figure 46 to illustrate relative performance with and without the satellite simulator within the transmission path. Within the range that comparative data were available, these results show that introduction of the satellite simulator was the system caused only a slight increase in the BEP. Figure 60 shows BEP performance in the HRF mode when biphase code modulation was employed -- both with and without the range tracking loop enabled.

*Note that the comparative data apply only to the case where biphase code modulation is employed.

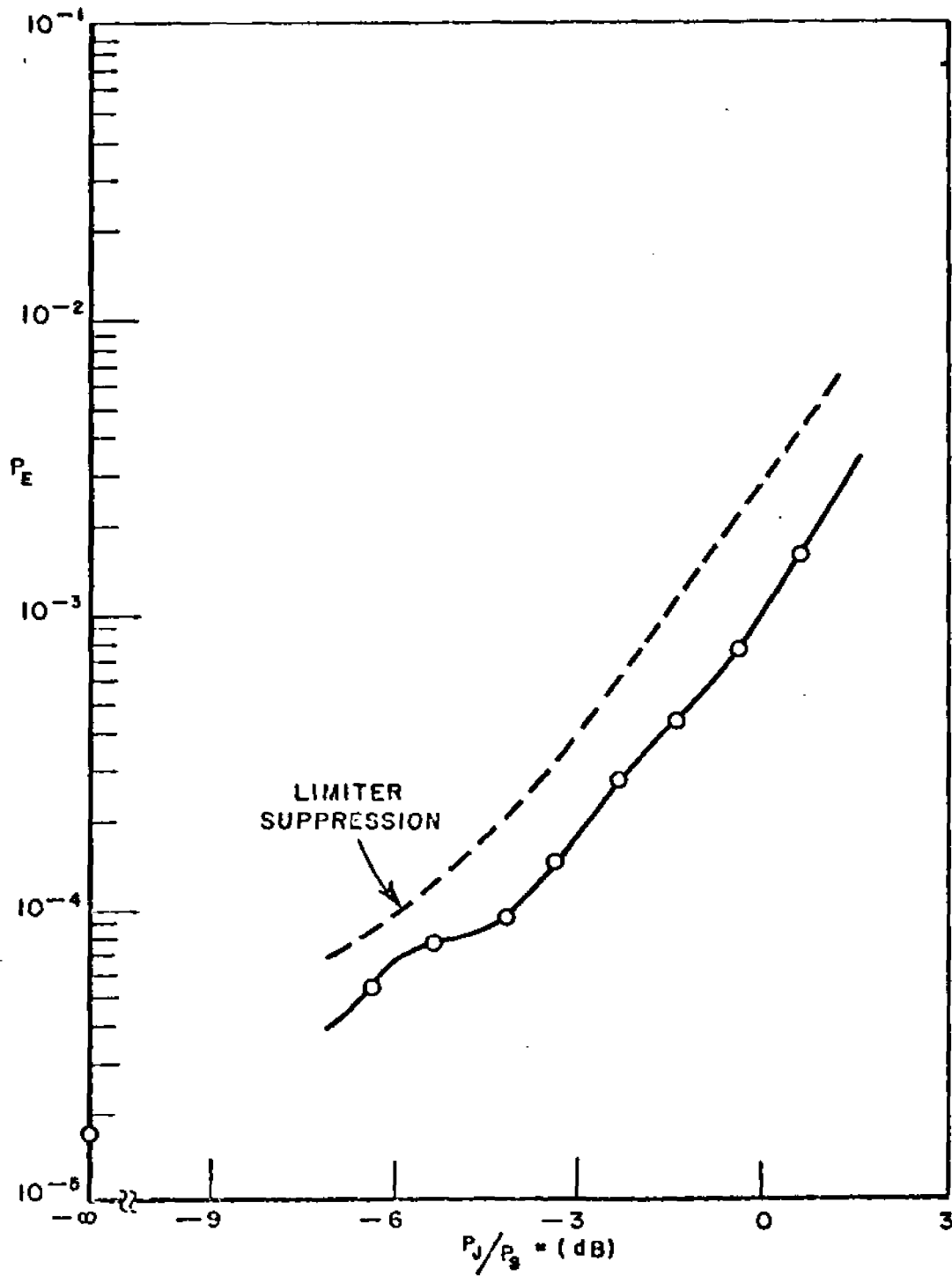


Figure 57--The bit error probability versus the interference-to-desired signal ratio at the input to the band-pass limiter with wideband interference. Interfering signal bandwidth = 560 KHz. Biphase code rate = 175.2 Kbps.

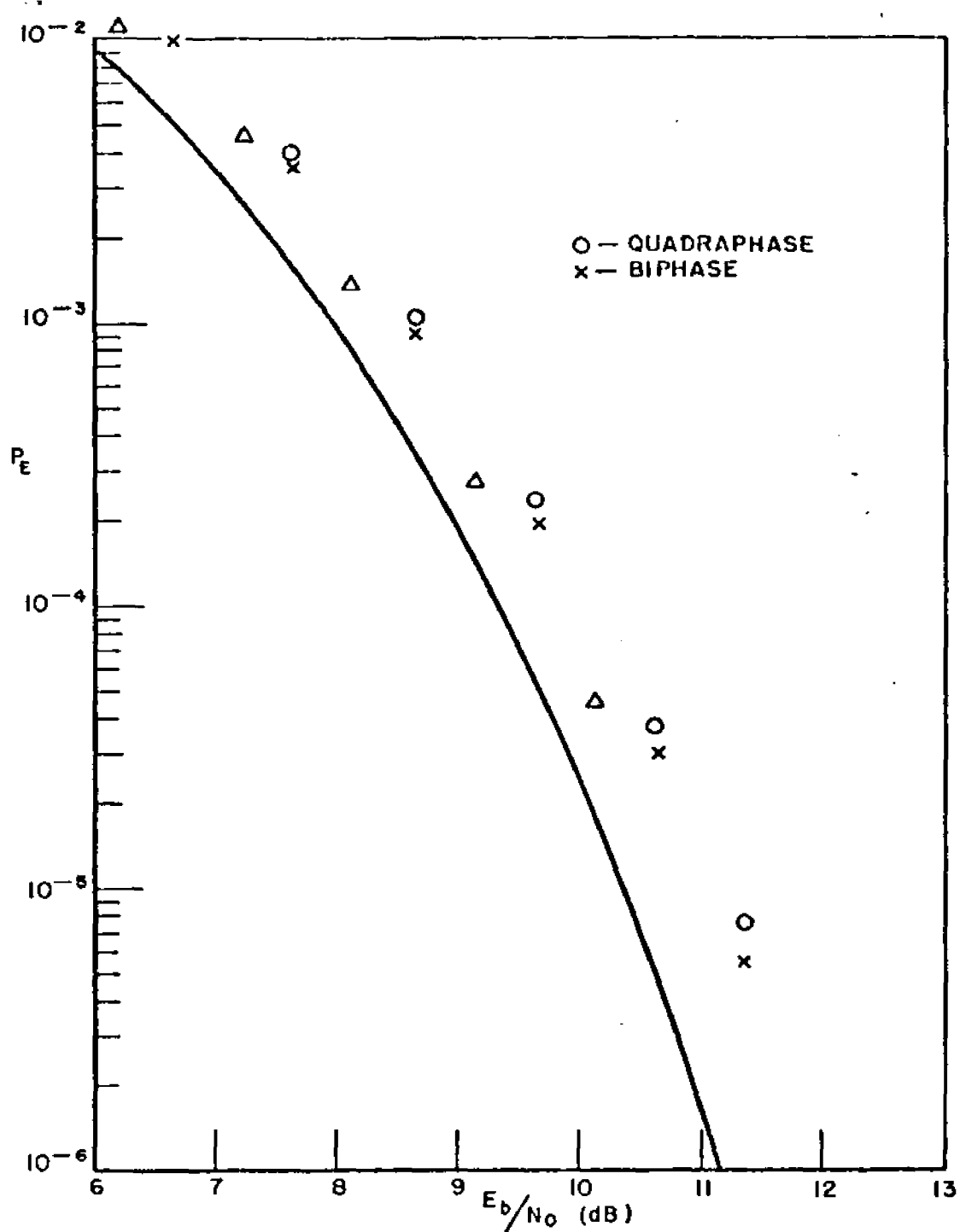


Figure 58--Performance of the experimental system versus the bit energy-to-noise density ratio at the detector input using quadrature and biphase modulation. LRF; $P_S/\sigma^2 = 0$ dB; array adapting. The timing error between the desired signal and the reference signal was set equal to zero.

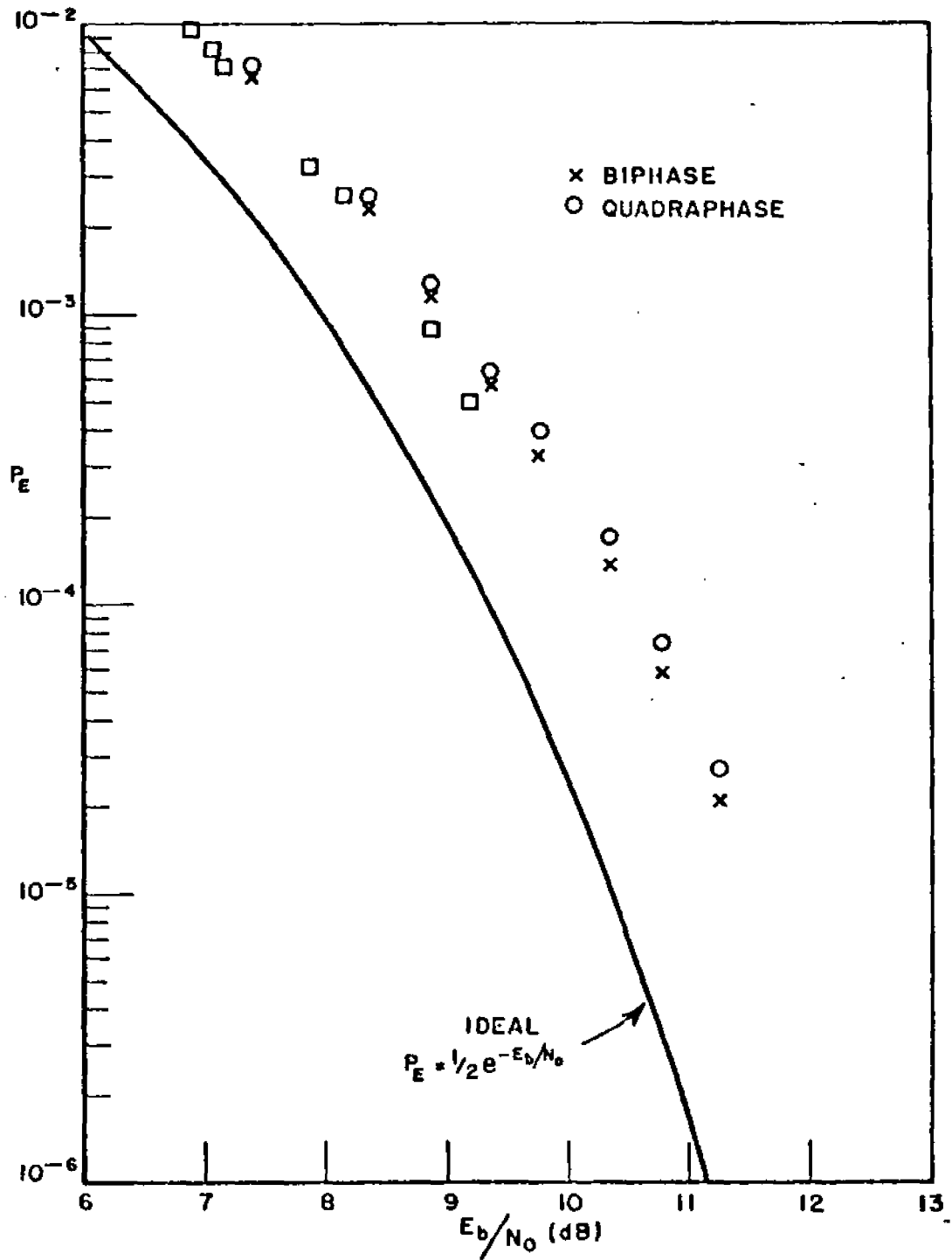


Figure 59--Performance of the experimental system versus the bit energy-to-noise density ratio using the range tracking loop to synchronize the transmit time base. Other conditions as in Figure 58.

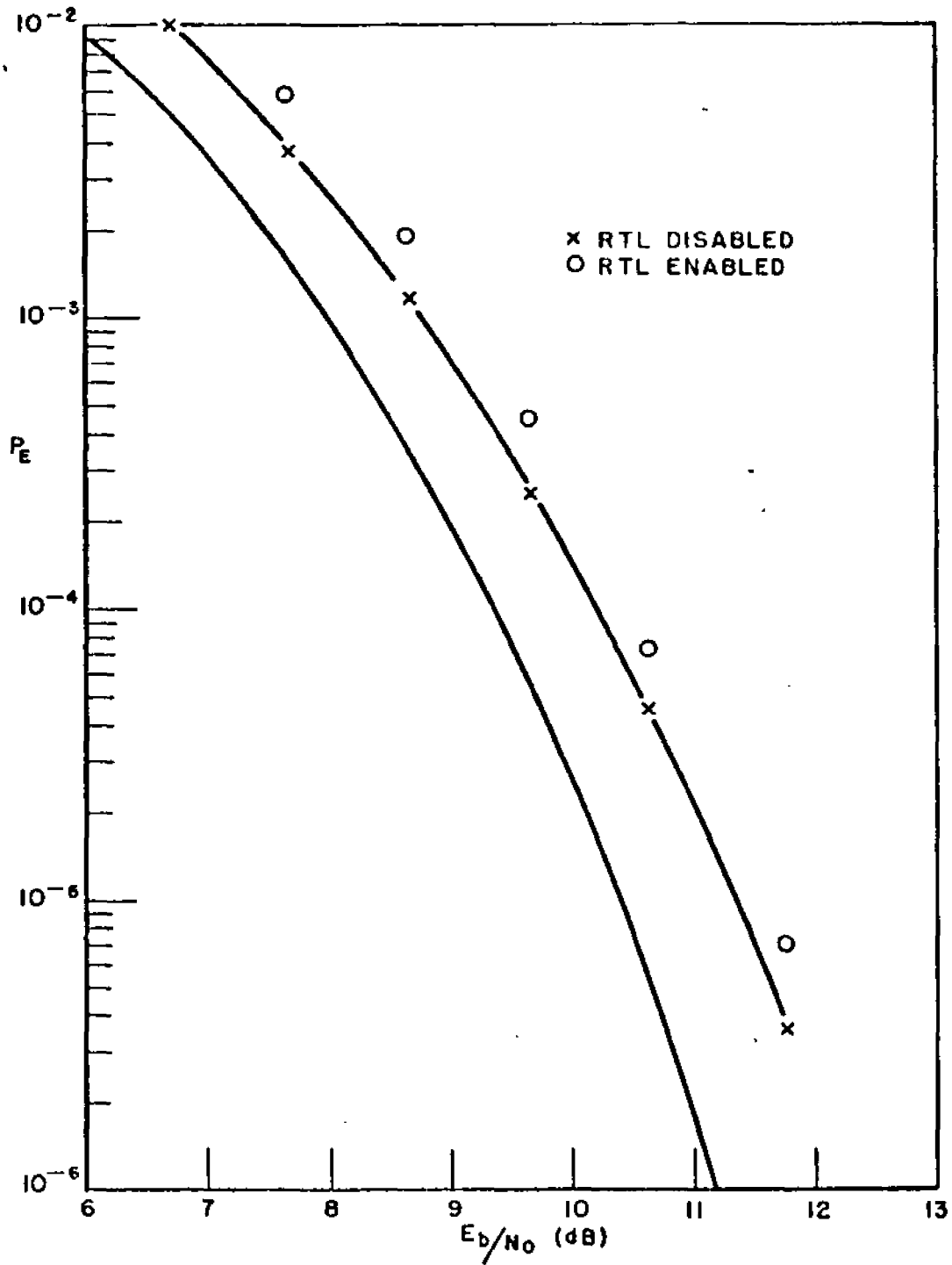


Figure 60--Performance of the experimental system versus the bit energy-to-noise density ratio in the HRF. The desired signal was biphas modulated.

The next set of measurements in Figures 61 and 62 illustrate adaptive array performance under cw interference conditions. In these measurements, the timing error between the desired signal and the waveform processed reference signal was set equal to zero (i.e., the RTL was disabled). BEP performance with the RTL enabled was not significantly different from the results presented for $\psi = 15^\circ$ in Figure 62, however, the output SNR was insufficient for acquiring and maintaining transmit time base synchronization. As to be discussed later in this section, the inability to acquire synchronization was not related to a basic limitation on the capability of the SDDL, but was related to the specific selection of parameters used at the modem for verifying transmit time base synchronization -- these parameters could easily be modified to permit operation at lower signal to noise ratios if so desired. The BEP measurements in Figure 61 and 62 were obtained by varying the level of cw interference at the input to the processor while holding the input desired signal to thermal noise ratio fixed at 0 dB per element. The 70.0001 MHz cw signal source was used to generate the interfering source, and biphase PN code modulation was used to spread the spectrum of the desired signal. The post-limiter attenuator was adjusted so that the BEP, measured in the absence of interference and with the array adapting, was approximately 1×10^{-4} . The solid curves drawn in each figure represent calculated bit error probabilities determined from BEP measurements in Figures 58 and 60 and by taking into account the limiter suppression factor (see Figure 44). To perform this calculation, thermal noise and interference were removed (i.e., no limiter suppression) and the bit energy to noise density at the detector input was measured. The signal was then removed and thermal noise was added. In the HRF (Figure 62), the spectral density of noise components at the bandpass limiter's output was about 8.6 dB smaller than the spectral density of the simulated down-link noise when the limiter input was thermal noise only. Thus, the energy to noise density at the detector input was approximated by

$$\frac{E_b}{N_o} = 11.7 \frac{\xi^2}{1 + \frac{(1 + \xi^2)}{7.24}} \quad (402)$$

where ξ is the limiter suppression factor.

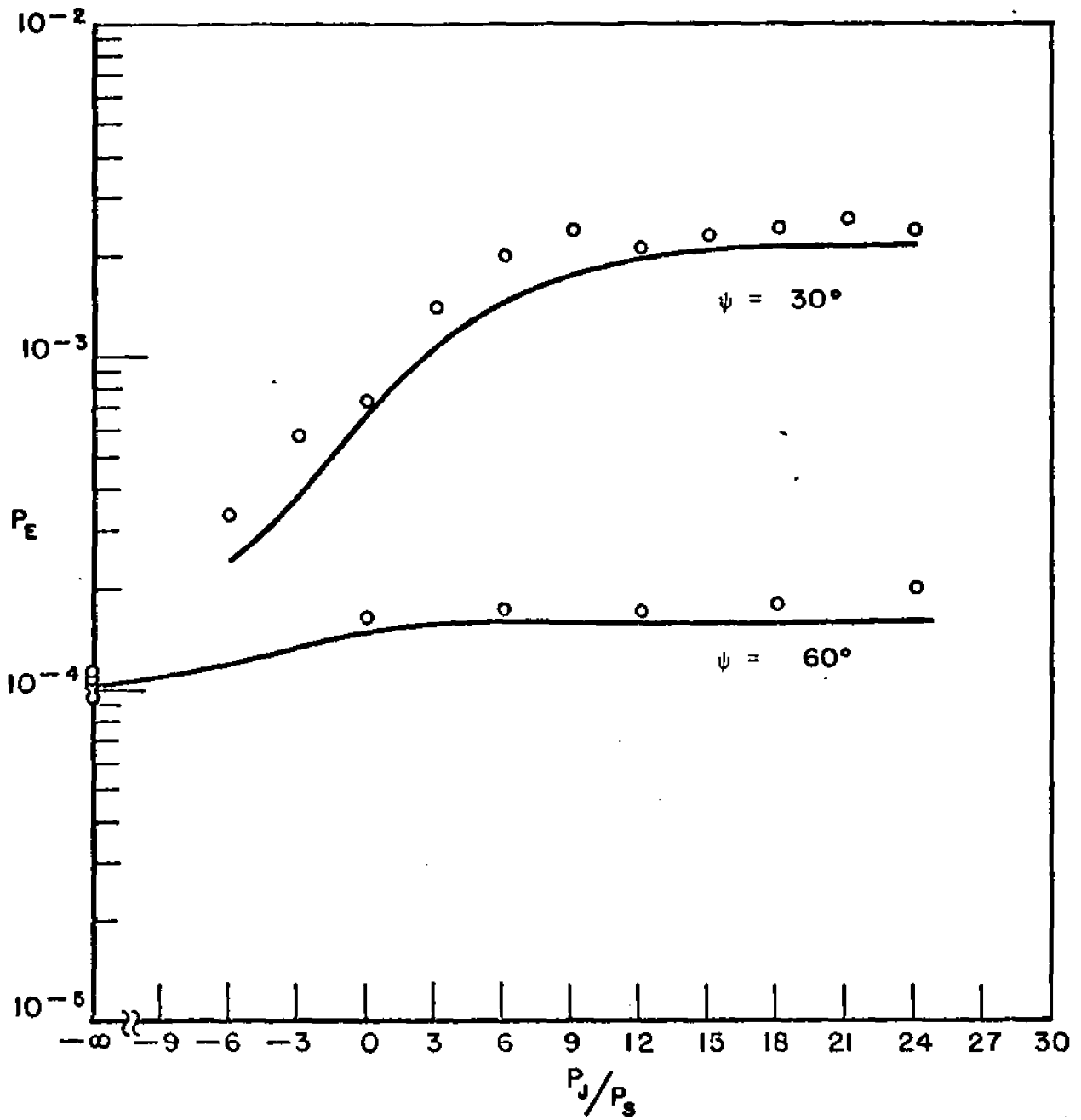


Figure 61--Performance of the experimental system versus the input interference-to-signal ratio for two values of the separation parameter ψ . C.W. interference frequency = 70 MHz + 100 Hz; LRF; transmit time base error = 0; $P_S'/\sigma^2 = 0$ dB.

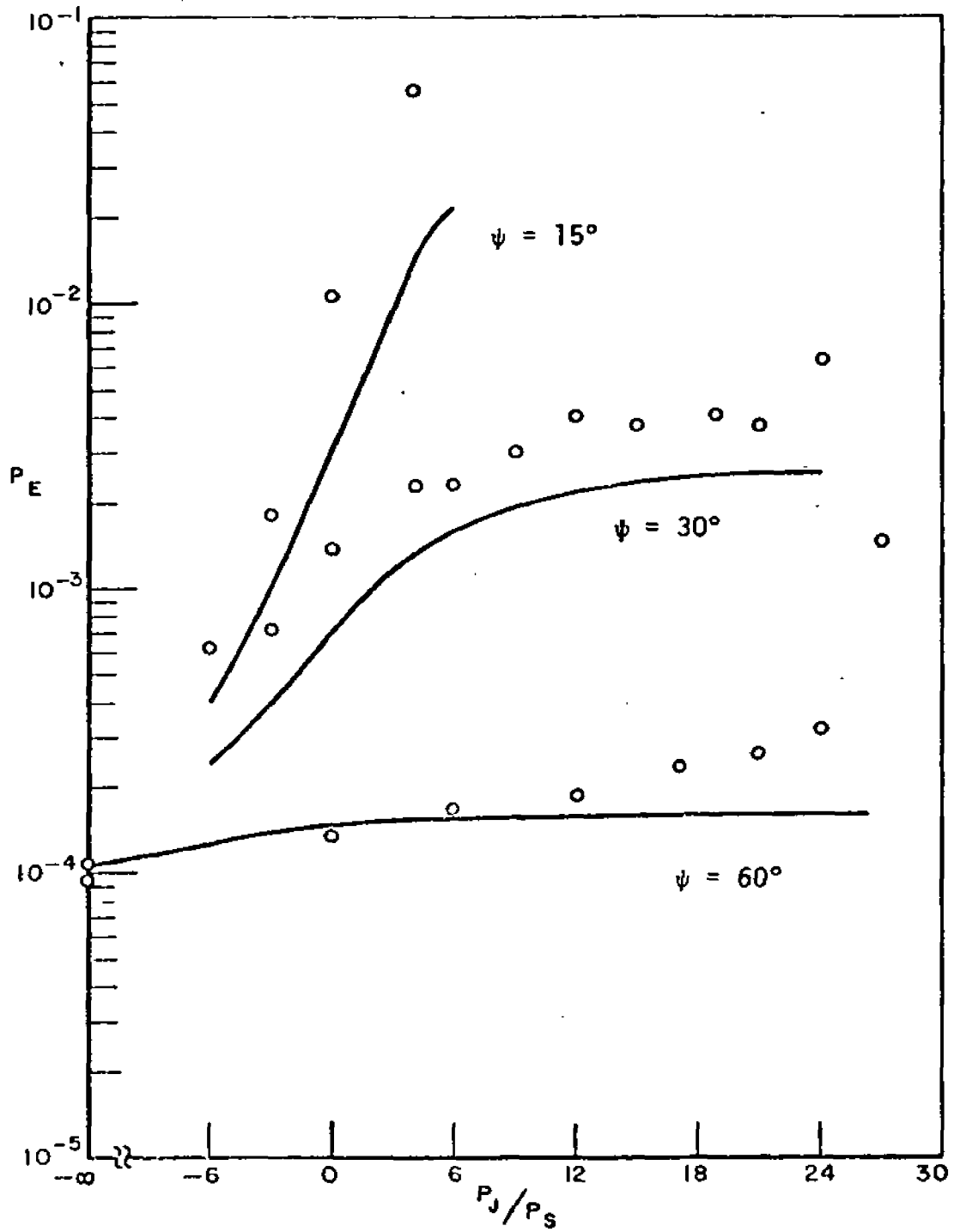


Figure 62--Performance of the experimental system versus the input interference-to-signal ratio for several values of the separation parameter ψ ; HRF. Other conditions as in Figure 61.

The multiplicative factor 11.7 represents the measured bit energy to noise density ratio when only the desired signal was applied to the bandpass limiter's input. The BEP versus P_J/P_S measurements agreed favorably with these calculated results in Figure 61 over a wide range of interference to signal ratios. Differences between the measured and calculated BEPs were slightly larger in Figure 62 for $\psi=30^\circ$ and much larger for $\psi=15^\circ$. The higher BEP for $\psi=30^\circ$ is attributed to the combined effects of non-ideal circuit components used to implement the array processor, including the effects of imperfect matching of the i.f. amplifiers bandpass characteristics and non-zero delay within the feedback loop. For $\psi=15^\circ$, these effects were magnified (note that the 29 nsec feedback delay represents a phase shift of approximately 18° at the 1.4 MHz code rate), and, at $P_J/P_S = 3$ dB, the calculated result becomes inaccurate since the output desired signal to interference ratio was only about -1.8 dB. In order to isolate the effects of non-ideal circuit components from the effects of weight jitter, most results to be presented were obtained by operating the SS/TDMA system in the lower-rate format. The larger deviations from the calculated result for large values of P_J/P_S in Figures 61 and 62 were caused by the effects of weight jitter -- this effect is investigated in the next section.

Experimental results also agreed favorably with the calculated results when the interfering signal was generated from a random source having a moderately wide bandwidth (563 KHz and 1.7 MHz doubled-sided). An example result is shown in Figure 63 for the 1.7 MHz case with $P_S/\sigma^2 = -4$ dB and $\psi=60^\circ$ per element.

An example illustrating system performance in a wideband interference environment is shown in Figure 64. For this example, the system was operated in the HRF and the 3 dB noise bandwidth of the interfering signal applied to the inputs of the i.f. amplifiers was approximately 12 MHz (double-sided), or about 8.5 times the code rate. The angular separation parameter ψ was fixed at 30° per element. The experimental results are shown to deviate significantly from the calculated result for values of P_J/P_S exceeding 9 dB. This performance degradation was caused by the inability of the ASP to form a sufficiently deep null on the interfering signal over the wide bandwidth, which contributed to additional desired signal suppression in the bandpass limiter stage. The degree of suppression was approximated in Figure 65 by calculating the signal-to-noise ratio at the bandpass limiter's input which would result in an equivalent BEP. For the purposes of comparison, the ideal output signal-to-noise ratio and the output signal-to-noise ratio with initial conditions set are also shown. The results in Figure 65 indicate that the output signal-to-noise ratio was within 3 dB of optimum when P_J/P_S was less than about

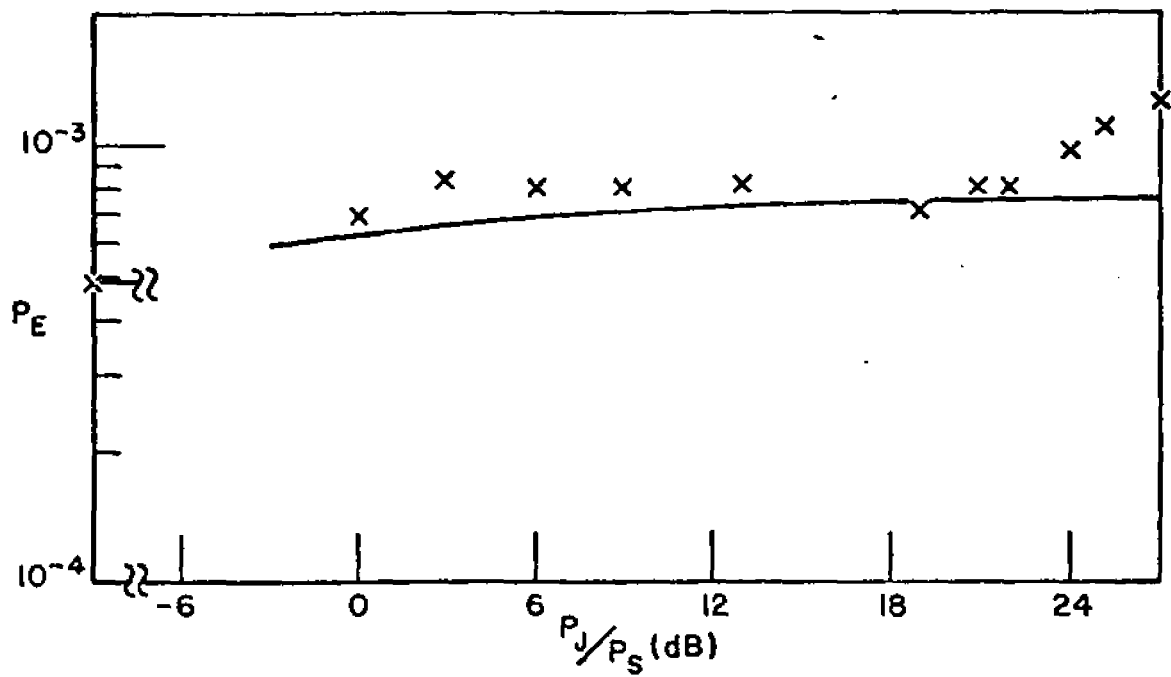


Figure 63--Performance of the experimental system versus the input interference-to-signal ratio for $\psi = 60^\circ$. Interfering signal bandwidth = 1.7 MHz centered on 70 MHz.

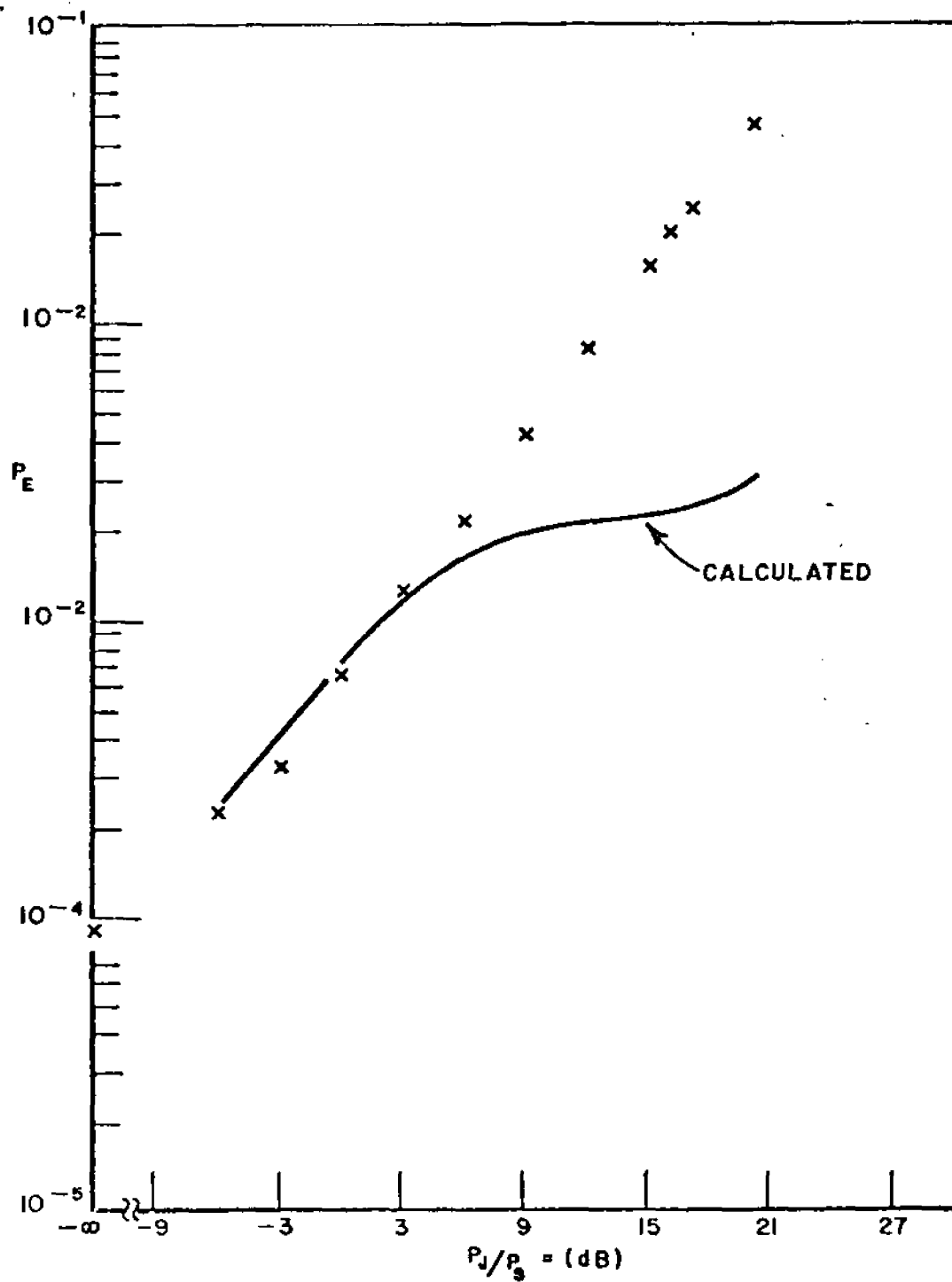


Figure 64--Performance of the experimental system versus the input interference-to-signal ratio for $\psi = 30^\circ$. Interfering signal bandwidth (3 dB) \approx 12 MHz centered on 70 MHz.

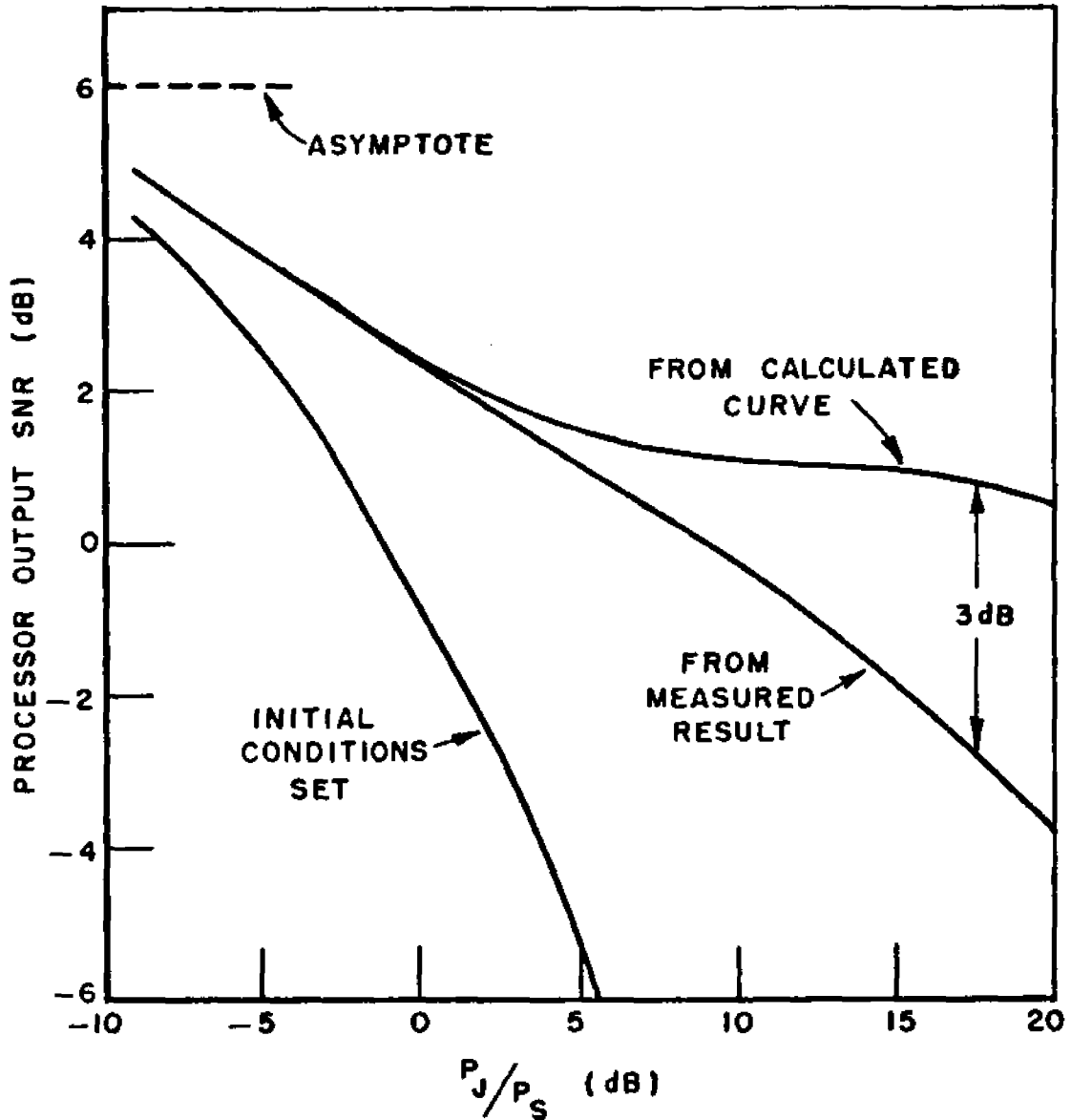


Figure 65--The array output signal-to-noise ratio versus the input interference-to-signal ratio. The curves were calculated from the results in Figure 64 using the limiter suppression factor.

16 dB -- the point at which the output noise power due to interference equals the output noise power due to input thermal noise. Note that, even though performance degraded from optimum for P_J/P_S greater than about nine decibels, the ASP continued to provide a significant processing gain.

Since nearly ideal performance was obtained for narrower-band interfering signals, insufficient wide-band interference suppression could only have been due to mismatched phase/amplitude versus frequency characteristics of the phase shifters, i.f. amplifiers, and processor control circuits and to the effects of non-zero loop delay. Using the results given in Figures 64 and 65 as an example, the interfering signal must be suppressed by about 17.5 dB to obtain the measured performance when $P_J/P_S = 17.5$ dB, i.e.,

$$\frac{P_J w^+ w}{w^+ M w} \doteq 17.5 \text{ dB} \quad (\doteq 56.2 \text{ numeric})$$

In order to obtain this amount of suppression, the amplitude and phase versus frequency characteristics of all signals that were combined to form the array output had to be matched to within about 1.2 dB and 7° , respectively, over the full interfering signal bandwidth. The phase matching requirement was not satisfied by the i.f. amplifiers (preceding each weight in Figure 38) over the 10 MHz bandwidth shown in Figure 39. Subsequent spot measurements indicated greater mismatches in amplitude and phase occurred beyond the 10 MHz band shown but within the 12 MHz interfering signal bandwidth. It thus appears that the mismatched bandpass characteristics of the i.f. amplifiers were the primary source of performance degradation under the wideband interfering signal condition, although the 37 nsec feedback delay (which is appreciable over this wide bandwidth) certainly magnified this effect. A reasonable attempt to match these characteristics and to minimize feedback delay over the bandwidth of interest would have significantly improved nulling capabilities under wideband interference conditions. Further studies in this area are recommended.

4. Steady-State Performance With Weight Jitter

The results of bit error probability measurements conducted under high loop gain conditions with the mean weights near their steady-state solution are presented in this section. The measurements were taken to determine the effects of weight jitter on SS/TDMA performance for signal environments encountered in practice.

In the preceding section, it was found that an analytical result could be used to predict system performance with good accuracy when the interfering signal spectrum was narrowband relative to the i.f. amplifier bandwidth. This was possible because (1) the signal-to-noise ratio at the output of the ASP was independent of the input signal bandwidths (provided the interfering signal continued to be narrowband with respect to the i.f. amplifier bandwidth) and (2) the limiter suppression factor was easily determined from T_0 . However, neither of these conditions are satisfied when the effects of weight jitter are to be investigated. The expression for excess noise due to weight jitter, i.e.,

$$P_{E_N} = \left[\frac{\alpha \Delta t P_I}{2 - \alpha \Delta t P_I} + \frac{(\alpha \Delta t P_I)^2}{2} \right] \frac{1}{1 + T_0},$$

was derived in Chapter IV under the assumption that the input thermal noise and interfering signals approximated ideal bandpass processes having a double-side bandwidth of B Hz, where $\Delta t = B^{-1}$. Since (1) the interfering signal bandwidths differed from the thermal noise bandwidths in most of the experimental results to be presented, (2) the excess noise generally cannot be assumed Gaussian, and (3) the excess noise is correlated with the desired signal, the above expression was not directly applicable. Formidable difficulties were also encountered in attempting to determine the effects of excess noise on the bandpass limiter output signal. Consequently, the analytical results could only be used to approximate, to set bounds on, or to predict general trends in the experimental results.

The first series of measurements shown in Figures 66-68 illustrate the effects of weight jitter when the thermal noise and the interfering signal bandwidths were approximately equal. For these measurements, the four thermal noise processes were bandlimited to 2 MHz (3 dB, double-sided) using single-tuned bandpass filters and the interfering signal had an effective noise bandwidth of approximately 1.7 MHz. Excluding the desired signal, the interval (Δt) between independent samples of the input signals thus approximated B^{-1} , where $B = 1.7$ MHz. The system was operated in the LRF mode with the timing error between the differential detector's input signal and the detector's LO signal set equal to zero thereby eliminating the effects of bit timing jitter. The method used to measure the effects of excess noise on SS/TDMA performance was to increase the loop bandwidth by increasing the interfering signal power while holding the circuit gains within the loop (proportional to α) constant. Using this method, the loop parameter $\alpha \Delta t P_I$ was

approximately proportional to the input interfering signal power when P_J/P_S was large. Results presented in Figure 66 show BEP versus P_J/P_S measurements for $\psi = 30^\circ$ and $P'_S/\sigma^2 = 0$ dB -- with and without down-link noise added to the bandpass limiter's output. When only thermal noise and the desired signal was applied to the input of the processor ($P_J/P_S = -\infty$ dB), the signal-to-noise ratio at the output of the ASP was about 6 dB, since the processor was (ideally) co-phased to the desired signal. The bit-energy-to-noise density ratio (E_b/N_0) at the detector's input was about 23.2 dB without down-link noise added* and about 10.1 dB with down-link noise added. The initial rise in the BEP as P_J was increased was attributed to a decrease in the optimum output signal-to-noise ratio due to nulling of the interfering signal (see previous section) which caused additional suppression of the desired signal at the bandpass limiter's output. If the effects of weight jitter had been negligible, the BEP versus P_J/P_S curve would have "leveled-off" as illustrated by the theoretical result given in Figure 66, which corresponds to $T_0 \approx 0.8$ dB for P_J/P_S large. That the measured BEP continued to increase was due to weight jitter effects. For $P_J/P_S = 21.2$ dB, the parameter αP_I was measured and found to be equal to about 8.2×10^5 (sec)⁻¹. Thus, the inverse of the important loop time constants were given by

$$\alpha \Delta t P_I \approx .48 \text{ (sec)}^{-1} \quad ; \quad P_J/P_S = 21.2 \text{ dB}$$

$$\alpha \Delta t \lambda_1 \approx .008 \text{ (sec)}^{-1}$$

$$\alpha \Delta t \sigma^2 = .0036 \text{ (sec)}^{-1}$$

where

λ_1 = eigenvalue associated with the desired signal

σ^2 = eigenvalue associated with thermal noise only.

Under these conditions, the time constants associated with beamforming to the desired signal and minimizing thermal noise were given by $0.09 T_S$ and $0.2 T_S$, respectively, where T_S equals the preamble interval (one time slot in the LRF mode). That is, the BEP measurements in Figure 66. also reflect system performance

* E_b/N_0 for this case was calculated using Equation (402).

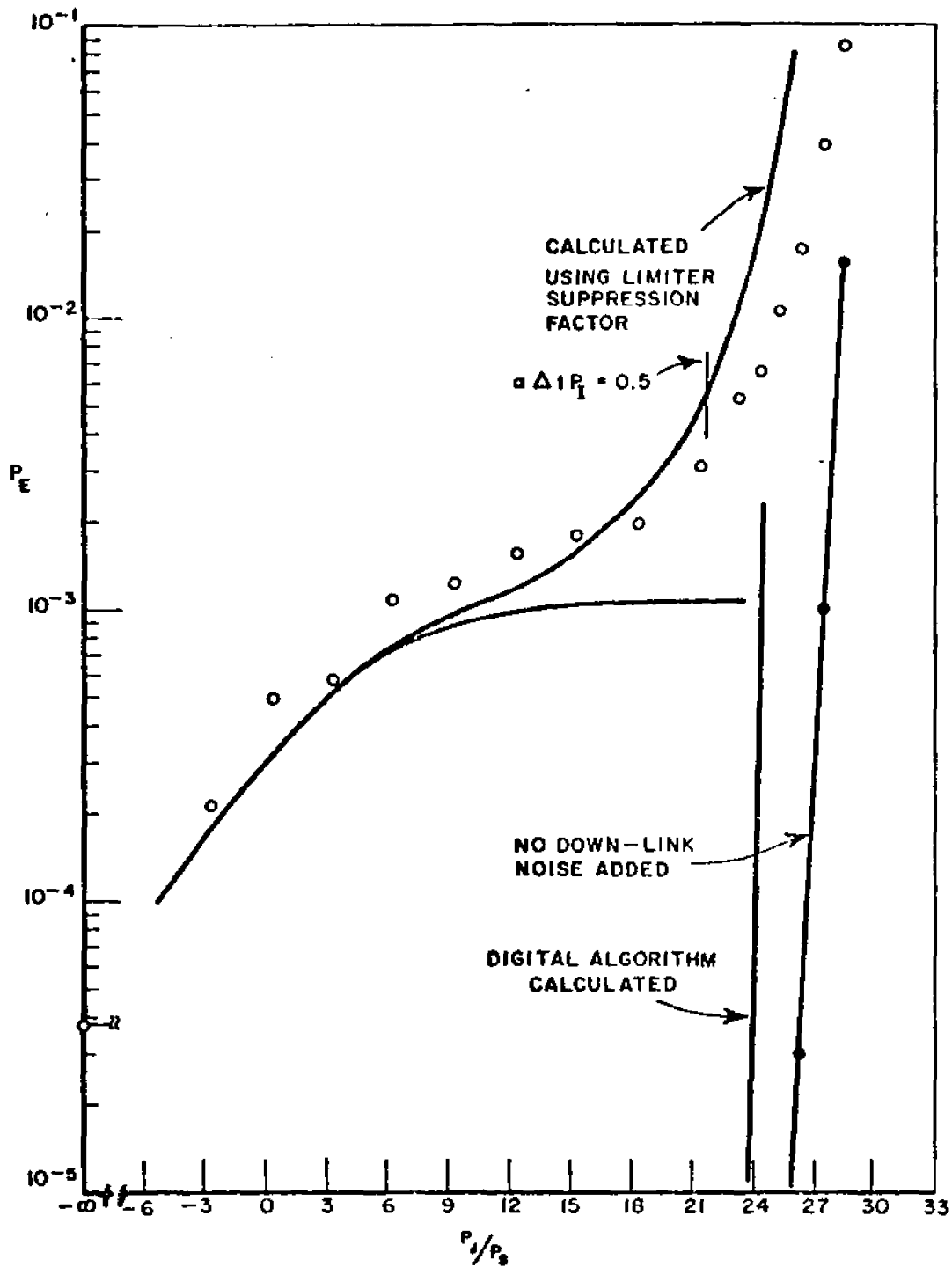


Figure 66--Performance of the experimental system versus the input interference-to-signal ratio for $\psi = 30^\circ$ with and without down-link noise added. Interfering signal bandwidth = 1.7 MHz; thermal noise bandwidth ≈ 2 MHz; $P_s'/\sigma^2 = 0$ dB.

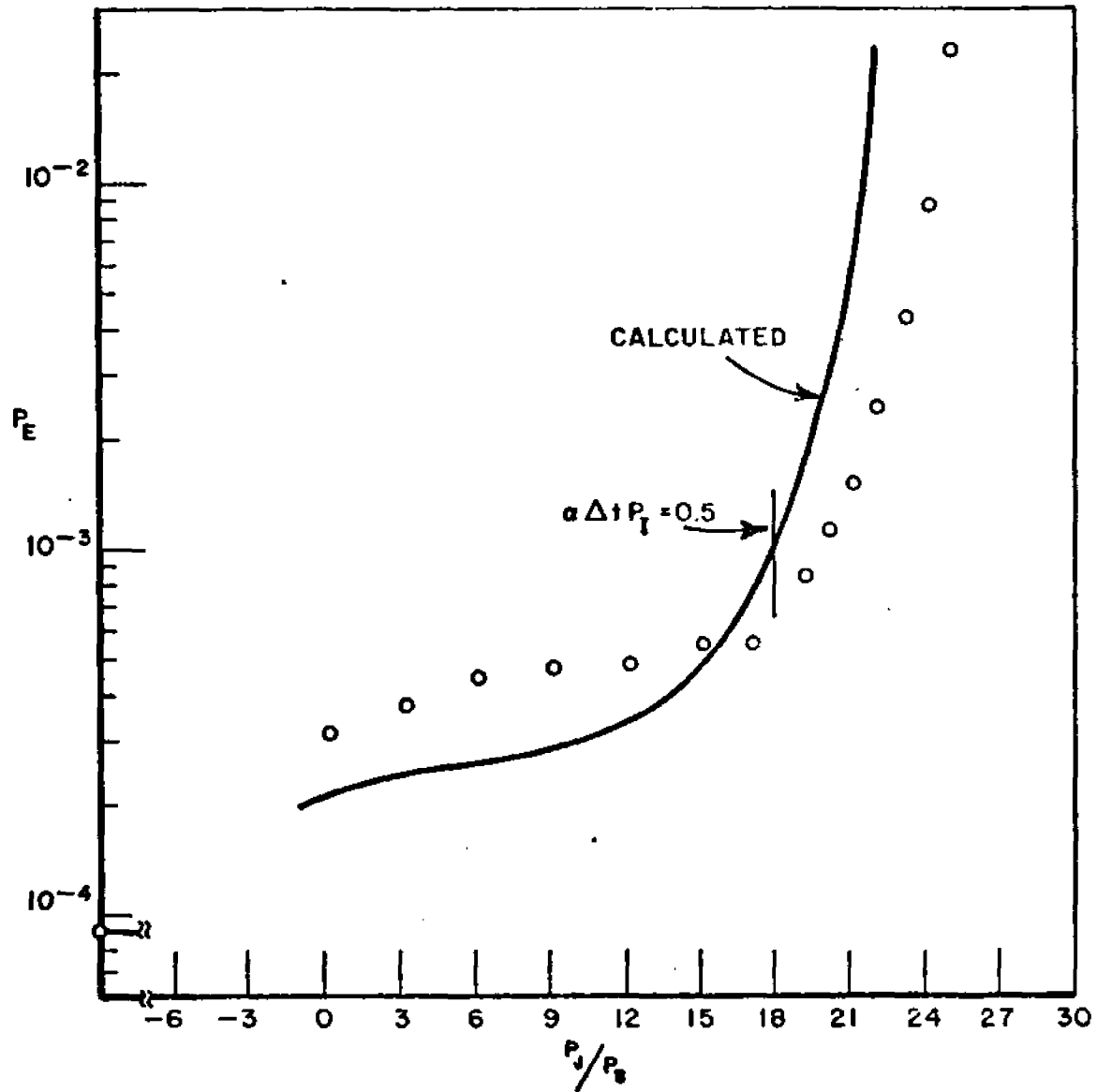


Figure 67--Performance of the experimental system for $P_S'/\sigma^2 = 4$ dB. Other conditions as in Figure 66 except E_b/N_0 is approximately 1 dB lower for $P_J/P_S = -\infty$ dB.

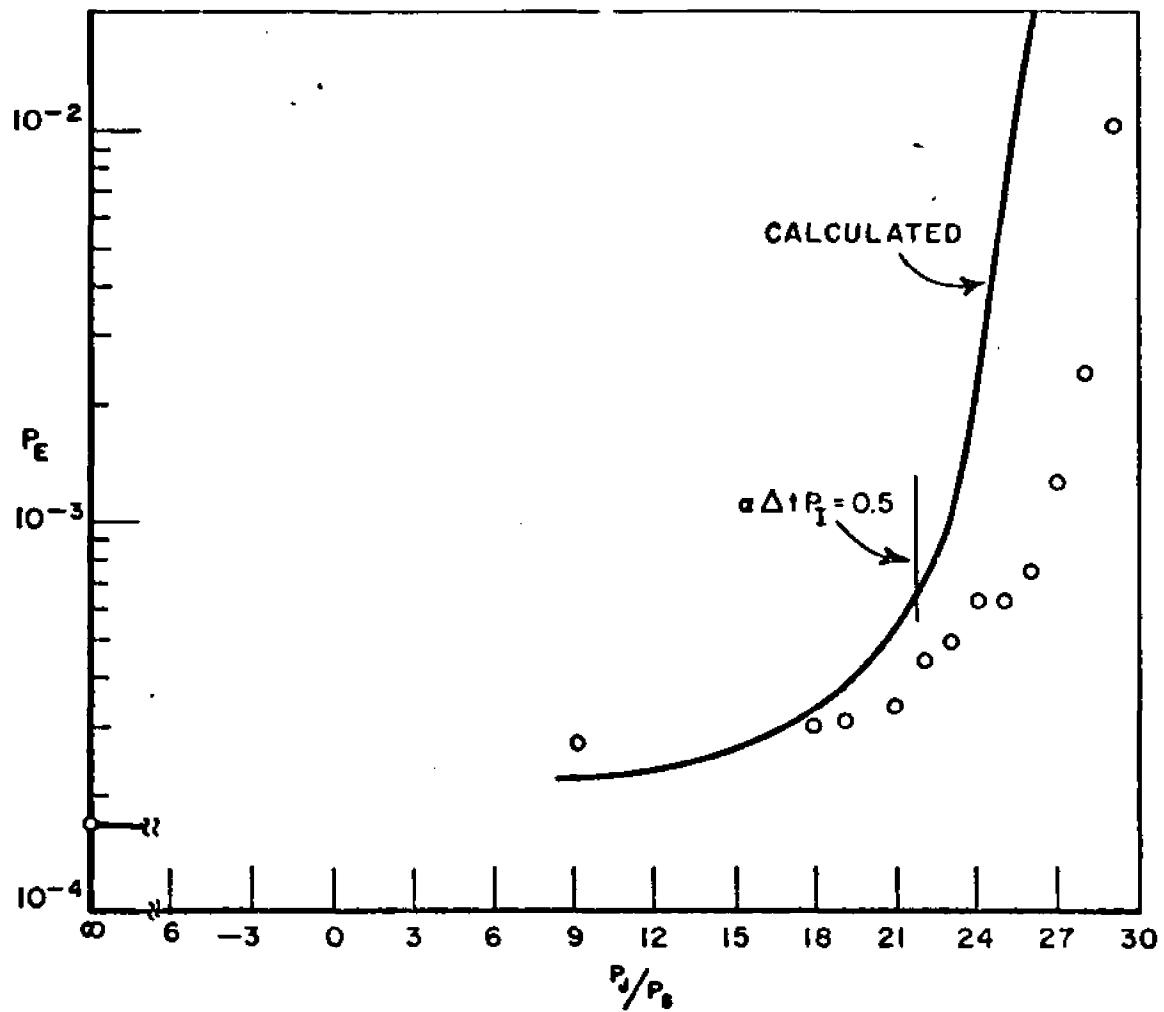


Figure 68--Performance of the experimental system for $\psi = 60^\circ$, and $P'_S/\sigma^2 = 0$ dB. Other conditions approximately the same as in Figure 67.

when the desired signal is pulsed in accord with the normally configured TDMA system described in Chapter II (measurements for this case are presented in the next section), since the longest time constant was much smaller than the preamble interval.* The results in Figure 66 indicate that excess noise due to jitter degraded performance by two mechanisms. One effect of the excess noise was to decrease the effective bit-energy-to-noise density ratio at the array output, as shown by the BEP measurements without down-link noise added. Although the analysis of the effects of weight jitter on DPSK detector performance were performed only for the digital implementation of the LMS algorithm, the measured result exhibits the same abrupt increase in the BEP predicted by the analytical result. For example, the detector performance measure D, as applied to a digital LMS algorithm implementation, was found to be approximated by [Equation (2560)]

$$D \doteq \frac{T}{\Delta t} T_0 \left[\frac{1}{1 + \frac{\alpha \Delta t c}{1 - \alpha \Delta t c} \frac{1 + T_0}{T_0}} \right] \quad (404)$$

which, in the high-level interfering signal environment under consideration, is approximated by

$$D \doteq \frac{T}{\Delta t} T_0 \left[\frac{1}{1 + \frac{\alpha \Delta t P_I}{2(1 - \alpha \Delta t P_I)} \frac{1 + T_0}{T_0}} \right] \quad (405)$$

The measurements given in Figure 66 can be compared with the theoretical performance of a digital LMS algorithm provided the effects of the bandpass limiter are taken into account. To make this comparison tractable, the bit-energy-to-noise density ratio at the output of the bandpass limiter is initially assumed proportional to the performance measure D. The result obtained under this assumption will be useful in demonstrating that the abrupt increase in the measured BEP is also predicted by the analytical result in Equation (405). When the weights were fixed at the optimum steady-state solution with $P_j/P_s = 24$ dB, the bit-energy-to-noise density ratio at the bandpass limiter's output was approximated by

*As will be shown in the next section, the loop bandwidth for this case is much wider than that required for acceptable performance under pulsed desired signal conditions.

$$\left. \frac{E_b}{N_0} \right|_{\alpha\Delta t P_I=0} \approx 58.2 \text{ (17.5 dB) .}$$

Applying the assumption discussed above, the expression for E_b/N_0 which includes the effects of weight jitter becomes

$$\frac{E_b}{N_0} \approx 58.2 \left[\frac{1}{1 + \frac{\alpha\Delta t P_I}{2(1 - \alpha\Delta t P_I)} \frac{1 + T_0}{T_0}} \right] \quad (406)$$

where $T_0 = 1.2$ (0.8 dB)

and $\Delta t \approx \frac{1}{1.7 \times 10^6}$.

The noise process at the bandpass limiter's output is clearly not Gaussian since the excess noise due to jitter is not Gaussian. However, as to be shown, this makes little difference when relating Equation (405) to the BEP, since E_b/N_0 increases very rapidly as $\alpha\Delta t P_I$ approaches one. The calculated result shown in Figure 66 for the digital LMS algorithm was obtained by simply substituting Equation (406) into the expression for the BEP of an ideal DPSK detector:

$$P_E = \frac{1}{2} e^{-\frac{E_b}{N_0}}$$

where P_E represents the bit error probability. The calculated BEP is similar to the measured BEP in that it exhibits an abrupt increase when the loop parameter $\alpha\Delta t P_I$ exceeds a certain value. However, the point at which the digital algorithm is predicted to "fail" occurs for $P_j/P_s \approx 24$ dB, which is about 2.5 dB lower than the measured result. Also, the slope of the BEP versus P_j/P_s curve is slightly smaller for the measured result. The differences between the measured and calculated results under high loop gain conditions are roughly in accord with the expected performance difference between the analog and digital LMS algorithms. For example, excess noise due to jitter was found in Chapter IV to be about a factor of two smaller for a given set of loop parameters when the analog LMS was used.

The difference can also be attributed to other factors, i.e., the level of correlation between excess noise and the desired signal is higher in the analog LMS case, as to be discussed subsequently.

When down-link noise was added to the bandpass limiter's output, as was the case in the second set of data points shown in Figure 66, the effect of excess noise on the limiter suppression factor had to be considered. As previously mentioned, the relationship between excess noise power due to jitter and the limiter suppression factor is difficult to determine since excess noise is not a Gaussian process and is in general correlated with the desired signal. Nevertheless, it is instructive to obtain an approximation for the limiter suppression factor by assuming that the limiter suppression characteristic of Figure 44 is applicable. The total noise power P_T at the input of the bandpass limiter can be approximated (for $\alpha\Delta t P_I \lesssim 0.5$) by summing the excess noise power (Equation (403)) with the quiescent noise power $T_0(1 + T_0)^{-2}$, i.e.,

$$P_T \doteq \frac{T_0}{(1 + T_0)^2} + \left[\frac{\alpha\Delta t P_I}{2 - \alpha\Delta t P_I} + \frac{(\alpha\Delta t P_I)^2}{2} \right] \frac{1}{1 + T_0}; \quad (407)$$

$\alpha\Delta t P_I \lesssim 0.5$.

Since $P_S \ll P_I$ for the range of P_J/P_S and $\alpha\Delta t P_I$ under consideration, weight jitter negligibly affected the desired signal power at the ASP's output (see section IV D3). Thus, the signal-to-noise ratio at the output of the ASP is approximated by

$$\left(\frac{S}{N_0} \right) = \frac{w_{opt}^+ \underline{s} \underline{s}^+ w_{opt}}{P_T} =$$

$$\frac{T_0}{1 + \left[\frac{\alpha\Delta t P_I}{2 - \alpha\Delta t P_I} + \frac{(\alpha\Delta t P_I)^2}{2} \right] \frac{1 + T_0}{T_0}} \quad (408)$$

The second calculated curve (with the highest BEP) shown in Figure 66 was obtained by assuming the limiter suppression factor ξ to be related to $(S/N)_0$ as in Figure 44. Using this value for ξ , the BEP was then determined from Figure 58 and the relation

$$\frac{E_b}{N_0} = 12.16 \frac{\xi^2}{1 + \frac{1 - \xi^2}{26.7}} \quad (409)$$

Excess noise due to jitter is shown to have a smaller effect on the measured BEP relative to the calculated result. In addition to the approximations which were made regarding the limiter suppression factor, the following factors also contributed to the difference between the calculated and measured results for $\alpha \Delta t P_I < 0.5$ (the region over which Equation (403) was assumed applicable): (1) the thermal noise bandwidth was wider than the effective noise bandwidth of the interfering signal; (2) Equation (403) represented an upper bound approximation to the excess noise power; and (3) the excess noise due to jitter was correlated with the reference (and thus the desired) signal. For the purposes of comparison, the calculated result is also shown for $\alpha \Delta t P_I > 0.5$. In this region, the slopes of the measured and calculated results were nearly the same, but the calculated result was displaced to the left by about 2.5 dB. Obviously, the calculated result does not apply in this case, since most of the measured performance degradation can be accounted for by adding the appropriate level of down-link noise to the measurements obtained without down-link noise. That is, the actual effects of excess noise on limiter suppression are secondary to the effects of weight jitter on DPSK receiver performance under these very high loop gain conditions.

Figure 67 shows the results of additional BEP measurements obtained when the input desired signal level was increased by 4 dB relative to the desired signal level in Figure 66, and Figure 68 shows results for $\psi = 60^\circ$. All other conditions, including the per-element thermal noise power, were the same as in Figure 66. Results calculated from the limiter suppression factor, evaluated as in Figure 66, are also shown. The degree of degradation (in terms of the effective value of E_b/N_0 determined from the expression $-\ln P_{E_m} + \ln 0.5$, where P_{E_m} is the measured BEP) due to jitter for a given value of $\alpha \Delta t P_I$ was smaller in both Figures 67 and 68 relative to the degree of degradation obtained in Figure 66. This is in accord with the theoretical results (Equation (407), for example) which showed that the ratio of excess noise power to quiescent noise power (i.e., when $w = w_{opt}$) was proportional* to $T_0^{-1} (1 + T_0)$.

*For $P_J/P_S = 12$ dB, the values for $T_0^{-1} (1 + T_0)$ in Figures were 1.82, 1.33, and 1.30, respectively. These values were nearly constant for $P_J/P_S > 12$ dB.

As was the case in Figure 66, the measured performance degradation due to jitter was less than that predicted by the calculated result, with the largest difference between calculated and measured results occurring for $\alpha \Delta t P_I \approx 0.5$. It is important to note, however, that the calculated result, along with the expression for $(S/N)_0$ given in Equation (407), can be highly useful in establishing bounds on system performance. For example, when $\alpha \Delta t P_I \approx 0.5$, the effect of weight jitter on the measured BEPs shown in Figures (66)-(68) was relatively small. This contrasted sharply with measured performance when $\alpha \Delta t P_I$ approaches a value of two -- the value for which the analytical result for the output SNR becomes unbounded; under this condition, the extent of degradation due to weight jitter was large enough to render the ASP ineffective for all practical purposes. Whether intermediate values of $\alpha \Delta t P_I$ -- a value of one, for example -- would yield acceptable performance would depend upon the application. Suppose that, in a particular application, the maximum acceptable BEP is 4×10^{-3} and that the condition under which the measurements in Figure 66 were obtained is the expected worst-case condition in terms of T_0 (i.e., $T_0 > 0.8$ dB in all expected input signal environments). In this case, the maximum value for αP_I (proportional to the convergence rate) for which these requirements can be satisfied is determined (using the measured results in Figure 66) by the relation

$$\alpha P_I \approx 0.4 (\Delta t)^{-1} = 0.72/\mu\text{sec} \quad .$$

The main point here is that the expression for $(S/N)_0$ can be used to establish reasonably tight bounds on worst-case system performance for a given value of α if the input signal bandwidth and the total input signal power are known.

The preceding results and discussions apply in cases where it is appropriate to assume that the input thermal noise plus interfering signal bandwidth approximates an ideal bandpass process and the ratio of the bandwidth to the data bit rate is large. Figures 69 and 70 show the results of measurements obtained for the case where the interfering signal bandwidth was much narrower than the thermal noise bandwidth, but still much wider than the data rate in the LRF. Specifically, the effective noise bandwidths of the thermal noise and the interfering signal were about 7.5 MHz and 563 KHz, respectively. The input signal spectra thus was significantly different from an ideal bandpass process. The theoretical results cannot be directly applied in this case, since the interval between independent samples of the interfering signal was about 13 times longer than the interval between independent samples of the thermal noise processes; an examination of the steps used to derive Equation (207) in Chapter IV would verify that the result would be significantly altered under this condition. In particular, the excess noise due to jitter is smaller (this can be

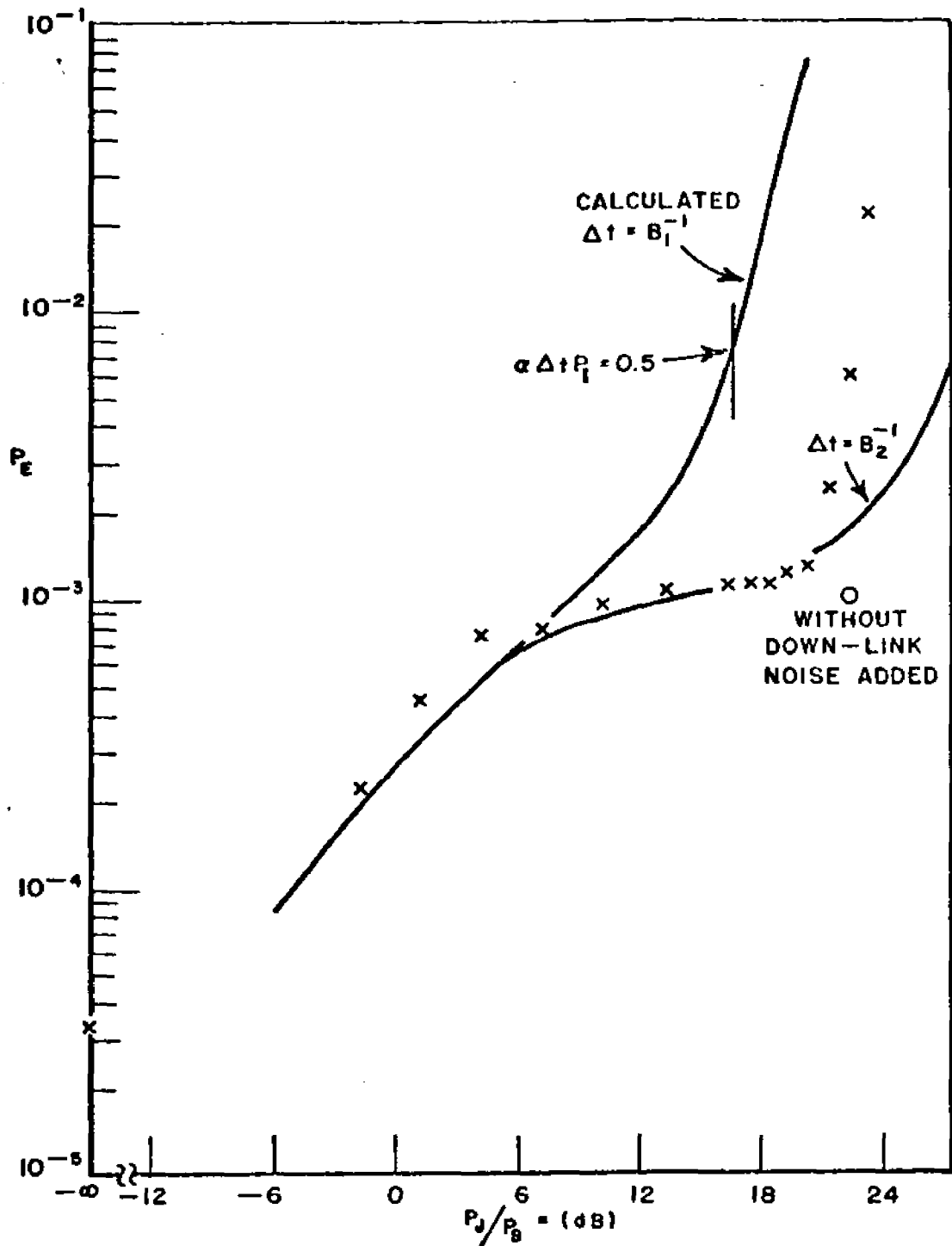


Figure 69--Performance of the experimental system versus the input interference-to-signal ratio for $\psi = 30^\circ$. Interfering signal bandwidth = 563 KHz; thermal noise bandwidth = 7.5 MHz; $P_s'/\sigma^2 = 0$ dB.

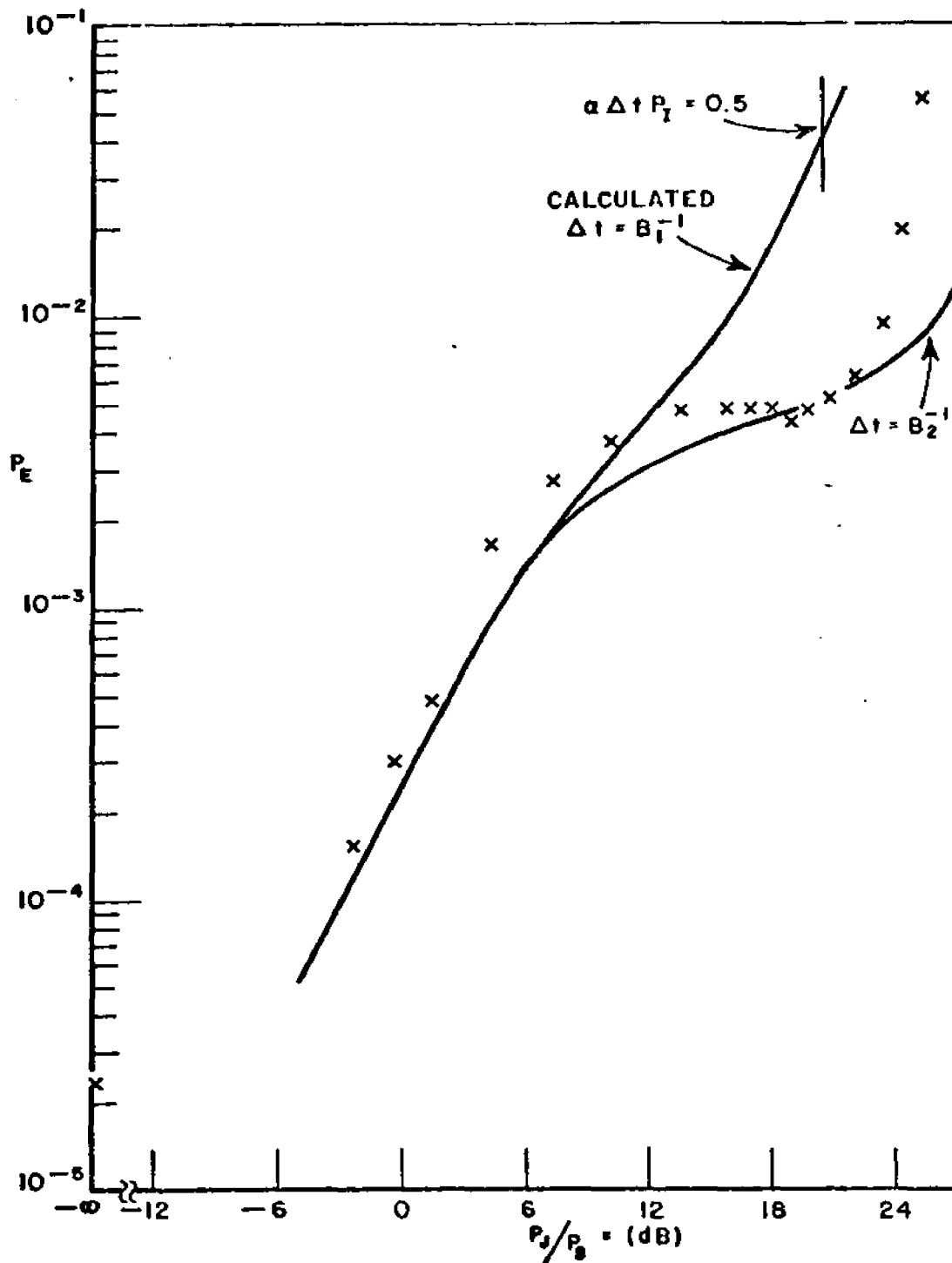


Figure 70--Performance of the experimental system for $P_s/\sigma^2 = -4$ dB. Other conditions as in Figure 69.

verified analytically) for a given input thermal noise power when the process has a wider bandwidth, because the percent of the total thermal noise power contained within the LMS loop response bandwidth is smaller. However, the impact that a smaller spectral density due to input thermal noise has on noise within the loop is obviously secondary compared with the effect of loop noise due to a high-level, narrowband, interfering signal when the parameter $\alpha \Delta t P_I$ (where $(\Delta t)^{-1} \cong 563 \times 10^3$) approaches a value of two. Therefore, the degree of performance degradation due to jitter should be very large when $\alpha \Delta t P_I = 2$, where $(\Delta t)^{-1}$ equals the effective noise bandwidth (double-sided) of the interfering signal. Furthermore, the degree of degradation should be smaller (for a given value of $\alpha \Delta t P_I$) relative to the degree of degradation obtained in Figures 66-68. These statements are confirmed by the BEP measurements shown in Figures 69 and 70, obtained for $\psi = 30^\circ$. The values of P_J/P_S which correspond to the condition $\alpha \Delta t P_I = 2$ in Figures 69 and 70 are 22.6 dB and 26.6 dB, respectively; at these levels of interference power, the effects of weight jitter caused the measured BEPs to increase at least an order of magnitude in both cases.

For the purposes of comparison, limiter suppression characteristics for the two cases $\Delta t = B_1^{-1}$ and $\Delta t = B_2^{-1}$, where B_1 is the interfering signal bandwidth and B_2 is the thermal noise bandwidth, were calculated and translated into the BEP measure using the limiter suppression factor as in Figures 66-68. The BEP, calculated using $\Delta t = B_2^{-1}$, is shown in Figures 69 and 70 to agree much more favorably with the measured results for $\alpha B_1^{-1} P_I < 1$, which indicates that the effects of weight jitter on system performance were considerably reduced in the wider-band thermal noise environment. For $\alpha B_1^{-1} P_I \cong 1$, the measured BEP increased sharply due to the presence of the narrower-band interfering signal, which was also in accord with the preceding discussion.

The results presented thus far have shown that the point at which the ASP "fails" due to weight jitter can be predicted with good accuracy by determining the point where $(S/N)_0$ (Equation (408)) becomes large, i.e., when $\alpha B^{-1} P_I \cong 2$, where B represents the effective noise bandwidth of the interfering signal. The expression for $(S/N)_0$ represents an upper bound on the degradation due to weight jitter for smaller values of $\alpha \Delta t P_I$. In all of the previous cases, the input thermal noise and/or interfering signals approximated ideal bandpass processes which had bandwidths exceeding the desired signal bandwidth, thus facilitating the selection of an appropriate value for Δt . Of course, it is entirely possible for an interfering signal to be narrowband with respect to the desired signal bandwidth (represented by the code rate in the present system). In order to evaluate the effects of

weight jitter on system performance for the narrowband case, BEP measurements were conducted under c.w. interfering signal conditions. The results of these measurements will be of greater value in determining appropriate loop gain parameters, since the effects of weight jitter are more pronounced in c.w. interfering signal environments. Again, Equation (408) may be used to approximate system performance even though it was derived assuming that the input signals were wideband random processes. If the frequency of a single high-level interfering signal is (nearly) equal to the desired signal carrier frequency, then, in addition to a d.c. term, the signals applied to the input of the integrators (Figure 38) contain components of the desired signal converted to baseband (desired signal by interfering signal cross-terms). The interval between uncorrelated samples of these cross-terms is approximately equal to the interval between uncorrelated samples of the PN code. Since the spectral density of the thermal noise process was much smaller than the desired signal spectral density within the loop response bandwidth for all c.w. interference tests conducted, the desired signal by interfering signal cross-term was the predominant source of weight jitter. Based on this argument, Equation (408) may be used to estimate the effects of weight jitter on system performance by employing the inverse of the code rate as an approximation for Δt . This assertion can also be deduced from the analytical expressions. Letting $\tilde{N}(t)$ represent the c.w. interfering signal, $\tilde{U}(t)$ the thermal noise process, and $\tilde{S}(t)$ the desired signal, the difference between the instantaneous and average input covariance matrix and cross-correlation vector used in the analysis of Chapter IV become

$$\begin{aligned} \phi(t) &\equiv \tilde{\underline{x}}(t) \tilde{\underline{x}}^\dagger(t) - K_x && (410) \\ &= [\tilde{\underline{u}}(t) + \tilde{\underline{N}}(t)] \tilde{\underline{s}}^\dagger(t) + \tilde{\underline{s}}(t) [\tilde{\underline{u}}^\dagger(t) + \tilde{\underline{N}}^\dagger(t)] + \tilde{\underline{u}}(t) \tilde{\underline{u}}^\dagger(t) - M \\ R_\Delta(t) &\equiv \tilde{\underline{x}}(t) \tilde{\underline{r}}^\dagger(t) = [\tilde{\underline{u}}(t) + \tilde{\underline{N}}(t)] \tilde{\underline{r}}^\dagger(t) \end{aligned}$$

where

$$M \equiv E \tilde{\underline{u}}(t) \tilde{\underline{u}}^\dagger(t)$$

$$E\phi(t) = 0$$

$$E R_\Delta(t) = [0]$$

The above results follow from the assumption that $\tilde{\underline{s}}(t)$, $\tilde{\underline{u}}(t)$, and $\tilde{\underline{N}}(t)$ are uncorrelated. An appropriate value for the interval

between "independent" samples of $\phi(t)$ and $R_{\Delta}(t)$ can be determined by evaluating the interval between uncorrelated samples of the signal by interfering signal cross-products (assumed to be the largest terms in $\phi(t)$ and $R_{\Delta}(t)$). It is well-known that the autocorrelation function of a PN code is approximated by

$$R_{PN}(\tau) = \begin{array}{ll} b(1 - \frac{\tau}{\Delta}) & ; \quad 0 < \tau < \Delta \\ b(1 + \frac{\tau}{\Delta}) & ; \quad -\Delta < \tau < 0 \\ 0 & ; \quad \text{elsewhere} \end{array} .$$

The interval between independent samples is thus approximately equal to the inverse of the code rate (Δ). It will be shown that this assumption leads to an approximation to measured results under c.w. interference conditions.

BEP measurements shown in Figure 71 illustrate system performance obtained under c.w. interfering signal conditions for $\psi = 60^\circ$. The conditions under which these measurements were performed differed from the wideband interfering signal measurements in that the loop gain (α) was reduced by a factor of about 9 dB and the receive time base was estimated at the TDMA modem by locking the SDDL to the NCS generated at the satellite simulator (although the transmit time base was still set for zero timing error). As in previous measurements, the value of α was held fixed. For $P_J/P_S = 20$ dB, the value of αP_I was about 8.3×10^4 per second; with Δt set equal to the inverse of the code rate, the corresponding value for the loop parameter $\alpha \Delta t P_I$ was approximately 0.47. The BEP measurements show that weight jitter was beginning to cause performance to degrade at this point. As P_J/P_S was further increased, the BEP increased in much the same manner as in the wideband interfering signal case, with the BEP increasing more than two orders of magnitude as $\alpha \Delta t P_I$ approached a value of two.

The calculated result shown in Figure 71 was evaluated by assuming that the effect of excess noise due to jitter was to suppress the desired signal power at the output of the bandpass limiter. The agreement with the measured result was roughly comparable to the agreement exhibited in Figure 66 (wideband interference case). Agreement between the calculated and measured results improved when the angular separation (ψ) of the desired signal and the c.w. interfering signal was reduced to thirty degrees (electrical) per element, as shown in Figure 72. It should be emphasized that although favorable agreement between calculated and experimental results was obtained in Figures 71 and 72, this does

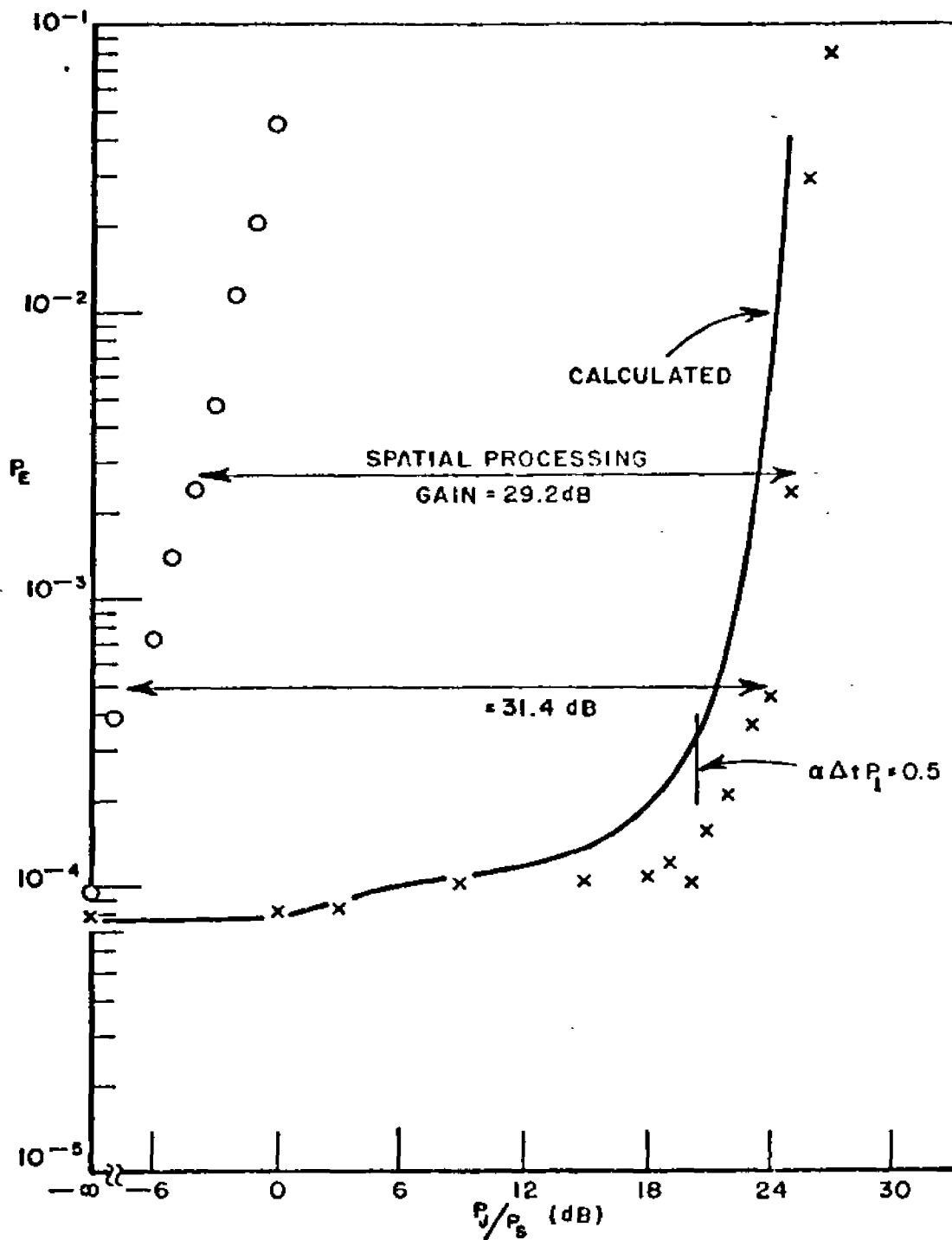


Figure 71--Performance of the experimental system versus the input interference-to-signal ratio for $\psi = 60^\circ$. The protection afforded by waveform processing is also shown. C.W. interference frequency = 70 MHz + 100 Hz; $P_S'/\sigma^2 = 0$ dB; biphasic modulated desired signal.

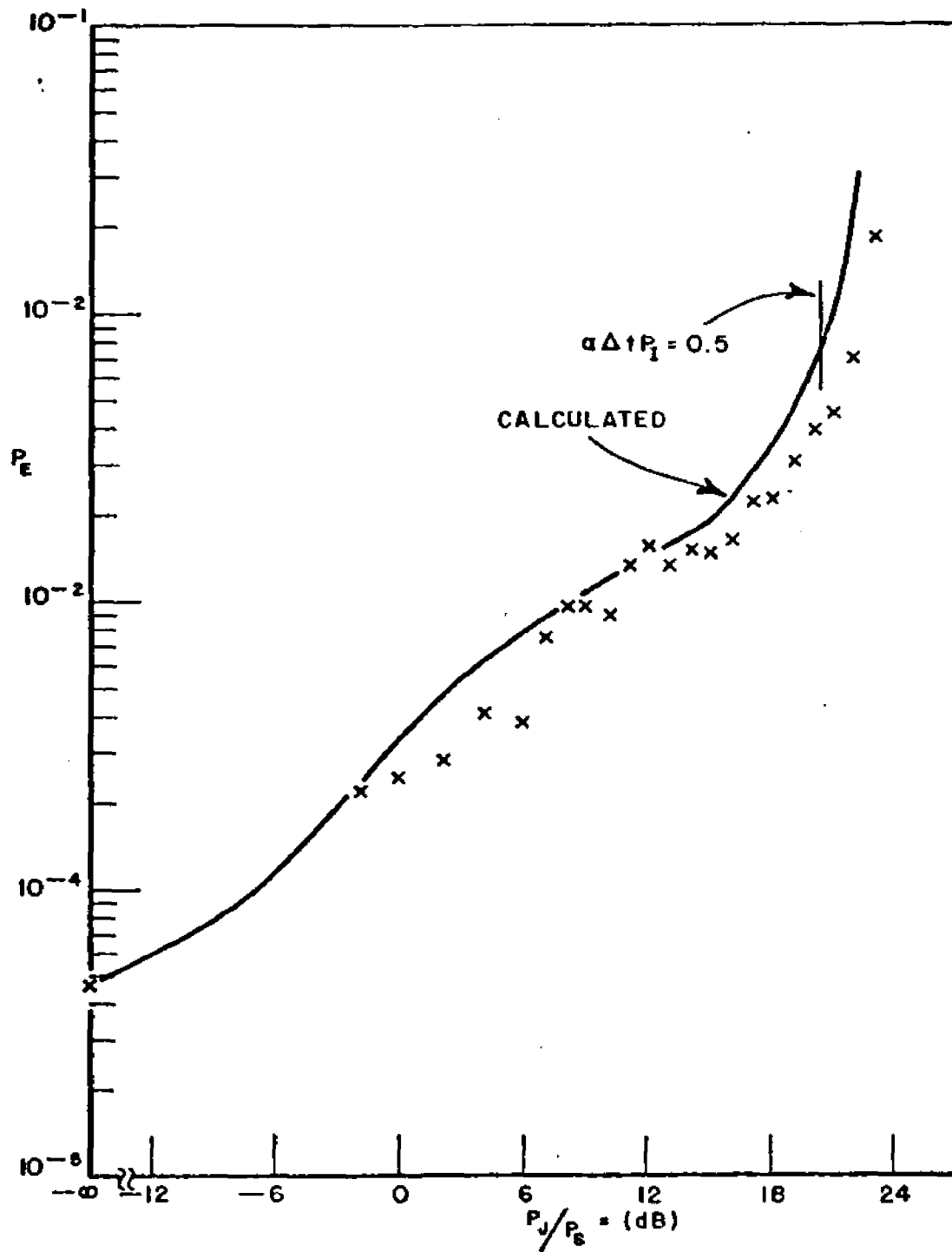


Figure 72--Performance of the experimental system for $\psi = 30^\circ$. Other conditions as in Figure 71 except E_b/N_0 is slightly higher for $P_J/P_S = -\infty$ dB.

not imply that similarly close agreement would be obtained for other PN code structures since an analytical result was not derived to support this assertion. In particular, the desired by interfering signal cross-terms in Equation (410) exhibit non-random characteristics, i.e., the PN code used to modulate the desired signal contained long intervals (up to seven chips in length) during which no bit transitions occurred. The excess noise level due to jitter is momentarily higher during these intervals since the effective interval between uncorrelated samples is momentarily higher.* In other words, the data presented apply specifically to a length 127 PN code and a spectrum-spreading ratio of 16. Improved results would generally be obtained by using higher spectrum-spreading ratios or shorter length PN codes. In order to determine whether the effects of weight jitter could be reduced by employing quadrature modulation to eliminate these long intervals between phase transitions of the desired signal, measurements were obtained with the SS/TDMA system operating in the quadrature modulation mode under c.w. interfering signal and high loop gain conditions with the angular separation parameter set equal to 30° per element. Even though the two (length 127) PN codes which were used to modulate the desired signal were structured so that the maximum interval between phase transitions of the desired signal was two code chip intervals, quadrature modulation provided only a small improvement in performance under high loop gain conditions, as shown in Figure 73. Apparently, the use of quadrature modulation is only marginally effective in providing additional protection in c.w. interference environments (at least with regard to DPSK detector performance).

Previous results presented in this section were obtained with the transmit timing fixed at a value corresponding to zero timing error between the NCS generated at the SS and the desired signal applied at the input to the SS. In these cases, the effects of weight jitter and down-link noise on the transmit time base correction circuits (the range tracking loop (RTL)) were eliminated from consideration. In order to evaluate system performance when the SS/TDMA system is configured for more normal operation (apart from the pulsed desired signal format, which is considered in section E), BEP measurements were conducted with the RTL enabled.

The BEP measurements shown in Figure 74 illustrate the effects of weight jitter and down-link noise on detector performance with and without the RTL enabled**; all other conditions were the same

*That this effect is significant was noted from preliminary experimental results in which the maximum interval between PN code transitions was reduced to three (length seven PN code). However, documentation was insufficient to merit inclusion in this report.

**When the RTL was disabled, the transmit timing error was set equal to zero.

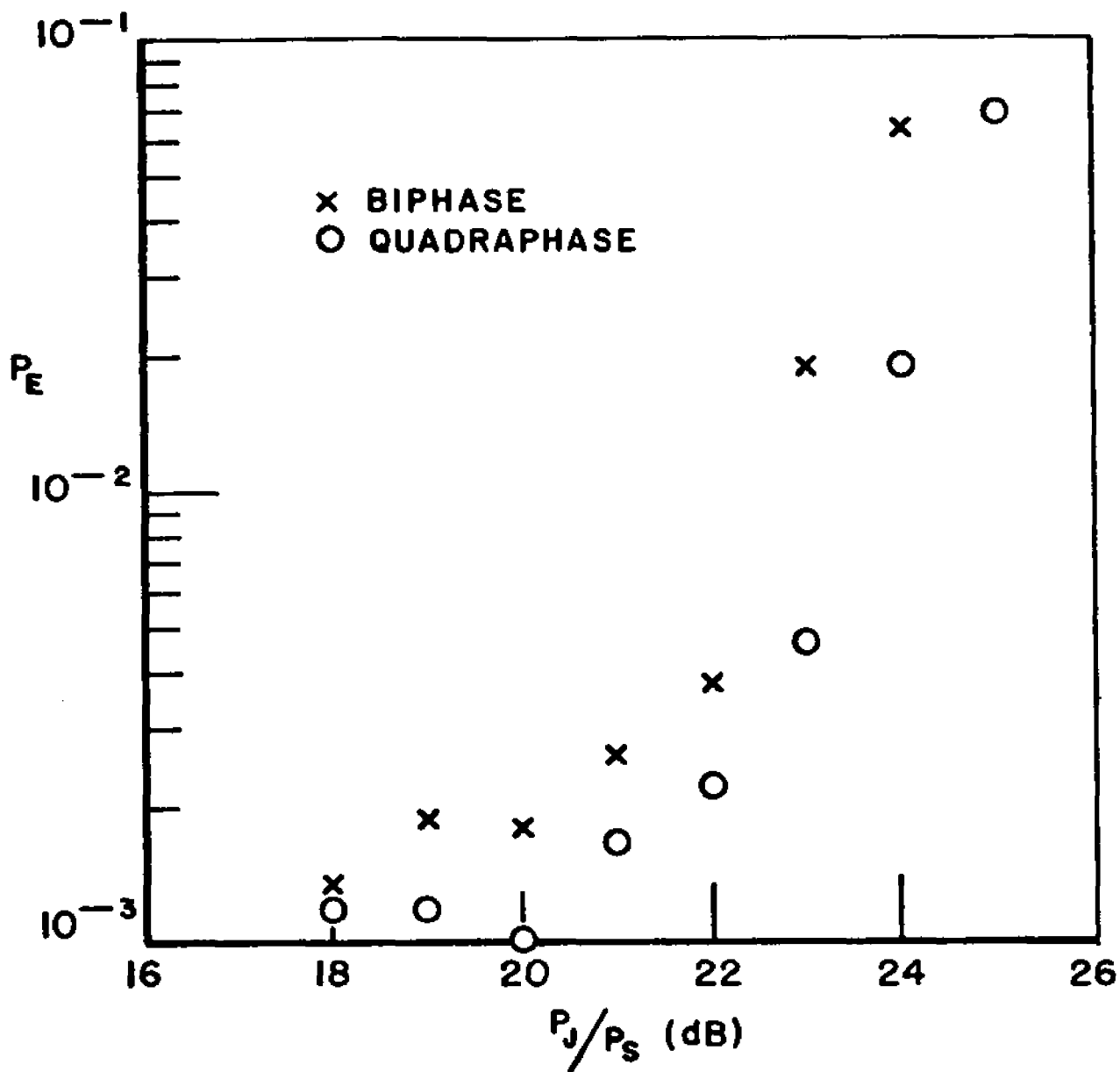


Figure 73--Performance of the experimental system versus the input interference-to-signal ratio for $\psi = 30^\circ$ using biphase and quadrature modulation. C.W. interference frequency - 70 MHz + 100 Hz; $P'_S/\sigma^2 = 0$ dB.

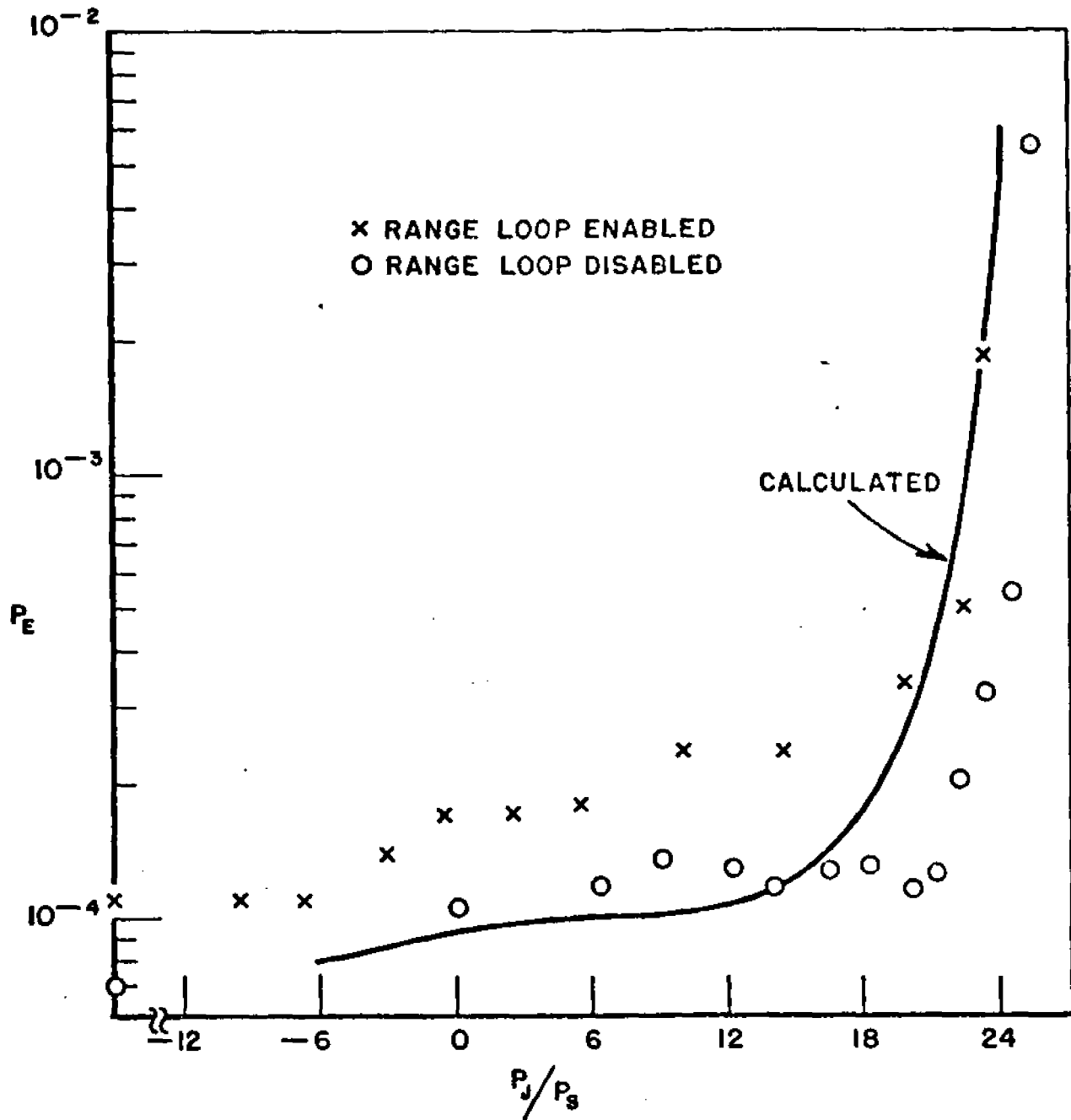


Figure 74--Performance of the experimental system versus the input interference-to-signal ratio for $\psi = 60^\circ$ with and without the range tracking loop enabled. When the range tracking loop was disabled, the transmit time base error was set equal to zero. C.W. interference frequency = 70 MHz + 100 Hz; $P_S'/\sigma^2 = 0$ dB; biphase modulation.

as in Figure 71. The BEP is shown to be larger with the RTL enabled and $P_J/P_S \approx 18$ dB, which is essentially in accord with the measurements given in Figures 58 and 59. The most important aspect of these comparative measurements is that the effects of weight jitter were more pronounced when the RTL was enabled. For example, the RTL occasionally lost lock when $P_J/P_S \approx 23.2$ dB (the data point shown was obtained during an interval when lock was maintained) and lock could not be maintained when $P_J/P_S \approx 24.2$ dB. As configured in the experimental tests, the loss of lock condition was determined within the modem based on the level of the post-waveform processed signal (i.e., after the correlation filters) measured during the range slot bursts. When this level dropped below a certain specified percentage (50%) of the level measured during NCS bursts, a possible loss of lock condition was flagged and the transmit time base corrections were inhibited. If the desired signal received at the TDMA modem during range slot bursts was less than this percentage in m out of n successive bursts ($m < n$) of the range pulses, a loss of lock condition was confirmed and the RTL attempted to reacquire lock by incrementing the transmit time base in a prescribed manner. While the details of this system will not be elaborated upon, it should suffice to say that the above-described algorithm used for validating the locked condition was necessary in order to minimize the possibility of locking the RTL to the wrong signal when the desired signal power received at the modem during range bursts dropped sharply. As applied to the system being investigated, a loss of lock condition was flagged when the level of correlation between the signal received during range bursts and the coded LO generated within the modem dropped to less than 50% of the level of correlation* between the NCS and the LO (recall that the system contains a bandpass limiter). The effectiveness of this technique in flagging a signal dropout condition was based on the assumption that the level of correlation between the coded LO and the excess noise at the ASP's output was small relative to its correlation with the desired signal component of the ASP's output. The relative level of correlation is easily determined under conditions of wideband (with respect to the code rate) interference, low loop gain ($\alpha \Delta t P_I \ll 1$), and zero timing error between the LO and the desired signal, by evaluating the expression**

*Note that the level of correlation between the signal received during NCS slots and the coded LO is approximately proportional to the received desired signal power.

**An ideal reference signal is assumed.

$$E \hat{r}(t) \hat{y}(t) = E \hat{r}(t) \hat{x}^*(t) w(t) \approx |\hat{r}|^2 \quad (411)$$

$$\left\{ \frac{T_0}{1+T_0} + \frac{\alpha \Delta t P_I}{2} \frac{1}{1+T_0} \right\} .$$

The first term is due to correlation with the desired signal and the second term is due to correlation with excess noise. Note that the effect of excess noise is to increase the total level of correlation, i.e., it is unclear as to whether the second term represents a measure of performance degradation. Much more formidable difficulties are encountered in attempting to determine a meaningful measure of these correlation effects under high loop gain, narrowband interference, or non-zero timing error conditions, or when the reference signal is derived via waveform processing. The only certainty is that the level of correlation (between excess noise and the coded LO) increases as $\alpha \Delta t P_I$ increases, since the LMS algorithm attempts to minimize the error between the output and the reference signal. If the level of correlation is sufficiently large -- specifically, much larger than the level of correlation between the desired signal and the coded LO -- the RTL can "lock" to the excess noise, thereby deriving transmit time base corrections from the timing of the reference signal rather than from the timing of the transmitted range pulse. That this mode of operation is possible was demonstrated experimentally for the case of a c.w. interfering signal centered on the desired signal's carrier frequency. It was found that if the loop gain parameter ($\alpha \Delta t P_I$) was sufficiently high (near a value of two), the RTL would remain locked (provided it was initially locked) even when the desired signal was removed from the ASP's input. Operation at such high values of $\alpha \Delta t P_I$ must therefore be avoided, since the loss of lock algorithm does not sense the false lock condition in this case.

The measurements presented in Table V were conducted to aid in the selection of an appropriate value for $\alpha \Delta t P_I$ when the RTL is enabled. The c.w. interference measurements were otherwise performed under the same conditions as Figure 71 except that post-limiter additive noise level was reduced to obtain a higher bit energy-to-noise density of 13.21 dB when P_J/P_S was set to 0 ($-\infty$ dB). Measurements were also obtained using a quadrature modulated desired signal. The results show that excess noise affects RTL performance in a very abrupt manner. In the biphase case, for example, the RTL retained lock for values of $\alpha \Delta t P_I$ up to 0.91, but would not stay locked for $\alpha \Delta t P_I = 1.44$. The effect is even more abrupt in the case of quadrature modulation, where the difference between the locked and unlocked condition occurs for $1.14 \approx \alpha \Delta t P_I \approx 1.44$. These results also show that the loss of lock algorithm was effective in preventing a false lock to the reference signal for

Table V. Experimental Performance of the Range Tracking Loop for Several Values of P_J/P_S Under c.w. and Wideband (563 KHz bandwidth) Interference Conditions.

P_J/P_S (dB)	$\alpha \Delta t P_I$	B-Biphase Q-Quadrature	RTL E-Enabled D-Disabled	ψ (elec. degrees)	Comment	
c.w. interference $\frac{E_b}{N_0} = 13.2$ dB						
262	21.8	0.72	B,Q	E,D	60°	No errors measured in 10^6 bits
	22.8	0.91	B	E	60°	BER = 9.2×10^{-6} , RTL retains lock
			Q	E	60°	No errors in 10^6 bits
			B,Q	D	60°	No errors in 10^6 bits
	23.8	1.14	B	E	60°	BER = 3.06×10^{-4} , almost all errors occurred when the transmit time base error was momentarily large
			Q	E	60°	No errors in 10^6 bits
			B,Q	D	60°	No errors in 10^6 bits
	24.8	1.44	B,Q	E	60°	Unable to retain lock
			B	D	60°	BER = 3×10^{-6}
			Q	D	60°	BER = 2×10^{-6}
	25.8	1.81	B	D	60°	BER = 8.7×10^{-4}
			Q	D	60°	BER = 1.2×10^{-4}
	26.8	2.27	Q	D	60°	BER = 2.56×10^{-2}

TABLE V (continued)

	P_J/P_S (dB)	$\alpha \Delta t P_I$	B-Biphase Q-Quadrphase	RTL E-Enabled D-Disabled	ψ (elec. degrees)	Comment
Wideband (563 KHz) interference, $\frac{E_b}{N_0} = 13.1$ dB						
263	28.8	1.10	B	E,D	60°	No errors
	29.8	1.38	B	E	60°	BER = 4.4×10^{-5} until loss of lock which occurred after 6.8×10^5 data bit
			B	D	60°	BER = 2.5×10^{-5}
	30.8	1.75	B	E	60°	Unable to retain lock for more than ten seconds
	31.8	2.20	B	D	60°	BER = 5.86×10^{-4}
	32.8	2.78	B	D	60°	BER = 1.2×10^{-3}

$\alpha \Delta t P_I$ as high as 1.44. Table V also shows BEP measurements obtained when the c.w. interfering signal was replaced by a wideband (563 KHz) interfering signal. That the RTL retained lock for a slightly higher value of $\alpha \Delta t P_I$ (≈ 1.75) may have been due to the effects of random envelope fluctuations which would tend to reduce, although not eliminate, the effects of correlation between excess noise and the coded LO.

The above considerations regarding the behavior of the RTL under high loop gain conditions were obtained to illustrate the effects of correlation between excess noise and the desired signal. Under lower loop gain conditions ($\alpha \Delta t P_I \approx 0.7$), the RTL was effective in both acquiring and maintaining transmit time base synchronization under all the test conditions presented in this chapter with the array adapting. Moreover, the length of time required to obtain synchronization under high-level interference conditions was no longer than the time required in the absence of interference. As a general rule of thumb, based on tests conducted in addition to those presented, transmit time base synchronization can be acquired and maintained when the desired signal is transmitted on a continuous basis* provided (1) the ratio of excess noise due to jitter to the output desired signal power during the range slot does not exceed a value of approximately one, and (2) the power level of the NCS pulse does not exceed the power level of the desired signal by more than 6 dB at the output of the bandpass limiter. The latter condition is necessary in order to insure that the level of correlation** between the LO and the desired signal was greater than 50% of the level of correlation between the NCS and the LO. From the limiter suppression characteristic (Figure 44), this implies that the output desired signal to total noise ratio must exceed approximately -4 dB. In the tests upon which the above-cited rules of thumb were based, the timing error between the transmitted desired signal and the PN code used to generate the waveform processed LO was initially offset by an integral number of code chips. Under this condition, the desired signal power at the array output was very small relative to its value when the array was beamformed to the desired signal, since the desired signal was treated as an interfering signal, i.e., the desired signal was uncorrelated with the reference signal due to the code timing offset. In the timing acquisition phase, the timing

*The case where the desired signal is pulsed, as it would be when the TDMA modem is configured for normal operation, is discussed in the following section.

**The term "level of correlation" has been applied loosely here and in the previous discussion to include the effects of the received power level on the correlation outputs.

of the PN code modulated desired signal was incremented in steps of one (code) chip using a prescribed search algorithm as described in [19]. At some point in the search algorithm, the timing error between the desired and reference signals was less than one-half code chip.* When this condition occurred, the array initiated a response to beamform to the desired signal. The interval of time between the increment and the transmission of the range signal pulse (used to test the timing of that increment) was sufficiently long (in all cases tested) to allow the array to settle to its steady-state condition (i.e., beamform to the desired signal and null the interfering signals). Even with a timing error of one-half code chip, the LMS algorithm will converge to the optimum output signal-to-noise ratio under low loop gain conditions, although the level of the desired signal will be reduced in proportion to the reduction in the level of correlation between the reference and the desired signal. However, the excess noise due to jitter will not change appreciably for a given set of loop parameters because of reference signal by input signal terms contained at the output of the error multipliers within the array feedback loop.** In other words, the excess noise due to jitter (Equation (407)) should not exceed one-half the steady-state output desired signal level

$$\left(0.5 |r|^2 \frac{T_0^2}{(1 + T_0)^2} \right)$$

in order to insure that transmit time base synchronization can be acquired.

In view of the favorable agreement between measured and calculated results under low-loop gain conditions, it is concluded that an adaptive array processor which converges to the optimum output signal-to-noise ratio can be implemented using a waveform processed reference signal. Moreover, it has been shown that the expression for excess noise power derived in Chapter IV can be used to obtain an approximate upper bound on the loop parameter $\alpha \Delta t P_I$ required for acceptable system performance. α is determined by circuit gains within the LMS feedback loop. Δt is determined from the input signal bandwidths. In cases where it is appropriate to assume the interfering signal bandwidth B is wider than the code rate and approximates an ideal bandpass process, then $\Delta t \approx B^{-1}$. If the signal environment contains a narrowband (with respect to the code rate) high-level interfering signal centered on the desired signal's carrier frequency, then an appropriate value for Δt was found to be the code chip interval. Note that this implies that the amount of degradation due to weight jitter is greater, for a given input signal power P_I , when

*In the tests, the timing error was approximately zero since the initial timing error was an integral number of code chips.

**Note that the reference by desired signal cross-terms disappear when the desired signal DOA (or its estimate) is used to discriminate the desired signal from interference.

the interference is narrowband. An effective method for preventing large degradation due to weight jitter would be to control the total power applied at the input to the array processor, i.e., implement an AGC control at each input. The AGC should have a rapid onset/slow release characteristic to minimize the effects that a high-level, repetitive pulsed, interfering signal would have on the control loops.

E. Experimental Performance Under Pulsed Desired Signal Conditions

The combined effects of finite adaption time and weight jitter on SS/TDMA system performance were evaluated by alternately switching between initial condition and integrate modes of operation under program control (see Figure 45). The TDMA modem was set to operate in the continuous transmit mode as in section D, but the position of the data and overhead slots in Figure 1 were selected so that they occurred one time-slot after a reset pulse. The conditions under which these tests were performed were therefore equivalent to the conditions encountered when the SS/TDMA system is configured for operation in the TDMA pulsed desired signal format, i.e., a period of one time-slot duration (preamble) was allocated to precede each data or overhead slot for the purpose of establishing a sufficiently high signal-to-noise ratio at the ASP's output prior to the onset of data (or the link/range pulse).

All results to be presented were obtained with the SS/TDMA system configured to operate in the LRF mode. The average data rate was 2400 bps (e.g., a vocoder channel). To accommodate an average data rate of 2400 bps employing an instantaneous rate of 10.95 K bps, data were transmitted in eight adjacent slots* (rather than a single slot), with the first slot occurring at the end of the preamble (see discussion, Chapter II). In this mode, there was one adaption (one reset) per sixty-four data bits, as opposed to one adaption per eight data bits had data been transmitted in single-slot bursts (i.e., if data had been transmitted at an average rate of 75 bps). Although the bit error probability in these two cases will generally differ since adaption continues during data slots (except during the reference delay interval), the BEP can be approximated in the single-slot-per-transient case by applying the theoretical results, as will be shown. The interfering signal in all tests was generated using a 70 MHz + 100 Hz c.w. source to simulate worst-case conditions for a given input interfering signal power.

*The duration of the link or range pulses remained equal to one-time slot.

It has been shown that the convergence properties of the LMS algorithm are greatly affected by the initial weight vector. Of the three initial weights considered in Chapter IV, the most appropriate, as applied to the experimental system being investigated, are the zero initial condition and the omnidirectional initial condition, since the reference signal was derived via waveform processing; that is, an ideal reference was not available for performing an estimate of the desired signal DOA in the present equipment. Consequently, the experimental tests focussed on evaluating system performance when three of the four initial weights were set equal to zero and the fourth weight was non-zero.

The set of measurements shown in Figures 75 and 76 illustrate the dependence of the BEP on the reference signal level for a fixed value of the initial weight vector

$$w^{\dagger}(t_0) = (5 + j 5, 0, 0, 0)$$

when both bit timing loops were enabled. The measurements therefore reflect system performance when the SS/TDMA system was configured for normal operation. The BEP was measured as a function of the input interfering signal power under the following conditions:

$$P_S/\sigma^2 = 0 \text{ dB}$$

$$\psi = 60^\circ/\text{element}$$

$$\sqrt{P_S} = 7.07 \text{ mv p-p} = \sqrt{P_S/m} = \sqrt{0.25 P_S}$$

$$(\alpha P_S)^{-1} = 7.5 T_S$$

where

$$T_S \triangleq 0.82 \text{ msec} = \text{one time-slot interval.}$$

The loop time constants under high-level interference conditions were therefore given by

$$(\alpha \lambda_1)^{-1} \triangleq 7.1 T_S$$

$$(\alpha \sigma^2)^{-1} = 30.4 T_S$$

$$(\alpha P_I)^{-1} \triangleq (\alpha P_J)^{-1} \quad .$$

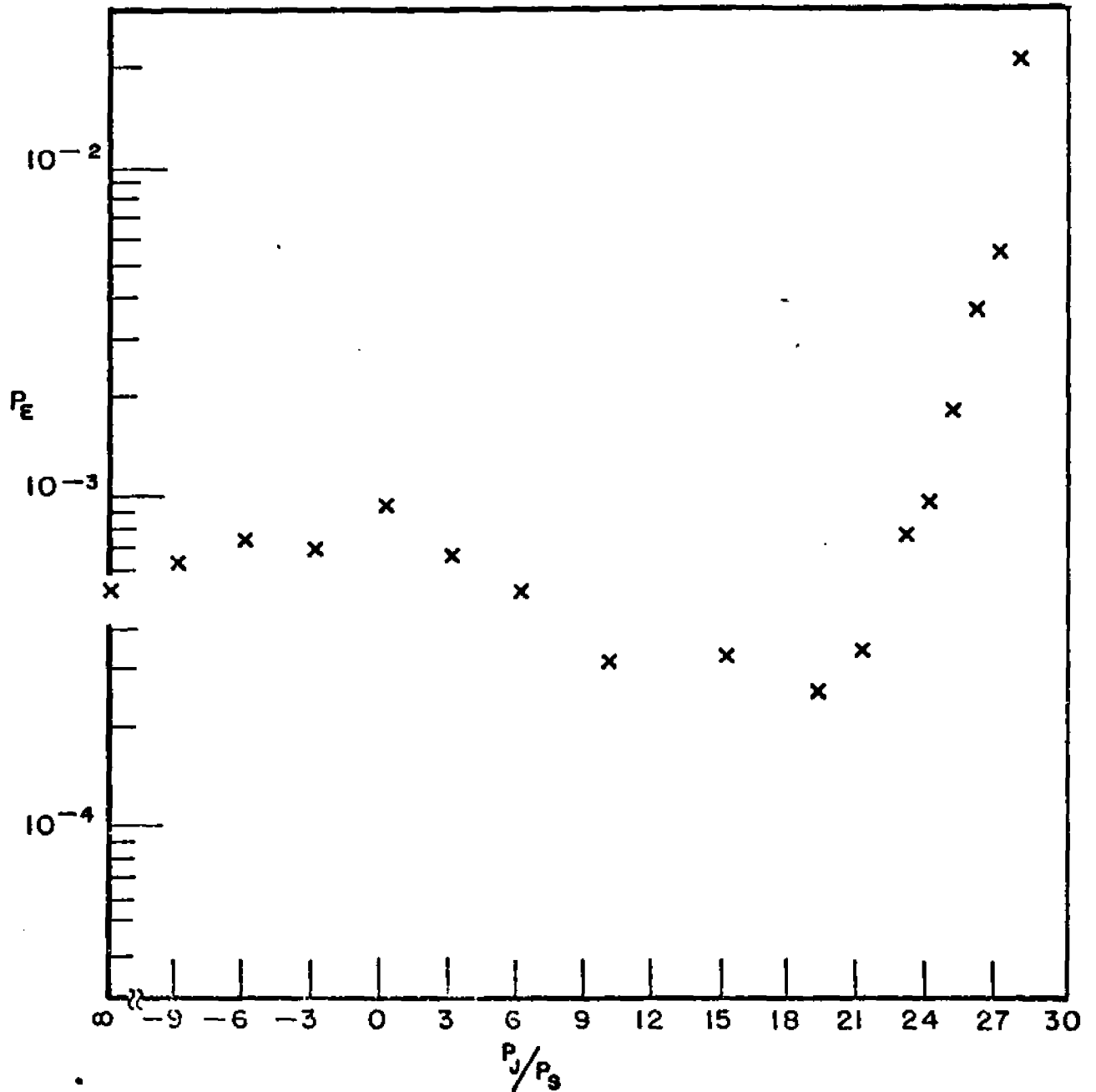


Figure 75--Performance of the experimental system versus the input interference-to-signal ratio for $\psi = 60^\circ$. TDMA/adaptive array system configured for normal operation in the LRF. The initial array pattern was omnidirectional. $E_b/N_0 \approx 10.9$ dB when the desired signal-to-thermal noise ratio (no interference) at the bandpass limiter's input was 6 dB. Input desired signal voltage = 2.5 mv rms; $P_s'/\sigma^2 = 0$ dB; C.W. interference frequency = 70 MHz + 100 Hz; $w^+(t_0) = [5 + j5, 0, 0, 0]$ volts; reference signal level = 97.2 mv rms; output desired signal level during reset = 25 mv rms; thermal noise bandwidth ≈ 2 MHz. $\alpha \Delta t P_I = 0.5$ for $P_J/P_S = 2.71$ dB.

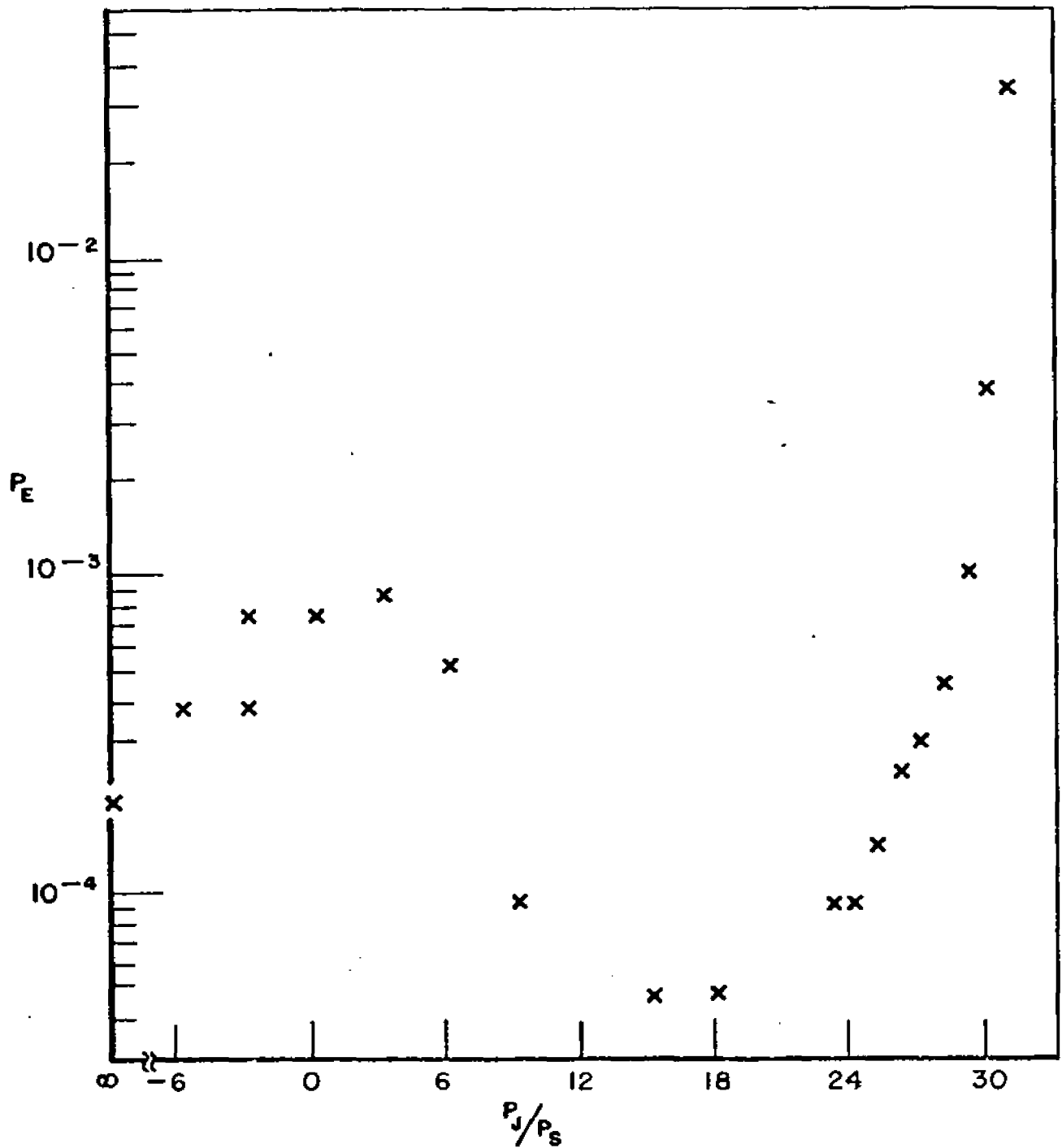


Figure 76--Performance of the experimental system with $E_b/N_0 \approx 11.9$ dB and a reference signal level of 68.5 mv rms. Other conditions as in Figure 75.

That is, the longest time constant was much greater than the preamble interval. As was shown in section IV B, the longest time constant can be eliminated from the weight transient by initializing the weights to zero. However, since this result was derived under the assumption that weight jitter effects are negligible, some caution must be exercised in applying the all zero initial condition under high loop gain conditions. The simulation results presented in Chapter V D show that relatively poor performance is obtained when (1) the output desired signal power is small relative to its optimum value and (2) an ideal reference signal is used to provide desired signal discrimination (rather than an estimate of the DOA). This same behavior was also noted in the experimental results. When the weights were initialized to zero under the test conditions of Figures 75 and 76, the output desired signal level was about 20 dB smaller than the reference signal level* at the beginning of the first data slot (i.e., after the preamble adaption interval), and thus 20 dB less excess noise could be tolerated. Since the level of excess noise caused by reference signal by input interfering signal cross-terms is approximately constant for a given value of $\alpha \Delta t P_I$ regardless of the output desired signal power, relatively poor performance was obtained when the weights were initialized to zero. The obvious solution is to increase the magnitude of one of the initial weights so that the desired signal has a higher level at the end of the preamble interval. Of course, this cannot be done without increasing the initial error along eigenvectors orthogonal to the desired signal DOA, thereby reducing the output signal-to-noise ratio during the transient. Moreover, the output SNR may not converge monotonically to its optimum value if the output desired signal power exceeds its steady-state value at some point in the transient. The selection of an initial weight vector therefore requires a compromise between minimizing the effects of weight jitter under high loop gain conditions and maximizing the output SNR during weight transients. The experimental results in Figures 75 and 76 illustrate this trade-off. During the reset interval, the ratio of the output desired signal power to the reference signal power was -11.8 dB in Figure 75 and -8.3 dB in Figure 76. At the end of a preamble adaption interval, the output desired signal level** was about 9.1 dB smaller than the reference signal in the conditions of Figure 75, whereas its level was only about

*The output desired signal power was also about 17 dB below its optimum value.

**These values were determined theoretically under high-level interfering signal conditions using a calculation technique as in Equation (409). Although an accurate measurement was difficult to obtain due to the low output signal-to-noise ratio, the actual values appeared to be close to the theoretical.

6.8 dB smaller in Figure 76. A comparison of the two sets of BEP measurements reveals that 3 dB more input interference power was tolerated when the output desired signal was higher. The result in Figure 76 also indicates that a further reduction in the reference signal level (equivalent to an increase in the initial weight value) would not have significantly increased the tolerance to higher level interfering signals since $\alpha \Delta t P_I = 0.94$ when $P_J/P_S = 30$ dB -- the region where abrupt failure begins to occur regardless of the desired signal level.

The effect of a slower response to nulling of the interfering signal is shown in both Figures 75 and 76 to cause an increase in the measured BEP for lower values of P_J (and $\alpha \Delta t P_I$). As an aid in determining the reason for this behavior, the output signal-to-noise ratio was calculated as a function of adaption time for each of the conditions of Figures 75 and 76; the results are given in Figures 77 and 78 for a number of selected input interference to desired signal ratios. The abscissa represents the actual adaption time normalized to T_S and thus does not account for the reference delay interval, during which adaption was halted (except during the preamble) in the experimental system. Since the reference delay interval was about one-quarter of a data bit, the results in Figures 77 and 78 can be applied by appropriately scaling the abscissa. Using this method, the output signal-to-noise ratio during the range pulse is approximated by the signal-to-noise ratio of Figures 77 and 78 in the interval $1.75 T_S < t < 2.5 T_S$. Similarly, the output signal-to-noise ratio during data slots (total of eight) is determined using the interval $T_S < t < 7 T_S$. Because the output SNR is not constant during these intervals, it is difficult to relate to the BEP in a precise manner. However, the following observations can be made:

- (1) The measured BEP was highest (for $P_J/P_S \approx 22$ dB) for -6 dB $\approx P_J/P_S \approx 6$ dB because of a slow response to null the interfering signal. The calculated output desired signal to interference ratio, shown in Figures 79 and 80 as a function of time (normalized to one time slot interval) for the test conditions in Figures 75 and 76, respectively, illustrates this slow response for several values of P_J/P_S . Figure 80, for example, shows that the output desired signal to interference ratio is as low as -0.3 dB at the end of the preamble interval when $P_J/P_S = 6$ dB, although the ratio increases rapidly as the adaption interval increases. This result, together with the waveform processing gain measurement in Figure 56, indicates that a low output desired signal to interference ratio was a predominant source of degradation. Although the desired signal to interference ratio is initially low (-3 dB) for

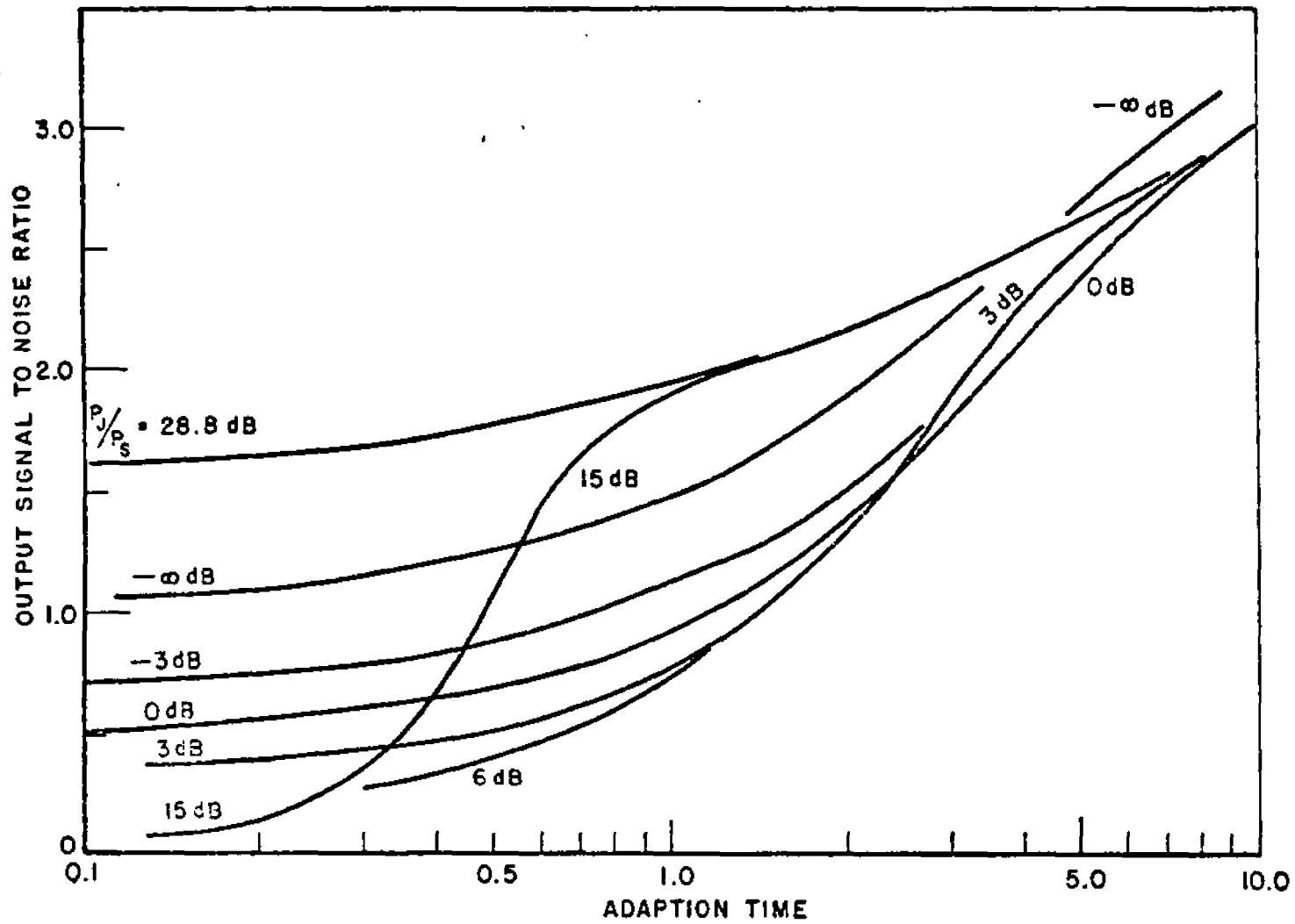


Figure 77--The output signal-to-noise ratio versus adaption time (normalized to the preamble interval) for several values of P_J/P_S under the same conditions as in Figure 75.

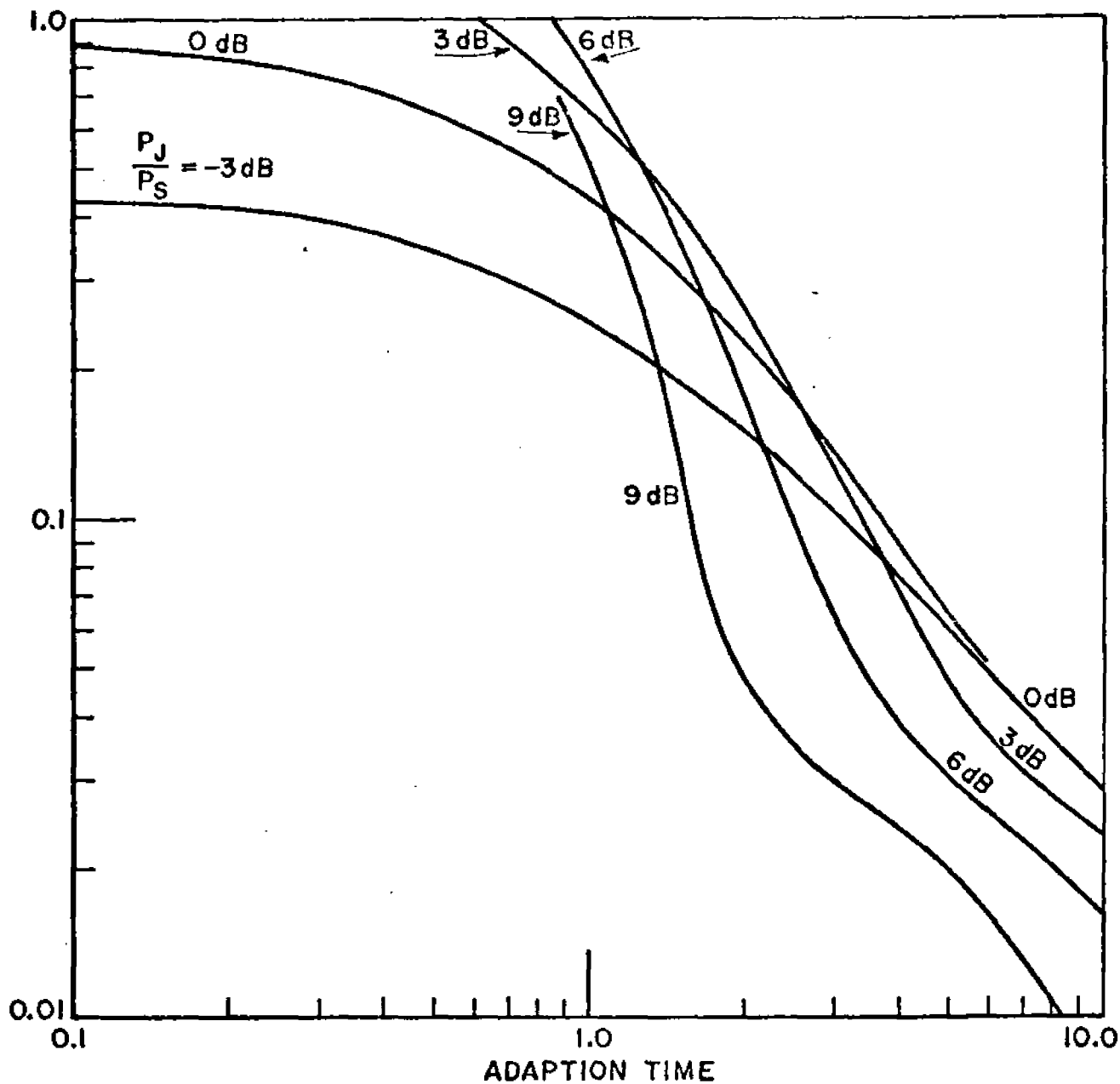


Figure 79--The output signal-to-interference ratio versus the normalized adaption time for several values of P_J/P_S under the same conditions as in Figure 75.

$P_J/P_S = 9$ dB and $t = T_S$, this ratio improves rapidly to 10 dB within the first data slot interval, and thus only a slight increase in the measured BEP (relative to the $P_J/P_S = 15$ dB case, for example) resulted in this case. The slower response for $P_J/P_S = 6$ dB, 3 dB, and 0 dB, exhibited by both the output SNR in Figures 77 and 78 and the desired signal to interference ratio in Figures 79 and 80, caused the measured BEP, which represents an average over the interval $T_S < t < 7 T_S$, to increase. In order to show that an inadequate output desired signal to interference ratio was the predominant source of degradation, rather than limiter suppression due to a low output signal to thermal noise ratio, the BEP was measured under conditions identical to those in Figure 76 except that the loop gain (α) was doubled. Since this corresponds to doubling the adaptation rate, Figures 78 and 80 can be applied by doubling the adaptation time (i.e., the end of the preamble corresponds to an adaptation interval of two rather than one). The measured BEP, shown in Figure 81, was considerably lower when P_J was near P_S compared to the measurements in Figure 76. Because the output desired signal to interference ratio increases significantly for $t > T_S$ when the adaptation rate is doubled, whereas the output SNR does not, it is concluded that the higher BEP in Figure 76 was primarily caused by an inadequate desired signal to interference ratio. This conclusion is also in accord with the result in Figure 75, which shows that the BEP is high when the ratio approaches 0 dB. It should be noted that the average BEP would have been significantly higher in Figure 76 -- up to at most a factor of eight -- if only one data slot had been used to convey data. The BEP would have also increased in Figure 81, but to a much lesser extent since the output desired signal to interference ratio is less than -5.5 dB for $t > T_S$.

- (2) Better performance was obtained (for $\alpha \Delta t P_I$ small) in Figure 75 compared to Figure 76 because the magnitude of the initial weight was smaller. (Note that E_b/N_0 , measured in the absence of interference and with the array continuously adapting, is 1 dB lower in Figure 75.) This result is also in accord with the calculated results of Figures 77-80. The reason for the improved performance is that the error introduced by the initial conditions in Figure 75 was smaller both initially and during the weight transient. For the purposes of comparison, calculated values of the output SNR and the

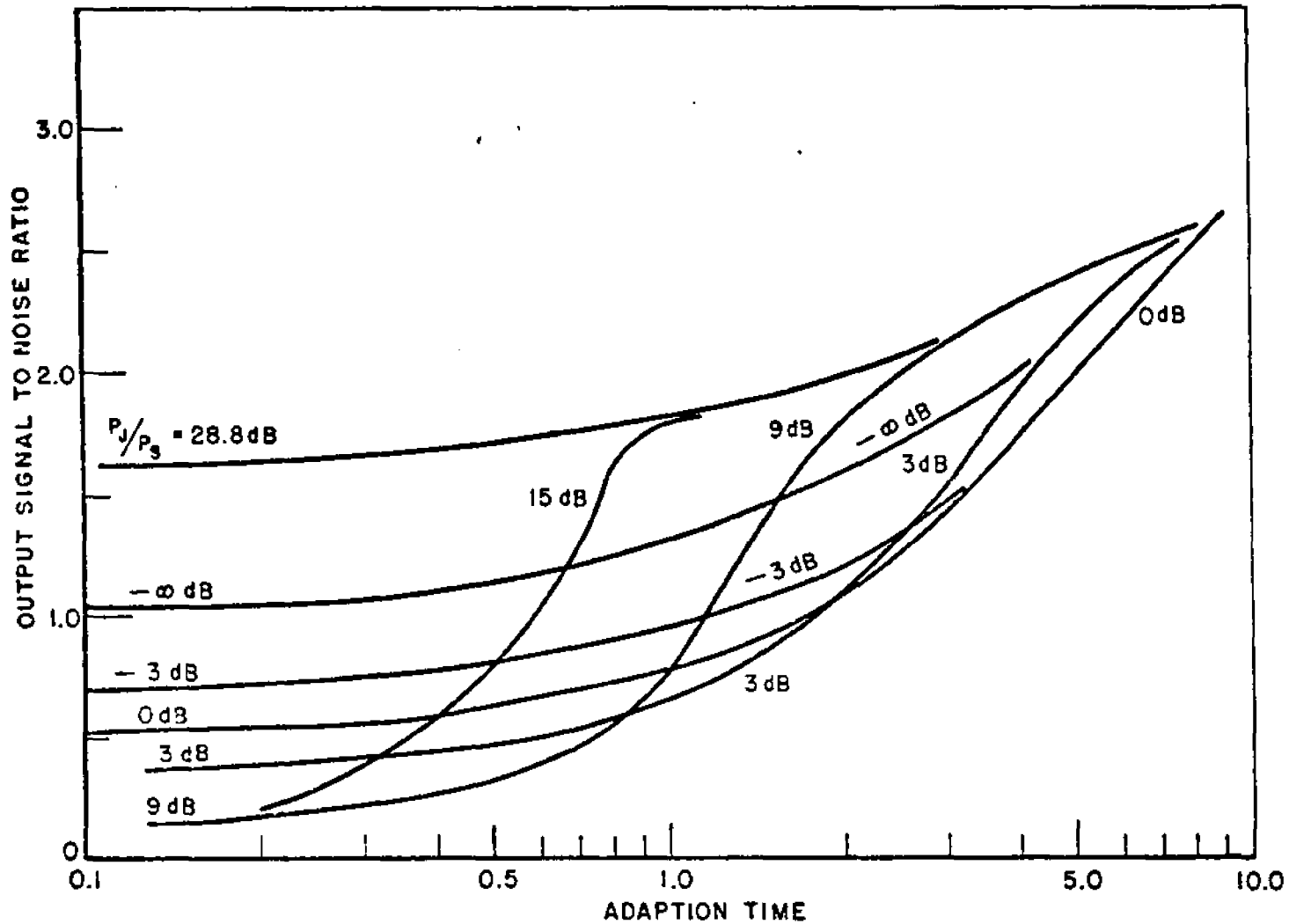


Figure 78--The output signal-to-noise ratio versus the normalized adaption time for several values of P_j/P_s under the same conditions as in Figure 76.

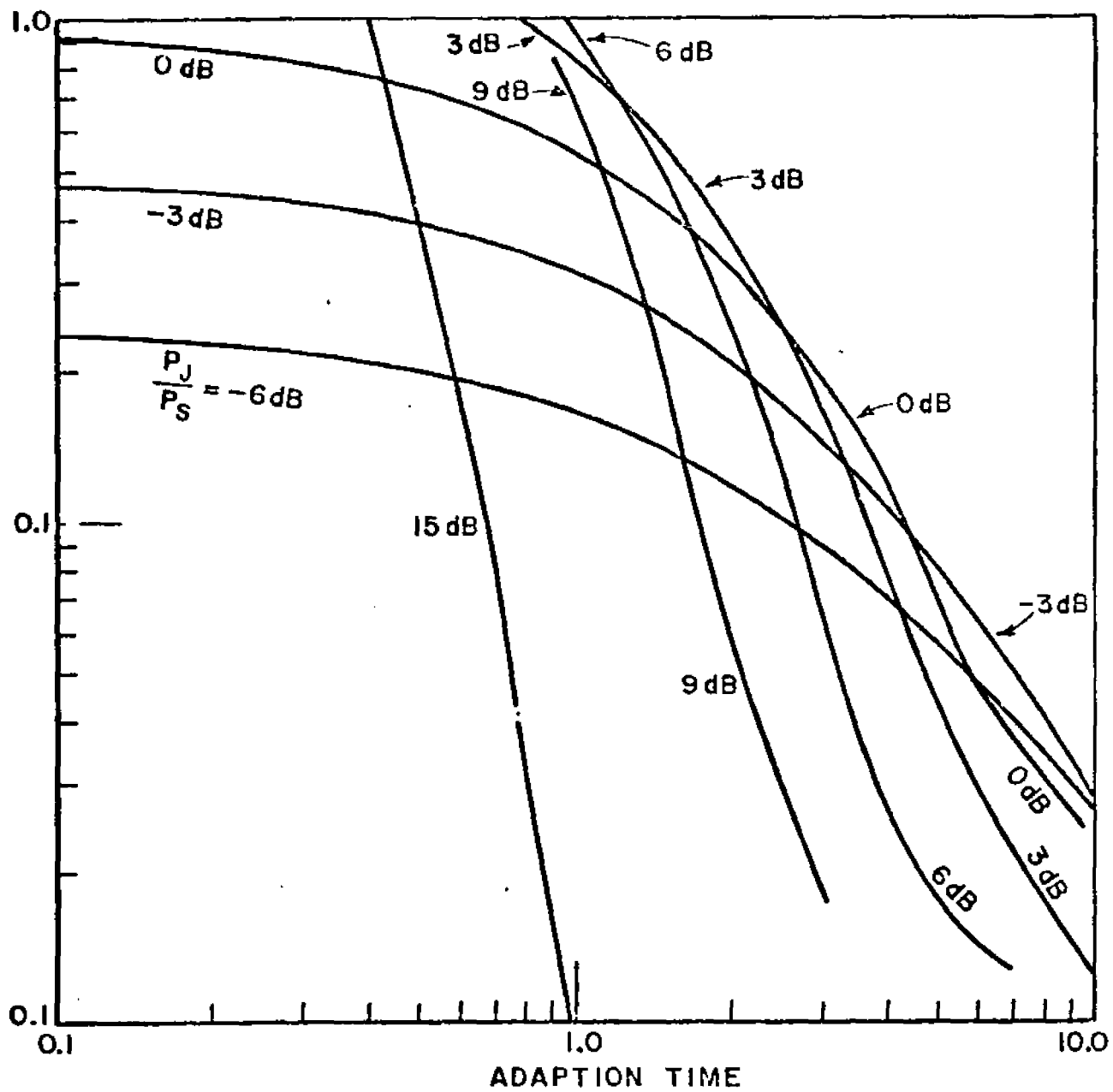


Figure 80--The output signal-to-interference ratio versus the normalized adaption time for several values of P_J/P_S under the same conditions as in Figure 76.

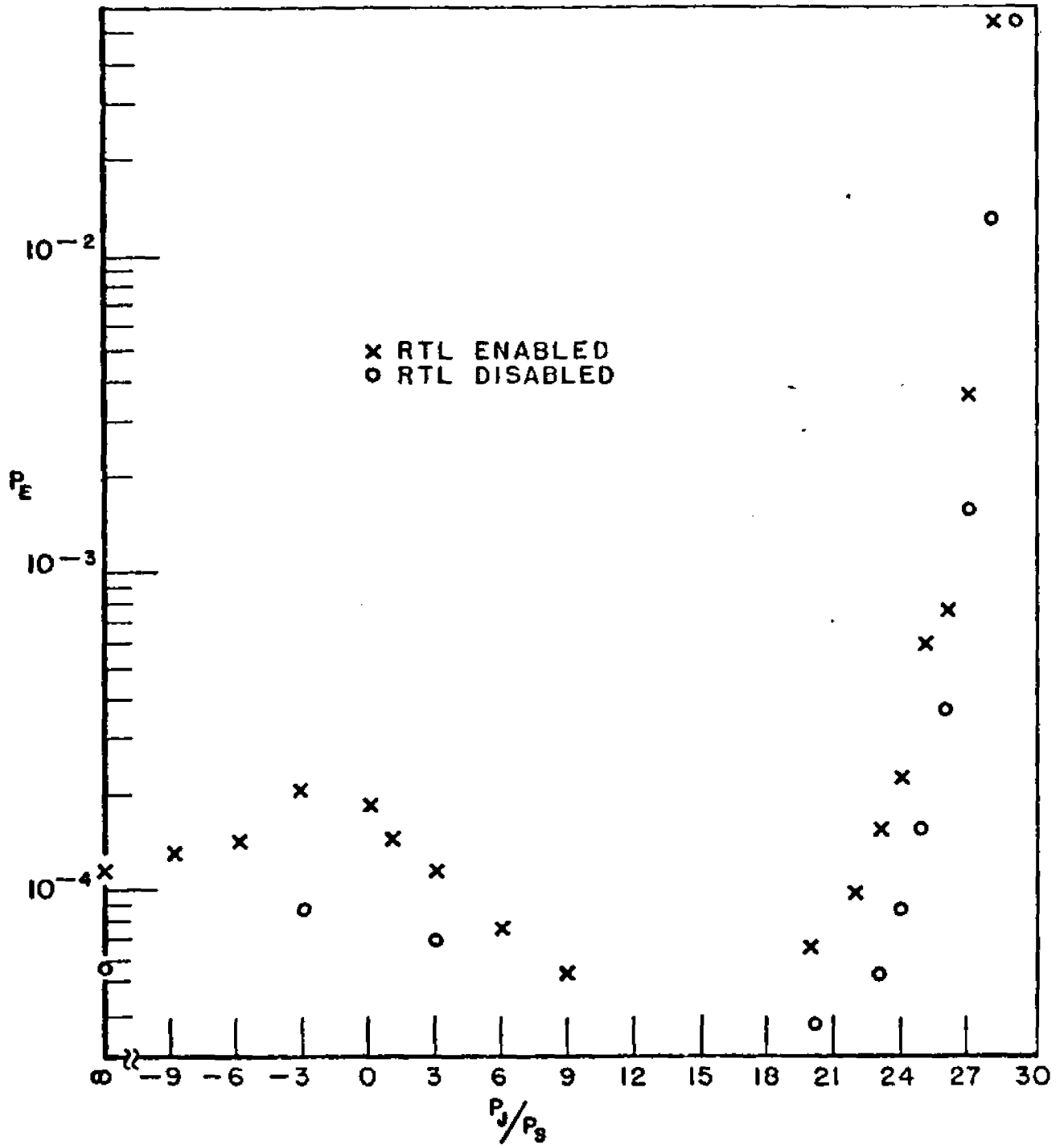


Figure 81--Performance of the experimental system versus the input interference-to-signal ratio with and without the range tracking loop enabled. Input desired signal level = 3.5 mv rms; $P'_S/\sigma^2 = 0$ dB. Other conditions as in Figure 75.

desired signal to interference ratio are shown in Figures 82 and 83 for the two cases $w(t_0) = [0]$ and $w^+(t_0) = \beta R_{xd}$, where β was selected so that the output desired level equalled the reference signal level when the weights were initialized. The results show that some improvement in performance (under worst-case values of P_J/P_S) would be obtained by initializing the weights to zero (assuming the effects of weight jitter are negligible). Initializing the weights to the desired signal DOA, however, would have resulted in significantly improved performance. Moreover, the output desired signal level is nearly as large as the reference signal level in this case, so that higher levels of excess noise could be tolerated during the transients.

Figure 81 also shows BEP measurements conducted with the error between the reference signal and the transmit time bases set equal to zero (RTL disabled). The comparative results indicate some improvement in performance with the RTL disabled, although the difference is small in terms of P_J/P_S under high level interference conditions. Under lower level interference condition ($\alpha \Delta t P_I \ll 1$), timing accuracy achieved by the RTL depended primarily on the signal-to-noise ratio of the signal received (at the TDMA modem) during the range tracking pulse. Since the preamble to the range tracking pulse was nearly two time-slots in duration, the signal-to-noise ratio was higher during the range tracking pulse than during the first data slot in Figures 75, 76, and 81. In particular, the ratio of the NCS signal power and the range tracking signal power at the bandpass limiter's output was less than approximately 3 dB, which was well within the 6 dB range of the loss of lock algorithm. Thus, no difficulties in acquiring or maintaining transmit time base synchronization were encountered in the tests for $\alpha \Delta t P_I$ small.

The result in Figure 76 has shown that the adaptive array is capable of providing greater than 29 dB of interference protection for $\psi = 60^\circ$ when the interfering signal was c.w. and centered on the desired signal carrier frequency. Based on the steady-state measurements presented in section C, higher levels of interference could be effectively processed if the interfering signal is wider band.* Also, BEP performance would improve for larger values of the angular separation parameter ψ . The theory predicts that system performance degrades, however, as the angular separation is reduced. Suppose, for example, that the initial conditions and the input desired signal and thermal noise powers are the same as in Figure 76, but the angular separation between the desired

*The interfering signal bandwidth must still be smaller than the i.f. amplifier bandwidths (10 MHz).

and interfering signals is reduced to $30^\circ/\text{element}$. One effect of the closer angular separation is to reduce the optimum output signal-to-noise ratio by 4.3 dB when P_J/P_S is large. A second effect is to reduce the rate at which the desired signal power converges to its optimum value. The third effect is to reduce to output desired signal power under transient as well as steady-state conditions. These effects can combine to significantly degrade system performance. In order to obtain performance comparable to Figure 76 for $\psi = 30^\circ$ under high loop gain conditions, the desired signal level at the end of the preamble interval must be increased by about 4 dB and the input desired signal to thermal noise ratio must be about 4.3 dB smaller. Assuming the same input desired signal power as in Figure 76, these requirements are satisfied if the magnitude of the initial weight vector is increased 4 dB, and the element thermal noise is decreased 4.3 dB, respectively. The calculated response of the output SNR and the output desired signal to interference ratio is shown in Figures 84 and 85 for $\psi = 30^\circ$ under these modified conditions. Comparing these results with Figures 78 and 80 shows that system performance for $\psi = 30^\circ$ would be poor relative to the $\psi = 60^\circ$ case, even though the element thermal noise power is 4.3 dB smaller. However, these results also indicate that the BEP would be lower (assuming $\alpha \Delta t P_i$ small) than the measured results in Figure 76 if the loop gain parameter α is increased by only a factor of two. Moreover, the effects of excess noise on performance under higher loop gain conditions would not be significantly different during weight transients since the output desired signal power is nearly as large in the $\psi = 30^\circ$ case as in the tests of Figure 76. Therefore, based on the c.w. measurements of Figure 76 and on the calculated results in Figures 78, 80, 84, and 85, it is concluded that system performance for a close angular separation of 30° per element would be comparable or better than the measured performance in Figure 76 for $P_J/P_S \approx 24$ dB if (1) the per element thermal noise power is 4.3 dB smaller, (2) the magnitude of the initial weight is 4 dB larger, and (3) the loop gain is increased by 3 dB. With these system parameters fixed, it is easily shown that better performance would be obtained in all cases if $\psi > 30^\circ$ or if the input desired signal power is, i.e., worst-case system performance occurs at the closest angular separation and the minimum input desired power.

The above results and discussions related to interference rejection capabilities of the SS/TDMA system may appear inappropriate in that AGC can be used to eliminate slow response to a lower level interfering signal, thereby significantly (by orders of magnitude) increasing the P_J/P_S capability. This technique can indeed be used to improve system performance provided only one interfering source is present in the environment. The

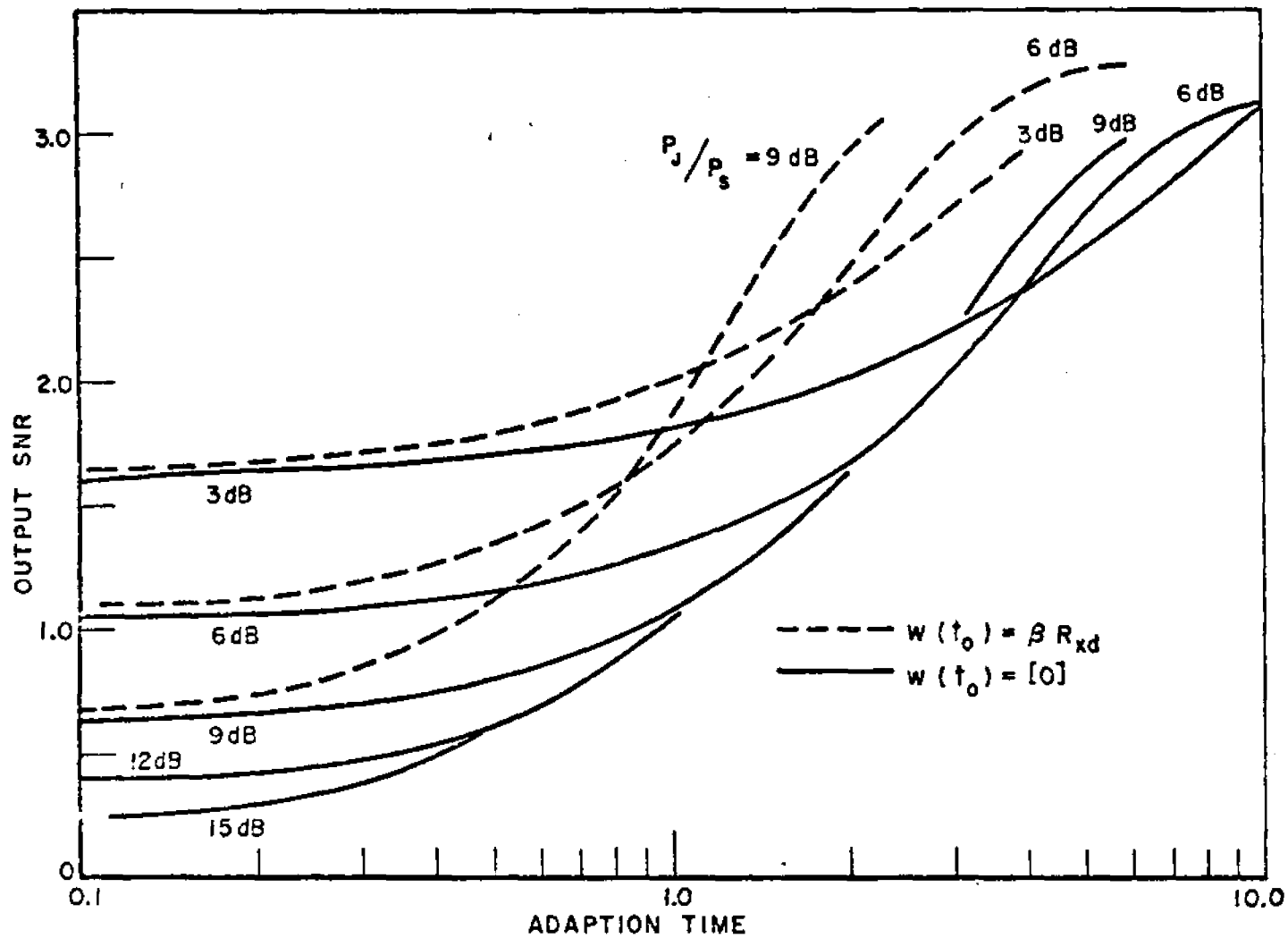


Figure 82--The output signal-to-noise ratio versus the normalized adaption time for $w(t_0) = [0]$ and $w(t_0) = (3.4 + j 3.4) [1, 1, 1, 1] = \beta R_{xd}$. Other conditions as in Figure 76.

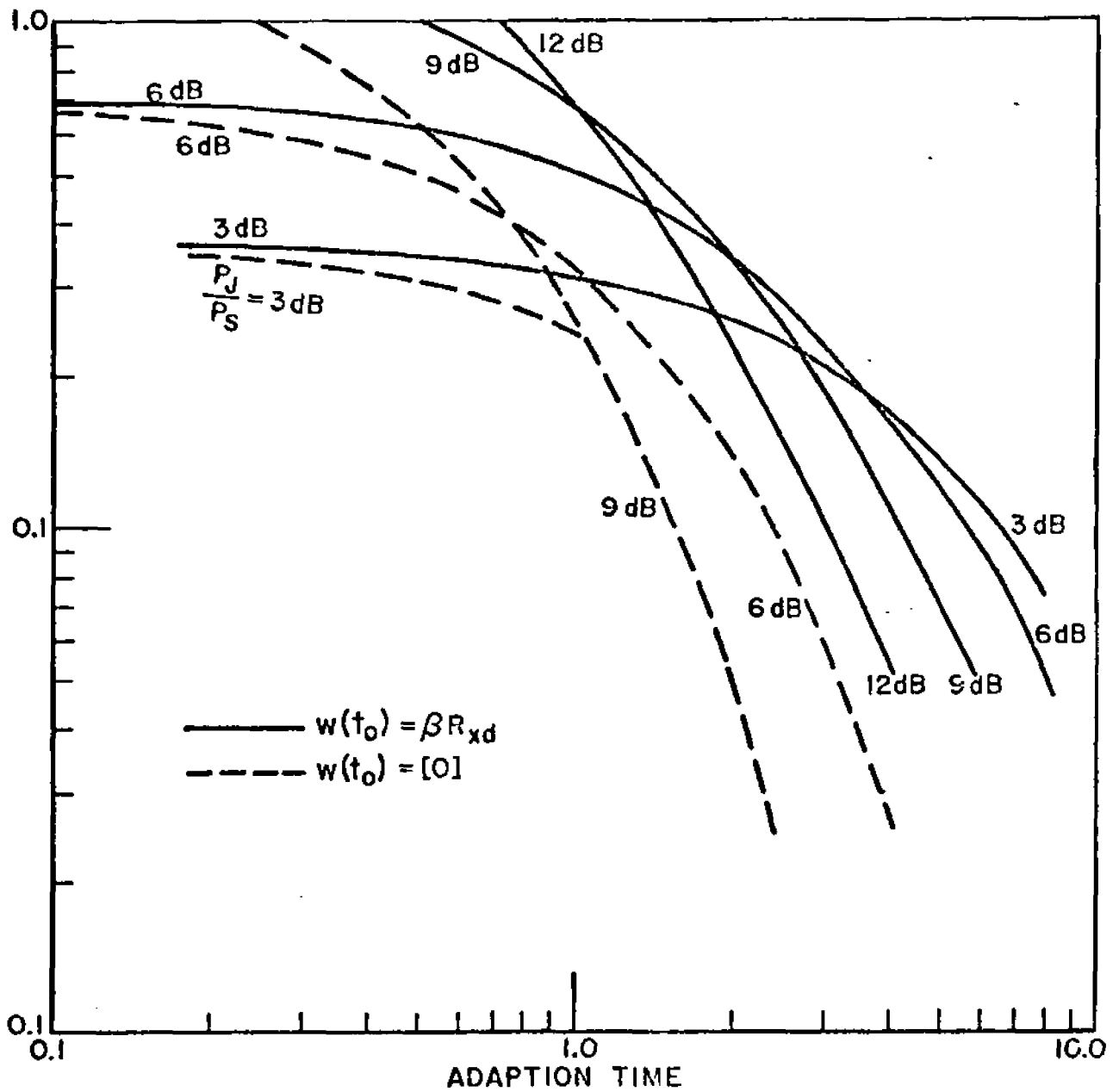


Figure 83--The output signal-to-interference ratio versus the normalized adaption time for $w(t_0) = [0]$ and $w(t_0) = 3.4 + j 3.4) [1, 1, 1, 1] = \beta R_{xd}$. Other conditions as in Figure 76.

presence of two or more interfering sources, however, alters the eigenvectors and eigenvalues of the input covariance matrix. Depending on the relative magnitude and angular separation of the interfering sources, one of the eigenvalues can be small relative to λ_{\max} , yet large (or of the same order of magnitude) relative to the eigenvalue associated with beamforming to the desired signal. Obviously, response to this smaller eigenvalue cannot be improved beyond a certain point as determined by the constraint $\alpha \Delta t P_I \approx \alpha \Delta t \lambda_{\max} \approx 1$. The effect of the longer time constant associated with this smaller eigenvalue on system performance is represented by performance obtained in Figures 75, 76, and 81 for smaller values of P_J/P_S (in the range -6 dB to 12 dB, for example). That system performance degraded for -6 dB $\approx P_J/P_S \approx 6$ dB indicates that the possible presence of a small eigenvalue (other than the eigenvalues associated with beamforming to desired signal and minimizing the output thermal noise power) could not be ignored in evaluating overall system performance.

In the present application, the signal environment is unknown a priori. Consequently, it is unrealistic to assume that an "optimal" initial weight can be used in all cases. One approach would be to determine an initial weight which yields good performance for most expected signaling situations in a given application. This could be rather tedious and perhaps impossible when the array size is large and when the array is subjected to a large number of interfering sources. A more feasible approach would be to estimate the desired signal DOA and use the estimate to provide desired signal discrimination within the feedback loop (see Figure 6). The ratio of excess noise to the output desired signal power could thus be eliminated from consideration, i.e., the initial weights could be set to zero. The weights could also be initialized to the desired signal DOA, which was shown in Chapter IV and in Figures 84 and 85 to further improve the convergence properties of the LMS algorithm. A subsystem for performing the DOA estimate could readily be implemented in the present system with only a moderate increase in circuit complexity by applying a reference signal to the error signal leg of the error by input signal multipliers and then averaging the error multiplier's output (after it has been down-converting to baseband) using an integrator or low-pass filter. This particular method of obtaining the estimate has the added advantage that the effects of non-ideal circuits and small phase errors within the error multipliers and down-converters are compensated. The reference signal could be generated autonomously within the satellite during the preamble -- even during the pre-lockup phase. The results of the analysis in Chapter V have shown that an adequate estimate of the DOA can be obtained in a relatively short interval of time (relative to the convergence rate of the LMS algorithm, for example), when the interfering signals approximate zero-mean Gaussian processes. It would appear that this estimate could be obtained

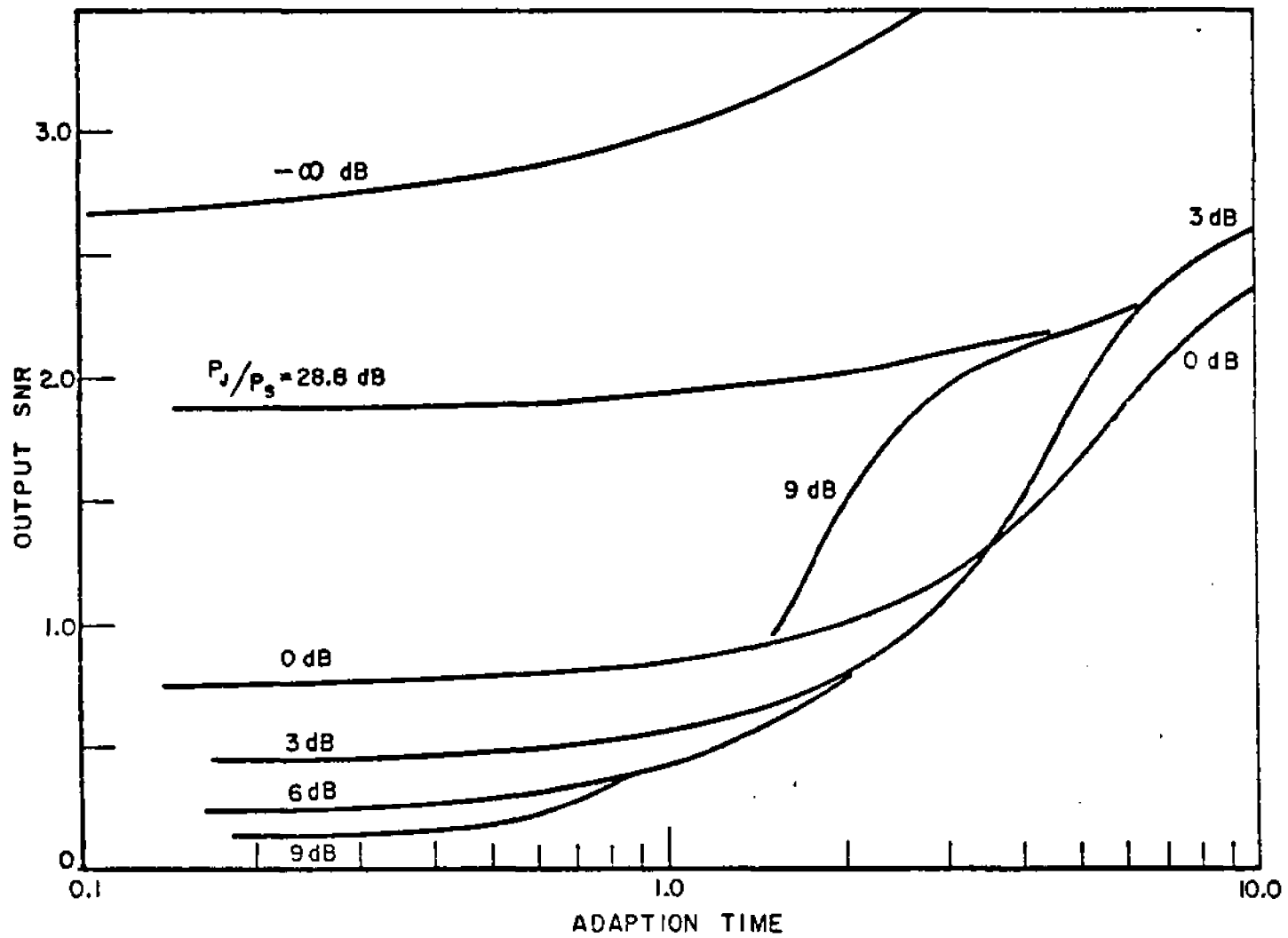


Figure 84--The output signal-to-noise ratio versus the normalized adaption time for $\psi = 30^\circ$. See text for parameter values.

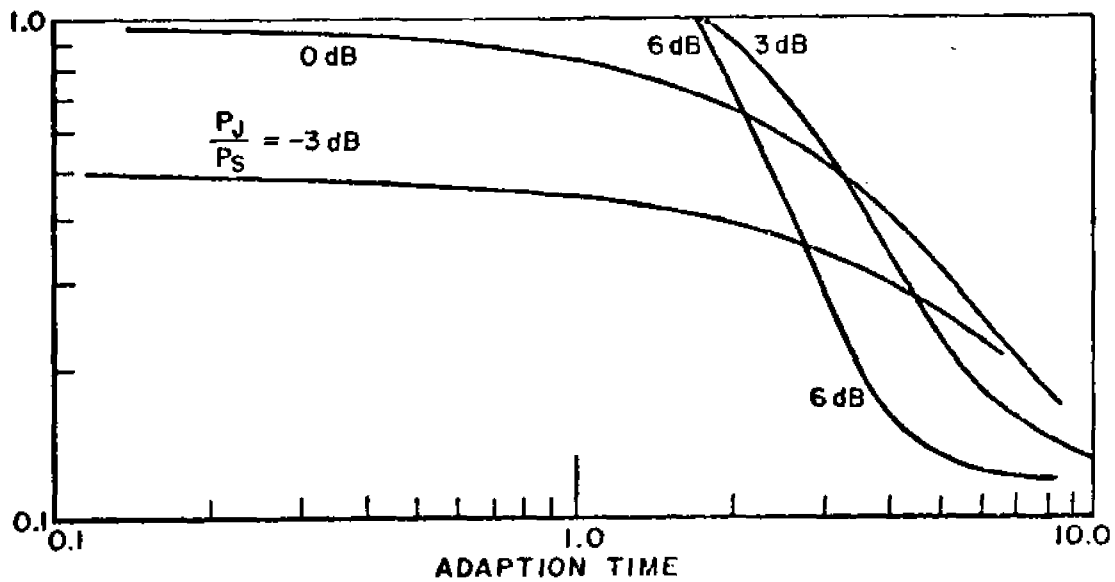


Figure 85--The output signal-to-interference ratio versus the normalized adaption time for $\psi = 30^\circ$. See text for parameter values.

rapidly in c.w. interference environments as well, although additional studies would be required to confirm this. Thus, only a portion of the preamble may be required to perform the estimate, with the remaining portion used for adaption. Alternatively, an interval preceding the preamble could be allocated for performing the estimate by utilizing a different PN code structure to distinguish the desired signal from other desired signals. Estimating the DOA has at least one additional advantage. In systems where it is appropriate to assume a constant desired signal DOA, the DOA estimate can be used to provide desired signal discrimination during data slots, thus eliminating the need for a waveform processed reference signal and reference delay compensation. In view of these considerations, further studies of the DOA estimation technique are indicated.

CHAPTER VII

SUMMARY AND CONCLUSIONS

The purpose of this research was to determine the characteristics and limitations of the transient response of adaptive arrays in coded communications system applications. To this end, the response of an adaptive array which employs the LMS algorithm to adjust the weighting coefficients was evaluated both analytically and experimentally. An analysis of the convergence properties of the direct matrix inversion algorithm was also performed in order to establish a basis for comparing LMS algorithm response with the response of an algorithm in which optimal adaptive processor parameters are directly computed.

In the analysis, loop parameters which result in maximizing the convergence rate of the LMS algorithm in a stationary signal environment were determined. Maximizing the rate of convergence in a stationary signal environment was shown to maximize the rate at which the array can respond to a time-varying signal environment (e.g., due to pulsed desired signals in a TDMA communications system). Initially, an idealized model of the LMS algorithm was analyzed under the assumption that the effects of jitter in the array weighting coefficients may be neglected to a first order approximation. This assumption is valid when the loop response bandwidth is much narrower than the input signal bandwidth. The rate at which the weights converge to their optimum values was shown to be proportional to the product of the loop gain constant and the eigenvalues of the input covariance matrix. This implies that the adaption interval required for the weights to converge is long when one or more of the eigenvalues is very small. The effect of this show convergence rate on adaptive array performance can be minimized by proper selection of the initial weights. Initializing the weights to the desired signal direction of arrival vector was shown to improve the output signal-to-noise ratio during transients compared to performance when all the initial weights except one were set equal to zero (omnidirectional case). Some improvement was also noted for the all zero initial condition. The next step in the analysis consisted of modifying the idealized model to include the effects of weight jitter. The effects of weight jitter on the steady-state performance of both the analog and digital (sampled data) approaches for implementing the LMS algorithm were considered in the analysis. Two approaches for distinguishing between the desired signals and interfering signals -- using an ideal reference signal or an accurate estimate of the desired signal direction of arrival vector -- were also considered. The excess noise power at the array output due to weight jitter was used as one measure of

performance. The excess noise power was shown to increase very abruptly when the loop response bandwidth exceeds approximately two-tenths of the input signal bandwidth in the analog LMS algorithm and approximately one-tenth in the digital LMS algorithm. The loop response bandwidth, which is approximately proportional to the product of the loop gain constant α and the total input power P_I , must not exceed these values for proper array operation. The upper bound on αP_I implies a constraint on the maximum ratio of input interfering signal power to desired signal power which can be effectively processed. The excess noise power due to weight jitter was also shown to depend on the parameter T_0 and the method used to distinguish the desired signal from undesired signals (see Equations (139), (158), and (206)). The parameter T_0 represents the optimum output signal-to-noise ratio which can be achieved with an adaptive array in a given signal environment, and therefore reflects the dependence of the excess noise power on the input signal levels, their relative angles of arrival, and the array geometry.

It was shown by analysis that weight jitter in the digital LMS algorithm does not significantly increase random fluctuations of the desired signal phase in most cases of interest: thus, an accurate estimate of the carrier phase required in coherent detection, e.g., PSK detection, can be obtained when the weights are near their steady-state solutions. Some caution must be exercised, however, in extrapolating this result to array transient conditions. In this case, it may not be possible to acquire and/or maintain carrier phase tracking at all, since the output desired signal can undergo radical phase and amplitude fluctuations during weight transients. It is partly for this reason that differential (DPSK) detection and envelope detection techniques, such as those employed in the prototype TDMA/adaptive array system for detecting data and establishing time base synchronization, are recommended in adaptive array applications. An expression indicating the effects of weight jitter on the performance of a PSK detector (with the weights near their steady-state solutions) was derived for the case of the digital LMS algorithm. The results indicated that increasing the ratio of the code rate to the data rate (spectrum-spreading factor) by increasing the code rate permitted an increased rate of convergence and also reduced the level of degradation due to weight jitter. This result was shown to apply as well to differential detection if appropriate (reasonable) conditions are satisfied.

In communications systems, desired signal characteristics (e.g., an ideal reference signal) are generally presumed known a priori without assuming prior knowledge of the angle-of-arrival. In some cases of interest, however, it was shown that the performance obtained with the LMS algorithm can be improved if an accurate estimate of the desired signal direction of arrival vector, rather than an ideal reference signal, is used within the feedback loop to discriminate between desired and undesired signals. A procedure for estimating the desired signal direction of arrival vector, based on

a maximum likelihood principle, was investigated analytically under the assumption that an ideal reference signal is available at the array processor. The results showed that an adequate estimate can be obtained within a time interval which is short compared to the adaption time required for LMS algorithm convergence. Therefore, with a small percentage increase in processing time, the desired signal direction of arrival vector can be estimated and used to initialize the weights and/or provide desired signal discrimination within the feedback loop, thereby improving adaptive array performance.

A procedure for estimating the input signal covariance matrix was also studied. This estimate, together with the estimate of the desired signal direction of arrival vector, formed a basis for implementing the direct matrix inversion algorithm mentioned previously. The direct matrix inversion algorithm differs from the LMS algorithm in that the array weights are computed directly from these estimates. The analysis of the convergence properties of the direct matrix inversion algorithm therefore represented a problem in estimation rather than feedback control theory. The rate at which the output signal-to-noise ratio converges to its optimum value was found to depend on the parameter T_0 , but does not depend explicitly on the eigenvalues of the covariance matrix as in the case of the LMS algorithm. A comparison with the LMS algorithm showed that the direct matrix inversion algorithm generally converges much more rapidly, particularly when the spread in eigenvalues is large (i.e., when high-level interfering signals are incident on the array). However, the higher convergence rate afforded in theory by the direct matrix inversion algorithm is difficult if not impossible to achieve in practice since the required digital computer speeds are beyond present technological capabilities in all but very narrowband, small array size applications. In particular, the LMS algorithm implementation described herein (Chapter IV) can achieve much higher rates of response in practice than could have been achieved with the direct matrix inversion algorithm. The LMS algorithm has additional advantages in that it is relatively simple to implement and it tends to compensate for circuit imperfections (refer to the analysis of the effects of circuit imperfections on LMS algorithm performance presented in Chapter VI-C). Although the comparison between the direct matrix inversion and LMS algorithms presented herein are based in theory rather than practice, applications of the "estimation" algorithms are expected to broaden with increased computer speeds, lower cost circuit components, and the further development of algorithms which solve some of the difficulties encountered when implementing the direct matrix inversion algorithm (e.g., the recursive algorithms[34]).

Experimental tests were conducted to evaluate the accuracy of the approximate analytical results and to demonstrate more conclusively that adaptive arrays can be utilized to suppress undesired signals in coded communications systems and TDMA communications

systems in particular. The experimental system consisted of a four element IF implementation of an adaptive array and a processor simulating a band-limiting satellite repeater. This adaptive array/satellite simulator, together with the prototype TDMA modem, was used to simulate a TDMA/adaptive array satellite communication system. To achieve the real-time adaption rates required, the analog LMS algorithm was employed. The reference signal was generated by waveform-processing the array output signal, which permitted array adaption to occur simultaneously with data reception.

Initial experimental tests were conducted with continuous received signals (i.e., the signals received at the array processor had constant power levels) and with the weights near their steady-state solutions. Among the results presented, it was shown that the experimental adaptive array suppresses a c.w. interfering signal 43 dB larger than the desired signal by more than 70 dB and simultaneously forms a beam on a properly-coded, properly-timed desired signal. An analysis indicated that a maximum interference to signal ratio of up to 60 dB could be accommodated with the present equipment by an appropriate choice of loop parameters. Performance of the system was further evaluated by conducting bit error probability (BEP) measurements on the differential detector contained within the TDMA modem. The experimental performance was shown to agree closely with the corresponding analytical results when the effects of control loop noise were negligible. A large increase in the measured BEP occurred with high-level, wideband (~ 10 MHz) interference as a result of mismatched bandpass characteristics of the IF amplifiers preceding each weight control. Basically, this degradation occurred because the interfering signal could not be adequately nulled over its full bandwidth by simply forming a linear combination of the input signals. Performance under wideband interference conditions could be greatly improved if a reasonable attempt is made to match the IF bandpass characteristics. This is an area recommended for future study. Additional experiments were conducted to evaluate the effects of control loop noise on system performance with the weights near their steady-state values. It was shown that the analytical results can be used to establish an upper bound on the level of degradation caused by weight hitter when the interfering signal is c.w. or wideband.

Finally, BEP measurements were conducted under conditions simulating the TDMA pulsed desired signal format. In order to allow for adaption prior to the transmission of data, each desired signal pulse transmitted from a TDMA modem contained a preamble of one time-slot duration in which a known code was transmitted. Adaption was initiated at the beginning of the preamble and continued during the transmission of data. With an initially omnidirectional pattern, it was shown that time base synchronization could be successfully established and an acceptable bit error probability obtained even when the level of a c.w. interfering signal centered on the desired

.....
signal carrier frequency exceeded the input signal power by 30 dB. Higher levels of interference could have been effectively suppressed if (1) the preamble adaption interval were increased, (2) the code rate were increased, (3) the input desired signal-to-thermal noise were higher, and/or (4) a more favorable initial pattern were selected. The level of suppression was also shown to depend on the angular separation between the desired signal and the interfering signal.

In view of the fact that both the analytical and experimental results indicated high levels of excess noise due to weight jitter when the loop bandwidth approached one- or two-tenths of the input signal bandwidth, an additional subsystem may be required to control the loop parameters. Utilizing AGC at each antenna element was proposed as a method for controlling the loop bandwidth which is relatively easy to implement.

It is concluded that an adaptive array can provide a significant capability for suppressing undesired signals in coded communications systems in general and TDMA systems in particular, and that the analytical and experimental results presented in this study can be used to design such systems.

APPENDIX I

Each term in Equation (118) is evaluated in this appendix using the properties of complex Gaussian processes. From Equation (102), the first term in Equation (118) may be written*

$$E[R_{\Delta j} R_{\Delta \ell}] = E \{ u_{\ell}^{\dagger} \tilde{r} \tilde{r}^{\dagger} \tilde{u}_j \} = |\tilde{r}|^2 M_{j\ell} \quad (I-1)$$

The last step follows from the assumption that the complex envelope of $\tilde{Y}(t)$ [and $\tilde{Z}(t)$] is constant. The procedure for evaluating the second term in Equation (118) is much more involved. Before proceeding, it will be convenient to express ϕ in the form

$$\begin{aligned} \phi(t) &\equiv \underline{\tilde{x}}(t) \underline{\tilde{x}}^{\dagger}(t) - K_x & (I-2) \\ &= [\underline{\tilde{u}}(t) + \underline{\tilde{s}}(t)] [\underline{\tilde{u}}(t) + \underline{\tilde{s}}(t)]^{\dagger} - M - \underline{s} \underline{s}^{\dagger} \\ &= \underline{\tilde{u}}(t) \underline{\tilde{u}}^{\dagger}(t) + \underline{\tilde{s}}(t) \underline{\tilde{u}}^{\dagger}(t) + \underline{\tilde{u}}(t) \underline{\tilde{s}}^{\dagger}(t) - M \end{aligned}$$

The last step follows from the relation $\underline{\tilde{s}}(t) \underline{\tilde{s}}^{\dagger}(t) = \underline{s} \underline{s}^{\dagger}$. The j th component of the vector $\phi P^{-1} y_{\Delta}$ is given by

$$\begin{aligned} [\phi P^{-1} y]_j &= \sum_{i=1}^m \phi_{ji} [P^{-1} y_{\Delta}]_i & (I-3) \\ &= \sum_{i=1}^m \sum_{k=1}^m \phi_{ji} [P^{-1}]_{ik} y_{k\Delta} \end{aligned}$$

Thus, the second term in Equation (118) is expressed as

*The explicit time dependence of variables will be omitted from the notation except when it is required for clarity.

$$\begin{aligned}
& E \{ (\phi P^{-1} y)_j (\phi P^{-1} y)_\ell^\dagger \} \quad (I-4) \\
& = E \left\{ \sum_{i=1}^m \sum_{k=1}^m \phi_{ji} (P^{-1})_{ik} y_{k\Delta} \sum_{f=1}^m \sum_{g=1}^m \phi_{f\ell} P_{gf} y_{g\Delta}^\dagger \right\} \\
& = \sum_{f=1}^m \sum_{g=1}^m \sum_{i=1}^m \sum_{k=1}^m [E(\phi_{ji} \phi_{f\ell})] (P^{-1})_{ik} (P)_{gf} \\
& \quad \cdot E(y_{k\Delta} y_{g\Delta}^\dagger) .
\end{aligned}$$

The last step follows from the independence of the processes ϕ and y_Δ at the sampling instants. The cross-correlation of the j th component of $\phi(t)$ and the f th component of $\phi(t)$ is given by

$$\begin{aligned}
E[\phi_{ji} \phi_{f\ell}] & = E \{ [\tilde{u}_j \tilde{u}_i^\dagger + \tilde{s}_j \tilde{u}_i^\dagger + \tilde{u}_j \tilde{s}_i^\dagger - M_{ji}] \quad (I-5) \\
& \quad \cdot [\tilde{u}_f \tilde{u}_\ell^\dagger + \tilde{s}_f \tilde{u}_\ell^\dagger + \tilde{u}_f \tilde{s}_\ell^\dagger - M_{f\ell}] \quad .
\end{aligned}$$

From the assumption that the input signals are uncorrelated, and using the properties of zero-mean Gaussian processes [Equation (11)], Equation (I-5) reduces to

$$E[\phi_{ji} \phi_{f\ell}] = M_{fi} K_{x_{j\ell}} + M_{j\ell} s_f s_i^\dagger \quad (I-6)$$

Substituting Equation (I-6) into Equation (I-4) yields

$$\begin{aligned}
& E \{ (\phi P^{-1} y_\Delta)_j (\phi P^{-1} y_\Delta)_\ell^\dagger \} \quad (I-7) \\
& = K_{x_{j\ell}} E \{ y_\Delta^\dagger P M P^{-1} y_\Delta \} + M_{j\ell} E \{ y_\Delta^\dagger P \underline{s} \underline{s}^\dagger P^{-1} y_\Delta \} .
\end{aligned}$$

Using the same procedure, the third term in Equation (118) becomes

$$E \{ (\phi w_{\text{opt}})_j (\phi w_{\text{opt}})_\ell^\dagger \} = K_{x_{j\ell}} w_{\text{opt}}^\dagger M w_{\text{opt}} \quad (\text{I-8})$$

$$+ M_{j\ell} w_{\text{opt}}^\dagger \underline{S} \underline{S}^\dagger w_{\text{opt}} \quad .$$

The steps used to evaluate the fourth term in Equation (118) are as follows:

$$E \{ R_{\Delta j} (\phi w_{\text{opt}})_\ell^\dagger \} = E \left\{ \sum_{i=1}^m R_{\Delta j} \phi_{i\ell} w_{i\text{opt}} \right\} \quad (\text{I-9})$$

$$= E \left\{ \sum_{i=1}^m \tilde{u}_j r^\dagger [\tilde{u}_i \tilde{u}_\ell^\dagger + \tilde{u}_i \tilde{s}_\ell^\dagger + \tilde{s}_i \tilde{u}_\ell^\dagger - M_{i\ell}] w_{i\text{opt}} \right\}$$

$$= \sum_{i=1}^m \{ M_{j\ell} r^\dagger \tilde{s}_i w_{i\text{opt}} \}$$

$$= \sum_{i=1}^m M_{j\ell} (R_{xd})_i^\dagger w_{i\text{opt}}$$

$$= M_{j\ell} R_{xd}^\dagger w_{\text{opt}} \quad .$$

Similarly,

$$E \{ (\phi w_{\text{opt}})_j R_{\Delta \ell}^\dagger \} = M_{j\ell} w_{\text{opt}}^\dagger R_{xd} \quad . \quad (\text{I-10})$$

Substituting Equation (I-1) and Equations (I-6)-(I-10) into Equation (118) yields the final result

$$\begin{aligned}
E [C_j C_\ell^\dagger] &= |\tilde{r}|^2 M_{j\ell} + K_{x_{j\ell}} E [y_\Delta^\dagger P M P^{-1} y_\Delta] \quad (I-11) \\
&+ M_{j\ell} E [y_\Delta^\dagger P \underline{s} \underline{s}^\dagger P^{-1} y_\Delta] + K_{x_{j\ell}} w_{\text{opt}}^\dagger M w_{\text{opt}} \\
&+ M_{j\ell} w_{\text{opt}}^\dagger \underline{s} \underline{s}^\dagger w_{\text{opt}} - M_{j\ell} R_{\text{xd}}^\dagger w_{\text{opt}} - M_{j\ell} w_{\text{opt}}^\dagger R_{\text{xd}} \\
&= |\tilde{r}|^2 M_{j\ell} + K_{x_{j\ell}} E [y_\Delta^\dagger \Lambda y_\Delta] - s_j s_\ell^\dagger E (y_\Delta^\dagger P \underline{s} \underline{s}^\dagger P^{-1} y) \\
&+ K_{x_{j\ell}} w_{\text{opt}}^\dagger K_x w_{\text{opt}} - s_j s_\ell^\dagger w_{\text{opt}}^\dagger \underline{s} \underline{s}^\dagger w_{\text{opt}} \\
&- M_{j\ell} R_{\text{xd}}^\dagger w_{\text{opt}} - M_{j\ell} w_{\text{opt}}^\dagger R_{\text{xd}} \quad .
\end{aligned}$$

APPENDIX II

This appendix defines the expression $M^{-1/2}$, where M is an $m \times m$, positive definite, Hermitian matrix. Let P' represent the unitary transformation which diagonalizes M ; i.e.,

$$\begin{aligned} P' M P'^{-1} &= \Lambda' & (II-1) \\ P' M^{-1} P'^{-1} &= \Lambda'^{-1} \end{aligned}$$

The diagonal elements of Λ'^{-1} are real and non-negative. Therefore, the square root of each element is defined. If $A^2 = \Lambda'^{-1}$, then a solution for the matrix A is given by

$$A = \Lambda'^{-1/2} \quad (II-2)$$

where $\Lambda'^{-1/2}$ is a diagonal matrix with the square root of the element of Λ'^{-1} as its elements. Define $M^{-1/2}$ as

$$M^{-1/2} = P'^{-1} \Lambda'^{-1/2} P' \quad (II-3)$$

It follows that

$$M^{-1/2\dagger} = M^{-1/2} \quad (II-4)$$

and that

$$\begin{aligned} M^{-1/2\dagger} M^{-1/2} &= M^{-1/2} M^{-1/2} = P'^{-1} \Lambda'^{-1/2} P' P'^{-1} \Lambda'^{-1/2} P' \\ &= P'^{-1} \Lambda'^{-1/2} \Lambda'^{-1/2} P' = P'^{-1} \Lambda'^{-1} P' = M^{-1}. \end{aligned} \quad (II-5)$$

APPENDIX III

The following specifications apply to the configuration of Fig. 20 when the 30 MHz gain adjustable amplifier is set to within one dB of maximum gain. All voltages are rms values unless otherwise noted.

Parameters	Measurement Point	Value	Units
<u>EACH III-PHASE OR QUADRATURE WEIGHT LOOP</u>			
Maximum recommended input signal level	A	650	mv. p-p
Two-tone third-order intermodulation intercept; Weight = 5 v	A	10	dBm
Ambient noise referred to input (B.W. = 10 MHz)		5×10^{-6}	volts
Stable input signal bandwidth	A	13.5	MHz
Gain; weight = 1 v	A to C	1.7	volts/volt
Gain @ weight = 1 v	A to B	12.5	$\frac{\text{d.c. volts}}{(\text{volts})^2}$
Feedback d.c. voltage	B	421	μvolts
2 mv p-p input, 200 mv p-p output	A,C		
d.c. voltage drift	B	15	$\mu\text{V}/\text{C}^\circ$
Baseband gain	B to J		
HRF		6.4×10^6	$(\text{sec})^{-1}$
LRF		8.0×10^5	$(\text{sec})^{-1}$
Loop gain constant (α)	B to B		
HRF		8.0×10^7	$(\text{sec})^{-1} (\text{volts})^{-2}$
LRF		1.0×10^7	$(\text{sec})^{-1} (\text{volts})^{-2}$
Weight time constant @ 600 mv p-p input	J		
HRF		2.8×10^{-7}	(sec)
LRF		2.2×10^{-6}	(sec)
Ratio of maximum output to minimum output versus weight control voltage (300 mv p-p c.w. signal applied at A)	C	32	dB
Range of weight voltages	J	± 10	d.c. volts
Range of reset voltages	J	± 5	d.c. volts
Minimum pulse duration required to reset	J,H		
HRF		2	μsec
LRF		20	μsec

Transition time to hold weights	J	1	μ sec
Transition time to shut off error feedback	E	200	nsec
Transition time to shut off reference signal	D	200	nsec
MAXIMUM OUTPUT VOLTAGE, no limiting in control loop (600 mv p-p signal applied at A, reference level = 0 v).	C	0.6	volts p-p

HT (FOUR IN-PHASE PLUS FOUR QUADRATURE) HEIGHTS IN LOOP

Minimum loop time constant (with 600 mv p-p input at A)	J		
HRF		68	nsec
LRF		550	nsec
Ratio of maximum output to minimum output (600 mv p-p c.w. signal applied at A)	C	>70	dB
Minimum input desired signal level required to obtain 200 mv p-p output	A	3	mv p-p
Minimum input signal level required for time constant of one time slot	A	17.2	mv p-p
Input signal level required for time constant of one code chip	A	207	mv p-p
Maximum linear output	C	3.5	volts p-p
Maximum stable loop bandwidth		2	MHz

Code rate		1.4016	Mbps
Data rate		87.6	Kbps
Time-slot length		103	μsec

Code rate		175.2	Kbps
Data rate		10.95	Kpbs
Time-slot length		0.83	m sec

REFERENCE NETWORK

Maximum output	D	350	mv p-p
Minimum input, limiting	C	10	mv p-p
Processing filters		Double tuned bandpass	
HRF 6 dB bandwidth		240	KHz
Envelope delay (HRF)	C to D	2.5	μsec
Processing gain to 70 MHz c.w. interfering signal (HRF)	C to D	8	dB
LRF 6 dB bandwidth		28	KHz
Envelope delay (LRF)	C to D	20	μsec
Processing gain to 70 MHz c.w. interfering signal (LRF)	C to D	8.3	dB

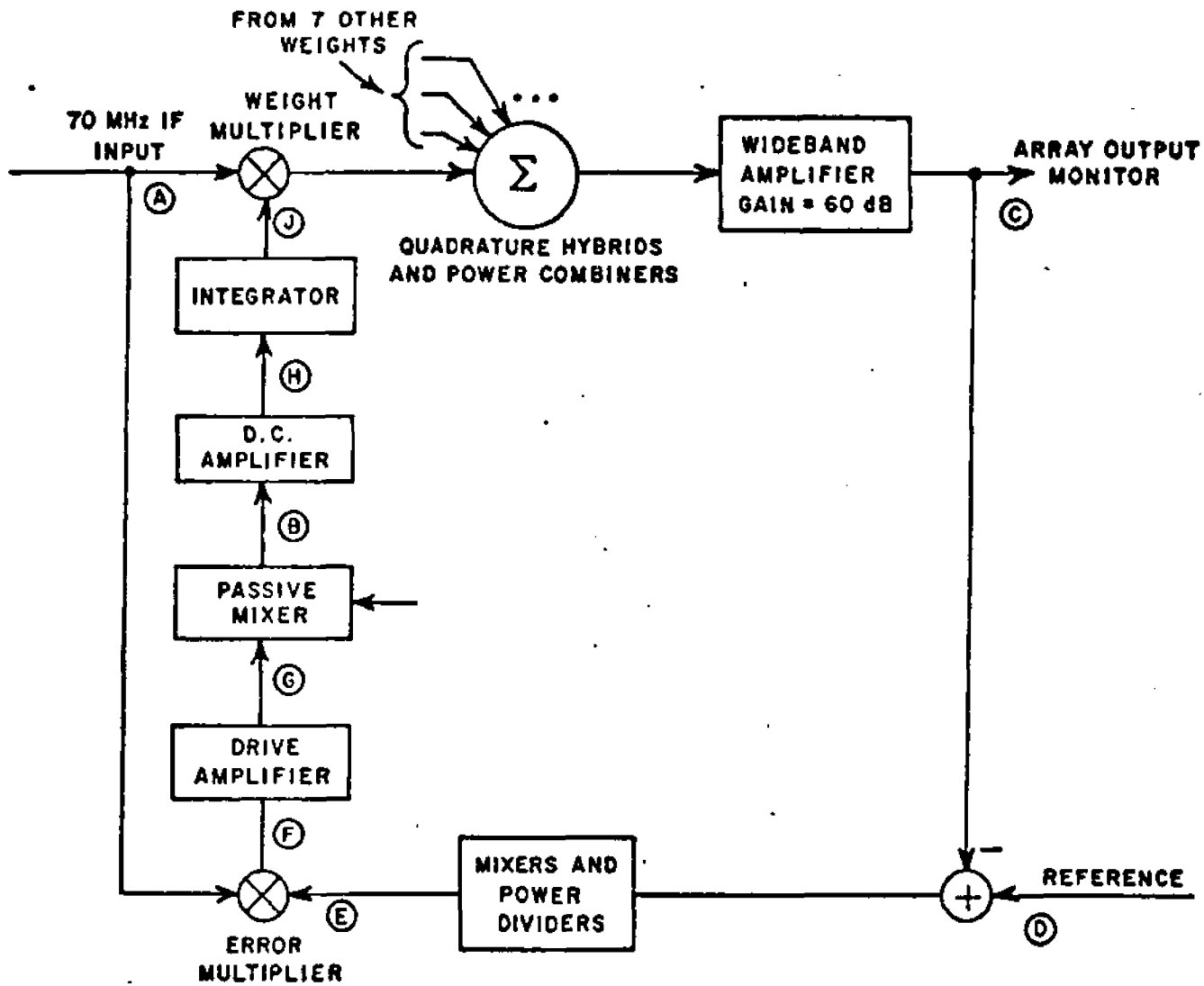


Figure 86. LMS loop showing points referenced in the specifications.

REFERENCES

1. Widrow, B., Mantev, P. E., Griffiths, L. J., and Goode, B. B., "Adaptive Antenna Systems," Proc. IEEE, 55 12 (December 1967), pp. 2143-2159.
2. Applebaum, S. P., "Adaptive Arrays," Special Projects Laboratory Report SPL-TR-66-1, August 1966, Syracuse University Research Corporation, Syracuse, N.Y.
3. Griffiths, L. H., "A Simple Adaptive Algorithm for Real-Time Processing in Antenna Arrays," Proc. IEEE, Vol. 57, pp. 1696-1704, Oct. 1969.
4. Brennan, L. E., Pugh, E. L., and Reed, I. S., "Control Loop Noise in Adaptive Array Antennas," IEEE Transactions, AES-7, 2 (March 1971), pp. 254.
5. Widrow, B., "Adaptive Filters I: Fundamentals," Systems Theory Laboratory, Stanford University, Stanford, Calif., Technical Report 6764-6, December 1966.
6. Reed, I. S., Mallet, J. D., and Brennan, L. E., "Rapid Convergence Rate in Adaptive Arrays," IEEE Trans. Aerospace and Electronic Systems, Vol. AES-10, pp. 853-863. November 1974.
7. Brennan, L. E., Mallet, J. D., and Reed, I. S., "Adaptive Radar Techniques," TSC-PD-096-2, Technology Service Corporation, Santa Monica, Calif., 27 April 1973.
8. Brennan, L. E., and Reed, I. S., "Theory of Adaptive Radar," IEEE Trans. AES, Vol. AES-9, March 1973.
9. McGuffin, A. L., "Adaptive Antenna Compatibility with Radar Signal Processing," Proc. of Array Antenna Conference, NELC, 22-24 February 1972.
10. Baird, C. A., Jr., Martin, G. P., Rassweiler, G. G., and Zahm, C. L., "Adaptive Processing for Antenna Arrays," Final Report, Radiation Systems Division, Melbourne, Florida, June 1972.
11. Zeger, A. E., and Abrams, B. S., "Interference Cancellation System for Sensors," Proc. Adaptive Antenna Workshop, Vol. I, 11-13 March 1974.

12. Riegler, R. L., and Compton, R. T., Jr., "An Adaptive Array for Interference Rejection," Report 2552-4, 16 February 1970, The Ohio State University ElectroScience Laboratory, Department of Electrical Engineering; prepared under Grant NGR-004-013 for National Aeronautics and Space Administration.
13. Huff, R. J., "TDMA Space Communications Systems: Concepts and Practical Techniques," November 1971.
14. Reinhard, K. L., "Adaptive Antenna Arrays for Coded Communication Systems," Report 3364-2, October 1973, The Ohio State University ElectroScience Laboratory, Department of Electrical Engineering; prepared under Contract F30602-72-C-0162 for Rome Air Development Center. (RADC-TR-74-102) (AD 782 395)
15. Reinhard, K. L., "Adaptive Antenna Arrays for Coded Communication Systems," Ph.D. Dissertation, The Ohio State University, 1973.
16. Compton, R. T., Jr., "Adaptive Antennas for Spread Spectrum Communication Systems," The Ohio State University ElectroScience Laboratory, Department of Electrical Engineering; prepared under Contract N00014-67-A-0232-0009 for Office of Naval Research, Arlington, Virginia.
17. Kolezar, G. E., "The Stochastic Properties of the Weights in an Adaptive Antenna Array," Ph.D. Dissertation, The Ohio State University, 1975.
18. Huff, R. J., "An Investigation of Time Division Multiple Access Space Communications System," Ph.D. Dissertation, The Ohio State University, 1969.
19. Huff, R. J., "Multifunction TDMA Techniques," Report 3364-3, August 1974, The Ohio State University ElectroScience Laboratory, Department of Electrical Engineering; prepared under Contract F30602-72-C-0162 for Rome Air Development Center. (RADC-TR-74-327) (AD/A004 196)
20. Miller, T. W., Caldecott, R., and Huff, R. J., "A Satellite Simulation with a TDMA-System Compatible Adaptive Array," Report 3364-4, January 1976, The Ohio State University ElectroScience Laboratory, Department of Electrical Engineering; prepared under Contract F30602-72-C-0162 for Rome Air Development Center.
21. Papoulis, A., Probability, Random Variables and Stochastic Processes, New York: McGraw-Hill, pp. 373-377, 1965.

22. Reed, I. S., "On a Moment Theorem for Complex Gaussian Processes," IEEE Trans. Information Theory, vol. IT-8, April 1962.
23. Friedman, B., Principles and Techniques of Applied Mathematics, New York: Wiley, pp. 6 and 7 and pp. 99-105, 1966.
24. Zielke, G., "Inversion of Modified Symmetric Matrices," Journal of the Association for Computing Machinery, vol. 15, no. 3, July 1968, pp. 402-408.
25. Baird, C. A., Jr., and Zahm, C. L., "Performance Criteria for Narrowband Array Processing," 1971 IEEE Conference on Decision and Control, Miami Beach, Florida, December 15-17, 1971.
26. Van Trees, H. L., Detection, Estimation, and Modulation Theory, Part I, New York: Wiley, pp. 65-67, 1968.
27. Van Trees, H. L., op. cit., pp. 96-97.
28. Hogg, R. V., and Craig, A. T., Introduction to Mathematical Statistics, London: Macmillan, pp. 182-184, 1970.
29. Hogg, R. V., et al., op. cit., pp. 325-327.
30. U. S. Government Printing Office, National Bureau of Standards, Applied Mathematics Series, No. 55, pp. 927-949, May 1968.
31. Lindsey, W. C., "Performance of Phase-Coherent Receivers Preceded by Bandpass Limiters," IEEE Trans. on Communication Technology, vol. COM-16, April 1968, pp. 245-251.
32. Huff, R. J., Reinhard, K. L., and Upp, D. C., "The Synchronization of Time Division Multiple Access Systems -- An Analytical and Experimental Study," Report 2358-9, 31 January 1969, The Ohio State University ElectroScience Laboratory, Department of Electrical Engineering; prepared under Contract F30602-67-C-0119 for Rome Air Development Center, Griffiss Air Force Base, New York. (AD 689 223)
33. Miller, T. W., "Imperfect Differential Detection of a Biphase Modulated Signal -- An Experimental and Analytical Study," Report 2738-5, 23 August 1971, The Ohio State University ElectroScience Laboratory, Department of Electrical Engineering; prepared under Contract F30602-69-C-0112 for Rome Air Development Center, Griffiss Air Force Base, New York.

34. Baird, C. A., "Recursive Processing for Adaptive Arrays,"
Proc. Adaptive Antenna Workshop, Vol. 1, 11-13 March 1974.